SYNTHESIS OF NORDIHYDROGUAIARETIC ACID (NDGA) ANALOGUES AND THEIR OXIDATIVE METABOLISM

A Thesis Submitted to the College of Graduate Studies and Research

in Partial fulfillment of the requirements

for the Degree of

Doctor of Philosophy

in the

College of Pharmacy and Nutrition

of the

University of Saskatchewan

Saskatoon, Saskatchewan

Canada

By

Isaac Asiamah

PERMISSION TO USE

In presenting this thesis in partial fulfillment of the requirements for a Postgraduate degree from the University of Saskatchewan, I agree that the Libraries of this University may make it freely available for inspection. I further agree that permission for copying of this thesis in any manner, in whole or in part, for the scholarly purposes may be granted by the professor(s) who supervised my thesis work or, in their absence, by the Dean of the College in which my thesis work was done. It is understood that any copying or publication or use of this thesis or parts thereof for financial gain shall not be allowed without my written permission. It is also understood that due recognition shall be given to me and to the University of Saskatchewan in any scholarly use made of any material in my thesis. Request for permission to copy or make other use of material in this thesis, in whole or in parts, should be addressed to:

The Dean

College of Pharmacy and Nutrition

University of Saskatchewan

110 Science Place

116 Thorvaldson Building

Saskatoon, SK Canada

S7N 5C9

ABSTRACT

Nordihydroguaiaretic acid (NDGA), is a naturally-occurring lignan isolated from the creosote bush (Larrea tridentata). The aqueous extract of this shrub, commonly referred to as Chaparral tea, was listed in the American pharmacopeia as an ethnobotanical used to treat tuberculosis, arthritis and cancer. Other documented traditional applications of creosote bush extract include treatment for infertility, rheumatism, arthritis, diabetes, gallbladder and kidney stones, pain and inflammation among many others. In spite of the numerous pharmacological properties, NDGA use has been associated with toxicities including hepatotoxicity in humans. Previous studies in our group showed that oxidative cyclization of NDGA (a di-catechol) at physiological pH forms a dibenzocyclooctadiene that may have therapeutic benefits whilst oxidation to *ortho*-quinone likely mediates toxicological properties.

In order to investigate the structural features responsible for pharmacological and toxicological properties, a series of NDGA analogues were designed, synthesized and characterized for the purpose of studying their oxidative metabolism. Literature procedures were modified to successfully prepare seven lignan analogues via multi-step synthesis. In our effort to understand the mechanisms of NDGA intramolecular cyclization, the prepared analogues were incubated under previously established conditions where NDGA autoxidized to yield the dibenzocyclooctadiene derivative. We also evaluated the stability of the analogues under the conditions of this study. Furthermore, we evaluated bioactivation potential of the prepared analogues with a goal of eliminating reactive metabolite liability through rational structural modification. We incubated NDGA and its analogues in rat liver microsomes (RLM) in the presence of glutathione as a nucleophilic trapping agent. Standards for comparison were generated by performing glutathione

trapping experiments with chemical and enzyme oxidation systems. The potential of the dibenzocyclooctadiene lignan **2** derived from NDGA under physiological conditions to contribute to toxicological properties via reactive metabolite formation was also evaluated. Glutathione conjugates were detected by electrospray ionization-mass spectrometry (ESI-MS) scanning for neutral loss (NL) 129 Da or 307 Da in positive ion mode or precursor ion (PI) scanning for 272 Da in negative ion mode and further characterized by liquid chromatography–tandem mass spectrometry (LC–MS/MS) or in a single LC-MS run using multiple reactions monitoring (MRM) as a survey scan to trigger acquisition of enhanced product ion (EPI) data.

We determined that NDGA autoxidation at pH 7.4 is dependent on substituents and/or substitution pattern on the two aromatic rings. In particular, spontaneous intramolecular cyclization to a dibenzocyclooctadiene required a di-catechol lignan, raising the possibility that o-Q formation may not be necessary for cyclization to occur. Cyclization was significantly inhibited in the presence of excess GSH which supports the involvement of free radicals as opposed to o-Q in the intramolecular cyclization process. The mono-catechol analogues **A1** and **A4** underwent oxidation to o-Q but no evidence of cyclization was found implying that electrophilic substitution cannot account for NDGA cyclization. The phenol-type analogues were oxidatively more stable in comparison with the catechol-type analogues at pH 7.4. The results demonstrate that electrophilic substitution makes no contribution to the intramolecular cyclization process and that a radical mediated process accurately describes the situation for NDGA.

Oxidative metabolism and bioactivation studies on NDGA and its analogues revealed that reactive metabolites formation is dependent on substitution and/or substitution pattern of the aromatic rings. Cytochrome P450-mediated oxidation of NDGA and its catechol-type analogues yielded electrophilic intermediates which reacted with GSH. The GSH mono-conjugates were

identified as ring adducts derived from o-Q although the position at which the GSH binds to the aromatic rings could not be determined. We also found that NL 129 or 307 scanning in positive ionization mode has potential diagnostic utility in distinguishing between aromatic and benzylic GSH conjugates although further studies may be required for validation. We found no evidence of p-QM either directly or via isomerization of o-Q intermediates suggesting that o-Q is the major reactive toxicophore responsible for reactive metabolite mediated toxicities associated with NDGA use. In addition, we demonstrated that the NDGA-derived dibenzycyclooctadiene lignan (cNDGA **2**) undergoes P450-mediated oxidation to a reactive metabolite which might have toxicological implications. There was no evidence of P450-mediated oxidation to reactive metabolites for the phenol-type NDGA analogues. It is concluded that structural modification efforts should focus on phenol-type analogues to potentially enhance the safety profile of NDGA.

DEDICATION

This thesis is dedicated to...

…my parents

my dear wife, Mercy and

my loving children John, Isaac Jr and Christabel.

ACKNOWLEDGEMENT

Primarily, I would like to express my sincere gratitude to my supervisor Dr Ed S. Krol for his continued support, guidance, compassion and the gift of optimistic encouragement during the course of my studies. In addition to caring about my academic progress, you also extended friendship beyond the confines of the laboratory to my family. I know I cannot thank you enough but I am sure of one thing. I hope to be a reflection of your curious personality in my own academic career. I also want to express my heartfelt appreciation to the Chair of my research committee Dr Fred Remillard, and the other members of the advisory committee Dr David Palmer, Dr Michel Gravel and Dr Brian Bandy for your valuable suggestions and constructive criticism which culminated in successful completion of this study. One person who deserves special mention is Dr Jane Alcorn for her continued encouragement, advice and helping me refine my knowledge and understanding of my area of research. I want to thank Dr J. Tusynski of the Cross Cancer Institute, University of Alberta, for the preliminary biological evaluations of the compounds synthesized for this study. I am also thankful to Dr Richard A. Manderville of the department of chemistry, University of Guelph for serving as my external examiner.

The following individuals have supported me in diverse ways and I am really grateful. Dr Jennifer Billinsky for her guidance and continued friendship, Ms Deboral Michel and Dr Josh Bush for LC-MS training, Dr Keith Brown for NMR training, my lab mates: Sabia Maini, Leah Mcgurn, Kholoud Algabbass, Yunyun Di and Ahmed Amousa for their help and support both scientifically and socially. I want to specially mention Heather Hodgeson, a summer student who worked in our group for successfully synthesizing one of the compounds studied in this project.

I am highly indebted to NSERC, the University of Saskatchewan and the University of Cape Coast in Ghana for the financial support without which this study would not have been possible

Lastly, but most importantly, I am grateful to my parents for the their unconditional love and prayers. I want to specially thank Mercy, John, Isaac Jr and Christabel Asiamah. Mercy for her love, support and for given me my life's most important assignment, John, Isaac Jr and Christabel. John and Isaac Jr have unique abilities to melt my frustrations with smiles and hugs. Christable was born to us ten day after successfully defending this work and has since been a blessing.

TABLE OF CONTENTS

LIST OF FIGURES

Figure……..……..Page

LIST OF SCHEMES

LIST OF TABLES

LIST OF ABBREVIATIONS

AAPH	2,2'-Azobis(2-amidinopropane) dihydrochloride
BHT	Butylated hydroxytoluene
BnBr	Benzyl bromide
BnCHO	Phenylacetaldehyde
BzOH	Benzoic acid
$CH(OEt)_3$	Triethyl orthoformate
CVD	Cardiovascular disease
d.w.	Dry weight
DCM	Dichloromethane
DDQ	2,3-Dichloro-5,6-dicyano-1,4-benzoquinone
DMF	Dimethylformamide
DMSO	Dimethylsulfoxide
DNA	Deoxyribonucleic acid
ER	Estrogen receptor
EtOH	Ethanol
EtONa	Sodium ethoxide

FDA	Food and Drug Administration
GI_{50}	50 % Growth inhibition
GRAS	Generally Recognized As Safe
GSH	Glutathione reduced
GSSG	Oxidized glutathione
HIV	Human immunodeficiency virus
HPV	Human papilloma virus
HSV	Herpes simplex virus
LC-MS/MS	Liquid Chromatography-tandem Mass Spectrometry
LDA	Lithium diisopropylamide
LFT	Liver function test
M4N	(tetra-O-methyl)nordihydroguaiaretic acid
MeI	Iodomethane
mM	Millimolar
mp	Melting point
MRM	Multiple reaction monitoring
MS	Mass Spectrometry

NAD(P)H	Reduced Nicotinamide adenine dinucleotide phosphate
NDGA	Nordihydroguaiaretic acid
NL	Neutral loss
NMR	Nuclear Magnetic Resonance
Nu	Nucleophile
o-Q	*ortho*-Quinone
PC	Pilot compound
Pd-C	Palladium on carbon
PI	Precursor ion
p-QM	*para*-Quinone methide
py	Pyridine
QMs	Quinone methides
R^2	Coefficient of determination
RM	Reactive metabolite
ROS	Reactive oxygen species
Rt	Retention time
rt	Room temperature

SAR	Structure activity relationship
SDG	Secoisolariciresinol diglucoside
SECO	Secoisolariciresinol
t-BuOH	*tert*-butyl alcohol
TFA-TFAA	Trifluoroacetic acid-trifluoroacetic acid anhydride
THF	Tetrahydrofuran
TsCl	Toluenesulfonyl chloride
TTFA	Thallium(III) tris(trifluoro acetate)

1 INTRODUCTION

The leaves of the plant creosote bush were used commonly in traditional medicines among the Native Americans for diverse beneficial effects.[1-3] The aqueous extract of this shrub, commonly referred to as Chaparral tea, was listed in the American pharmacopeia as an ethnobotanical used to treat tuberculosis, arthritis and cancer.[3] Documented traditional applications of the plant extract include treatment for infertility, rheumatism, arthritis, diabetes, gallbladder and kidney stones, pain and inflammation among many others.[1,2] Creosote bush is rich in lignans particularly nordihydroguaiaretic acid (NDGA, **1**) (up to 15% dry weight (d.w.)).[1] This natural polyphenol is generally accepted as responsible for both the beneficial and adverse effects associated with creosote bush, mainly because of its high content in the plant.[1,2, 4-6] NDGA **1** has been shown to have promising applications in the treatment of multiple diseases, including cardiovascular diseases,[7, 8] neurological disorders[9-13] and cancers.[2,14-20] It has also been reported to potently inhibit viruses such as human immunodeficiency virus (HIV-1), herpes simplex virus (HSV), human papilloma virus (HPV) and influenza virus.[1,21] The radical scavenging[22,23] and antioxidant effects[24] as well as anti-inflammatory[25, 26] and anti-proliferative properties may be of relevance in different diseases. Despite its broad pharmacological activities, NDGA **1** use is associated with toxicity especially when ingested at higher doses.[27] Reports of severe hepatic[24, 27-29] and renal injuries[30-32] associated with NDGA **1** use are likely linked to bioactivation to reactive ortho-quinones (o-Qs).[32-34]

Interestingly, incubation of NDGA **1** at pH 7.4 gave a schisandrin-like dibenzocyclooctadiene lignan **2**.[35] This appears to be an intramolecular cyclization although the

mechanism is yet unknown. The conditions of preparation of Chaparral tea[2] and biological evaluations of NssDGA **1**[5,36,37] favour autoxidation suggesting that any biological action by NDGA treatment could result from either NDGA itself or its oxidation products.[37] Also, lignans with the dibenzocyclooctadiene structural moiety have received much research attention and are known to exhibit a wide variety of interesting biological activities,[38,39] including antiviral,[40] anticancer,[41] anti-inflammatory,[42] and hepatoprotective effects.[43] On the other hand, Billinsky *et al.*,[33] reported that oxidative metabolism of NDGA gives rise to an o-Q but does not appear to form a para-quinone methide (p-QM). This is surprising given that under similar oxidative conditions secoisolariciresinol (SECO, **9**), a structurally similar lignan, converts to lariciresinol **21** likely via a p-QM intermediate.[33, 44] It is noteworthy that oral consumption of SECO is not reported to cause serious toxic effects in humans whilst use of NDGA in the food industry as an antioxidant was banned following reports of nephrotoxicity.[31]

Research interest in NDGA continues to rise due to its encouraging treatment benefits in conditions such as cardiovascular diseases, neurological disorders and cancers.[6] Several medicinal properties have been supported by *in vitro* and *in vivo* experimental studies, as well as historical reports. Studies suggest that NDGA derivatives such as tetramethyl-O-NDGA (M4N, **14**) and tetra-acetyl NDGA **15** exhibit similar or even higher anti-viral activities than natural compounds. It is worth mentioning that M4N **14** is currently under clinical evaluations for treatment of human cancers.[45] Perhaps, the most startling observation is with 1,4-bis-(3,4-dihydroxyphenyl) butane **17**, a simplified NDGA, which is 10 times more potent as a proliferative inhibitor of H-69 small lung cancer cells than NDGA.[36] Given that chemical modification of NDGA may reduce toxicity, combined with enhancing therapeutic effects, the possibility that derivatives of NDGA may become important drugs in the future has been well recognized as evidenced by increasing research interest.

Unfortunately, the structural features that govern both pharmacological and toxicological properties of NDGA are poorly understood. At present, the usefulness of NDGA and its derivatives is hindered by the lack of understanding of the mechanisms of not only the beneficial activities but also toxicity. A thorough understanding of pharmacological and toxicological pathways may lead to rational design of NDGA analogues with improved safety profile. While a great deal of observational and correlative data has been reported, there have been few comprehensive mechanistic or structure-function studies conducted on NDGA. Therefore, the overall goal of this study is to synthesize analogues of NDGA to investigate the mechanisms of pharmacological and toxicological pathways. The study is expected to provide insight into the structural features which modulate biological properties of NDGA and likely lead to development of new treatments for human diseases in the future. The results will certainly advance our understanding of structure-activity-relationships of NDGA and direct efforts towards discovery of new NDGA analogues with better safety profiles.

2 LITERATURE REVIEW

2.1 Lignans

Lignans constitute an important class of natural products derived from oxidative dimerization of two phenylpropanoid units. They are widely distributed in the plant kingdom and probably play important roles in plants' defense mechanisms against various biological pathogens and pests.[46] Structurally, lignans have two C_6C_3 structural units linked through β and β′ (or C8 and C8′) carbons to form 18 carbon basic skeleton[46, 47] (Figure 2-1).

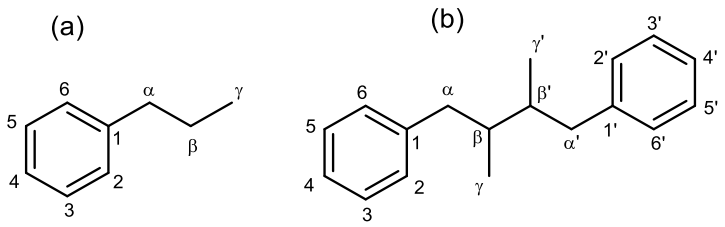

Figure 2-1: Structures for (a) C_6C_3 phenylpropane subunit and (b) basic lignan skeleton.

Lignans continue to attract much research attention due largely to their significant pharmacological properties including antitumor, anti-inflammatory, immunosuppressive, cardiovascular, antioxidant and antiviral actions.[48,49] In addition to their staggering biological activities, lignans show enormous structural diversity which partly accounts for an upsurge in research interest. Lignans have been classified into different families on the basis of their general chemical structure.[49,50]

2.2 Nordihydroguaiaretic Acid (NDGA)

2.2.1 Source and Traditional Uses

Nordihydroguaiaretic acid NDGA **1** is a lignan present at concentrations of up to 15% by dry weight of creosote bush leaves.[1] Creosote bush (*Larrea tridentata)*, is a common shrub of the arid regions of northern Mexico and the south-western United States. Traditionally, the shrub has been used by the indigenous people of these areas to treat numerous health problems.[2, 51] Extracts and preparations of the plant were used for varied reasons including treatment for infertility, rheumatism, arthritis, diabetes, gallbladder and kidney stones, pain and inflammation among others.[2, 4]

2.2.2 Structure and Physical Properties

Structurally, NDGA **1** possesses two catechol moieties linked via a butane bridge with two methyl substitutions at C_2 and C_3. This polyphenol occurs naturally as a *meso* compound (Figure 2-2). Its strong antioxidant properties are believed to result from the presence of four phenolic hydroxyl groups. NDGA **1** is classified as a dibenzylbutane lignan because the phenylpropanoid dimers are joined only by β-β′ bonds[47]. Its molecular formula and weight are $C_{18}H_{22}O_4$ and of 302.26 g/mol respectively. It is solid at room temperature (mp 185-186 °C). NDGA **1** is also referred to as 2,3-bis(3,4-dihydroxybenzyl)butane, 4,4'-(2,3-dimethyl-1,4-butanediyl)bis[1,2-benzenediol] and 4,4'-(2,3-dimethyltetramethylene)dipyrocatechol and trivially as masoprocol.

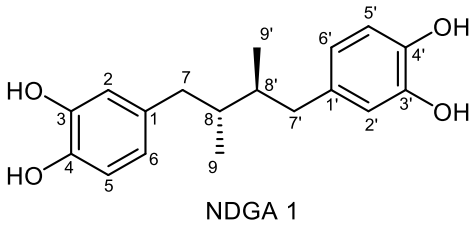

Figure 2-2: Molecular Structure of Nordihydroguaiaretic Acid (NDGA **1**).

2.2.3 Pharmacological Properties of NDGA

The natural antioxidant NDGA **1** has been under study for numerous pharmacological activities including its anti-inflammatory and anti-cancer properties. A topical form of NDGA (Actinex®, Chemex Pharmaceuticals, Denver CO) was approved by the FDA for treatment of actinic keratosis. After a short while on the market, Actinex® was voluntarily withdrawn due to reports of skin hypersensitivity.[4] NDGA **1** has shown benefit in cancer chemoprevention, cancer therapy, antimicrobial, fertility and hypoglycaemic effects in *in vitro* and *in vivo* studies as well as human clinical trials[1]. In addition, NDGA is a known potent inhibitor of lipoxygenase,[4, 24] HPV,[2] HSV and HIV.[1, 4] It is particularly touted for its antioxidant properties. However, its long use as antioxidant in the food industry[52] was discontinued following reports of NDGA-induced cystic nephropathy in rats.[31] The use of NDGA for therapeutic purposes is currently limited due largely to toxicity concerns.

2.2.4 NDGA and Autoxidation

A study in the 1980s reported that nordihydroguaiaretic acid underwent conversion to "activated NDGA" in the presence of oxygen.[37] The structure of the oxidation product remained unstudied until a recent literature report suggesting the "activated NDGA" is a

dibenzocyclooctadiene.[35] In this study, Billinsky *et al*.,[35] showed that NDGA underwent rapid oxidative cyclization in aqueous solution at physiological pH (7.4) to a schisandrin-like dibenzocyclooctadiene lignan. The structure of the oxidation product (Figure 2-3) was unequivocally determined from NMR and MS experiments.

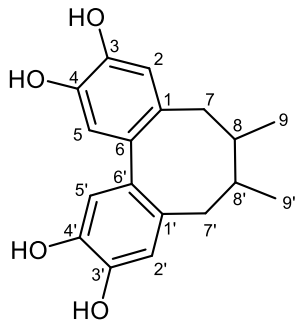

cNDGA, 2

Figure 2-3: Structure of the NDGA-derived dibenzocyclooctadiene (cNDGA).

2.2.5 Biological Implications of NDGA-derived Dibenzocyclooctadiene

NDGA-derived dibenzocyclooctadiene lignan probably makes contribution to therapeutic effects attributed to NDGA. The "activated" NDGA originally reported by Wagner et al.,[37] formed a stable complex with duplex DNA. This suggests that any biological action by NDGA treatment could result from either NDGA itself or its oxidation products[37] since many antimicrobial and antineoplastic agents are known to function by interacting with DNA and subsequently affecting nucleic acid metabolism.[53, 54] Unlike NDGA itself, the "activated" NDGA interacted with duplex DNA via hydrophobic association. Further, no evidence of intercalation was seen suggesting that complexation might not lead to DNA structure modification. In addition, the following important observations lend support to potential involvement of NDGA oxidation products in therapeutic claims.

Firstly, the traditional method of preparation of products from creosote bush normally involves boiling the leaves in water. Under such extraction conditions, NDGA possibly converts to dibenzocyclooctadiene lignan.[35] Secondly, reported conditions of biological activity evaluations involving NDGA favour its oxidation and therefore NDGA-derived dibenzocyclooctadiene lignan likely makes contribution to reported biological activities especially where biological studies were conducted under aerobic conditions for extended periods of time at pH 7.4 or higher.[35] For example, anticancer activity reported by McDonald et al.,[36] was carried out for 7 days under conditions that favour oxidation. NDGA autoxidation is rapid[35] and therefore the observed activity may not result entirely from the natural polyphenol. Lastly, lignans with dibenzocyclooctadiene structural moiety exhibit a wide variety of interesting biological activities,[38,39,55] including antiviral,[40] anticancer,[41] anti-inflammatory,[42] and hepatoprotective effects.[43] For instance, gomisin J and derived dibenzocyclooctadiene lignans are reported to have effective anti-HIV activity[56] and schisantherin D and kadsuranin showed similarly effective anti-HIV activity.[57] A study[58] involving a series of dibenzylbutanediols reported enhanced anti-tumor activity and benefit in breast cancer cell inhibition following introduction of the dibenzocyclooctadiene structural moiety. These findings suggest that an NDGA-derived dibenzocyclooctadiene likely makes contribution to therapeutic properties of NDGA.

2.2.6 Proposed Mechanisms of NDGA Autoxidation

Nordihydroguaiaretic acid autoxidation to dibenzocyclooctadiene probably occurs via a radical-mediated reaction.[35, 59] A proposed mechanism involves sequential 2 proton 2 electron loss leading to a di-radical **4a** which subsequently undergoes coupling via its resonance form **4b** to the dibenzocyclooctadiene lignan **2** as shown in Scheme 2-1.[35, 59] This mechanism is supported by the

biosynthesis of the dibenzocyclooctadiene family of lignans in plants which is known to involve enzymatic intramolecular biaryl oxidative coupling of phenolic precursors via radical cations, as a key step.[38, 60]

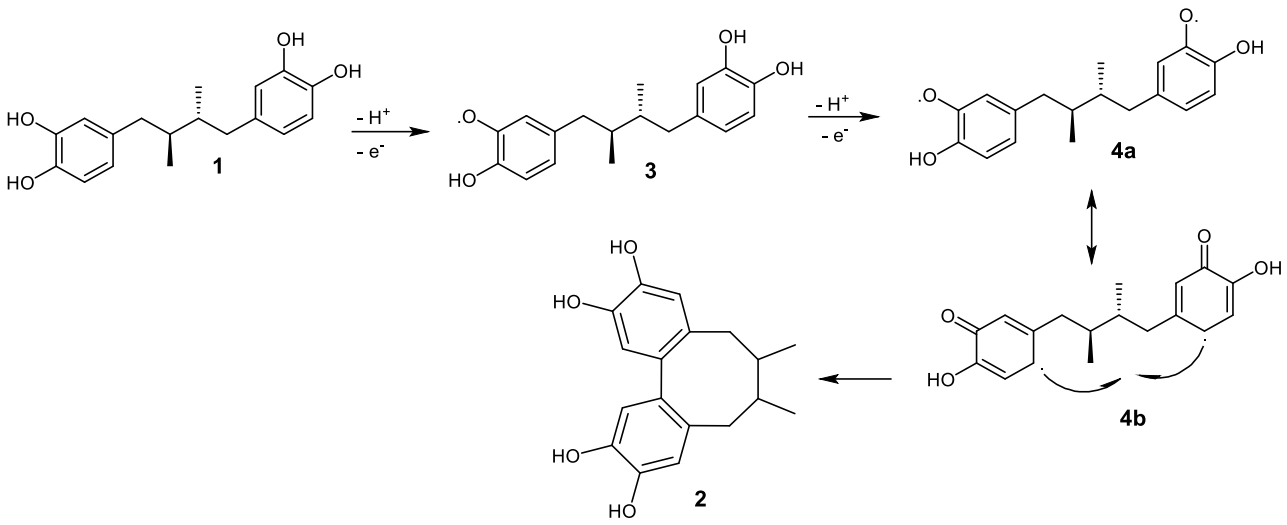

Scheme 2-1: Proposed mechanism for NDGA autoxidation via radical addition.

In addition, the dibenzocyclooctadiene family of lignans has been successfully prepared by biomimetic synthetic methods.[38, 59, 60] Whilst all described approaches involve oxidative aryl coupling, the reagents used are critical for the success of the reactions. Coupling of lignans containing phenol functions have been achieved using milder oxidative coupling reagents such as vanadium(V) oxyhalides,[61] thallium(III) tris(trifluoroacetate) (TTFA),[62] hypervalent iodine reagents,[63] ruthenium oxide,[60] and others.[38] On the other hand, non-phenol substrates required oxidizing agents such VOF_3.[64] Attempts at minimizing the accompanying side reactions led to a variety of transition metal oxides or their salts, such as Tl(III), Mn(II), Fe(III), Co(III), and Ru(IV), which promote aryl-aryl couplings including intramolecular cases.[38] In particular, ruthenium(IV) dioxide in trifluoroacetic acid-trifluoroacetic acid anhydride (TFA-TFAA) medium is a versatile reagent for the synthesis of bridged biaryls from non-phenolic precursors.[60] Chattopadhyay et al.,[65]

demonstrated for the first time the use a cheap, readily accessible non-transition metal based reagent 2,3-Dichloro-5,6-dicyano-1,4-benzoquinone (DDQ) as oxidative coupling reagent for non-phenols. This reagent has been widely used in non-phenol oxidative coupling reaction as illustrated with the general structure in Scheme 2-2.

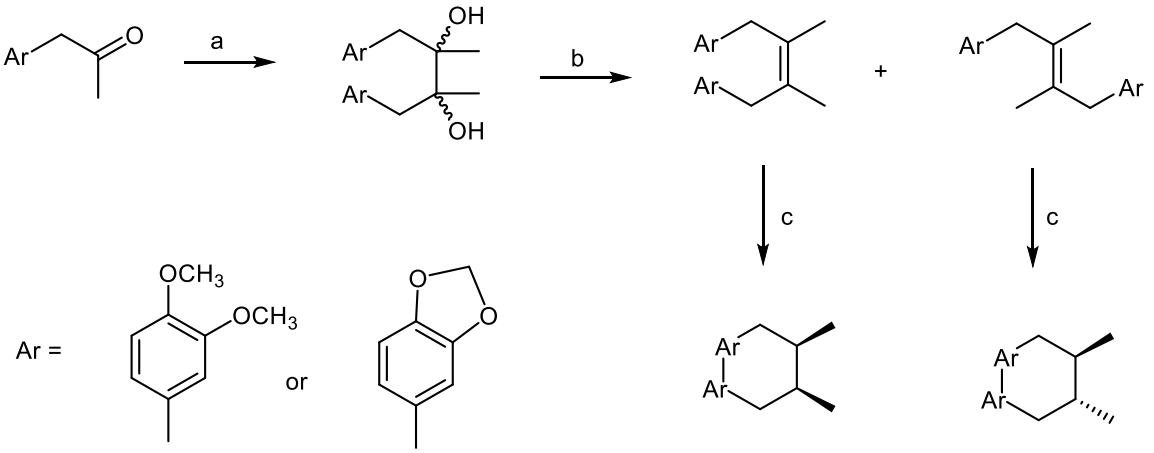

Scheme 2-2: Oxidative coupling of non-phenol lignans using DDQ.
Reagents: a) $TiCl_4/Zn$; b) $CH(OEt)_3$, BzOH; c) (i) H_2, PtO_2; (ii) DDQ, TFA

Notwithstanding the proposed radical mediated mechanism, autoxidation of NDGA could also result from electrophilic substitution[66] as illustrated in Scheme 2-3. This mechanism also involves a 2 proton, 2 electron loss as in the case of radical-mediated addition. The sequential loss of 2 protons and 2 electrons is expected to occur at only one of the two equivalent rings leading to a di-radical **5a** which possesses the resonance form o-Q **5b**. A subsequent nucleophilic attack of the unoxidized ring on the o-Q is expected to yield the dibenzocyclooctadiene product **2**. The two catechol moieties of NDGA are equivalent and therefore exclusive oxidation of one ring seems unlikely as suggested by Galano et al.[22] However, only one of the two equivalent phenol rings of secoisolariciresinol (SECO, **9**) was oxidizable with 2,2'-azobis(2-amidinopropane) dihydrochloride (AAPH).[51] Given that SECO **9** and NGDA **1** are structurally similar and oxidation of NDGA in the

presence of GSH could result in a mono-conjugate derived from o-Q,[33] an electrophilic substitution mechanism cannot be ruled out.

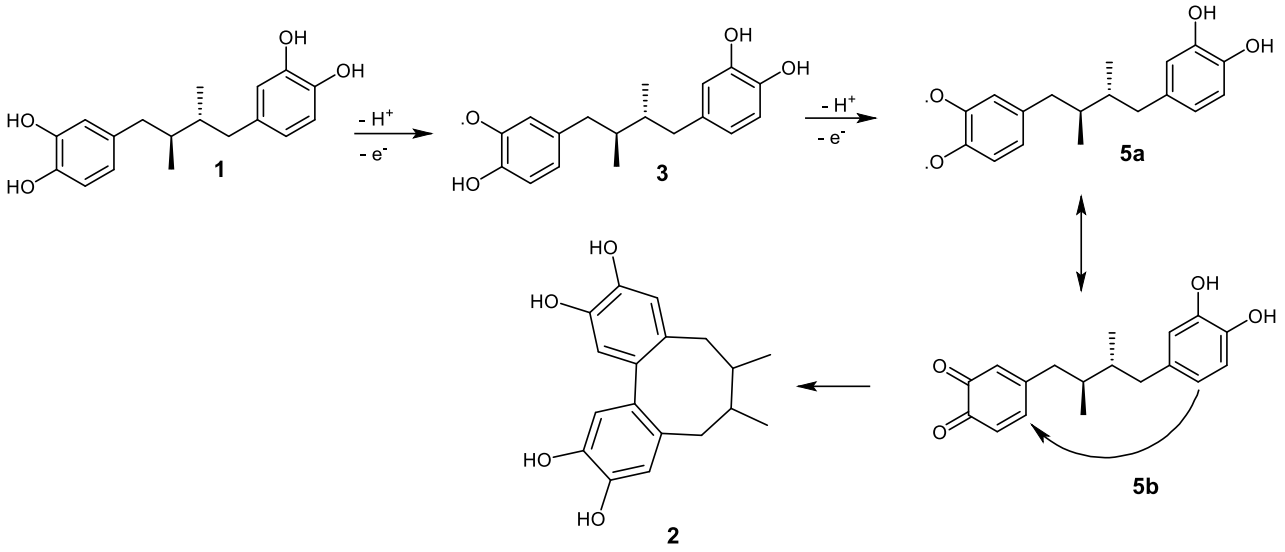

Scheme 2-3: Autoxidation of NDGA via electrophilic substitution mechanism.

This mechanism is further supported by observations with polyphenols present in tea. Oxidations have resulted in dimers such as **8** and other oligomers, whose formation is suggested to occur via intermolecular nucleophilic attack of an unoxidized ring of one molecule **6** on an o-Q **7** derived from oxidation of a second molecule.[66, 67] Flavonoids undergo enzymatic or non-enzymatic reactions known to proceed via oxidation of the 3,4-dihydroxy function of the B-ring to the corresponding *o*-Qs such as **7**. The o-Qs have electrophilic properties and are able to react with surrounding nucleophilic molecules including unoxidized polyphenols[68] such as **6** via an electrophilic substitution mechanism. Oxygen-dependent dimerization of dihydrochalcone aspalathin **6** occurred via electrophilic substitution as illustrated in Scheme 2-4[66]. Interestingly, aspalathin was treated under the same conditions of incubation (phosphate buffer, pH 7.4 and 37 ^{o}C) as in the NDGA autoxidation study. Although, the coupling is intermolecular, the fact that an initially formed o-Q reacts with a nucleophilic phenolic ring suggests that NDGA *o*-Q **5b** possibly

undergoes intramolecular coupling with its unoxidized catechol ring. It should be noted however that this mechanism was not demonstrated conclusively and a radical-mediated process remains a possibility for the formation of **8**.

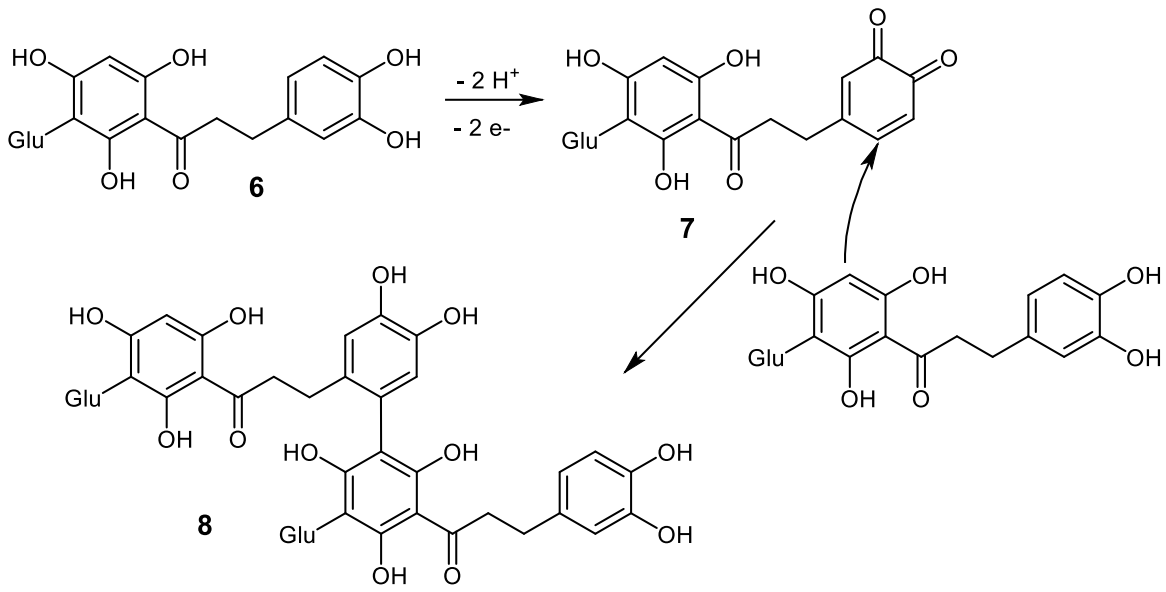

Scheme 2-4: Dimerization of aspalathin via oxidative coupling.[66]

The exact mechanisms of NDGA oxidative cyclization remain unknown but likely depend on substituents and/or substitution patterns on both aromatic rings. Understanding the mechanisms will be critical to designing NDGA analogues with higher propensity to undergo cyclization at physiologically relevant conditions. Also, NDGA analogues resistant to autoxidation can be designed and synthesized to investigate the contribution of cyclization product **2** to pharmacological activity and/or toxicity.

2.3 Toxicological Properties of NDGA

Creosote bush has been utilized in traditional healing practices for many years in a wide range of remedies, but its use in clinical setting is currently limited due to toxicity concerns. For instance,

chronic exposure to Chaparral tea, an aqueous extract of creosote bush is known to cause liver damage. Individuals who consumed Chaparral tea over time suffered drug-induced hepatitis.[2, 24, 27] With exception of one specific case report of total hepatic failure[24, 28] and a few cases of progression to liver cirrhosis,[24] hepatotoxicity was reversible when ingestion is discontinued.[2, 24, 27, 28] In 1968 the Canadian Food and Drug Directorate found evidence of NDGA-induced cystic nephrotoxicity in rats.[31] Consequently, NDGA use as food preservative was banned in Canada. Furthermore, NDGA lost its "Generally Recognized As Safe" (GRAS) status and was removed from the US Food and Drug Administration's list following several reports of toxicity.[1, 31]

2.3.1 Secoisolariciresinol (SECO) versus Nordihydroguaiaretic acid (NDGA)

Secoisolariciresinol (SECO, **9**) belongs to the dibenzylbutanediol class of lignans. It is closely related to NDGA **1** in structure. Like NDGA, is linked only by a β-β′ bond. However, SECO **9** has hydroxymethyl groups at C_2 and C_3 of the butane bridge and methoxy substitutions at 3 and 3′ positions of the aromatic rings (Figure 2-4). Both NDGA **1** and SECO **9** have been under study for their diverse pharmacological properties and potential as lead drug candidates.

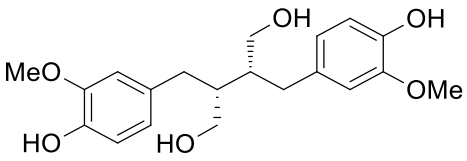

9

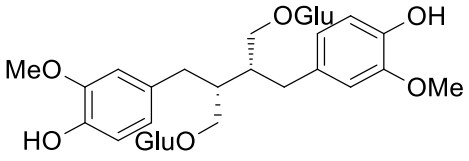

10

Figure 2-4: Molecular structure of Secoisolariciresinol (SECO, **9**) and its diglucoside (SDG, **10**).

The consumption of flaxseed has shown benefits in humans. Experimental evidence suggests that the lignan secoisolariciresinol diglucoside (SDG, **10**) present in flaxseed and its

mammalian metabolites may protect against CVD and metabolic syndrome by reducing lipid and glucose concentrations, lowering blood pressure, and decreasing oxidative stress and inflammation.[69] A reduction in cancer risk by preventing pre-cancerous cellular changes and by reducing angiogenesis and metastasis following ingestion of flax lignans has also been suggested.[69] Therefore, dietary SDG **10** has been proposed as having the potential to decrease the incidence of several chronic diseases. Despite its close structural similarity to NDGA **1**, flaxseed lignan SECO **9** appears to be well tolerated among adult populations[69] and no known significant toxicity in humans has been reported.[44]

2.3.2 Quinones and Toxicity

Quinones represent a class of toxicological intermediates which have been implicated in a variety of xenobiotic toxicities *in vivo*, including cytotoxicity, immunotoxicity, and carcinogenesis. Formation of quinones from xenobiotics may be mediated by monooxygenase enzymes, peroxidases and in some cases molecular oxygen. Quinone-mediated toxic effects may have varied and often complex mechanisms.[70] However, the main theories proposed over the years to explain quinone toxicity include alkylation or covalent binding, and oxidative stress mechanisms of cytotoxicity.[71]

2.3.3 Theories of Quinones Toxicity

2.3.3.1 Alkylation of Macromolecules

The major non-protein sulfhydryl present in cells, glutathione (GSH, **11**) is generally considered to protect cells from oxidative damage because its thiol function serves as “sacrificial”

nucleophile, preventing critical sites on cellular macromolecules from irreversible modification.[70] The physiological concentration of GSH in the liver is approximately 7mM[72] of which nearly 90% is found in the cytosol.[73]

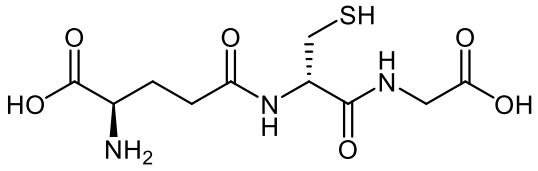

GSH, 11

Figure 2-5: Structure of glutathione (GSH, **11**).

The presence of electrophiles in the cellular environment causes a reaction with cellular GSH **11** leading to its depletion. Following GSH **11** depletion, nucleophilic groups on cellular macromolecules, such as proteins or DNA, react covalently with electrophiles (Figure 2-6) leading to irreversible structural and/or functional changes resulting in cell death.[70,71] DNA modifications likely mediates cytotoxicity of rapidly dividing cells, such as tumor cells, whilst in resting or non-dividing cells alkylation of essential protein thiol or amine groups and/or oxidation of essential thiols by activated oxygen species and/or GSSG is the molecular basis of quinone cytotoxicity.[71]

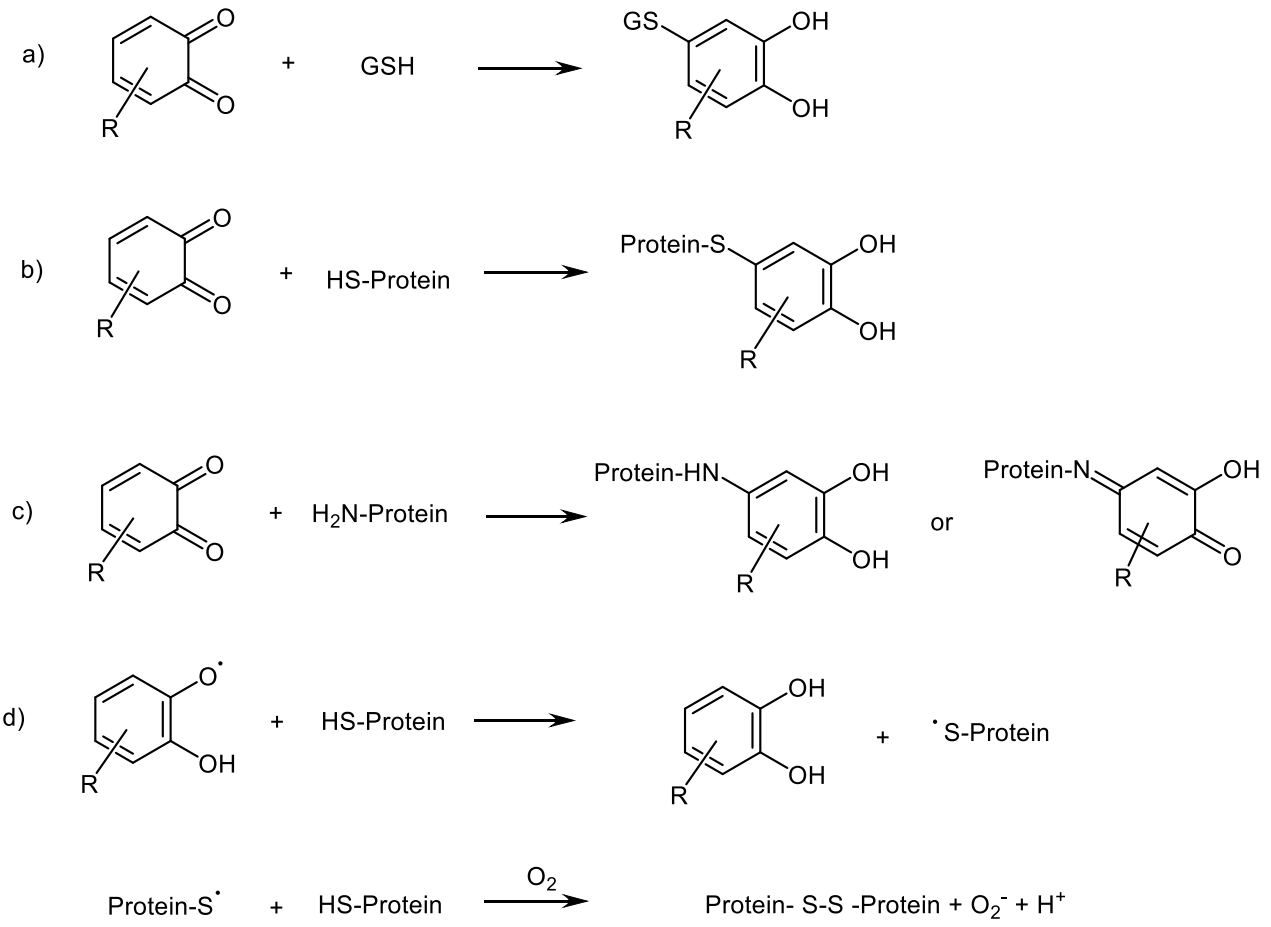

Figure 2-6: Covalent binding of electrophiles with (a) GSH and three possible forms of electrophile-protein interactions: interaction with (b) thiol group (c) amine group of protein and (d) reduction of semiquinone radical by sulfhydryl group and subsequent protein cross-linking in the presence of oxygen.[74]

2.3.3.2 Oxidative Stress

Quinone toxicity may result from oxidative stress. Oxidative stress arises when there is a disturbance in the prooxidant-antioxidant balance in favour of the former, leading to potential damage.[75] Quinones are potent redox active compounds which can undergo enzymatic or non-enzymatic redox cycling with their semi-quinone radicals, leading to formation of reactive oxygen species (ROS) such as superoxide anion radicals (Scheme 2-5). Superoxide anion radicals may cause damage on their own or react further with hydrogen peroxide, formed from enzymatic or

spontaneous dismutation of superoxide anion radical to give hydroxyl radicals. Hydroxyl radicals are powerful oxidizing species that may be responsible for most of the damage to essential macromolecules involved in oxidative cytotoxicity (Scheme 2-5)[70, 71].

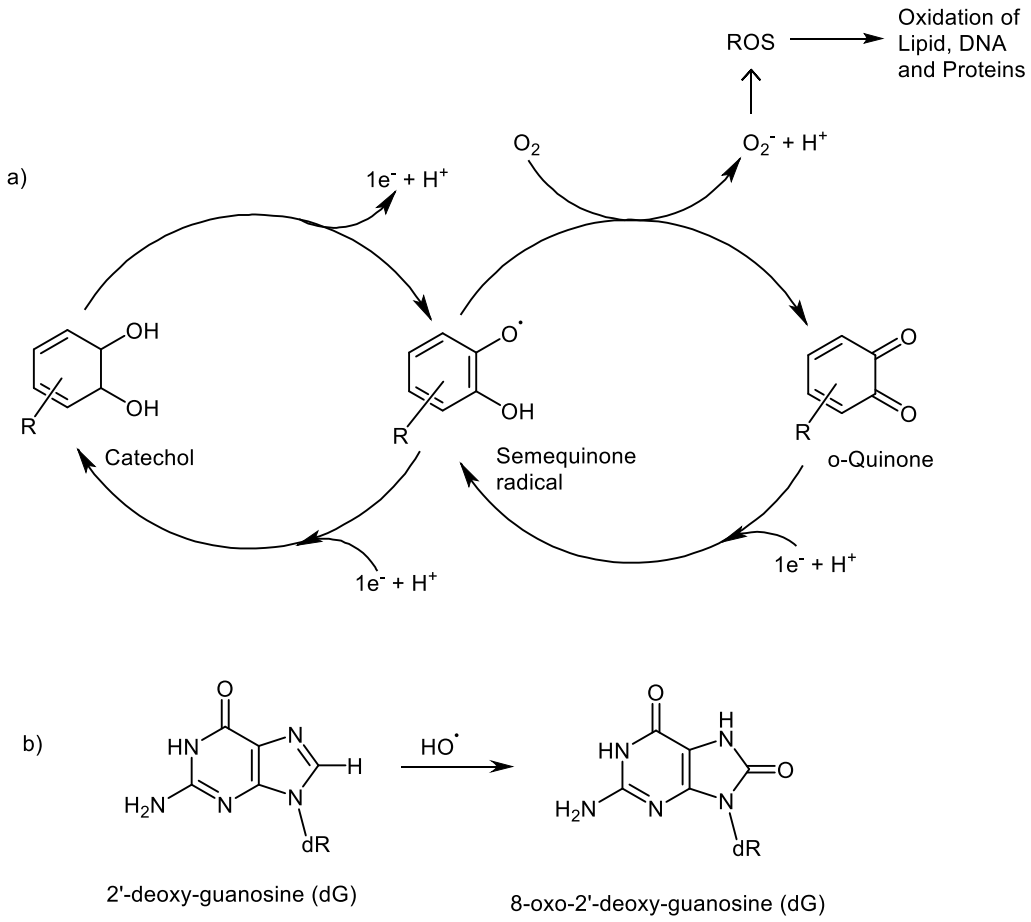

Scheme 2-5: (a) Redox cycling of quinones generating reactive oxygen species (ROS) and (b) Oxidation of 2-deoxy-guanosine by hydroxyl radical.

2.3.4 NDGA and Quinones Formation

The mechanisms of NDGA toxicity remain unclear although quinone formation has been implicated in hepatotoxicity. In theory, the structure of NDGA **1** suggests possible direct oxidation to either o-Q **5b** or p-QM **5c** (Scheme 2-6). Such transformations may be cytochrome P450-

mediated or catalysed by other oxidases.[28] Formation of NDGA o-Q **5b** has been reported in the literature.[32, 33, 76] Surprisingly, NDGA does not appear to form p-QM **5c**[33] even though its o-Q **5b** meets structural requirements for isomerization.[77, 78] The presence of benzyl protons available for abstraction suggests that NDGA o-Q **5b** can tautomerize to p-QM **5c.**[79] In addition, extended π-conjugation at the para or 4-position of a catechol[78] as well as acidity of the benzyl proton[80] enhances o-Q to p-QM isomerization rate. On the contrary, steric hindrance at the benzyl position slows down tautomerization rate and may lead to non-detectable levels of p-QM. This has previously been cited as a possible explanation for the absence of p-QM **5c** in NDGA oxidation experiments.[33]

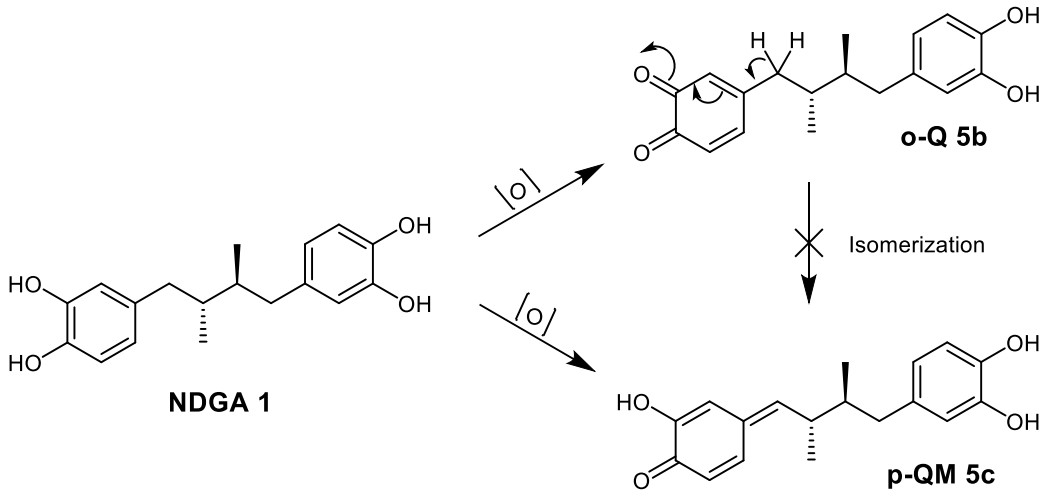

Scheme 2-6: Oxidation of *meso*-NDGA to o-Q and p-QM derivatives.

2.3.5 ortho-Quinones and Reactive Oxygen Species

In general, catechols undergo two successive 1-electron oxidations catalysed by a variety of oxidative enzymes, metals ions and in some situations molecular oxygen to generate reactive

metabolites called o-Qs (Scheme 2-5a).[71] For example, tyrosinase oxidizes phenols and/or catechols directly to o-Qs.[81, 82] o-Qs are redox active molecules with potential to undergo non-enzymatic two-electron reduction with cellular reducing equivalents [NAD(P)H] or enzymatic one-electron reduction. The ensuing redox cycling (Scheme 2-5a) increases production of reactive oxygen species (ROS), including superoxide, hydrogen peroxide and ultimately hydroxyl radical.[70] Production of ROS in the cellular environment is known to cause severe oxidative stress through the formation of oxidized macromolecules, including lipids, proteins, and DNA (Scheme 2-5b). The intermediate semiquinone radical (Scheme 2-5a) may cause deleterious damage on its own[74] or oxidizes further to the o-Q. Cytotoxicity of o-Qs appears to be mainly due to oxidative stress[70] although the potential to react with cellular nucleophiles can occur due to the o-Q's ability to act as electrophilic Michael acceptors. NDGA o-Q **5b** is therefore likely to mediate toxicological effects via oxidative stress resulting from redox cycling with its intermediate semiquinone radical **3** although covalent modification of cellular macromolecules may also occur as illustrated in Scheme 2-7. The o-Q **5b** has intrinsic potential to isomerize to the more electrophilic p-QM **5c** tautomer which may also contribute to toxicity.

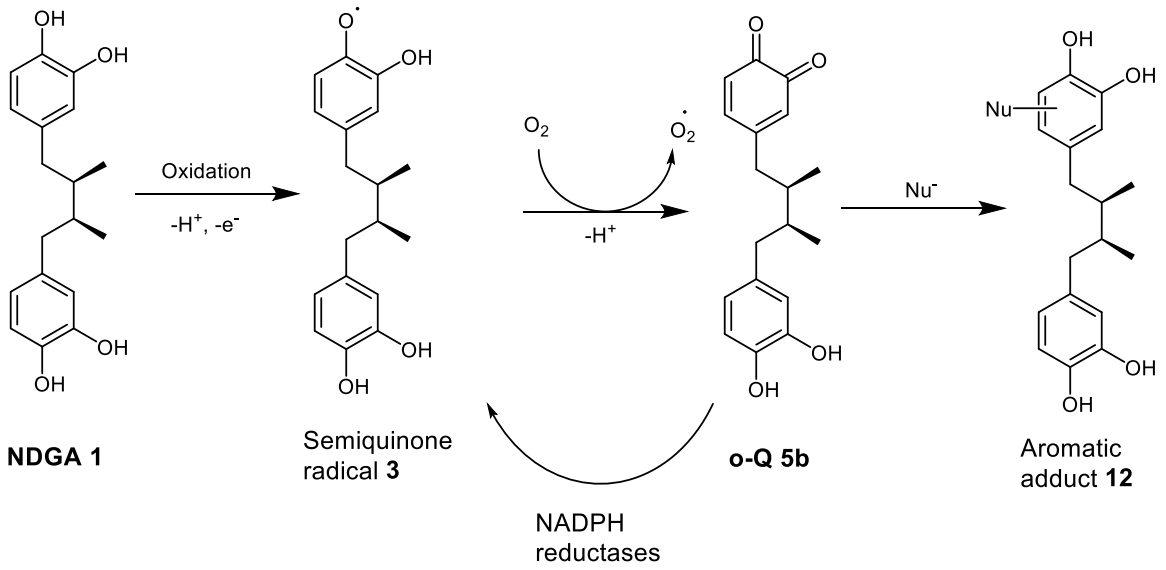

Scheme 2-7: Proposed toxicological pathways for NDGA. The redox cycling of NDGA o-Q **5b** with its semi-quinone radical **3** leads to ROS which may cause oxidative stress. The o-Q **5b** may bind covalently to cellular nucleophiles (Nu) forming aromatic adducts.

2.3.6 p-Quinone Methide and Adduct Formation

Quinone methides (QMs) differ structurally from quinones (Figure 2-7), as one carbonyl group is replaced by a methylene or substituted methylene group.[77] QMs have been implicated in toxicity of certain exogenous compounds including food additives such as eugenol and butylated hydroxytoluene (BHT).[79]

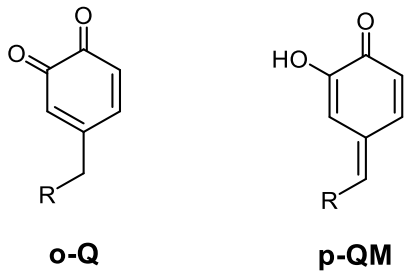

Figure 2-7: General structures of *ortho*-quinone and *para*-quinone methides.

Oxidative metabolism generates QM by one of two major mechanisms. Firstly, phenols with at least one benzylic proton may be directly oxidized to the corresponding phenoxy radical as a

result of monooxygenase[83, 84] or peroxidase activity.[85, 86] The phenoxy radical is subsequently oxidized to a QM which is probably non-enzymatic but is likely to be enzyme-catalysed in the presence of cytochrome P450.[87] A second pathway involves indirect conversion of a catechol to a QM via isomerization of the initially formed o-Q. However, this tautomerization is dependent on the presence of a benzylic hydrogen available for abstraction[79] and steric factors around the benzyl position.[33]

In theory, NDGA **1** should form both o-Q and p-QM. Given that the o-Q **5b** has benzylic hydrogens it is expected to isomerize to the more electrophilic p-QM **5c** as shown below (Scheme 2-8) although there is no evidence yet for NDGA p-QM **5c**. The p-QM **5c** is anticipated to be highly electrophilic in nature and expected to exhibit higher reactivity than o-Q tautomers.[88] Therefore, NDGA p-QM, if formed, will more readily react with cellular nucleophiles than the o-Q tautomer implying a higher toxicity. On this basis, the molecular mechanism of toxicity for a p-QM will be mainly characterized by alkylation of cellular nucleophiles rather than redox chemistry.

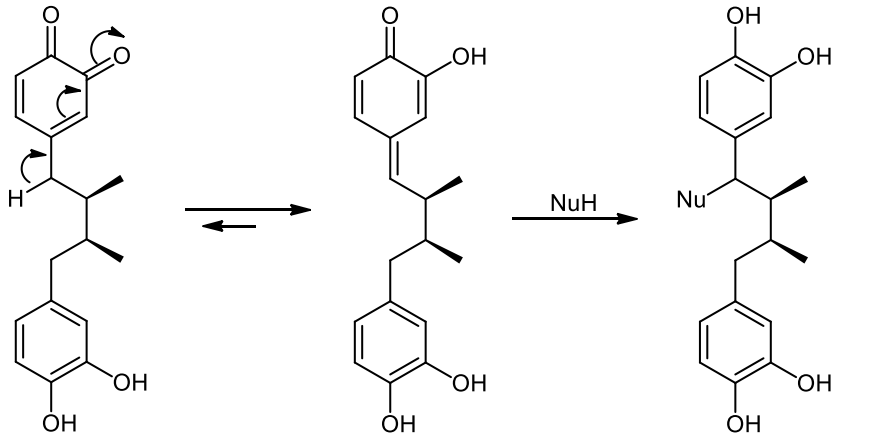

Scheme 2-8: Isomerization of NDGA o-Q **5b** to p-QM **5c** and subsequent reaction with cellular nucleophile (Nu) to form a benzylic adduct **13**.

2.4 Structure Activity Relationship (SAR) Studies on NDGA

McDonald et al.,[36] examined activities of various NDGA analogues against H-69 small cell lung cancer cell line. The primary objective was to establish relationships between structure and potency as proliferative inhibitor of H-69 lung cancer cell line. The authors report that the optimum carbon spacing between the two catechol moieties is four as analogues with less or greater than C_4 bridge showed decreased activity. Findings of McDonald and co-workers as well as those of others[21, 89-91] also suggest that the catechol moiety has little, if any, effect on activity. A tetra-O-methyl-nordihydroguaiaretic acid (M4N **14**) is strikingly more effective,[21, 92] non-toxic and currently in clinical trials against human cancers.[91] Other hydroxyl-substituted analogues (Figure 2-8) such as a tetraacetate of NDGA (TA **15**) and the prodrug tetraglycinylated-NDGA (G4N **16**) have also shown antiviral activity.[21, 89] Lambert et al.,[5] have observed a positive correlation of O-methylation with potency for NDGA and have suggested increased lipophilicity which allows the compounds to traverse lipid membranes as one probable reason for the enhanced activity. Since NDGA binds to estrogen receptors (ERs) to elicit estrogenic response, the potent inhibition of MCF7 breast cancer line by methylated NDGA analogues may be related to increased affinity for ER which are expressed in MCF7 cells.[5]

NDGA potently inhibits lipoxygenase by a mechanism which involves reduction of ferric iron into inactive ferrous form, and concomitant oxidation of the catechol moiety of NDGA to a semiquinone.[93] Whitman et al.,[94] found that "masking" of the phenolic groups of NDGA removes lipoxygenase inhibitory activity. It follows then that pharmacologically active analogues with masked phenolic groups act via a lipoxygenase independent mechanism thus suggesting NDGA acts at multiple targets. Although M4N **14** and other hydroxyl-substituted analogues display similar[36] or better potency than NDGA,[91] the catechol moiety is required for lipoxygenase activity

and also largely accounts for NDGA antioxidant activity. NDGA possibly possesses cytotoxic activity independent of pro-oxidant capability but its antioxidant properties have also been cited in many beneficial applications. For instance, NGDA is a potent *in vitro* scavenger of peroxynitrite, singlet oxygen, hydroxyl radical, superoxide anion and hypochlorous acid.[23] In fact, NDGA is a more effective hydroxyl radical scavenger than other recognized hydroxyl radical scavengers like uric acid, dimethylthiourea, trolox and mannitol.[23] In addition, the inhibition of cytotoxicity induced by *t*-butylhydroperoxide[63] and hydrogen peroxide[74] in mammalian cells is also consistent with the antioxidant effect of NDGA. Therefore, suggestions that the *o*-hydroxyl functions may not be critical to biological activities of NDGA are misleading and possibly simplistic. Perhaps the most striking SAR report is the observation that 1,4-bis(catechol-yl-)-butane **17**, a double demethylated NDGA (Figure 2-8), is 10 times more potent than NDGA as proliferative inhibitor of H-69 small cell lung cancer cells.[36] This raises the question of whether or not NDGA's internal planes of symmetry are necessary for pharmacological activity. NGDA and its racemate showed similar potency as proliferative inhibitor of H-69 small cell lung cancer cells[36]. There are no systematic evaluations of stereochemical influence on biological activity for NDGA.

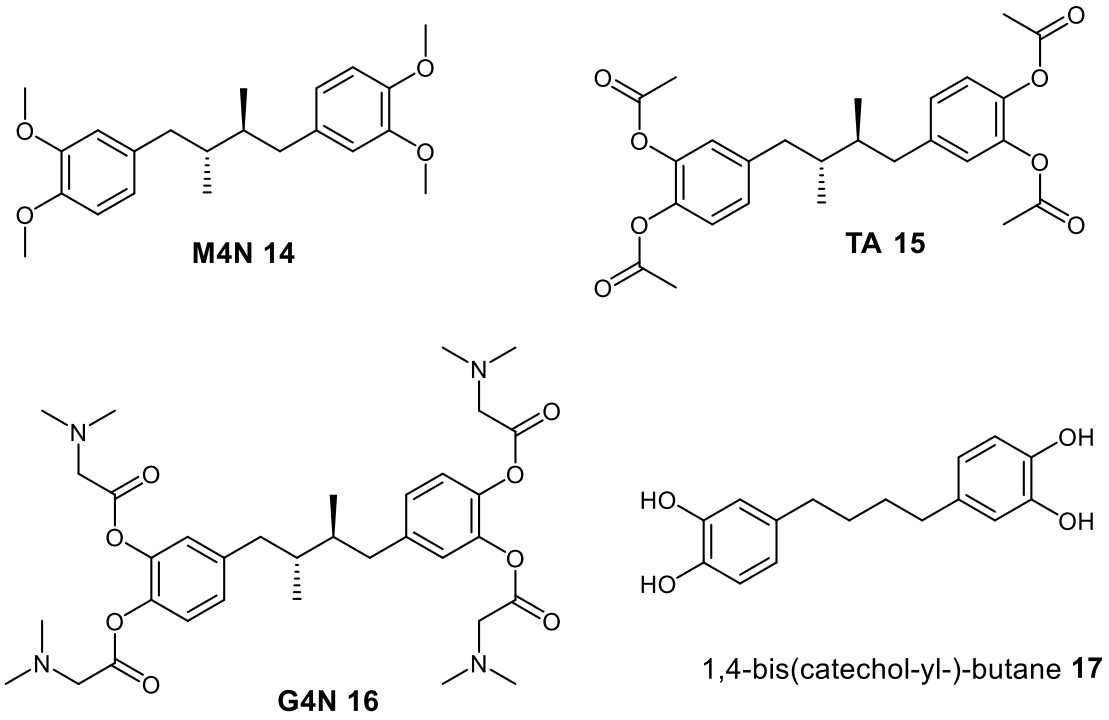

Figure 2-8: Examples of pharmalogically active *o*-hydroxy-substituted analogues of NDGA and a simplified NDGA **17**.

2.5 Design of NDGA Analogues

A radical mediated mechanism (Scheme 2-9 pathway A) has been proposed to explain NDGA **1** autoxidation to dibenzocyclooctadiene[35, 59] but could also result from an electrophilic substitution[66] mechanism (Scheme 2-9 pathway B). Although the exact mechanism of the intramolecular cyclization remains unknown, it likely depends on substituents and/or substitution patterns on both aromatic rings. Access to approapriate NDGA analogues will allow for investigations into the effect of aromatic rings and/or butane bidge substitutions on dibenzocyclooctadiene product formation. This will untimately provide insight into the structural features which modulate NDGA pharmacological and toxicological effects. Therefore, we proposed the synthesis of of eigth NDGA analogues (Figure 2-9) to primarily verify the proposed

mechanisms of NDGA intramolecular cyclization and whether oxidative conversion to reactive metabolites depends on substituents and/or substitution pattern of the aromatic rings.

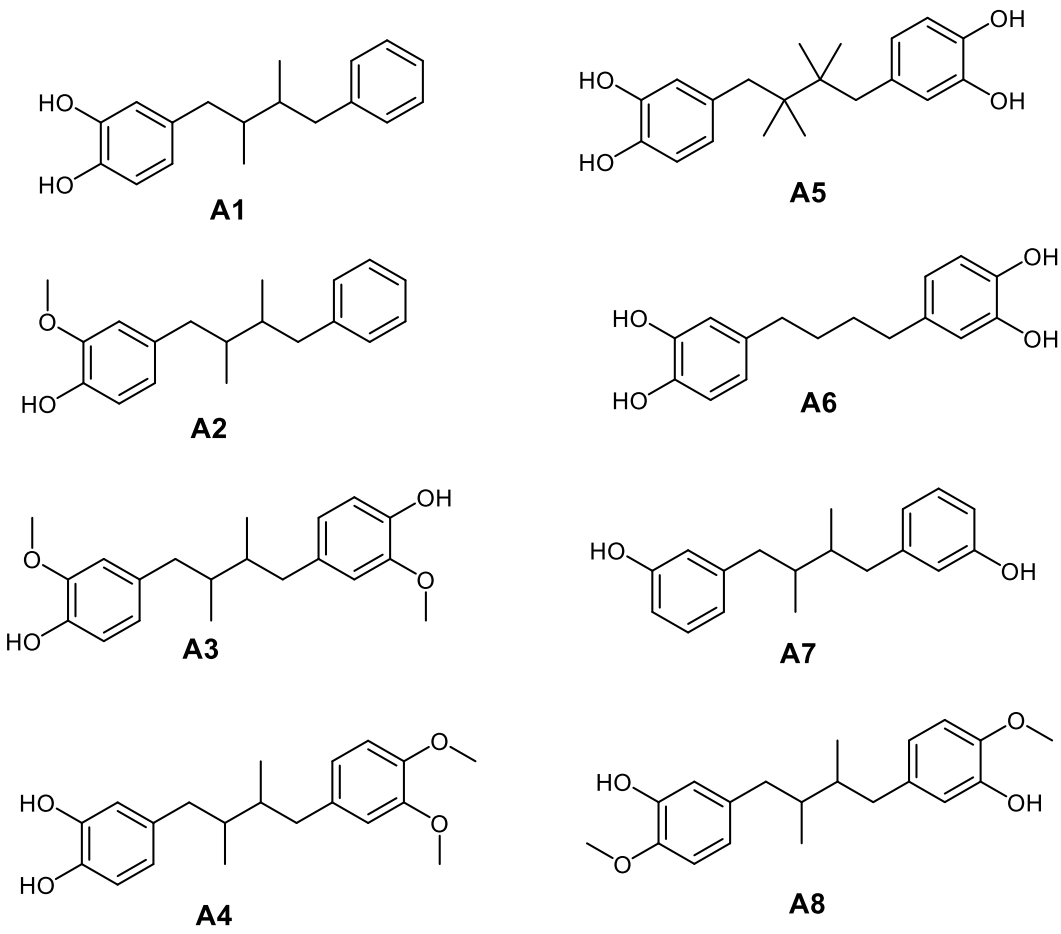

Figure 2-9: Structures of proposed NDGA analogues for this project.

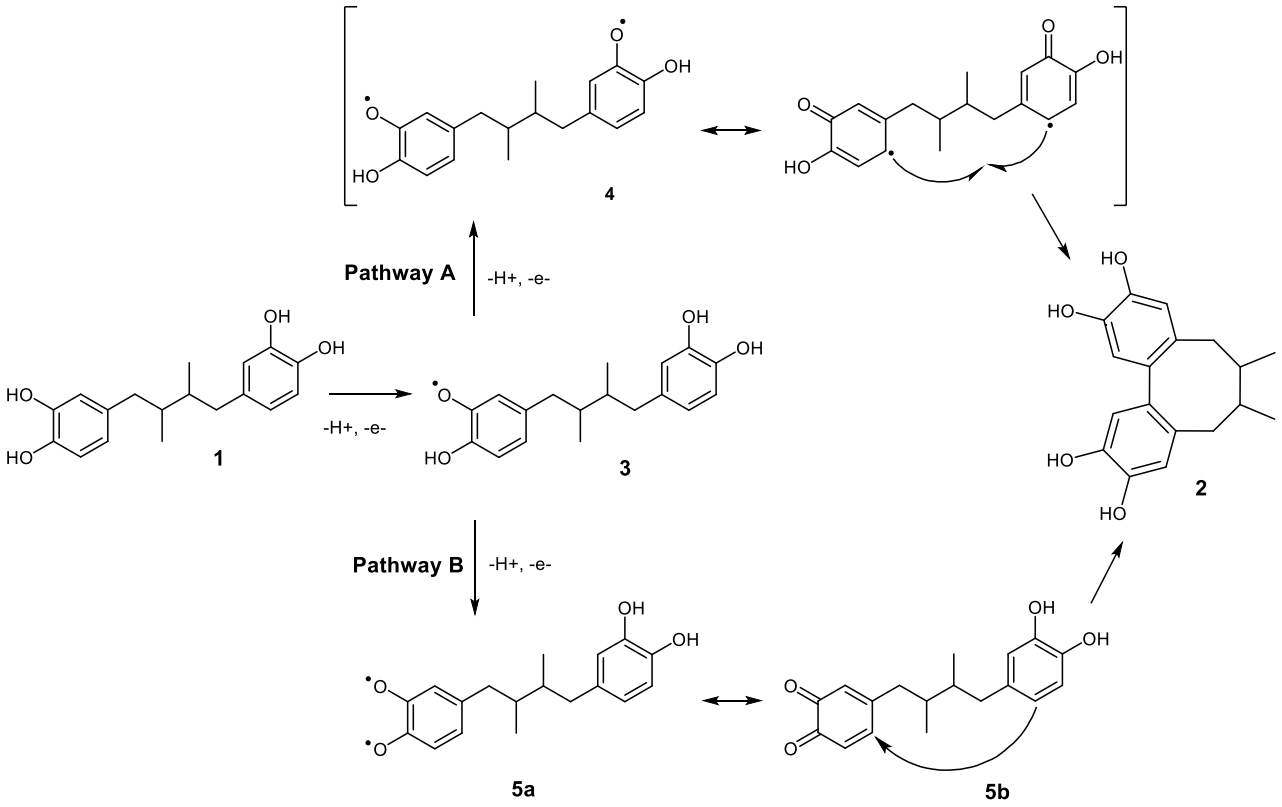

Scheme 2-9: Proposed mechanisms of NDGA autoxidation. Pathways A and B represent radical-mediated and electrophilic substitution mechanisms respectively.

2.6 Rationale for the Proposed NDGA Analogues

A radical-mediated addition mechanism (Scheme 2-9, pathway A) requires initial formation of a di-radical **4**, followed by radical coupling. This mechanism is dependent on a di-catechol moiety or the presence of free 3-OH and 3′-OH groups, suggesting that a mono-catechol NDGA and other analogues lacking 3 and 3′ OH structural units may not undergo the intramolecular cyclization under similar conditions. On the other hand, an electrophilic substitution mechanism (Scheme 2-9, pathway B) requires at least a catechol moiety which oxidizes to an o-Q **5b** via a di-radical intermediate **5a** and the potential of the other ring to act as a nucleophile.

A mono-catechol **A1** (Figure 2-9) lacks readily ionizable -OH groups on the unsubstituted ring and could only cyclize via an electrophilic substitution mechanism. The Hammett constants for

substituents σ (Table 2-1),[95] suggest that the mono-catechol **A1** is less nucleophilic and therefore expected to undergo autoxidation at a greatly reduced rate in comparison to NDGA. **A4** is comparable to NDGA in nucleophilicity and will be expected to autoxidize at a rate comparable to that reported for NDGA if the cyclization follows electrophilic substitution mechanism. However, the lack of free –OH functions on both aromatic rings of **A4** means that the radical-mediated pathway cannot occur for **A4**. Therefore, absence of autoxidation in **A4** could imply that a radical-mediated process more accurately describes NDGA oxidative cyclization. Compounds **A5** and **A6** are expected to behave like NDGA under oxidative conditions although intramolecular cyclization to a dibenzocyclooctadiene derivative is expected to occur at different rates. Given the potential of compound **A6** to cyclize under oxidative conditions, we were motivated to verify whether a dibenzocyclooctadiene derivative possibly contributes to the remarkable anti-proliferative activity reported by McDonald et al.[36] Compound **A5** was intended to investigate the effect of butane-bridge substitution on intramolecular cyclization rate. Lastly, if the intramolecular cyclization follows a radical-mediated addition mechanism, compounds **A7** and **A8** will be expected to form dibenzocyclooctadiene derivatives.

Table 2-1: Hammett constants for substituents[95] on the prepared NDGA analogues.

Substituents	Hammett constant (σ)
H	0.00
m-OH	0.12
p-OH	-0.37
m-OCH_3	0.12
p-OCH_3	-0.27

Unlike NDGA **1**, oxidation of SECO **9** did not form reactive intermediates capable of interacting with biological nucleophiles.[33] Instead, SECO converts to lariciresinol (Scheme 2-10) which is resistant to further oxidations[96]. The lack of reactive metabolites likely explains the relative safety profile reported for SECO.[33]

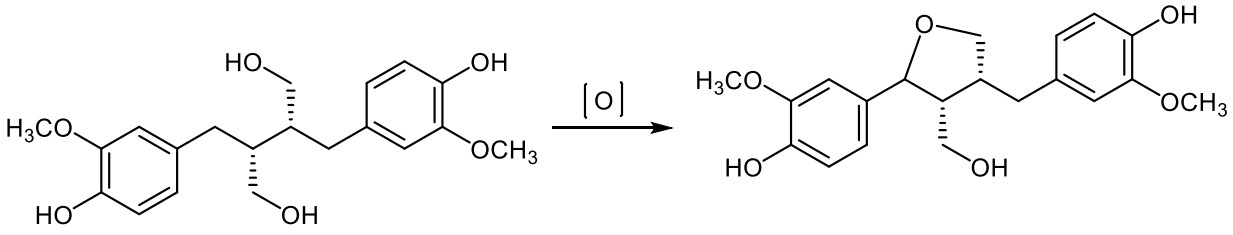

SECO 9 Lariciresinol **23**

Scheme 2-10: Conversion of SECO to lariciresinol under oxidative conditions.

The methoxy substituents of the di-phenolic lignan SECO **9** possibly prevent metabolic conversion to quinones (Scheme 2-11). Metabolism studies of **A2** and **A3** which lack the potential for o-Q formation are expected to aid in understanding the contribution of o-Qs and/or p-QMs to NDGA **1** toxicity. Oxidative metabolism studies of the analogues will help us to better appreciate

metabolism of lignans and possibly lead to development of some understanding of structure-activity relationships for lignans, an area where data is currently lacking.

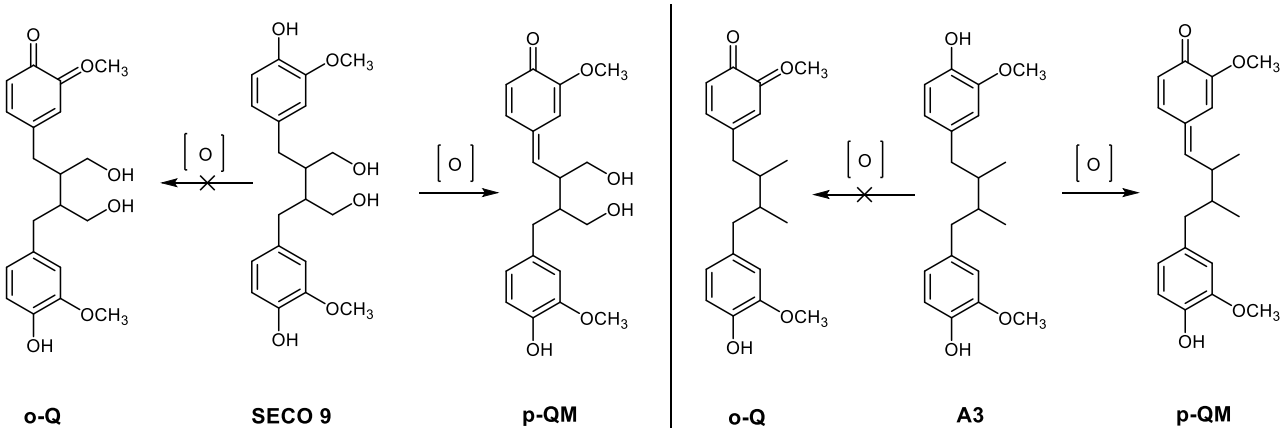

Scheme 2-11: Oxidation of secoisolariciresinol (SECO **9**) and nordihydroguaiaretic acid (NDGA) analogue 3 (**A3**) to quinones.

2.7 Synthesis of NDGA and its Analogues

Synthesis of lignans and their analogues continues to attract attention due to their interesting biological properties and potential for use as medicines. One such lignan with interesting pharmacological properties is NDGA. In a recent review, Chen[48] described various approaches to prepare NDGA analogues. Synthetic analogues were categorized broadly into three families (Figure 2-10) based on the modification type as a) hydroxyl-substituted NDGA derivatives, b) butane-bridge modified NDGA derivatives and c) phenyl-ring NDGA derivative[48]

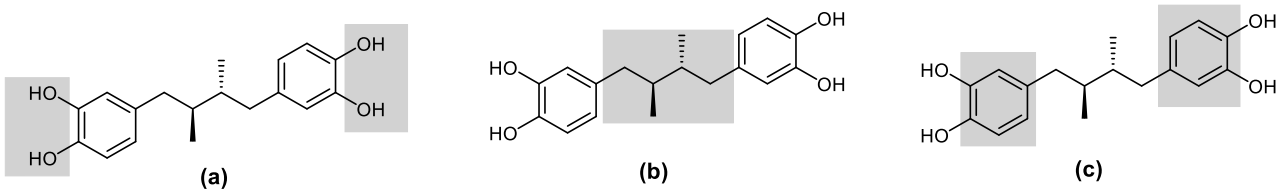

Figure 2-10: Modifications of the backbone of NDGA to (a) hydroxyl-substituted NDGA derivatives (b) butane-bridge modified NDGA derivatives and (c) phenyl-ring NDGA derivatives (shaded areas are sites of modification).[48]

Approaches to syntheses of lignans and their analogues described in the literature involve the use of a limited number of vital reactions to construct the basic 18-carbon skeleton which is subsequently modified via cyclization, reduction, oxidation or hydration among others to the desired target compound. The compounds of interest for this project are all hydroxyl-substituted NDGA derivatives. This section reviews a number of approaches with emphasis on their applicability to the synthesis of our anticipated NDGA analogues. Based on retrosynthetic analysis, hydroxyl-substituted NDGA type derivatives can be prepared via four major routes (Figure 2-11)[48] depending on synthetic objective and factors such as availability of starting materials, yield and stereoselectivity among others.

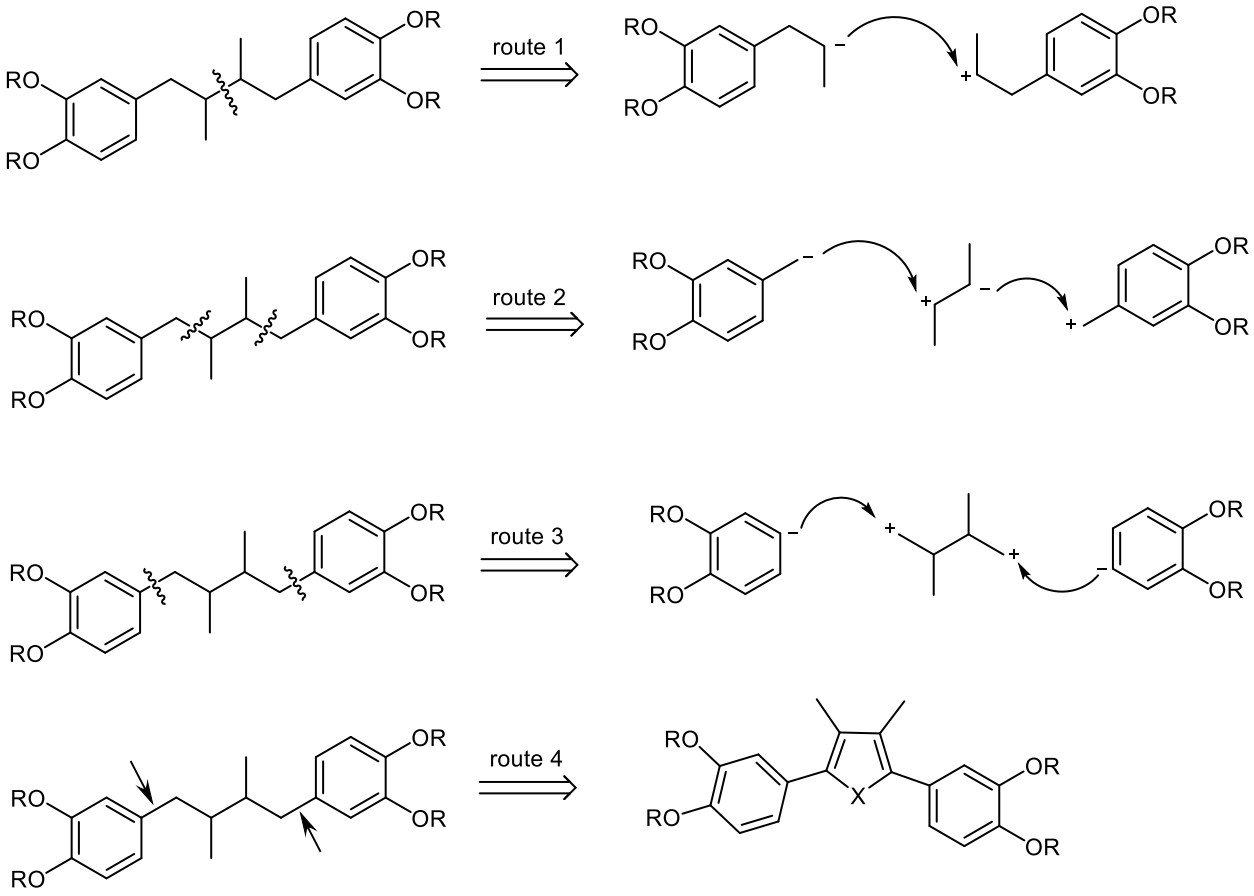

Figure 2-11: Retrosynthetic approach for synthesis of hydroxyl-substituted NDGA derivatives.

2.7.1 Consecutive Stobbe Condensation

The Stobbe condensation reaction has been used extensively in the literature for constructing the basic skeleton of lignans due largely to its versatility. The reaction involves treating an aromatic aldehyde **18** with a succinate ester **19** in the presence of a base to give a trans-benzylidene succinate monoester **20**.[97] The mechanisms (Scheme 2-12) involve intramolecular cyclization leading to formation of a 5-membered lactone[97, 98] which subsequently cleaves via β-elimination to form the trans-benzylidene product **20**. The intermediate 5-membered lactone has been confirmed by isolation.[97] Stereochemistry of the trans-benzylidene product **20** was

unambiguously established through NMR studies.[98] The diamagnetic anisotropic deshielding effect of the carbonyl group causes the olefenic proton in the *E* configuration to appear beyond 7.5 ppm, downfield from the *Z* proton arrangement.[98]

A consecutive Stobbe condensation of the trans-benzylidene diester **21** with another equivalent of aromatic aldehyde **18** in refluxing alkoxide/alcohol affords the diarylbutanediene basic structure **22**. A couple of subsequent reductive steps lead to the desired lignan.[99, 100] The approach provides a flexible way for preparing lignans in good yield with individual steps ranging from 73-99% in the literature. The major drawback, however, is lack of stereo-control for the forming stereogenic centers. This has led to various modifications aimed at controlling stereochemistry as reviewed in the subsequent sections.

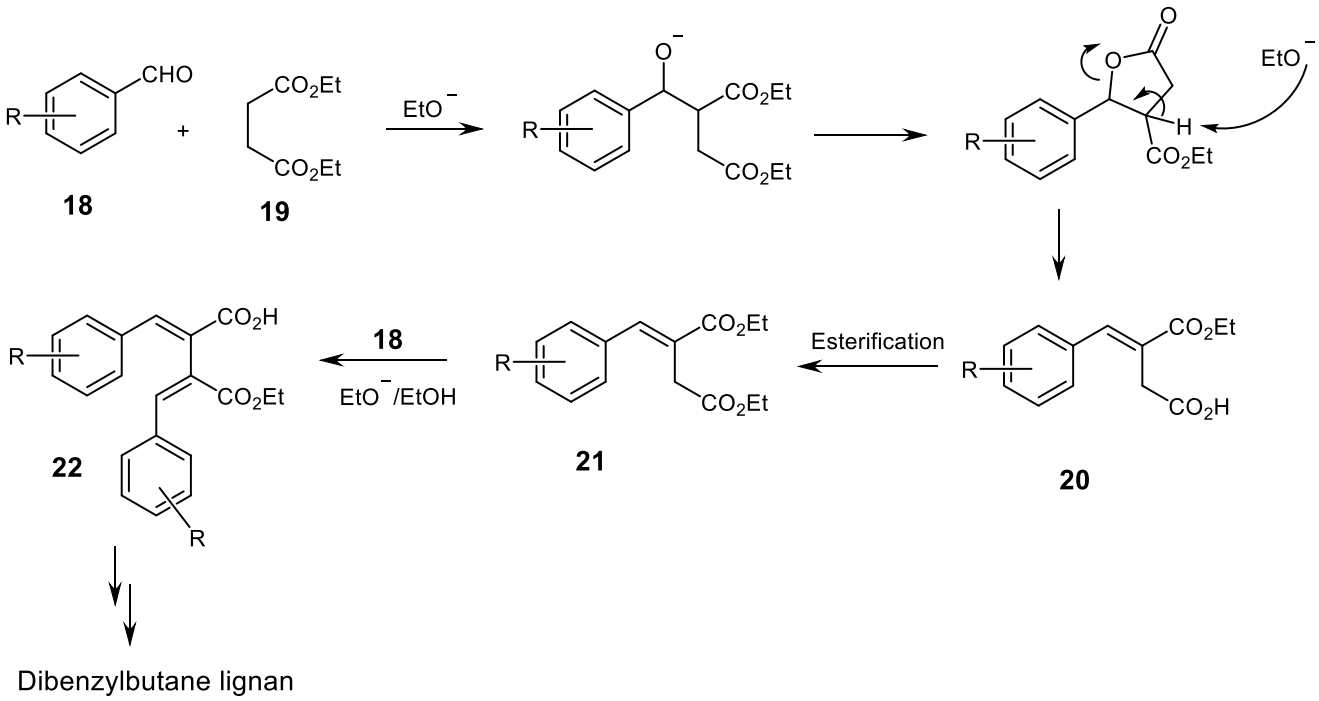

Scheme 2-12: General mechanism of Stobbe condensation reaction.

The analogues of interest for this project can all be synthesized by using a double Stobbe condensation approach as illustrated below for **A1** (Scheme 2-13). In the case of **A2, A3, A4**, **A7** and **A8** protection of the active phenol group in the starting aromatic aldehyde may be necessary to prevent side reactions.

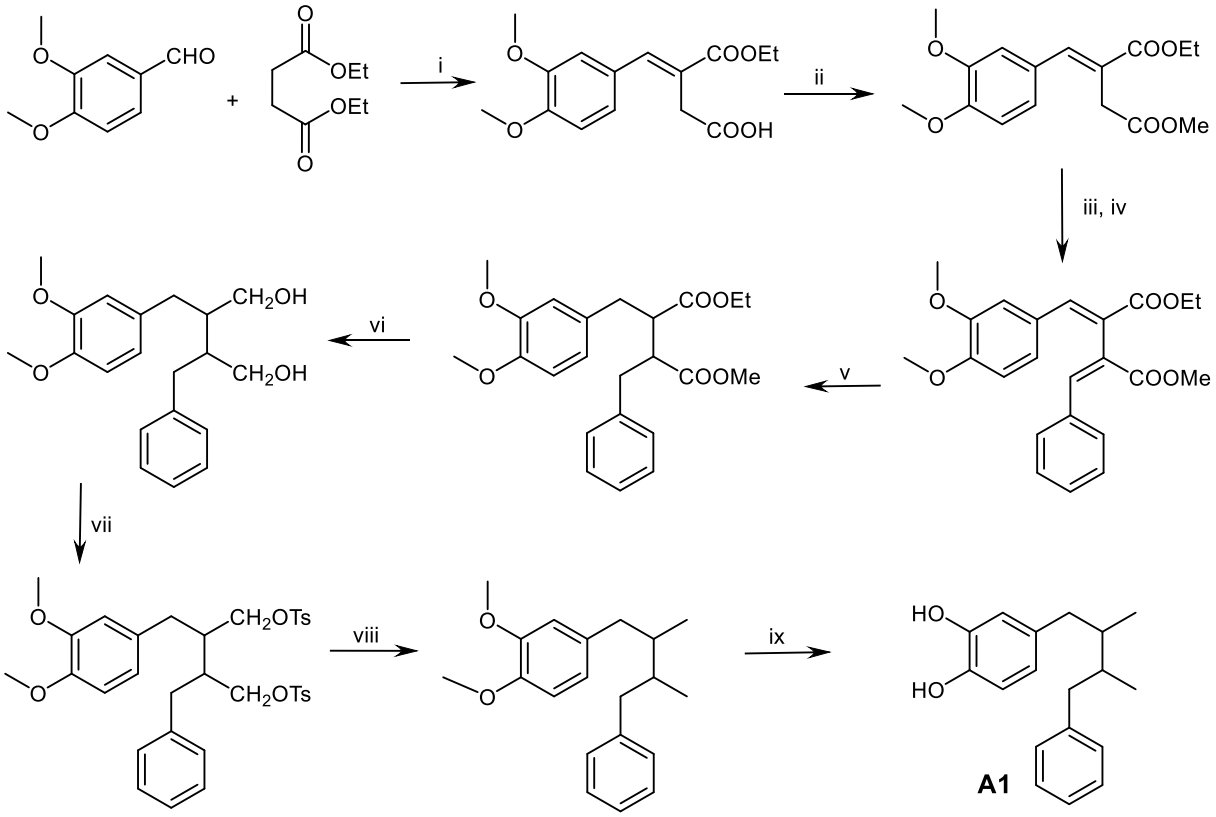

Scheme 2-13: Consecutive Stobbe condensation approach for synthesis of **A1**.
Reagents and Conditions: i) EtONa/EtOH, reflux; ii or iv) MeI, K_2CO_3/DMSO, rt; iii) BnCHO, EtONa/EtOH, reflux; v) H_2, Pd-C, vacuum; vi or viii) $LiAlH_4$/THF, rt; vii) TsCl/py, 0°C; ix) BBr_3/DCM, -78°C.

Following hydrogenation, the resulting four stereoisomers in the case of **A1, A2** and **A4** for example are expected to exist as two pairs of enantiomers which should be separable chromatographically.[101] **A3, A7** and **A8** will exist as a *meso*-compound and a pair of enantiomers which are separable chromatographically.[101] Figure 2-12 shows the possible stereoisomers of **A1,**

A2, A3 and **A4** following hydrogenation. It is not known whether any preference for the formation of any specific stereoisomers will occur, but it remains a possibility.

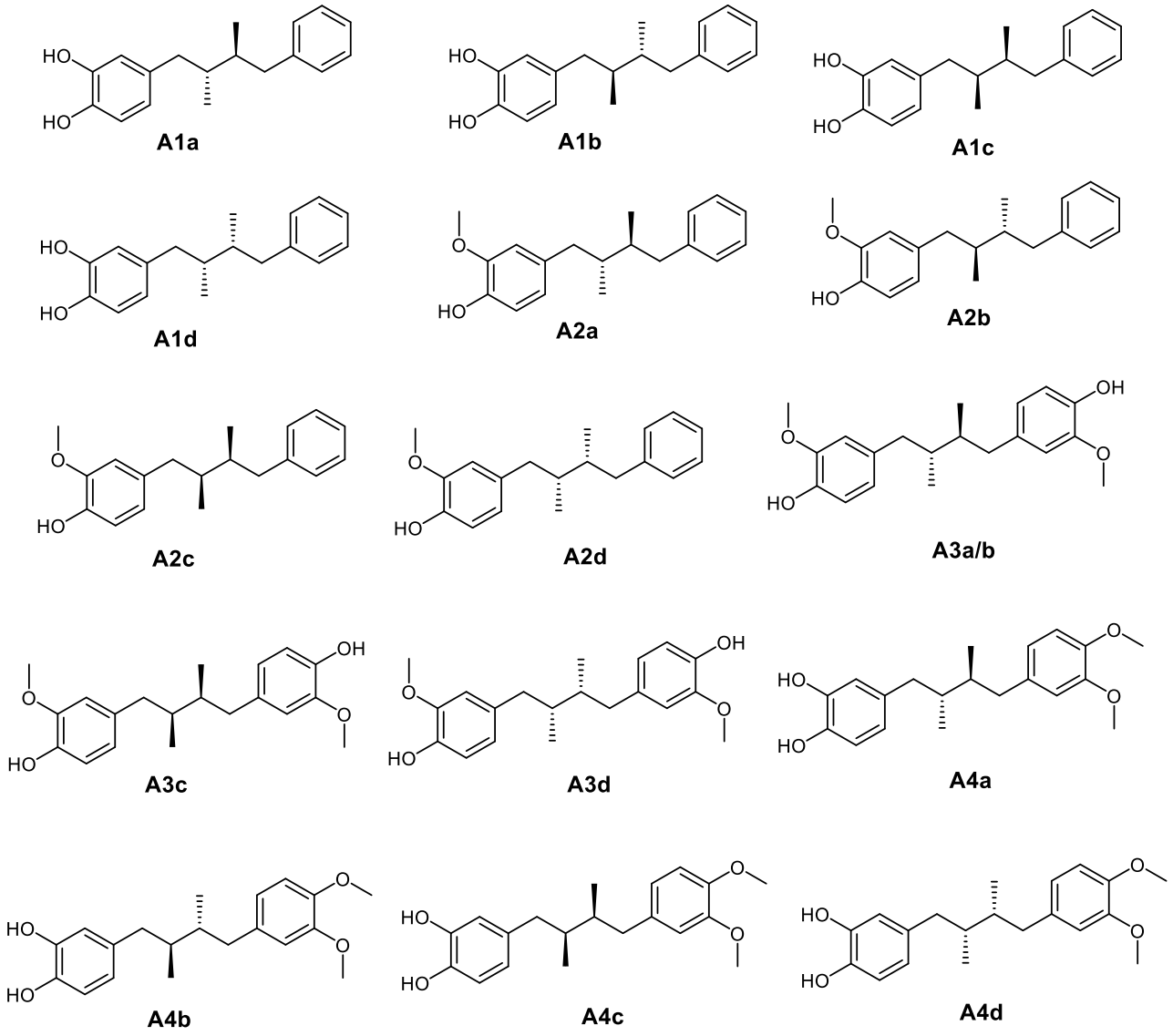

Figure 2-12: Stereoisomers of analogues **A1, A2, A3** and **A4**.

2.7.1.1 Approach to controlling stereochemistry of the Stobbe Condensation

2.7.1.1.1 Stobbe Condensation-Alkylation

Xia et al.,[58, 102] described an approach for enantioselective synthesis of NDGA, (–)-saururenin and their analogues using a Stobbe condensation followed by alkylation as key synthetic steps (Scheme 2-14). The Stobbe condensation product, a benzylidene half-ester was esterified and treated with appropriate alkylating agent in the presence of LDA to give the basic lignan structure. After basic hydrolysis, the resulting diacids were resolved via their quinine salts. Hydrogenation of esterified (+) or (-) acid followed by $LiAlH_4$ reduction gave diols which were readily separable by chromatography. Further reductive steps gave the desired stereospecific lignans with individual yields varying from 38-92%.

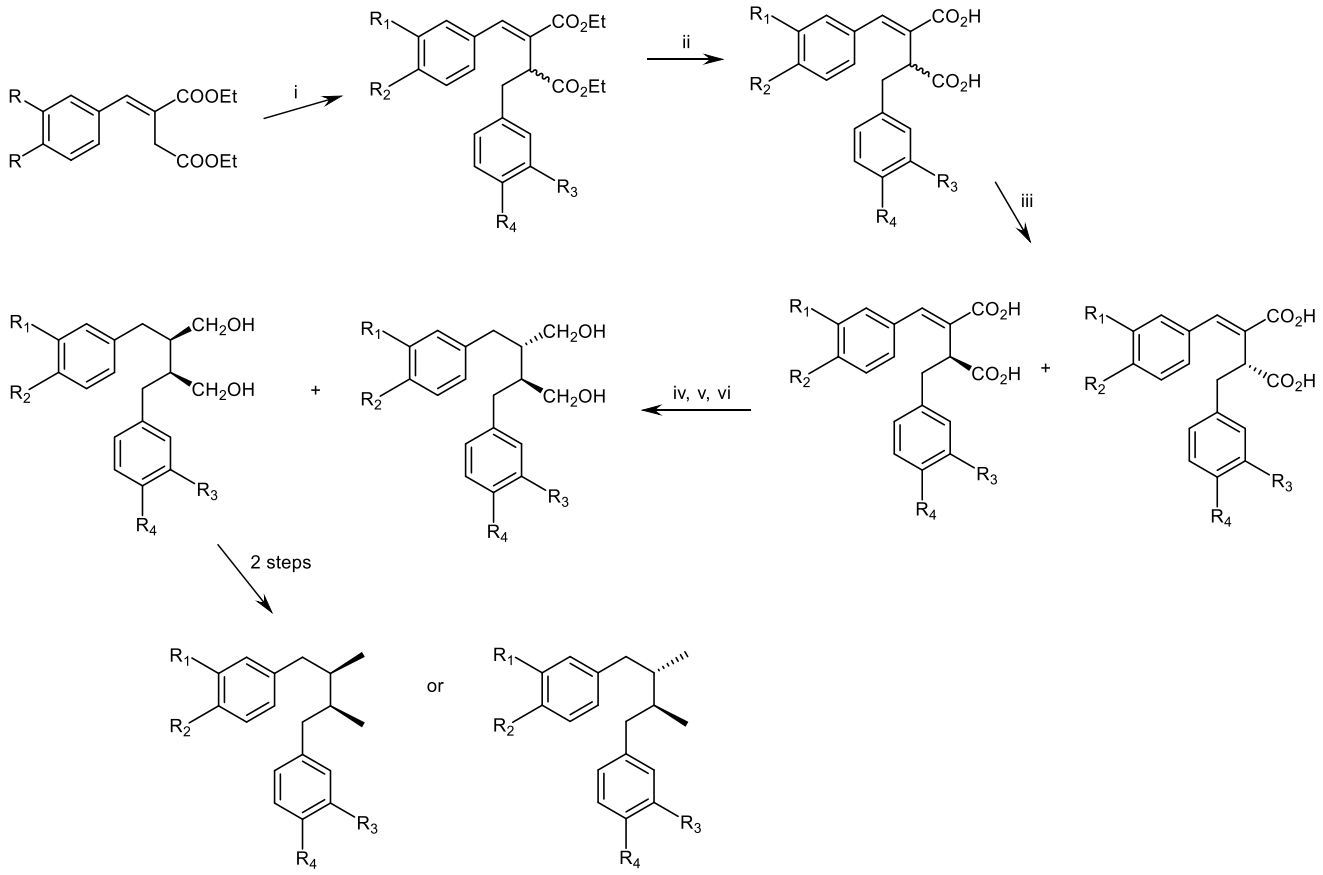

Scheme 2-14: Enantioselective synthesis of NDGA analogues by Stobbe Condensation-alkylation approach.
Reagents and conditions: i) substituted BnBr, LDA/THF, -78°C; ii) $NaOH/H_2O$, reflux; iii) (-)-quinine resolution; iv) $EtOH/C_6H_6$, H^+; v) H_2, Pd-C; vi) $LiAlH_4$/THF, rt.

This approach will allow access to **A1** and **A2** needed for this project as illustrated in Scheme 2-15 for **A2**. The key advantage of this approach is stereo-control leading to analogues with defined stereochemistry. The major drawback is the lack of general applicability as appropriate alkylating agents needed may not be readily available.

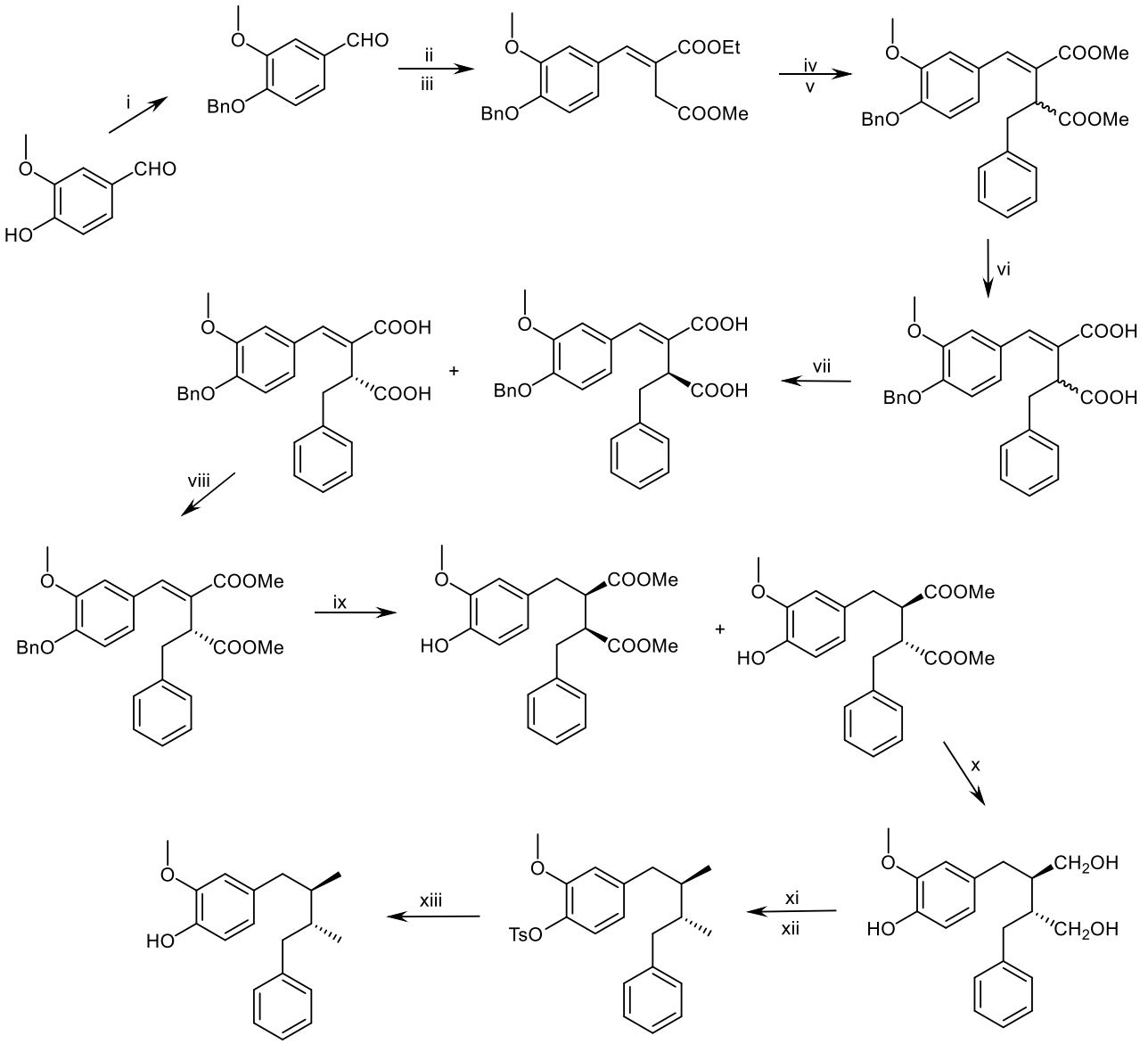

Scheme 2-15: Synthesis of A2 via Stobbe condensation-alkylation method.
Reagents and Conditions: i) BnBr, K_2CO_3/DMF; ii) EtONa/EtOH, reflux; iii, v or viii) MeI, K_2CO_3/DMSO, rt; iv) BnBr, LDA/THF, -78°C; vi) NaOH/H_2O, reflux; vi) (-)-quinine resolution; ix) H_2, Pd-C; x or xii) $LiAlH_4$/THF, rt; xi) TsCl, Pyridine, 0 °C; xii) KOH/EtOH-H_2O (1:1), reflux.

2.7.1.1.2 Stobbe Condensation-Lactonization

The backbone conformation of NDGA analogues can be established by catalytic hydrogenation of a racemic lactone.[101, 103] The Stobbe condensation product, benzylidene half-ester is hydrogenated over Pd/C to give the corresponding saturated hemiester which is chemoselectively

reduced and lactonized with $Ca(BH_4)_2$ in ethanol to give the racemic lactone in good yield (Scheme 2-16). Stobbe condensation of the lactone with another equivalent of substituted benzyladehyde followed by catalytic hydrogenation with Pd/C yields the cis-lactone exclusively, which was reduced to the diol with $Ca(BH_4)_2$.[48] The approach is useful for stereoselective synthesis of dibenzylbutane type lignans.

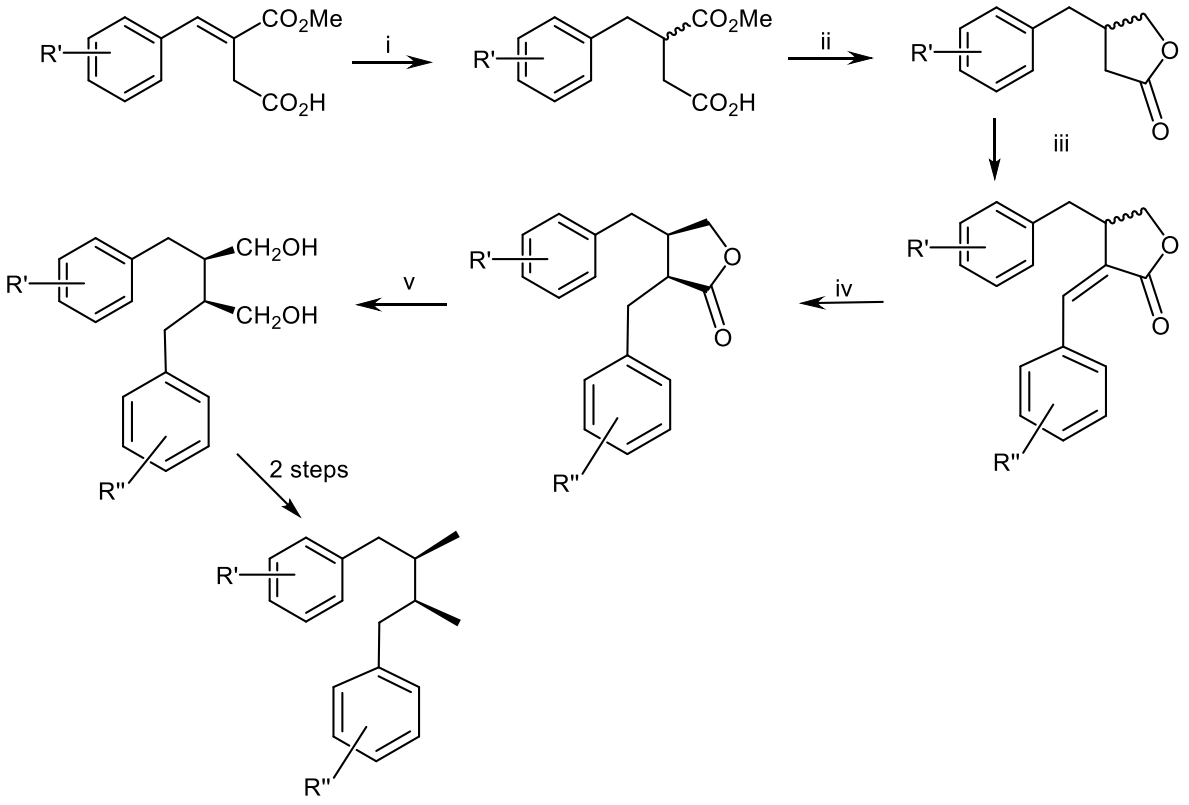

Scheme 2-16: Synthesis of NDGA analogues via Stobbe condensation-lactonization approach. *Reagents and Conditions:* i) : (i) H_2, Pd-C; (ii) KOH, $Ca(BH_4)_2$; (iii) NaH, THF, ArCHO, reflux; (iv) H_2, Pd-C; (v) $Ca(BH_4)_2$, THF, H_2O.

2.7.2 Grignard Reaction

Lieberman et al.,[104] used the coupling of 1-piperonyl-1-bromoethane and its Grignard derivative as a key step to make the skeleton of NDGA. This approach has been modified without success to improve yield and stereo-control in the literature.[105] Son et al.,[106] developed a modified

procedure via 1,4-di(substituted-phenyl)-2,3-dimethyl- butan-2-ol as a key intermediate for the synthesis of NDGA and related lignans (Scheme 2-17).

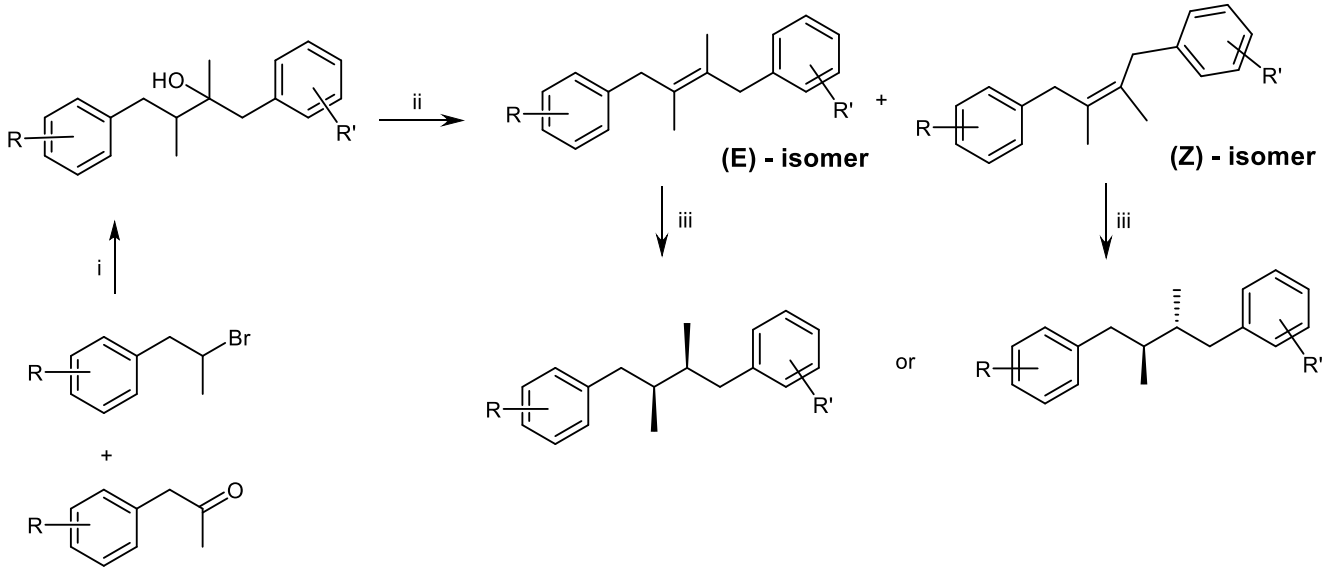

Scheme 2-17: Synthesis of NDGA analogues via Grignard synthesis approach.
Reagents and Conditions: i) (a) Mg/ether, (b) then H_3O^+; ii) H_2SO_4; iii) H_2/PtO_2.

Following dehydration, the resulting (*E*) and (Z) stereoisomers were readily separable since the (*E)* and (*Z*) forms were crystalline and oily respectively at room temperature.[106] The effect of various ring substitutions on these physical states is unknown and likely not general. However, this approach has a wider applicability because it allows access to both symmetrical and unsymmetrical NDGA analogues. In addition, the method uses ketones which are readily available and cheap as electrophilic coupling reagents. The overall yields range from 45-54%. The attractiveness of this approach may, however, be limited by lack of stereoselectivity although isomers following hydrogenation may be separable by chromatography.[101] In principle, this approach is expected to allow synthesis of all four analogues of interest. Following hydrogenation, the two pairs of enantiomers in the case of **A1, A2, A4** and the *meso*-compound and a pair of enantiomer of **A3** (Figure 2-12) should be separable by chromatography.[101]

2.7.3 McMurry Coupling Reaction

Ti-induced carbonyl-coupling reactions of substituted phenylacetones, surprisingly, resulted in 1,4- disubstituted-butane-2,3-diols instead of expected McMurry type butenes. This finding provides an attractive alternative route to NDGA and its non-*meso* isomer using (3,4-dimethoxyphenyl)-acetone as starting material as shown in Scheme 1-18.[107] The method is simple and stereoselective although yields were not fully reported. Also, the approach offers many possibilities to produce a wide variety of NDGA derivatives, since carbonyl containing compounds are easily accessible.

However, applicability is limited to symmetrical NDGA analogues since McMurry coupling reactions between two different ketones are rarely successful.[108] Therefore, **A3, A6, A7** and **A8** may be obtainable via this approach as illustrated in Scheme 2-19 for **A3**. We have also observed that an electron-withdrawing substituent on the OH para to the benzyl carbon prevents the coupling reaction, resulting only in reduction of starting material to the alcohol (unpublished work). Hence the need for an electron-donating group such as trimethylsilyl (TMS) group shown in Scheme 2-19. Dehydroxylation of the resulting butanediol is expected to give both *Z* and *E*-butenes. As reported previously for NDGA,[108] the *Z* and *E*-isomers may be separable by crystallization. Subsequent hydrogenations should either form the *meso*-compound or a racemic mixture of **A3**.

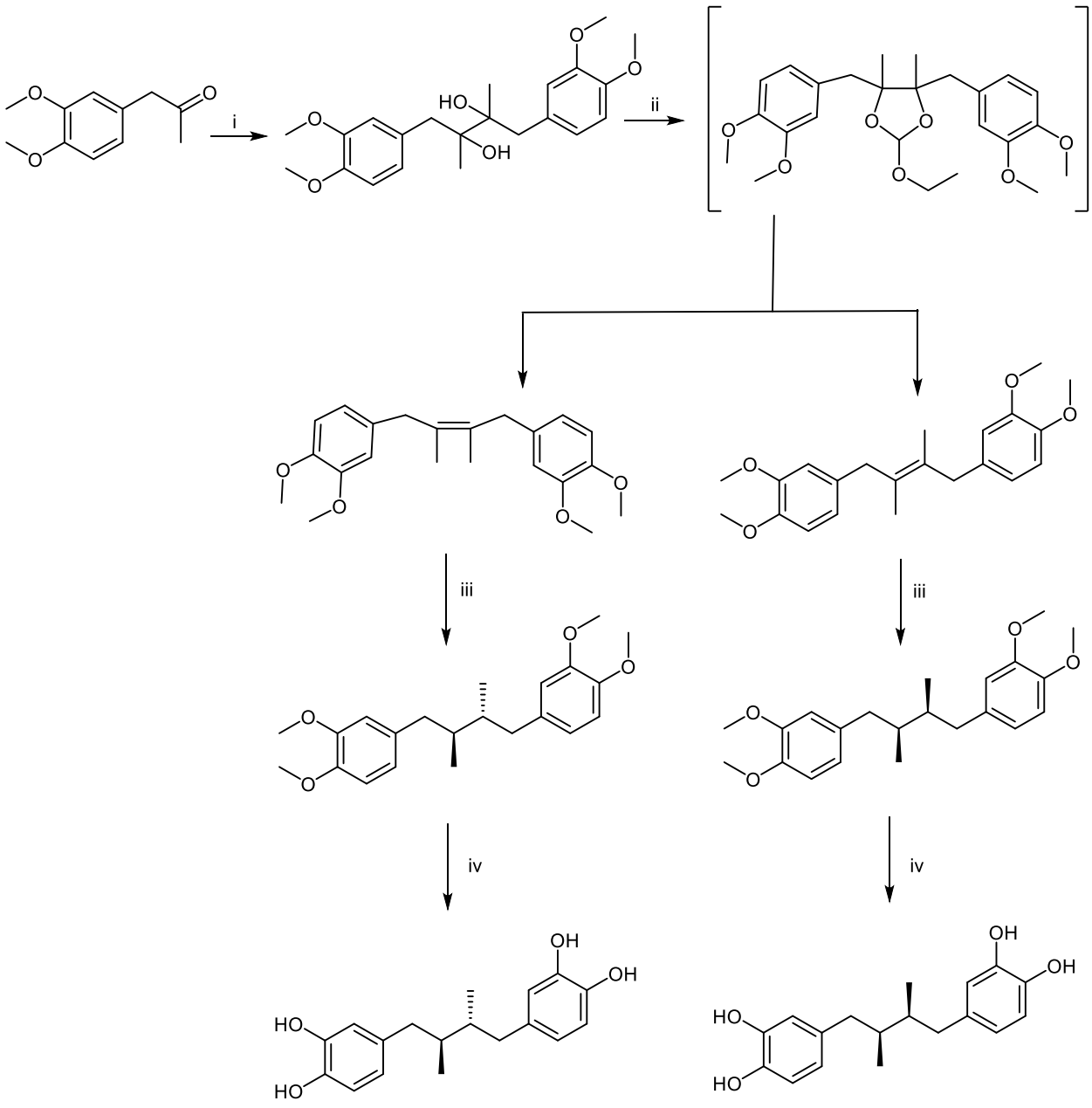

Scheme 2-18: Synthetic route to NDGA and its stereoisomer using Ti-induced carbonyl-coupling reaction.
Reagents and Conditions: i) $TiCl_4$/Zn, THF; ii) $CH(OEt_3)$, BzOH; iii) H_2/PtO_2; iv) BBr_3.

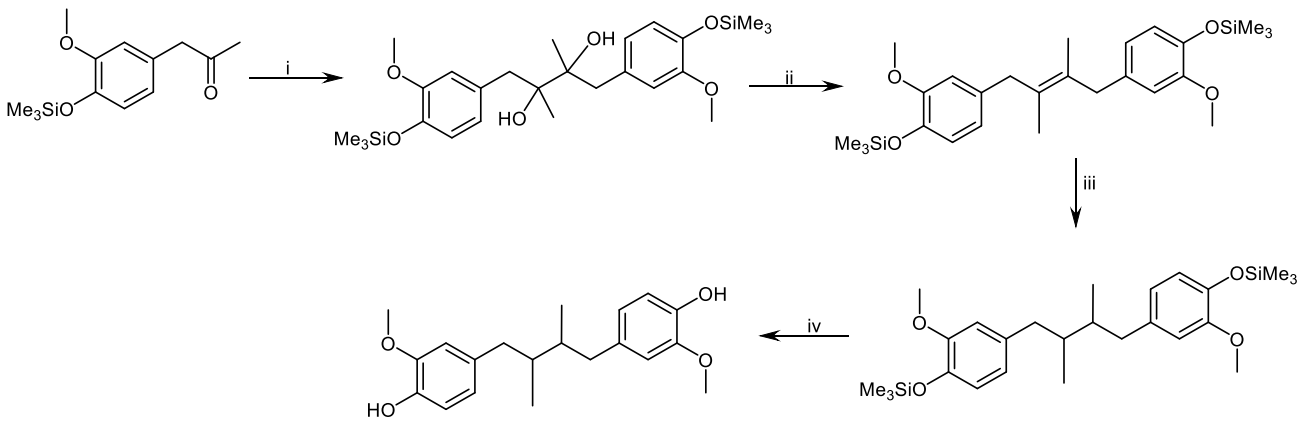

Scheme 2-19: Synthesis of **A3** via McMurry coupling reaction.
Reagents and Conditions: i) $TiCl_4$/Zn, THF; ii) $CH(OEt_3)$, BzOH; iii) H_2/PtO_2; iv) H_2O/H^+.

2.7.4 Oxidative Coupling Approach

Matairesinol has been synthesized through oxidative coupling of ferulic acid as a key step.[109] The poor control of regiochemistry in the oxidative coupling step led to low yield of the desired coupling product. Oxidized ferulic acid exists in three mesomeric forms (Figure 2-13) which allows for six different coupling patterns leading to a mixture of coupling products.[101, 110] The major coupling pathway seems to be β-5 linked compound.[111]

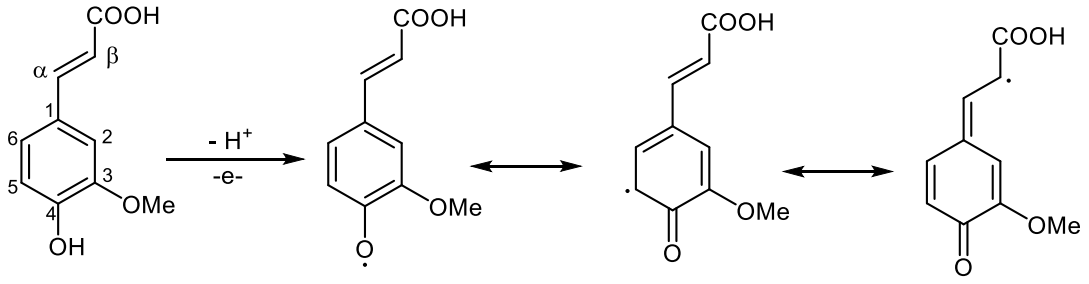

Figure 2-13: Mesomeric forms of oxidized ferulic acid.

This strategy has been modified over the years to improve regioselectivity of the coupling reaction. Notably, the use of *tert*-butyl protection at C_5 of the phenyl ring enhances the desired β-β coupling by blocking the major β-5 pathway.[101, 110] The attractiveness of this approach, however, is

limited by its applicability. It does not allow access to unsymmetrical lignan skeletons and therefore applicable only to **A3** as shown in Scheme 2-20.

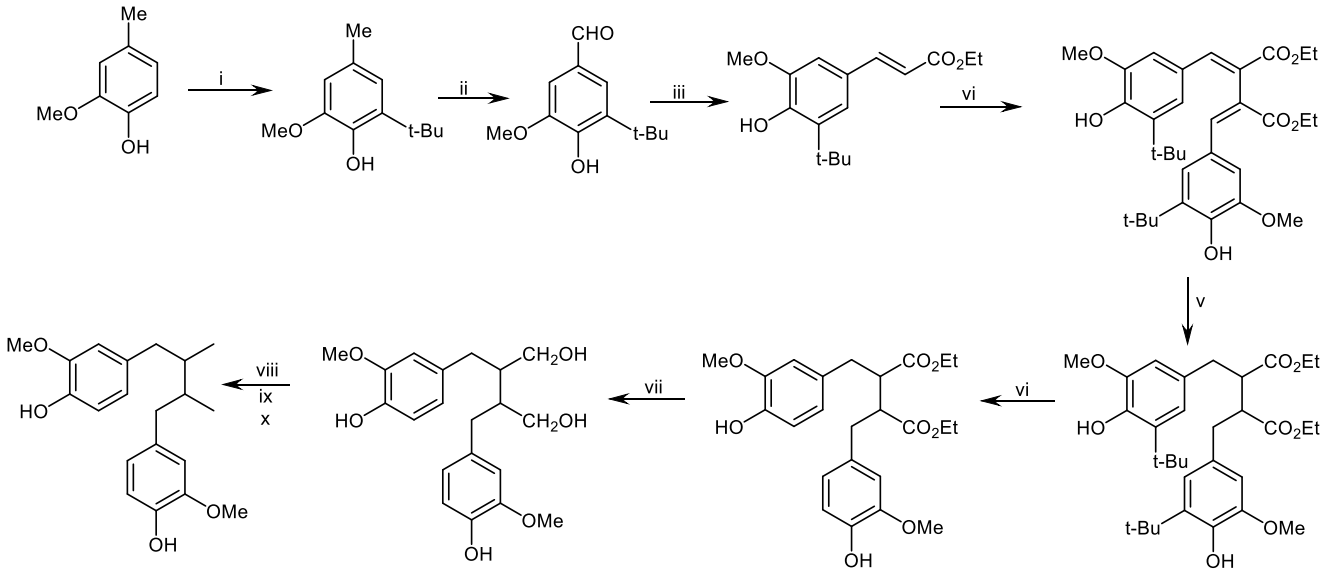

Scheme 2-20: Synthesis of A3 via oxidative coupling approach.
Reagents and Conditions: i) t-BuOH, 85% H_3PO_4, 75°C; ii) Br_2, t-BuOH, r.t.; iii) $Ph_3PCHCOOEt$, $CH_3OCH_2CH_2OCH_3$, reflux; vi) $K_3[Fe(CN)_6]$, KOH, C_6H_6-H_2O, rt; v) H_2, Pd/C(10%); vi) $AlCl_3$, C_6H_6, 50°C; vii) $LiAlH_4$/THF, rt.; viii) TsCl, Pyridine, 0°C; ix) $LiAlH_4$/THF, rt; x) KOH/EtOH-H_2O (1:1), reflux.

2.8 Oxidative Metabolism

In order to facilitate elimination from the body, xenobiotics are metabolized by various oxidation and conjugation enzymes to more electrophilic metabolites. However, this generally accepted detoxification process may lead to chemically reactive metabolites *in vivo*, a process known as bioactivation. Most reactive metabolites are electrophilic in nature and can react with nucleophiles. Due to a possible link between reactive metabolites and drug toxicity, screening for metabolic activation has become integral part of the drug development process.[112, 113]

2.8.1 Metabolism of Nordihydroguaiaretic Acid

The low bioavailability of NDGA is attributed to efficient first-pass metabolism as opposed to low absorption given that NDGA readily forms glucuronides, and liver function test (LFT) abnormalities have been detected in multiple patients indicating delivery of NDGA to the hepatocyte.[114] Lambert et al.,[4] detected mono- and diglucuronides of NDGA within minutes in the plasma of mice following intravenous treatment. When incubated with human hepatic microsomes, however, NDGA formed only the monoglucuronide. While this finding suggests that glucuronidation may be a major detoxification pathway for NDGA, it remains to be determined whether differences in mouse and human glucuronosyltransferases accounted for this observation or it simply reflects *in vitro* versus *in vivo* situations.[4] Rats fed 0.5-1.0 % NDGA in the diet developed cystic reticuloendotheliosis of the paracaecal lymph nodes and vacuolation of kidney epithelium. Subsequent isolation of o-Q intermediate of NDGA from kidney extracts suggests that the observed kidney lesions are mediated by the o-Q reactive metabolite.[32] In another study, Woodrats which had adapted to a creosote bush diet had elevated levels of cytochrome P450s (CYP2B, CYP1A) and glutathione conjugation liver enzymes compared to Woodrats on a traditional juniper diet, indicating the importance of these enzymes in the metabolism and elimination of NDGA metabolites.[115]

2.8.2 Assessment of Bioactivation Potential

Catechols and phenols form quinones and/or quinone methides via oxidative metabolism which may be enzyme-catalyzed.[33, 34, 70, 71, 84, 86, 87] Like other reactive metabolites, the high reactivity of quinones and quinone methides preclude their detection by traditional analytical methods. However, reactive metabolites are generally analyzed by LC-MS/MS after chemical

trapping with nucleophilic agents such as GSH **11**.[113,116-119] This approach traps the otherwise highly unstable electrophilic intermediates as GSH adducts to allow structural elucidation of the stable conjugates by LC-MS/MS and/or NMR methods. The data obtained provide indirect information about the structure of the electrophilic species, and hence the bioactivation mechanism.[113] GSH **11** as nucleophilic trapping agent is known to work well with 'soft' electrophiles but does not trap effectively some 'hard' electrophiles.[119] Therefore, other nucleophilic trapping agents, such as semicarbazide or methoxylamine[120, 121] and potassium cyanide[122, 123] that are capable of trapping 'hard' electrophiles have been employed for comprehensive screening protocols for reactive metabolite. A few other trapping agents have also been suggested in the literature for simultaneously trapping both 'soft' and 'hard' electrophiles.[124, 125]

2.8.3 Methods for Studying GSH Adducts

2.8.3.1 Nuclear Magnetic Resonance (NMR) Approach

Glutathione conjugates of NDGA o-Q **5b** have previously been studied by NMR and LC-MS methods.[33] The GSH conjugate of p-QM **5c** of NDGA will be distinguishable by NMR as it forms exocyclic GSH adduct **13** whilst the o-Q generally yields ring conjugates **12**.[33, 78] (Scheme 2-21).

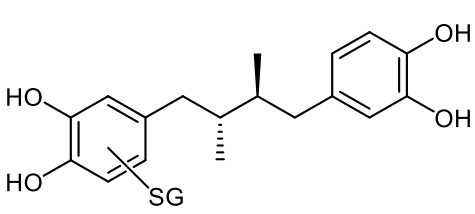

Aromatic adduct **12**

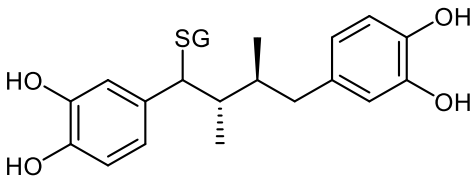

Benzylic adduct **13**

Scheme 2-21: Glutathione conjugates derived from NDGA o-Q **12** and p-QM **13**.

2.8.3.2 Liquid Chromatography-tandem Mass Spectrometry (LC-MS/MS) Approach

LC-MS/MS techniques have been routinely utilized in *in vitro* evaluations of new chemotypes for reactive metabolites via GSH trapping experiments. Dieckhaus et al.,[116] demonstrated that precursor ion (PI) scanning of *m/z* 272 (deprotonated γ-glutamyl-dehydroalanyl-glycine) in the negative ion mode (Scheme 2-22) provides a general survey scan applicable for the detection of a wide variety of GSH conjugates.[116]

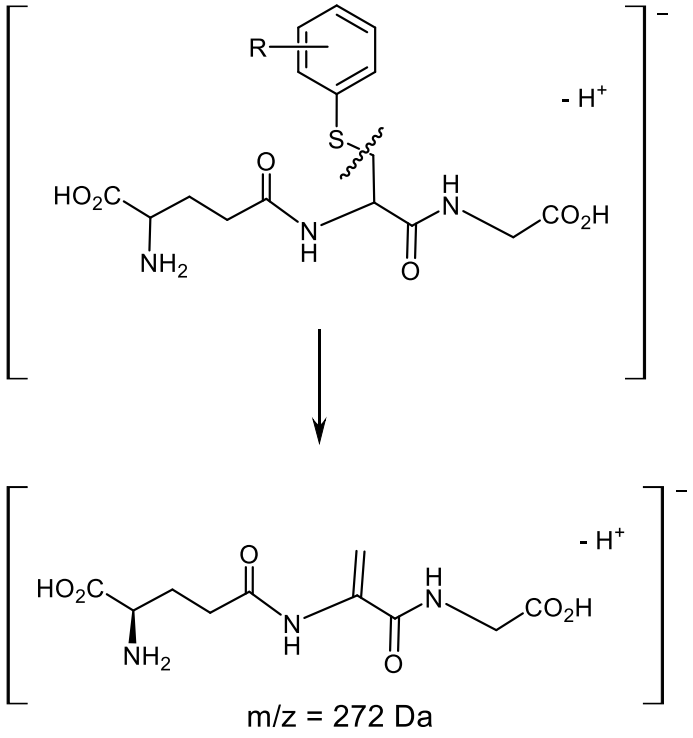

Scheme 2-22: Detection of GSH conjugates via precursor ion (PI) scan of *m/z* 272 in the negative ion mode.

Previously, a triple quadrupole MS technique employing neutral loss (NL) of *m/z* 129 (pyroglutamic acid moiety) in the positive ion mode (Scheme 2-23) was largely used for screening GSH-trapped reactive metabolites.[126] Neutral loss 307 (glutathione) has also been employed as a

detection technique.[116, 126] The structure of a suspected glutathione conjugate is elucidated following a product ion scanning of the parent ion (MH^+).[116, 126] However, general applicability of NL 129 as a detection technique suffers from low sensitivity and limited selectivity resulting from the interference of endogenous compounds and background noise.[116]

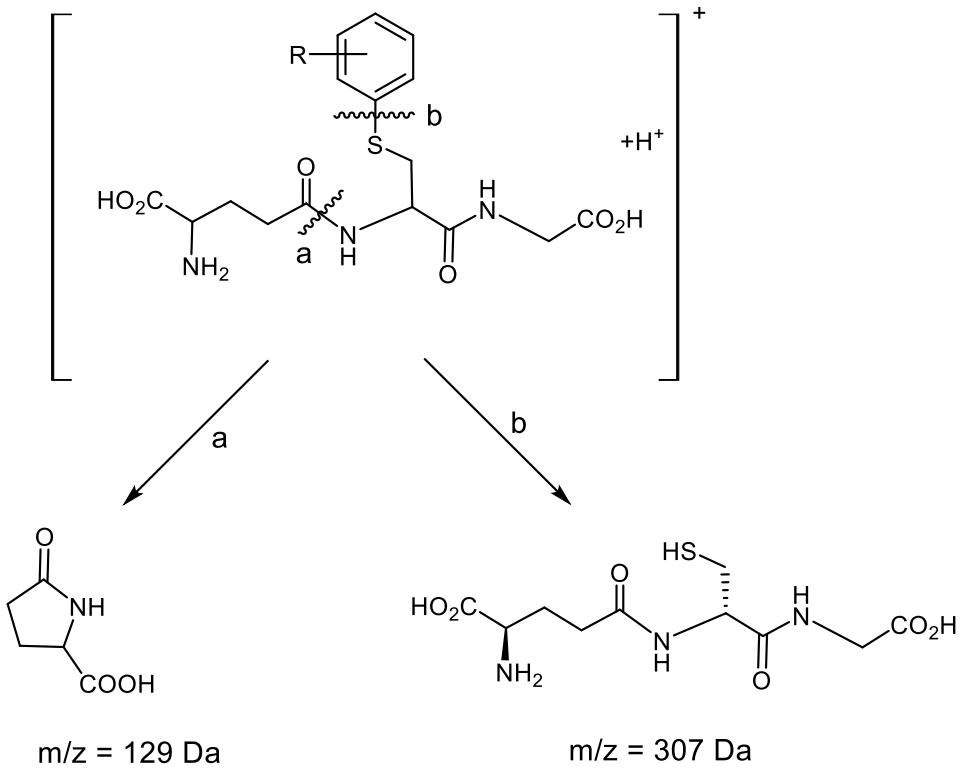

Scheme 2-23: Detection of GSH conjugates via neutral loss scan (NL) of m/z 129 or 307 in the positive ion mode.

More recently, a complementary technique utilizing multiple reaction monitoring (MRM) as a survey scan to trigger the acquisition of enhanced product ion (EPI) spectra has been reported.[127] Although this MRM-based approach seems to provide superior sensitivity and selectivity for GSH adducts, it only detects the GSH adducts pre-set on an MRM transition protocol. Therefore MRM-EPI approach must be used in conjunction with PI or NL when comprehensive analysis of predicted and unpredicted GSH conjugates is desired.[127] Recent developments in mass spectrometry have

revolutionized reactive metabolites analysis in the drug discovery process. For example, the quadrupole-linear ion trap mass spectrometry (Q-trap) retains the MS/MS scan functions of both the triple quadrupole and the ion trap.[128] In addition to speeding the data acquisition process, the Q-trap allows information dependent acquisitions which provide the advantages of combining the selectivity of PI, NL and MRM scans by the triple quadrupole and the sensitivity of MS/MS spectral acquisition by the ion trap.[129] The Q-trap allows detection and MS/MS acquisition of analytes to be accomplished in a single LC-MS run.

2.9 Perspective

The structural features that govern both pharmacological and toxicological properties of NDGA are poorly understood. In the drug discovery process, chemical modification is commonly used to reduce toxicity and/or enhance pharmacological effects of potential drug candidates or new chemotypes. It is likely that NDGA **1** toxicity is related to its catechol moieties.[32-34] The structurally similar lignan secoisolariciresinol (SECO **9**) which exists as a di-phenol has limited toxicity suggesting that the o-dihydroxy function in the case of NDGA **1** is possibly culpable. Also, the rapid intramolecular cyclization to a dibenzocyclooctadiene derivative reported[35] for NDGA **1** at physiological conditions did not seem to occur when SECO **9** was treated under similar conditions. Instead, SECO **9** yields lariciresinol **23**[44] which likely occurs via a para-quinone methide intermediate as shown in Scheme 2-24.

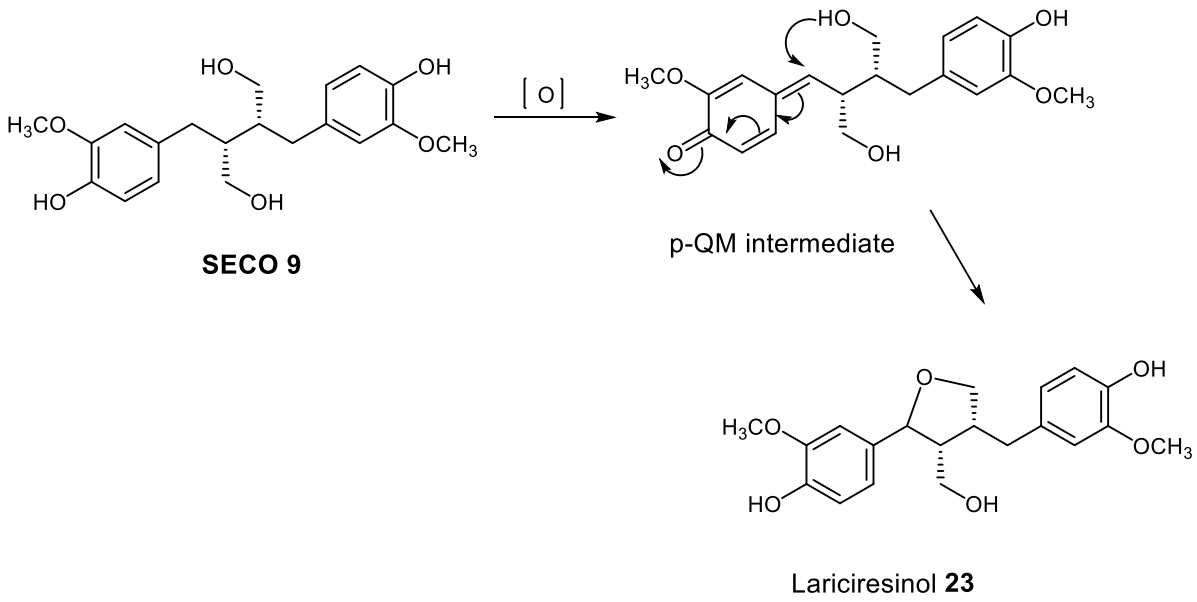

Scheme 2-24: Proposed mechanism of SECO oxidation to Lariciresinol.

In theory, a p-QM **5c** derived from NDGA is expected to be formed directly or via isomerization of the o-Q **5b** as depicted by Scheme 2-6. The p-QM **5c**, if formed, will be expected to contribute to toxicity (Scheme 2-25) as has been confirmed for the o-Q.[32] It is unclear why NDGA does not seem to form the p-QM **5c** and will be investigated in these studies. The structural features which govern the pathways to reactive metabolites and intramolecular cyclization which likely have toxicological and pharmacological implications respectively (Scheme 2-25) were of interest in this study.

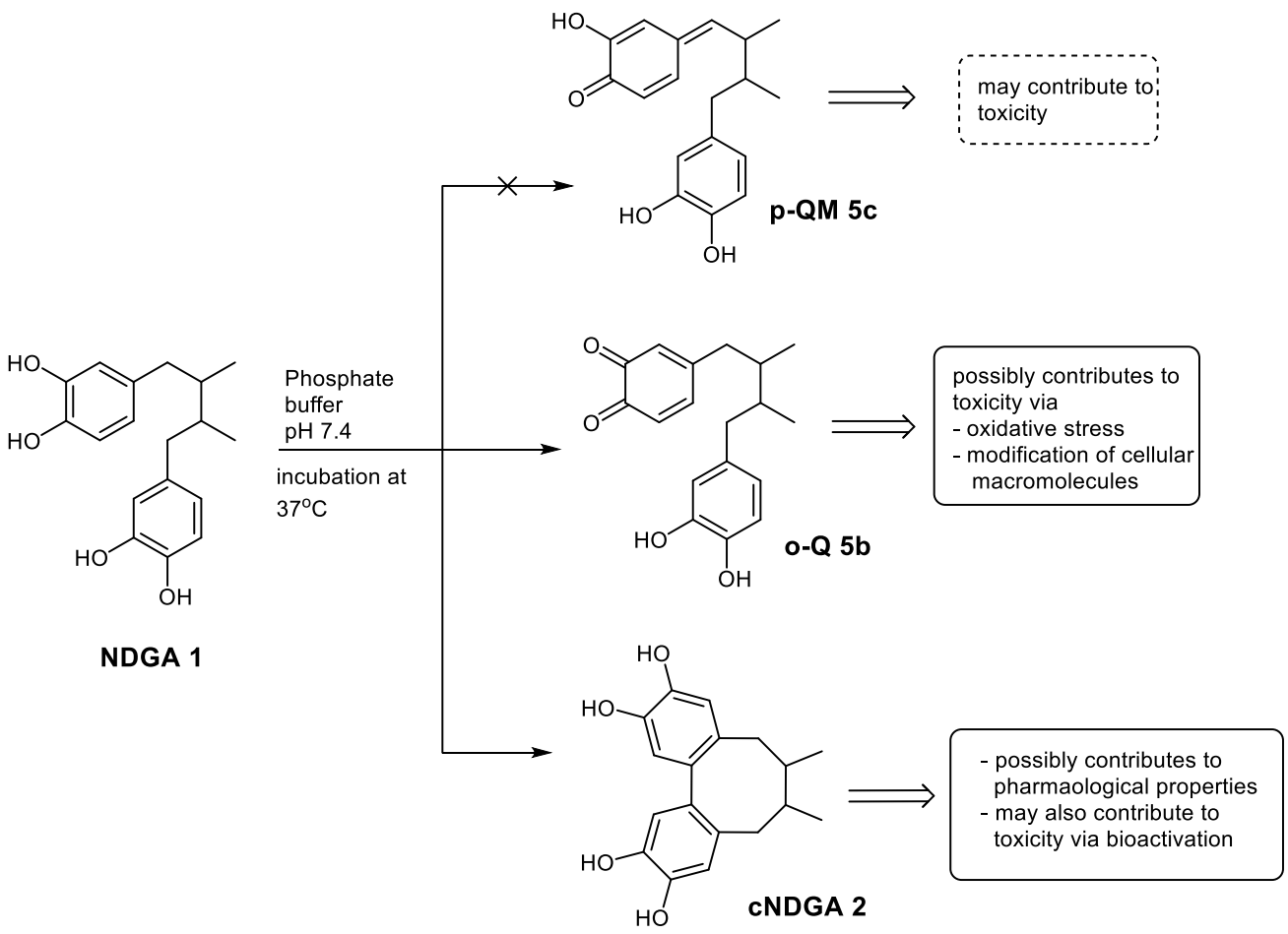

Scheme 2-25: Autoxidation of NDGA **1** at physiological conditions to a dibenzocyclooctadiene lignan (cNDGA **2**) and ortho-quinone (o-Q **5b**). There is no evidence yet for a para-quinone methide (p-QM **5c**).

2.10 Purpose of this Project

2.10.1 Rationale

Nordihydroguaiaretic acid has a broad spectrum of important biological activities but its usefulness is hindered by toxicity concerns. Rational modifications of the structure of NDGA will allow for identification of its pharmacophore and toxicophore and likely lead to design and synthesis of analogues with better safety profiles in the future. The pathways mediating pharmacological and toxicological effects of NDGA are presently unclear. Therefore, understanding the mechanistic pathways is the way forward to develop NDGA analogues with better safety profiles. To this end, there is the need to design and synthesize appropriate NDGA analogues (Figure 2-9) that will provide vital information to unravel the mechanisms of its oxidative conversion to a dibenzocyclooctadiene derivative which likely has pharmacological implications. The conditions of formation[35] and the known biological properties of the dibenzocyclooctadiene family of lignans[55] suggest that this oxidation product likely contributes to the pharmacological effects of NDGA. Autoxidation studies on appropriate analogues will aid in understanding the mechanisms of NDGA-derived dibenzocyclooctadiene formation and the design of analogues with higher propensity to convert to a dibenzocyclooctadiene under physiologically relevant conditions. Also, oxidation studies on the prepared analogues will provide vital information about structural features which influence reactive metabolite formations. This is expected to help in design strategies to metabolically block reactive intermediates formation with potential implication for ameliorating the safety profile of NDGA analogues. The overall outcome of this study is expected to advance our understanding of structural features that influence biological activities of NDGA and likely lead to discovery of analogues with improved pharmacological effects and safety profile.

2.10.2 Hypotheses

The following hypotheses were tested in this study:

1. Nordihydroguaiaretic acid intramolecular cyclization to dibenzocyclooctadiene involves a radical mediated addition mechanism.
2. Formation and type of quinoid species is dependent on substitution and/or substitution pattern of the aromatic rings
3. A p-QM of nordihydroguaiaretic acid contributes to its toxicity

2.10.3 Objectives and Aims

In order to verify our hypotheses, the following objectives and aims were outlined.

2.10.3.1 Objective 1

Synthesis and characterization of NDGA analogues for the purpose of understanding structural features that influence pharmacological and toxicological properties of NDGA. The two specific aims of this objective are:

1. To develop synthetic protocols for the preparation of the NDGA analogues
2. To purify and characterize prepared analogues using various chromatographic, mass spectroscopy (MS) and nuclear magnetic resonance (NMR) methods

2.10.3.2 Objective 2

Evaluate the synthesized NDGA analogues for their potential to undergo autoxidative cyclization under physiologically relevant conditions. This study is expected to help explain the mechanisms of NDGA oxidative cyclization in a phosphate buffer (pH 7.4) at 37°C and provide

information about structural features that influence pharmacological properties of NDGA. The two specific aim of objective 2 are:

1. To develop an HPLC method for detection and quantification of the autoxidation products and subsequently quantify the rates of autoxidation
2. To isolate and elucidate the structures of the autoxidation products.

2.10.3.3 Objective 3

Study the oxidative metabolism and bioactivation of the NDGA analogues. This will provide understanding of the effect of aromatic rings substitution and/or substitution pattern on quinoid species formed under oxidative conditions and also help determine the major toxicophore responsible for NDGA's toxicity. The two specific objective are:

1. Perform enzymatic and chemical oxidation on the prepared analogues and trap reactive quinones as glutathione conjugates for HPLC and LC-MS analyses.
2. Perform *in vitro* microsomal incubations and identify glutathione-trapped conjugates by MS and/or NMR techniques

2 MATERIALS AND METHODS

3.1 Materials/Chemicals

The following chemicals were purchased from Sigma-Aldrich (St. Louis, MO): Benzaldehyde, 3,4-dimethoxybenzaldehyde, vanillin, 3-hydroxy-4-methoxybenzaldehyde, 4-hydroxy-3-methoxybenzaldehyde, 3,4- dihydroxybenzaldehyde, 3-hydroxybenzaldehyde, diethyl succinate, benzyl bromide, lithium diisopropylamide, CH_3I, eugenol, BBr_3 (1 M in DCM), p-toluenesulfonyl chloride, methanesulfonyl chloride, Pd/C (10%), anhydrous DMSO, anhydrous pyridine, $AgNO_3$, $LiAlH_4$, anhydrous THF, anhydrous DCM, molecular sieves 3Å, $MgSO_4$, trifluoroacetic acid (TFA), nordihydroguaiaretic acid (NDGA), reduced glutathione (GSH), mushroom tyrosinase, reduced nicotinamide adenine dinucleotide phosphate (NADPH) tetrasodium salt, 3,4-dimethoxyphenyl acetone (DMPA), K_2HPO_4, $MgCl_2$, salicylamide. NaOH and silica gel 60 (0.040-0.063 mm) used in flash columns were obtained from EMD. K_2CO_3, $NaHCO_3$, H_2SO_4, Na_2HPO_4, KOH, formic acid and perchloric acid were obtained from BDH Chemicals (Toronto). Celite® 545, H_3PO_4, HCl, NaCl, citric acid and sea sand used in the flash columns were obtained from Fisher Scientific (Fairlawn, NJ); ethanol (it was distilled and stored over sieve under $N_{2(g)}$ prior to use) was obtained from Commercial Alcohols Inc. (Brampton, ON); $CDCl_3$, CD_3OD, and DMSO-d6 were obtained from Cambridge Isotope Laboratories Inc. (Andover, MA). Silver oxide (Ag_2O) was freshly prepared from $AgNO_3$ and KOH according to literature procedure.[130] NaOEt solution in ethanol was prepared by addition of $Na_{(s)}$ to dry ethanol. Hydrogenation of eugenol gave PC2; PC1 was obtained from PC2 by demethylation with BBr_3 solution in DCM; NDGA analogues were prepared according to literature procedures with modifications where appropriate as described in Section 3.3. All other solvents were of the highest grade purity obtained from EMD (Gibbstown,

NJ). HPLC runs were done with HPLC grade water and acetonitrile. LC/MS grade water, methanol and acetonitrile were used for all LC-MS analyses.

3.2 Equipment/Instrumentation

TLC aluminium sheets were coated with silica gel 60 F254 purchased from EMD Chemicals Inc. (Gibbstown, NJ). Rotary evaporator systems consisted of Büchi Rotavapor R-200, and Büchi v700 vacuum pump with attached v850 vacuum controller. Samples in test tubes were concentrated using Eppendorf Concentrator 4301 with Büchi Vac V-500 with attached v850 vacuum controllers. Incubates were centrifuged using an Eppendorf Centrifuge 5417C. Trace amounts of solvent and moisture were removed using an Edwards High Vacuum Pump. Vortexed reactions utilized a Janke & Kunkel IKA-Vibrax VXR with VX2 attachment. Incubations were done in a VWR incubating orbital shaker. Water was purified with a Millipore Milli-Q system with a Quantum EX Cartridge (Mississauga, ON). HPLC system consisted of Waters Alliance 2695 connected to Waters 2996 photodiode array detector. The HPLC system was controlled by, and data interpreted with the Waters Empower software. NMR experiments were performed on a Bruker AVANCE DPX-500 spectrometer, and data processed by X-WIN NMR 3.5 software or TopSpin 3.2. All compounds were named using ACD/ChemSketch. MS experiments were conducted using AB SCIEX 4000 QTRAP (AB SCIEX instruments) quadrupole linear ion trap mass spectrometer coupled to an Agilent 1100 system consisting of an Agilent 1100 G1311A pump and an Agilent 1100 G1329A autosampler (Agilent Technologies, Mississauga, ON). Data acquisition and analysis was performed using Analyst 1.5.1 software from AB SCIEX.

3.3 Experimental 1: Synthesis and Characterization of NDGA Analogues

3.3.1 Synthesis of (3E)-4-(3,4-dimethoxyphenyl)-3-(ethoxycarbonyl)but-3-enoic acid (25)[100, 102]

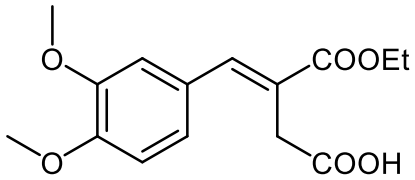

Sodium ethoxide (28%) solution (44.5 ml, 180.54 mmol), dried ethanol (180.5 ml) were transferred into the reaction flask under nitrogen gas. 3,4-dimethoxybenzyladehyde (15 g, 90.27 mmol) was added to the stirring mixture. Diethyl succinate (22.6 ml, 135.40 mmol) was added via syringe in drops and the mixture refluxed for 4 h. Ethanol was removed and the resulting orange solid was acidified (5 M HCl) and extracted with ethyl acetate (70 ml × 3). The combined organic layer was extracted with satd. $NaHCO_3$ (80 ml). The $NaHCO_3$ extract was acidified to pH 2, and the resulting oily solution re-extracted with EtOAc (20 ml × 3). The combined organic extract was dried over $MgSO_4$, filtered and evaporated in *vacuo* to give yellowish brown oil. On further drying under vacuum, yellowish solid form which was recrystallized form ethyl acetate/petroleum ether (26 g, 98 %). ^{1}H NMR (500 MHz, $CDCl_3$): δ (ppm) 1.35 (t, J = 7.1Hz, 3H), 3.63 (s, 2H), 3.89 (s, 3H), 3.91 (s, 3H), 4.31 (q, J = 7.1Hz, 2H), 6.91 (d, 1H), 7.00 (d, 2H), 7.87 (s, 1H), 11.60 (bs, 1H). ^{13}C NMR (500 MHz, $CDCl_3$): δ (ppm) 14.4, 34.2, 56.1, 61.7, 111.3, 112.4, 122.9, 123.4, 127.5, 142.69, 149.1, 150.2, 168.3, 176.8. ESI-MS (m/z) = 293.0 $[M-H]^-$.

3.3.2 Synthesis of 1-ethyl 4-methyl (2*E*)-2-(3,4-dimethoxybenzylidene)butanedioate (26)[102]

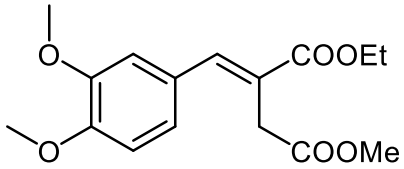

DMSO (176 ml) and K_2CO_3 (24.80 g, 179.46 mmol) were stirred for 5 min in the reaction flask at RT. The half-ester **25** (35.21 g, 119.64 mmol) was added followed by iodomethane (11.2 ml, 179.46 mmol). After stirring 2 h at RT, water (1000 ml) was added and extracted with DCM (100 ml × 4). The combined DCM layer was washed with water (1000 ml), and the aqueous layer re-extracted with DCM (50ml). The combined DCM extract was dried over $MgSO_4$, filtered and evaporated in *vacuo*. Flash chromatography over silica (2:1 PE/EtOAc) gave the product as yellowish oil (34.4 g, 93 %). ^{1}H NMR (500 MHz, $CDCl_3$): δ (ppm) 1.30 (t, J = 7.1Hz, 3H), 3.56 (s, 2H), 3.69 (s, 3H), 3.84 (s, 3H), 3.86 (s, 3H), 4.24 (q, J = 7.1Hz, 2H), 6.85 (d, 1H), 6.93 (m, 2H), 7.81 (s, 1H). ^{13}C NMR (500 MHz, $CDCl_3$): δ (ppm) 14.2, 33.5, 51.9, 55.7, 60.9, 110.6, 112.3, 122.5, 124.2, 127.3, 141.7, 148.7, 149.7, 167.37, 171.7. ESI-MS (m/z) = 309.1 $[M+H]^+$.

3.3.3 Synthesis of compound 27[102]

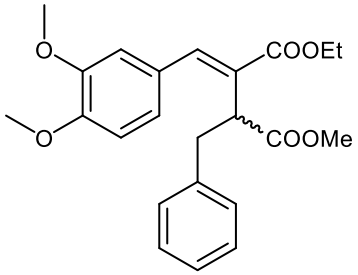

A well-stirred solution of the diester **26** (11.15 g, 36.16 mmol) in THF (45 ml) was added dropwise to a solution of LDA (39.78 mmol, 2 M in THF) in THF at -78°C under nitrogen atmosphere. After stirring at -78°C for 20 min, benzyl bromide (6.80 g, 39.78 mmol) in THF (22.6

ml) was added in drops. The mixture was stirred at -78°C for 2h, then allowed to warm up to room temperature. THF solvent was evaporated in vacuo after which excess saturated aqueous NH_4Cl solution was added. The mixture was extracted with DCM (40 ml × 3), washed with brine (50 ml), dried over $MgSO_4$ and evaporated *in vacuo*. Flash chromatography over silica (3:2 Pet. Ether/EtOAc) gave orange oil (10.5 g, 73%). ^{1}H NMR (500 MHz, $CDCl_3$): δ (ppm) 1.33 (t, J = 7.1Hz, 3H), 3.00 (dd, 1H), 3.44 (dd, 1H), 3.72 (s, 6H), 3.86 (s, 3H), 4.13 (dd 1H), 4.28 (q, 1H), 6.44 (s, 1H), 6.58 (d, 1H), 6.74 (d, 1H), 6.92 (d, 2H), 7.12 (m, 3H), 7.69(s, 1H). ^{13}C NMR (500 MHz, $CDCl_3$): δ (ppm) 14.2, 36.1, 45.5, 52.0, 55.8, 60.8, 110.6, 111.4, 121.3, 126.0, 127.9, 128.1, 129.2, 129.7, 139.1, 142.4, 148.6, 149.3, 166.7, 173.3. ESI-MS (m/z) = 399.2 $[M+H]^+$.

3.3.4 Synthesis of compound 28[99-101]

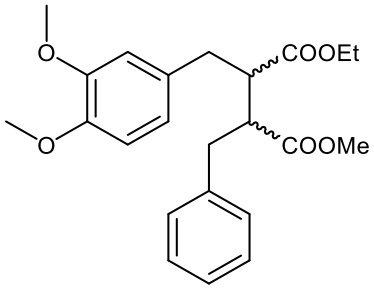

The reaction flask was evacuated and Pd/C (10%, 2.0g) added under N_2 gas. The flask was sealed, then ethanol (700 ml) and TFA (100 µl) were added. The diester **27** (10 g, 25.09 mmol) in ethanol (100 ml) was added. The flask was evacuated until the solvent just begun to bubble, then flushed with N_2 gas several times. The N_2 gas was replaced with H_2 gas. After flushing three times the mixture was left to stir under H_2 for 132 hours. The reaction was filtered through a pad of celite and washed with ethanol. The solvent was evaporated and after flash chromatography over silica gave yellow oil (8.8g, 88 %). ^{1}H NMR (500 MHz, $CDCl_3$): δ (ppm) 1.20 (t, 3H), 3.01 (m, 4H),

3.62 (s, 3H), 3.79 (s, 3H), 3.85 (s, 3H), 4.09 (m, 4H), 6.57 (d, 1H), 6.75 (m, 2H), 7.09 (m, 2H), 7.21(m, 3H). ESI-MS (m/z) = 401.2 $[M+H]^+$.

3.3.5 Synthesis of compound 29[100, 102]

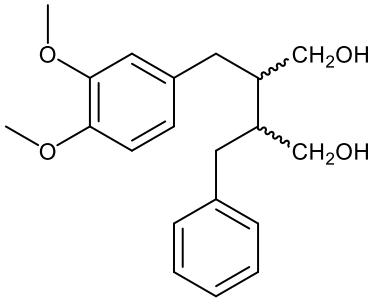

A suspension of $LiAlH_4$ (3.0 g, 79 mmol) in THF (90 ml) was stirred under N_2 and cooled to 0°C. The diester **28** (7.6 g, 18.97 mmol) in THF (150 ml) was slowly added. The mixture was allowed to come to RT and stirred 2h. The mixture was diluted with ether (50 ml) and cooled to 0°C. Water (3 ml) was carefully added via syringe, followed with 15% NaOH (3 ml) after stirring 5 min. Water (15 ml) was added after allowing the mixture to come to RT. EtOAc (50ml) and anhy. $MgSO_4$ were added and stirred overnight. The mixture was filtered, evaporated in vacuo and the resulting crude product chromatographed via flash column over silica gel (1:1 Pet ether/ethylacetate) to give white solid (4.1 g, 65 %) ^{1}H NMR (500 MHz, $CDCl_3$): δ (ppm) 1.92 (m, 2H), 2.78 (m, 4H), 3.54 (m, 4H), 3.83 (s, 3H), 3.87 (s, 3H), 6.66 (s, 1H), 6.71 (m, 1H), 6.78 (d, J = 8.1, 1H), 7.16 (d, J = 7.1, 2H), 7.21 (t, J = 5.1, 7.2, 1H), 7.28 (t, J = 7.2, 7.5, 2H). ^{13}C NMR (500 MHz, $CDCl_3$): δ (ppm) 35.9, 36.4, 43.1, 55.9, 56.1, 60.6, 111.0, 112.3, 121.2, 126.3, 128.5, 129.4, 133.2, 140.6, 147.4, 148.9. ESI-MS (m/z) = 329.1 $[M-H]^-$.

3.3.6 Synthesis of compound 30[100, 102, 144]

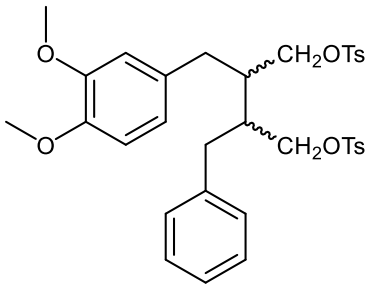

Pyridine (7.8 ml) was added via syringe to the diol **29** (2.0 g, 6.053 mmol) in the reaction flask under nitrogen. The mixture was stirred at 0°C for 20 min. Toluenesulfonyl chloride (2.77 g, 14.53 mmol) was added to the mixture and stirred 2 h at 0°C. HCl (60ml, 2M) was added and filtered by suction. The filtrate was extracted with EtOAc (30ml×3). The combined organic layer was washed with water (30 ml), brine (30ml) and dried over $MgSO_4$. After evaporation in vacuo, the crude product was purified by flash chromatography over silica gel to give white solid (1.0 g, 26 %). ^{1}H NMR (500 MHz, $CDCl_3$): δ (ppm) 2.10 (m, 2H), 2.47 (s, 6H), 2.52 (m, 2H), 2.69 (m, 2H), 3.81 (s, 3H), 3.87 (s, 3H), 3.96 (m, 4H), 6.48 (d, J = 8.1, 1H), 6.55 (s, 1H), 6.69 (d, J = 8.1, 1H), 7.17 (m, 3H), 7.34 (d, J = 8.7, 4H), 7.72 (m, 4H). ESI-MS (m/z) = 639.4 $[M+H]^+$.

3.3.7 Synthesis of compound 31[100, 102]

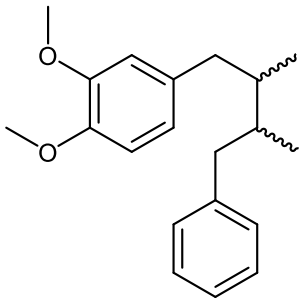

To a stirred suspension of $LiAlH_4$ (0.26, 6.85 mmol) in THF (12 ml) at 0°C under nitrogen was added the substrate **30** (0.99 g, 1.56 mmol) in THF (12 ml) slowly via syringe. The mixture

was stirred 2 h at RT. Diethyl ether (20ml) was added to the mixture and cooled to 0°C. Water (0.26 ml) was carefully added via syringe, followed with 15% NaOH (0.26 ml) after stirring 5 min. Water (0.81 ml) was added after allowing the mixture to come to RT and stirring continued for 15 min. EtOAc (20 ml) and anhy. $MgSO_4$ were added and stirred overnight. The mixture was filtered and evaporated in vacuo. Flash chromatography over silica gel (hexane-EtOAc 9:1) gave yellowish oil (0.4 g, 82 %). ^{1}H NMR (500 MHz, $CDCl_3$): δ (ppm) 0.88 (d×2, 6H), 1.82 (m, 2H), 2.40 (m, 1H), 2.43 (m, 1H), 2.65 (m, 1H), 2.83 (m, 1H), 3.84 (s, 3H), 3.89 (s, 3H), 6.61 (s, 1H), 6.67 (d, J = 8.1, 1H), 6.79 (m, 1H), 7.12 (d, J = 7.1, 1H), 7.20 (d, J = 7.2, 2H), 7.28 (m, 2H) ^{13}C NMR (500 MHz, $CDCl_3$) 14.1, 16.3, 37.9, 41.1, 41.7, 55.9, 56.0, 111.0, 112.1, 121.0, 125.8, 125.8, 128.3, 128.3, 129.2, 129.3, 134.3, 141.8, 147.1, 148.8. ESI-MS (m/z) = 299.2 $[M+H]^+$.

3.3.8 Synthesis of 4-(2,3-dimethyl-4-phenylbutyl)benzene-1,2-diol (A1)[100, 106]

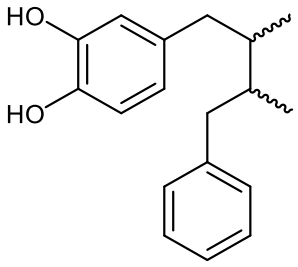

To a stirred solution of the substrate **31** (0.20g, 0.67 mmol) in DCM (6.67 ml) at -78 °C under nitrogen was added 1M BBr_3 in DCM (3.35ml, 3.35 mmol) carefully via syringe. The mixture was stirred 2 h at -78 °C. After warming to RT, the reaction was quenched with water (6.67 ml) and extracted with EtOAc (15ml, 7ml×3). The combined organic layer was washed with 10 ml each of $NaHCO_3$ (10%), HCl (1 M), water, and brine. It was dried over $MgSO_4$, filtered and the solvent evaporate in vacuo to give purplish dark oil (180 mg, > 99 %). ^{1}H NMR (500 MHz, $CDCl_3$): δ (ppm) 0.84-0.87 (6H, 2×d, J = 4.3, H9, 9'), 1.74-1.84 (2H, m, H8, 8'), 2.32-2.36 (1H, dd, J = 8.5, 13.4, H7α), 2.43-2.48 (1H, dd, J = 8.6, 13.4, H7α'), 2.55-2.59 (1H, dd, J = 6.4, 13.6, H7β), 2.66-

2.70 (1H, dd, J = 6.2, 13.6, H7β'), 5.78 (2H, bs, o, p-ArOH), 6.55-6.57 (1H, dd, J = 1.9, 8.1, H6), 6.64 (1H, d, J = 1.9, H2), 6.79 (1H, d, J = 7.9, H5), 7.14 (2H, d, J = 7.2, H2', 6'), 7.21 (1H, t, J = 7.4, H4'), 7.30 (2H, t, H3', 5'). ^{13}C NMR (500 MHz, $CDCl_3$): δ (ppm) 13.9, 16.2, 38.1, 39.3, 40.8, 41.5, 115.2, 116.1, 121.6, 125.6, 128.2, 128.2, 129.1, 129.2, 134.9, 141.3, 141.8, 143.3. ESI-MS (m/z) = 269.1 $[M-H]^-$.

3.3.9 Synthesis of 4-(benzyloxy)-3-methoxybenzaldehyde (32)[46]

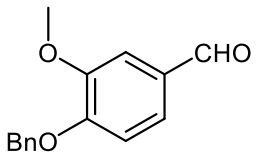

Vanillin (10 g, 65.72 mmol) and K_2CO_3 (13.7g, 98.58 mmol) were stirred in DMF (60 ml) under nitrogen atmosphere at room temperature. Benzyl bromide (9.4 ml, 78.86 mmol) was slowly added via syringe with agitation. The mixture was stirred at RT for 1 h. The reaction mixture was diluted with water (27 ml), neutralized with 50% HCl (20 ml) and extracted with EtOAC (67 ml, 20 ml ×2). The combined EtOAc extract was wash with water, brine (67 ml each) and dried with $MgSO_4$. The solvent was evaporated in vacuo to give orange solid which after recrystallization from heptane-EtOAc (9:1) gave white crystals (84 %). ^{1}H NMR (500 MHz, $CDCl_3$): δ (ppm) 3.95 (s, 3H), 5.25 (s, 2H), 6.99 (d, J = 8.2, 1H), 7.33 (t, J = 7.3, 1H), 7.39 (m, 3H), 7.44 (d, J = 7.3), 9.84 (s, 1H). ^{13}C NMR (500 MHz, $CDCl_3$): δ (ppm) 56.1, 70.9, 109.3, 112.4, 126.6, 127.2, 128.2, 129.0, 130.3, 136.0, 150.1, 153.6. ESI-MS (m/z) = 243.1 $[M+H]^+$ obs; 243.1016 Da calc.

3.3.10 Synthesis of (3*E*)-4-[4-(benzyloxy)-3-methoxyphenyl]-3-(ethoxycarbonyl)but-3-enoic acid (33)[100, 102]

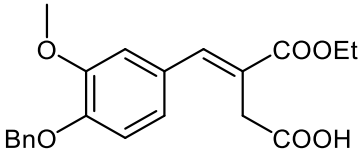

The procedure described for **25** but starting with **32** (9.6 g, 39.63 mmol) gave compound **33** as yellow oil (98 %). ^{1}H NMR (500 MHz, $CDCl_3$): δ (ppm) 1.25 (t, J = 7.1, 3H), 3.61 (s, 2H), 3.87 (s, 3H), 4.14 (q, J = 7.1, 2H), 5.16 (s, 2H), 6.89 (m, 2H), 6.97 (s, 1H), 7.30 (m, 1H), 7.35 (t, J = 7.3, 7.6, 2H), 7.42 (d, J = 7.3, 2H), 7.84 (s, 1H), 11.39 (s, 1H). ESI-MS (m/z) = 369.0 $[M-H]^-$ obs; 269.1332 Da calc.

3.3.11 Synthesis of compound 34[102]

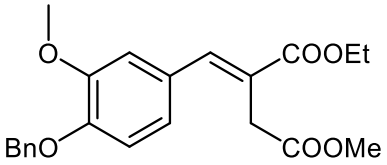

Following the procedure described for **26** but starting with **33** (20.9 g, 54.24 mmol)**,** compound **34** was obtained as yellow oil (92 %). ^{1}H NMR (500 MHz, $CDCl_3$): δ (ppm) 1.33 (t, J = 7.1, 3H), 3.58 (s, 2H), 3.72 (s, 3H), 3.88 (s, 3H), 4.27 (q, J = 7.1, 2H), 5.18 (s, 2H), 6.87 (s, 2H), 6.96 (s, 1H), 7.30 (t, J = 7.3, 5.1, 1H), 7.37 (t, J = 7.2, 7.7, 2H), 7.42 (d, J= 7.3, 2H), 7.83 (s, 1H). ^{13}C NMR (500 MHz, $CDCl_3$): δ (ppm) 14.3, 33.7, 52.2, 56.0, 60.9, 70.9, 112.7, 113.5, 122.4, 124.4, 127.2, 127.9, 128.7, 136.9, 141.8, 148.9, 149.4, 167.5, 171.8. ESI-MS (m/z) = 385.2 $[M+H]^+$ obs; 285.1645 Da calc.

3.3.12 Synthesis of compound 35[102]

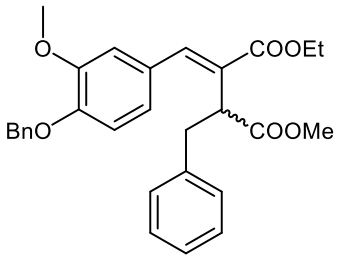

Following the procedure described for **27** but starting with **34** (10.22 g, 26.57 mmol)**,** compound **35** was obtained as orange oil (92 %). ^{1}H NMR (500 MHz, $CDCl_3$): δ (ppm) 1.37 (t, J = 7.1, 3H), 3.04 (dd, 1H), 3.47 (dd, 1H), 3.76 (s, 3H), 3.77 (s, 3H), 4.16 (m, 1H), 4.31 (q, J = 7.1, 2H), 5.18 (s, 2H), 6.49 (s, 1H), 6.56 (d, J = 8.2, 1H), 6.78 (d, J = 8.2, 1H), 6.92-6.94 (m, 2H), 7.11-7.14 (m, 3H), 7.39-7.42 (m, 3H), 7.46 (d, J = 7.2, 2H), 7.72 (s, 1H). ESI-MS (m/z) = 475.2 $[M+H]^+$obs; 475.2115 Da calc.

3.3.13 Synthesis of compound 36[102]

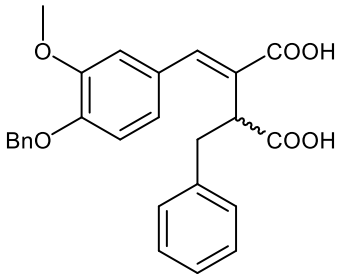

A 20% sodium hydroxide solution (2.44 ml, 12.2 mmol) was added to the diester **35** (0.29 g, 0.61mmol) and refluxed for 6 h. After cooling to room temperature, the mixture was washed with ethyl acetate (5 ml×3) and acidified until pH ≤ 2. The mixture was extracted with ethyl acetate (10 ml×4), dried over anhy. $MgSO_4$ and solvent evaporated *in vacuo.* Recrystallization from acetic acid gave the product as white crystals (57 %). ^{1}H NMR (500 MHz, $CDCl_3$): δ (ppm) 3.13 (dd, 1H), 3.48 (dd, 1H), 3.82 (s, 3H), 4.20 (dd, J = 4.7, 4.5, 1H), 5.26 (s, 2H), 6.79 (s, 2H), 7.11-7.15 (m, 3H),

7.28-7.31 (m, 3H), 7.56-7.63 (m, 5H), 7.72 (s, 1H), 12.63 (s, 2H). ESI-MS (m/z) = 431.1 $[M-H]^-$ obs; 431.1489 Da calc.

3.3.14 Synthesis of compound 37[58]

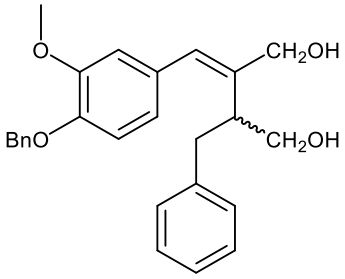

To a stirred suspension of $LiAlH_4$ (1.93 g, 50.83 mmol) in THF (100 ml) was added $AlCl_3$ (2.04 g, 15.26 mmol) under N_2. After stirring 20 min, the mixture was cooled to 0 °C. The substrate **13** (5.86 g, 12.35 mmol) in THF (40 ml) was slowly added via syringe. The mixture was allowed to come to RT and stirred 2.5 h. The mixture was diluted with ether (50 ml) and cooled to 0°C. Water (2 ml) was carefully added via syringe, followed with 15% NaOH (2 ml) after stirring 5 min. Water (6 ml) was added after allowing the mixture to come to RT. EtOAc (50ml) and anhy. $MgSO_4$ were added and stirred overnight. The mixture was filtered, evaporated in vacuo and the resulting crude product chromatographed via flash column over silica gel eluting with ethyl acetate to give white solid (3.67g, 73.5%) ^{1}H NMR (500 MHz, $CDCl_3$): δ (ppm) 2.73-2.84 (m, 2H), 3.05 (bs, 2H), 3.38-3.44 (m, 1H), 3.69-3.76 (m, 2H), 3.82 (s, 3H), 4.10 (d, J = 11.8, 1H), 4.43 (d, J = 11.8, 1H), 5.16 (s, 2H), 6.57-6.61 (m, 2H), 6.63 (s, 1H), 6.81 (d, J = 7.1, 1H), 7.00 (d, J = 7.0, 2H), 7.14-7.21 (m, 3H), 7.32 (t, J = 7.2, 1H), 7.39 (t, J = 7.4, 2H), 7.45 (d, J = 7.4, 2H). ^{13}C NMR (500 MHz, $CDCl_3$): δ (ppm) 36.0, 43.1, 56.1, 64.9, 65.2, 71.2, 112.7, 113.8, 121.2, 126.2, 127.5, 128.1, 128.41, 128.8, 129.1, 130.4, 133.3, 137.3, 139.8, 140.8, 147.3, 149.4. ESI-MS (m/z) = 403.2 $[M-H]^-$.

3.3.15 Synthesis of 2-benzyl-3-(4-hydroxy-3-methoxybenzyl)butane-1,4-diol (39)[99]

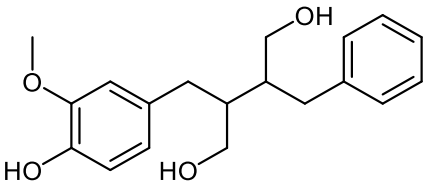

The diol **37 (**0.812 g, 2.0 mmol**)** in ethanol (150 ml) and catalytic amount of TFA (50 µl) is stirred under hydrogen atmosphere for 24 h in the presence of 10 % Pd/C (162 mg). The reaction mixture was filtered through a pad of celite and solvent removed in vacuo. Flash chromatography over silica gel (3:1 EtOAc/Pet. ether) gave the desired product as two pairs of enantiomers. ^{1}H NMR (500 MHz, MeOD): δ (ppm) 1.91 (m, 1H), 1.96 (m, 1H), 2.62 (m, 2H), 2.68 (m, 2H), 3.56 (m, 4H), 3.73 (s, 3H), 6.54 (d, J=7.9Hz, 1H), 6.65 (m, 2H), 7.11 (m, 3H), 7.19 (m, 2H). ^{13}C NMR (500 MHz, MeOD): δ (ppm) 35.6, 36.4, 44.4, 44.5, 56.4, 62.0, 62.1, 113.7, 115.9, 122.8, 126.9, 129.4, 130.3, 133.9, 142.9, 145.7, 148.9. ESI-MS (m/z) = 315.1 $[M-H]^-$.

3.3.16 Synthesis of compound 40[101]

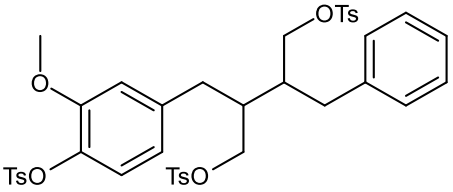

Pyridine (0.98 ml) was added via syringe to the diol **39** (308 mg, 0.76 mmol) in the reaction flask under nitrogen. The mixture was stirred at 0°C for 20 min. Toluenesulfonyl chloride (1.16 g, 6.06 mmol) was added to the mixture and stirred 4 h at 0°C. HCl (4 ml, 2M) was added and the oil mixture extracted with ethyl acetate. The combined organic layer was washed with water, brine and dried over $MgSO_4$. After evaporation in vacuo, the crude product was purified by flash chromatography over silica (363.6 mg, 62%). ^{1}H NMR (500 MHz, $CDCl_3$): δ (ppm) 2.10 (m, 2H),

2.47 (s, 6H), 2.52 (m, 2H), 2.69 (m, 2H), 3.81 (s, 3H), 3.87 (s, 3H), 3.96 (m, 4H), 6.48 (d, J = 8.1, 1H), 6.55 (s, 1H), 6.69 (d, J = 8.1, 1H), 7.17 (m, 3H), 7.34 (d, J = 8.7, 4H), 7.72 (m, 4H). ESI-MS (m/z) = 639.4 $[M+H]^+$.

3.3.17 Synthesis of compound 42[100]

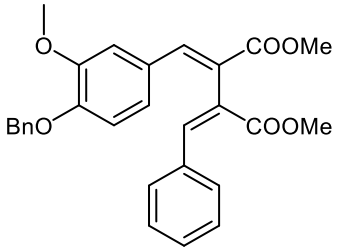

Following the procedure described for **25** but starting with substrate **34** (7.65g, 19.90 mmol) and benzaldehyde **41** (2.32 g, 21.89 mmol), the resulting half-ester was esterified according the the procedure described for **26** to give compound **42** as yellow oil (> 90 %). ^{1}H NMR (500 MHz, $CDCl_3$): δ (ppm) 1.11 (t, J = 7.1, 3H), 3.56 (s, 3H), 3.74 (s, 3H), 4.14 (q, J = 7.1, 2H), 5.12 (s, 2H), 6.75 (s, 1H), 6.77(s, 1H), 7.01 (t, J = 6.6, 8.2, 2H), 7.11 (d, J = 8.5, 1H), 7.16 (d, J = 8.4, 1H), 7.20 (s, 1H), 7.25 (s, 2H), 7.44-7.46 (m, 3H), 7.89 (m, 1H), 8.05 (s, 1H), 8.08 (s, 1H).

3.3.18 Synthesis of 4-(2,3-dimethyl-4-phenylbutyl)-2-methoxyphenol (A2)[101]

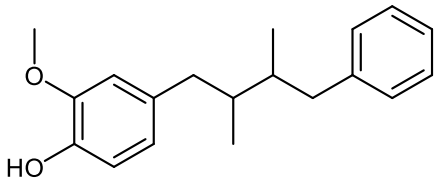

To a stirred suspension of $LiAlH_4$ (88.57 mg, 2.33 mmol) in THF (7 ml) at 0 °C under nitrogen was added the substrate **40** (363.6 mg, 0.47 mmol) in THF (4 ml) slowly via syringe. The mixture was stirred 2 h at RT. The reaction mixture is diluted with ether and cooled to 0 °C. The reaction is quenched with saturated sodium sulfate solution and H_2SO_4 (10%) solution. The mixture

is extracted with EtOAc, washed with brine and dried over anhy. $MgSO_4$. The solvent is removed in vacuo. The resulting residue in 3% KOH in ethanol-water (1:1) solution is refluxed overnight (12 h). On cooling to rt, the mixture is neutralized with acetic acid and extracted with ether. Combined ether is washed brine, dried over $MgSO_4$ and solvent removed in vacuo. Flash chromatography over silica (4:1 hexane/EtOAc) gave pale yellow oil (54.4 mg, 41 % in 2 steps) ^{1}H NMR (500 MHz, $CDCl_3$): δ (ppm) 0.86-0.88 (6H, overlapping d, H9, 9'), 1.77-1.85 (2H, m, H8, 8'), 2.38-2.49 (2H, m, H7α, 7α'), 2.57-2.68 (2H, m, H7β, H7β'), 3.84 (3H, s, OC<u>H</u>$_3$), 5.51 (1H, bs, p-ArO<u>H</u>), 6.58 (s, 1H), 6.62-6.65 (1H, m,), 6.84-6.88 (1H, m,), 7.13 (d, J = 7.2, 1H), 7.18-7.23 (m, 2H), 7.23-7.33 (m, 2H). ^{13}C NMR (500 MHz, $CDCl_3$): δ (ppm) 13.95, 16.11, 37.81, 38.94, 41.09, 41.45, 55.84, 111.34, 113.97, 121.67, 125.64, 128.15, 129.08, 133.57, 141.73, 143.55, 146.29. ESI-MS (m/z) = 283.18 $[M-H]^-$ obs; 283.17 Da calc.

3.3.19 Synthesis of compound 44[100]

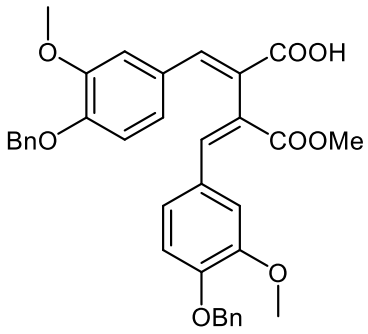

Following the procedure described for **25** but starting with substrates **32** (7.83, 32.31) and **34** (11.29 g, 29.37 mmol), compound **44** was obtained as yellow powder (72 %). ^{1}H NMR (500 MHz, $CDCl_3$): δ (ppm) 1.07 (t, J = 7.1, 3H), 3.56 (s, 6H), 3.64 (s, 3H), 3.65 (s, 3H), 4.12 (q, J = 7.1, 2H), 5.07 (s, 4H), 7.01 (t, J = 6.6, 8.2, 2H), 7.11 (d, J = 8.5, 1H), 7.16 (d, J = 8.4, 1H), 7.20 (s, 1H), 7.25 (s, 2H), 7.30-7.33 (m, 2H), 7.35-7.40 (m, 8H), 7.79 (s, 2H), 12.53 (bs, 1H).

3.3.20 Synthesis of compound 45[100]

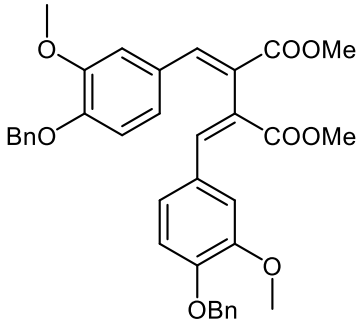

The esterification procedure described for **26** but starting with **44** (10.79 g, 18.59 mmol) was employed to obtain **45** as sparkling yellow crystals (87 %). ^{1}H NMR (500 MHz, $CDCl_3$): δ (ppm) 1.11 (t, J = 7.1, 3H), 3.69 (s, 3H), 3.76 (s, 6H), 4.16 (q, J = 7.1, 2H), 6.80 (d, J = 7.5, 2H), 7.03 (d, J = 8.3, 2H), 7.16 (s, 2H), 7.30 (m, 2H), 7.36 (m, 4H), 7.39 (m, 4H), 7.86 (s, 2H). ^{13}C NMR (500 MHz, $CDCl_3$): δ (ppm) 14.3, 52.6, 56.1, 61.2, 70.9, 112.5, 112.9, 124.7, 124.9, 125.1, 127.1, 128.2, 128.8, 136.7, 142.3, 142.5, 149.4, 149.7, 167.3, 167.9.

3.3.21 Synthesis of compound 46[58]

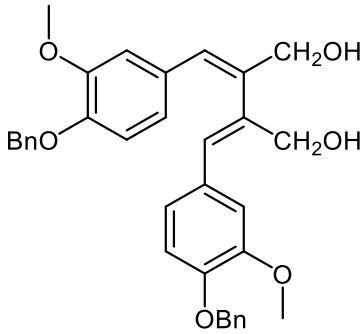

The reduction method described for **37** but starting with **45** (9.42 g, 15.83 mmol) afforded **46** as yellow powder (6.2 g, 74%). ^{1}H NMR (500 MHz, $CDCl_3$): δ (ppm) 2.51 (bs, 2H), 3.76 (s, 6H), 4.16 (s, 4H), 5.14 (s, 4H), 6.65 (s, 2H), 6.79 (d, J = 8.3, 2H), 6.97 (d, J = 8.3, 2H), 7.14 (s, 2H), 7.30 (m, 2H), 7.36 (m, 4H), 7.42 (m, 4H). ^{13}C NMR (500 MHz, $CDCl_3$): δ (ppm) 56.0, 66.9, 70.9, 111.5,

113.6, 121.1, 127.2, 127.9, 128.6, 129.2, 129.5, 136.9, 137.4, 147.9, 149.4. ESI-MS (m/z) = 537.20 $[M-H]^-$ obs; 537.22 Da calc.

3.3.22 Synthesis of *meso*-secoisolariciresinol (47a) and racemic (±)-secoisolariciresinol (47b)[99, 101]

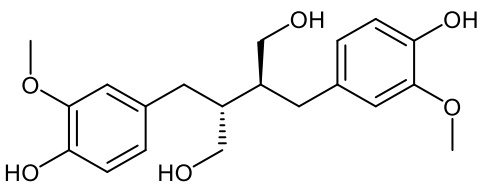

meso-Secoisolariciresinol **47a**

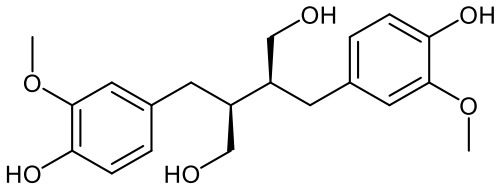

(±) Secoisolariciresinol **47b**

Hydrogenation procedure described for **28** but starting with **46** (2.38 g, 4.43 mmol) afforded *meso*- and *rac*(±)-secoisolaricirenol as pale yellow oil (747.4 mg, 47 %) and as pale orange solid (771.7 mg, 48 %) respectively after flash chromatography over silica (3:1 EtOAc/hexanes). **47a,** off-white solid, ^{1}H NMR (500 MHz, $CDCl_3$), δ (ppm): 1.91 (m, 1H), 1.96 (m, 1H), 2.62 (m, 2H), 2.68 (m, 2H), 3.56 (m, 4H), 3.73 (s, 3H), 6.54 (d, J=7.9Hz, 1H), 6.65 (m, 2H), 7.11 (m, 3H), 7.19 (m, 2H). ^{13}C NMR (500 MHz, MeOD): δ (ppm) 35.6, 36.41, 44.4, 44.5, 56.4, 62.0, 62,1, 113.7, 115.9, 122.8, 126.9, 129.4, 130.3, 133.9, 142.9, 145.7, 148.9. ESI-MS (m/z) = 315.1 $[M-H]^-$.

3.3.23 Synthesis of 4,4'-[(2*S*,3*S*)-2,3-dimethylbutane-1,4-diyl]bis(2-methoxyphenol) (A3)[101]

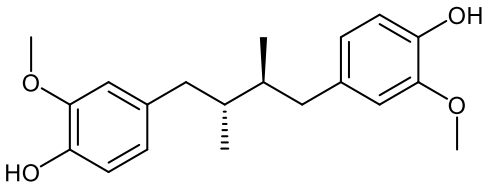

A3a

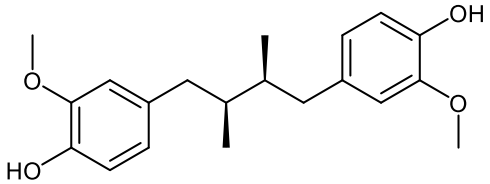

A3b

To *meso*-secoisolariciresol **47a** (443.2 mg, 1.22 mmol) in pyridine (1.6 ml) was added tosyl chloride (1.86 g) at 0^{O}C and stirred 4h. The reaction was quenched with HCl (2M) solution and

extracted with ethyl acetate. After drying over MgSO4, the solvent is removed in vacuo. The crude product was added to a suspension of $LiAlH_4$ (270 mg, 7 mmol) in THF (25 ml) at $0^{O}C$ under nitrogen and stirred at room temperature overnight (12 h). The reaction was quenched with saturated N**A**$_2SO_4$ solution and 10% H_2SO_4 solution. The clear mixture was extracted with ethyl acetate, washed with brine, dried over $MgSO_4$ and solvent removed in vacuo to give colourless oil (983 mg). KOH (3%, 25 ml) solution in ethanol-water (1:1) of was added to the oil and refluxed overnight (12h). On cooling to RT, the mixture was neutralized with acetic acid and extracted with ether. Combined ether layer was washed with brine, dried over $MgSO_4$ and solvent removed in vacuo. Flash chromatography over silica (3:1 pet. ether/EtOAc) gave **A3a** as off white solid (296.9 mg, 73.47% in 3 steps). The procedure was repeated with (±)-secoisolariciresol **47b** (476.3 mg, 1.31 mmol) to afford **A3b** as white solid (276.1 mg, 64 % in 3 steps). **A3a,** off-white solid, mp 79-80°C; ^{1}H NMR (500 MHz, $CDCl_3$): δ (ppm) 0.83-0.86 (6H, overlapping d, J = 6.4, H9, 9'), 1.72-1.76 (2H, m, H8, 8'), 2.26-2.32 (1H, dd, J = ,H7α), 2.37-2.41 (1H, dd, J = 7.4, 13.4, H7α'), 2.51-2.55 (1H, dd, J = 7.4, 13.7, H7β), 2.72-2.76 (1H, dd, J = 4.1, 12.9, H7β'), 3.82 (3H, s, *p*-OC$\underline{H}_3$), 3.87 (3H, s, *o*-OC$\underline{H}_3$), 5.58 (2H, bs, p-ArO$\underline{H}$), 6.55 (1H, s, H2), 6.60 (1H d, J = 7.8, H6), 6.64 (1H, s, H2'), 6.68 (1H, d, J = 7.8, H6'), 6.83 (1H, d, J = 8.0, H5), 6.85 (1H, d, J = 8.0, H5'). ^{13}C NMR (500 MHz, $CDCl_3$) δ (ppm) 14.0, 16.4, 21.3, 37.6, 39.1, 39.4, 41.3, 55.9, 56.0, 60.6, 111.5, 111.6, 114.0, 114.2, 121.8, 121.9, 133.8, 133.9, 143.7, 143.7, 146.4, 146.5. ESI-MS m/z: 329.1 $[M-H]^-$ obs; 329. 18 Da calc.

A3b, δ (ppm) 0.83-0.86 (6H, overlapping d, J = 6.8, H9, 9'), 1.72-1.76 (2H, m, H8, 8'), 2.28-2.32 (1H, dd, J = 9.3, 13.3 ,H7α), 2.37-2.42 (1H, dd, J = 7.7, 13.7, H7α'), 2.51-2.55 (1H, dd, J = 7.3, 13.7, H7β), 2.72-2.76 (1H, dd, J = 5.2, 13.7, H7β'), 3.82 (s, 3H, *p*-OC$\underline{H}_3$), 3.87 (s, 3H, *o*-OC$\underline{H}_3$), 5.50 (bs, 2H, p-ArO$\underline{H}$), 6.53 (1H, s, H2), 6.60 (1H, d, J = 7.7, H6), 6.63 (1H, s, H2'), 6.68 (1H, d, J

= 8.0, H6'), 6.81 (1H, d, J = 7.7, H5), 6.84 (1H, d, J = 7.7, H5'). ^{13}C NMR (500 MHz, $CDCl_3$) δ (ppm) 13.9, 16.3, 37.5, 38.9, 39.2, 41.1, 55.8, 55.9, 111.3, 111.5, 113.9, 114.0, 121.7, 121.7, 133.6, 133.8, 143.5, 143.6, 146.3, 146.3. ESI-MS m/z: 329.13 $[M-H]^-$ obs; 329. 18 Da calc.

3.3.24 Synthesis of compound 49[46]

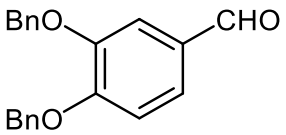

Benzylation procedure described for **32** but starting with 3,4-dihydroxybenzaldehyde **48** (15.06 g, 109.04 mmol) gave **49** as white crystals (84%). ^{1}H NMR (500 MHz, $CDCl_3$): δ (ppm) 5.23 (s, 2H), 5.27 (s, 2H), 7.03 (d, J = 8.2, 1H), 7.34 (m, 2H), 7.39 (m, 5H), 7.47 (m, 5H), 9.82 (s, 1H). ^{13}C NMR (500 MHz, $CDCl_3$): δ (ppm) 31.1, 70.9, 71.1, 112.5, 113.2, 126.9, 127.2, 127.5, 128.2, 128.3, 128.8, 128.8, 130.5, 136.4, 136.7, 149.3, 154.4, 191.0. ESI-MS m/z: 319.10 $[M+H]^+$ obs; 319.13 Da calc.

3.3.25 Synthesis of compound 50[100, 102]

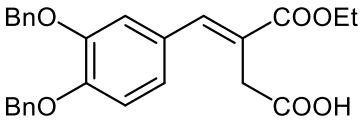

Stobbe condensation procedure described for **25** but starting with **49** (24.95 g, 78.23 mmol) gave **50** as yellow solid (98 %). ^{1}H NMR (500 MHz, $CDCl_3$): δ (ppm) 1.33 (t, J = 7.1 Hz, 3H), 3.51 (s, 2H), 4.28 (q, J = 7.1 Hz, 2H), 5.21 (s, 2H), 5.22 (s, 2H), 6.96 (s, 2H), 7.03 (s, 1H), 7.38 (m, 5H), 7.46 (m, 5H), 7.82 (s, 1H), 11.48 (bs, 1H). ESI-MS m/z: 445.10 $[M-H]^-$ obs; 445.16 Da calc.

3.3.26 Synthesis of compound 51[102]

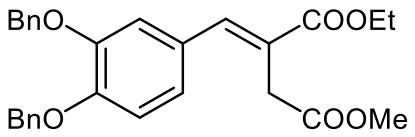

Esterification procedure described for **26** but starting with **50** (35.05 g, 78.56 mmol) gave **51** as yellow oil (98 %).^{1}H NMR (500 MHz, $CDCl_3$): δ (ppm) 1.34 (t, J = 7.1 Hz, 3H), 3.51 (s, 2H), 3.74 (s, 3H), 4.28 (q, J = 7.1 Hz, 2H), 5.19 (s, 2H), 5.20 (s, 2H), 6.96 (s, 2H), 7.04 (s, 1H), 7.36-7.40 (m, 5H), 7.45-7.46 (m, 5H), 7.82 (s, 1H). ESI-MS m/z: 461.20 $[M+H]^+$ obs; 461.19 Da calc.

3.3.27 Synthesis of compound 52[99]

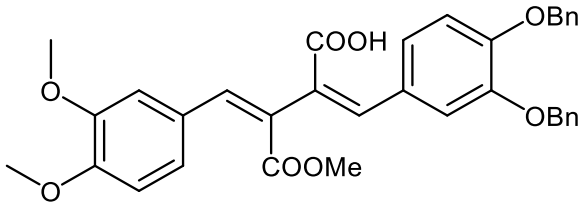

Following the procedure described for **25** but starting with **51** (10 g, 21.71 mmol) and 3,4-dimethylbenzylaldehyde **24** (3.97g, 23.89 mmol), compound **52** was obtained as yellow solid (> 90%). ^{1}H NMR (500 MHz, $CDCl_3$): δ (ppm) 1.07 (t, J = 7.1, 3H), 3.56 (s, 6H), 3.64 (s, 3H), 3.65 (s, 3H), 4.12 (q, 2H), 5.07 (s, 4H), 7.01 (t, J = 6.6, 8.2, 2H), 7.11 (d, J = 8.5, 1H), 7.16 (d, J = 8.4, 1H), 7.20 (s, 1H), 7.25 (s, 2H), 7.31 (m, 2H), 7.37 (m, 8H), 7.79 (s, 2H), 12.53 (bs, 1H).

3.3.28 Synthesis of compound 53[100, 102]

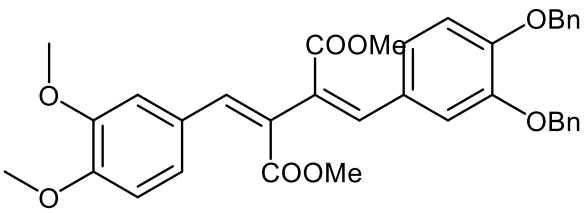

Esterification procedure described for **26** but starting with compound **52** (12.6 g, 21.71 mmol) gave the desired product as orange oil (98 %). ^{1}H NMR (500 MHz, $CDCl_3$): δ (ppm) 1.09 (t, J = 7.0 Hz, 3H), 3.67 (s, 3H), 3.71 (s, 3H), 3.87 (s, 3H), 4.13 (q, J = 7.0 Hz, 2H), 5.16 (s, 2H), 5.19 (s, 2H), 6.78 (d, 1H), 6.83 (d, 1H), 7.01-7.01 (m, 3H), 7.33-7.38 (m, 5H), 7.39-7.43 (m, 3H), 7.81 (s, 1H), 7.82 (s, 1H).

3.3.29 Synthesis of compound 54[99]

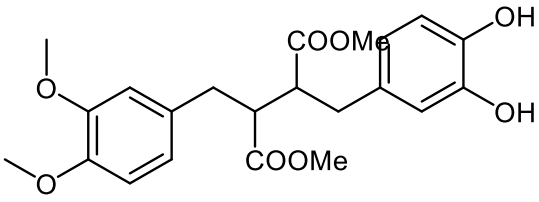

Hydrogenation procedure described for **28** but starting with **53** (8.42 g, 13.84 mmol) afforded the desired product **54** in > 99% yield. ^{1}H NMR (500 MHz, $CDCl_3$): δ (ppm) 1.09 (t, J = 7.0 Hz, 3H), 3.67 (s, 3H), 3.71 (s, 3H), 3.87 (s, 3H), 4.13 (q, J = 7.0 Hz, 2H), 6.78 (d, 1H), 6.83 (d, 1H), 7.01-7.01 (m, 2H), 7.81 (s, 1H), 7.82 (s, 1H).

3.3.30 Synthesis of compound 55[46]

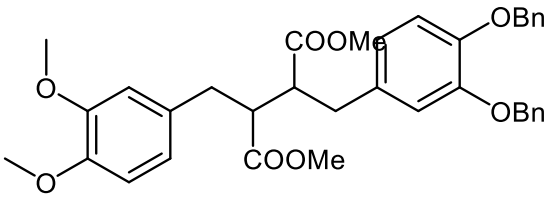

Benzylation procedure described for **32** but starting with compound **54** (5.8 g, 13.41 mmol) gave **55** as white solid (63 %) after flash chromatography over silica (2:1 pet. Ether/EtOAc). ^{1}H NMR (500 MHz, $CDCl_3$): δ (ppm) 5.23 (s, 2H), 5.27 (s, 2H), 7.03 (d, J = 8.2, 1H), 7.34 (m, 2H), 7.39 (m, 5H), 7.47 (m, 6H), 9.82 (s, 1H). ^{13}C NMR (500 MHz, $CDCl_3$): δ (ppm) 31.1, 70.9, 71.1, 112.5, 113.2, 126.9, 127.2, 127.5, 128.2, 128.3, 128.8, 128.8, 130.5, 136.4, 136.7, 149.4, 154.4, 191.0.

3.3.31 Synthesis of compound 56[100]

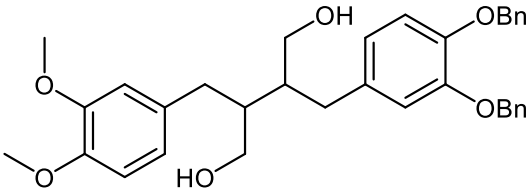

To a stirred suspension of $LiAlH_4$ (1.45 g, 38 mmol) in THF (80 ml) at 0°C under nitrogen was added the substrate **55** (3.9 g, 6.36 mmol) in THF (45 ml) slowly via syringe. The mixture was stirred 4 h at RT. The reaction mixture was diluted with ether and cooled to 0°C, then quenched with saturated sodium sulfate solution and H_2SO_4 (10%) solution. The mixture was extracted with EtOAc, washed with brine and dried over anhy. $MgSO_4$. The solvent is removed in vacuo to give compound **56** as colourless oil. ^{1}H NMR (500 MHz, $CDCl_3$): δ (ppm) 2.43-2.49 (m, 4H), 2.59-2.66 (m, 2H), 3.32-3.38 (m, 4H), 3.79 (s, 3H), 3.83 (s, 3H), 5.07 (s, 2H), 5.12 (s, 2H), 6.40 (d, J = 7.8 ,

1H), 6.44 (d, J = 7.8, 1H), 6.55 (s, 1H), 6.64-6.68 (m, 2H), 6.74 (d, J = 8.0, 1H), 7.30-7.32 (m, 6H), 7.36-7.38 (m, 4H), 7.44-7.46 (m, 4), 7.70-7.72 (m, 4H).

3.3.32 Synthesis of compound 57[101]

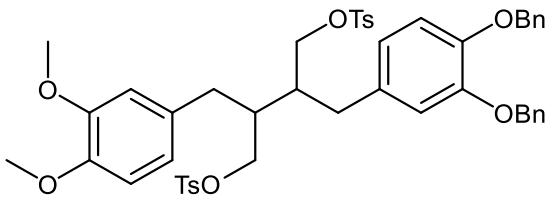

Pyridine (8.22 ml) was added via syringe to the substrate **56** (3.45 g, 6.36 mmol) in the reaction flask under nitrogen. The mixture was stirred at 0°C for 20 min. Toluenesulfonyl chloride (4.85 g, 25.44 mmol) was added to the mixture and stirred 4 h at 0°C. Addition of HCl (20 ml, 2M) gave a mixture of white solid and pale yellow oil. The oil was extracted into ethyl acetate and the white solid into DCM. The two organic extracts were washed separately with water, brine and dried over $MgSO_4$. The white solid obtained by DCM extraction **57a** was pure by NMR and was used without further purification (1.60g, 30 %). ^{1}H NMR (500 MHz, $CDCl_3$): δ (ppm) 2.10 (s, 6H), 2.43-2.49 (m, 4H), 2.59-2.66 (m, 2H), 3.79 (s, 3H), 3.83 (s, 3H), 3.86-3.94 (m, 4H), 5.07 (s, 2H), 5.12 (s, 2H), 6.40 (d, J = 7.8 , 1H), 6.44 (d, J = 7.8, 1H), 6.55 (s, 1H), 6.64-6.68 (m, 2H), 6.74 (d, J = 8.0, 1H), 7.30-7.32 (m, 6H), 7.36-7.38 (m, 4H), 7.44-7.46 (m, 4), 7.70-7.72 (m, 4H). ^{13}C NMR (500 MHz, MeOD): δ (ppm) 35.6, 36.4, 44.4, 44.5, 56.4, 62.0, 62,1, 113.7, 115.9, 122.8, 126.9, 129.4, 130.3, 133.9, 142.9, 145.7, 148.9. ESI-MS (m/z) = 851.20 [M-H$^+$]. After evaporation, the ethyl acetate extract was purified by flash chromatography over silica to yield 57 **57b** (2.97g, 55 %).

3.3.33 Synthesis of compound 58[101]

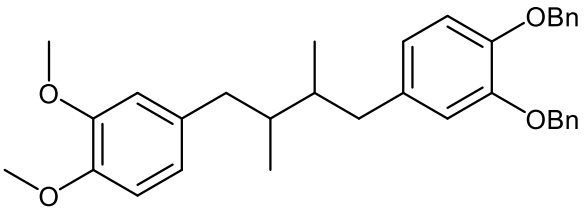

$LiAlH_4$ reduction described for compound **56** but starting with **57a** (1.6 g, 1.85 mmol) resulted in **58a**. Flash chromatography over silica gel (2:1 Pet. Ether/EtOAc) gave **58a** as colorless oil (632.6 mg, 67%). ^{1}H NMR (500 MHz, $CDCl_3$): δ (ppm) 0.79-0.81 (2 d, 6H), 1.71-1.74 (m, 2H), 2.34-2.40 (m, 2H), 2.51-2.57 (m, 2H), 3.82 (s, 3H), 3.85 (s, 3H), 5.11 (s, 2H), 5.14 (s, 2H), 6.58 (s, 1H), 6.60-6.63 (m, 2H), 6.70 (s, 1H), 6.76 (d, J = 8.9, 1H), 6.84 (d, J = 8.1 , 1H), 7.29-7.32 (m, 2H), 7.34-7.38 (m, 4H), 7.45-7.47 (m, 4H). ^{13}C NMR (500 MHz, MeOD): δ (ppm) 35.6, 36.4, 44.4, 44.5, 56.4, 62.0, 62,1, 113.7, 115.9, 122.8, 126.9, 129.4, 130.3, 133.9, 142.9, 145.7, 148.9. ESI-MS (m/z) = 511.2 [M+H$^+$] obs; 511.28 Da calc. The procedure was repeated with **57b** to obtain **58b**.

3.3.34 Synthesis of 4-[4-(3,4-dimethoxyphenyl)-2,3-dimethylbutyl]benzene-1,2-diol (A4)[99]

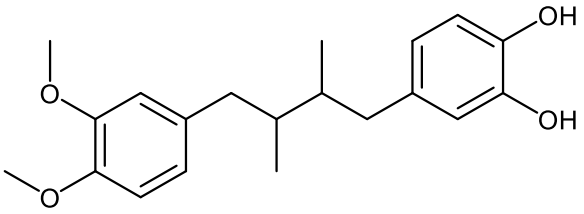

Treatment of **58a (**0.812 g, 2.0 mmol**)** or **58b** with excess H_2 in the presence of Pd-C(10%) as described for compound **28** gave compound **A4a** as dark purple solid (323.7 mg, 98%) or compound **A4b. A4a,** dark purple solid, mp 105-108 °C, ^{1}H NMR (500 MHz, $CDCl_3$): δ (ppm) 0.81-0.83 (6H, overlapping d, J = 4.5, H9, 9'), 1.69-1.76 (2H, m, H8, 8'), 2.31- 2.33 (2H, dd, J = 7.8, 13.4, H7α), 2.38-2.42 (1H, dd, J = 7.7, 13.4, 7α'), 2.46-2.51 (1H, dd, J = 7.0, 13.3, H7β), 2.51-2.55 (1H, dd, J = 7.3, 13.5, 7β'), 3.82 (3H, s, *p*-OC$\underline{H}_3$), 3.86 (3H, s, *o*-OC$\underline{H}_3$), 6.50 (1H, d, J = 6.2),

6.56 (1H, s), 6.58 (1H, s), 6.77-6.78 (m, 2H). ^{13}C NMR (500 MHz, MeOD): δ (ppm) 13.8, 13.9, 37.3, 37.4, 40.7, 40.9, 55.9, 55.99, 111.0, 112.3, 115.0, 115.9, 121.2, 121.5, 134.4, 134.7, 141.5, 143.3, 146.9, 148.6. ESI-MS (m/z) = 329.13 $[M\text{-}H^+]^-$ obs; 329. 18 Da calc.

3.3.35 Synthesis of compound 59

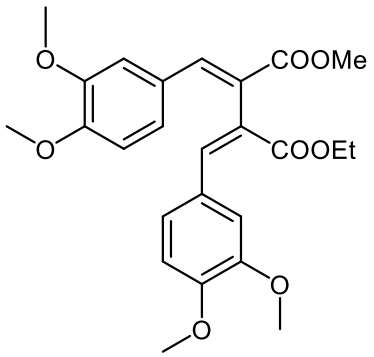

Stobbe condensation procedure described for **25** but starting with substrates **26** (7.50g, 24.32 mmol) and **24** (4.45g, 24.33 mmol), gave a yellow oil which was esterified with MeI in K_2CO_3/ DMSO as describe for **26** to afford compound **59.** ^{1}H NMR (500 MHz, $CDCl_3$): δ (ppm) 1.12 (t, J = 7.1 Hz, 3H), 3.59 (s, 3H), 3.73 (s, 3H), 3.74 (s, 3H), 3.84 (s, 3H), 3.85 (s, 3H), 4.12 (q, J = 3.4, 7.1, 2H), 6.77-6.80 (m, 2H), 7.11-7.17 (m, 4H), 7.90 (s, 1H), 7.94(s, 1H).

3.3.36 Synthesis of compound 60

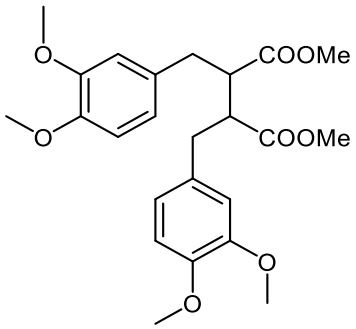

Compound **59** (12.85, 29.04 mmol) was hydrogenated in excess H_2 atmosphere in the presence of Pd-C(10%) as described for **28** to afford compound **60**. ^{1}H NMR (500 MHz, $CDCl_3$): δ (ppm) 1.12 (t, J = 7.1 Hz, 3H), 2.87-2.90 (m, 2H), 2.93-2.98(m, 2H), 3.54 (s, 3H), 3.78 (s, 6H), 3.83 (s, 6H), 4.12 (q, J = 3.4, 7.1, 2H), 6.55 (s, 2H), 6.60-6.62 (m, 2H), 6.63-6.74 (m, 2H).

3.3.37 Synthesis of compound 64

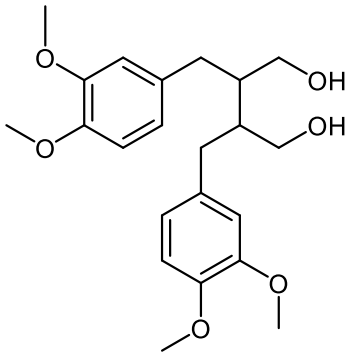

$LiAlH_4$ reduction described for compound **56** but starting with **60** (6.5 g, 14.11 mmol) resulted in **64** as a white solid (91 %). ^{1}H NMR (500 MHz, $CDCl_3$): δ (ppm) 0.86-0.88 (m, 2H), 2.66-2.70 (dd, 2H, J = 5.8, 13.7 Hz), 2.76-2.80 (dd, 2H, J = 8.4, 13.7 Hz), 3.19 (s, 2H), 3.52-3.55 (dd, 3H, J = 4.4, 11.1 Hz), 3.60-3.63 (dd, 1H, J = 7.1, 11.1 Hz), 3.83 (s, 4H), 3.86 (s, 8H), 6.66 (s, 2H), 6.69 (d, 2H, J = 7.7 Hz), 6.77 (d, 2H, J = 7.7).

3.3.38 Synthesis of tetra-O-methyl NDGA (14)

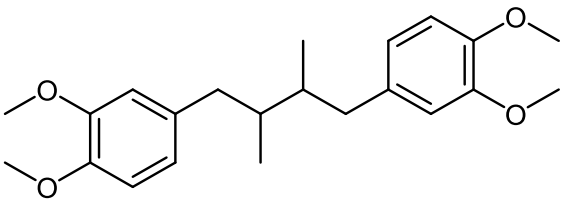

Compound **64** (3.5, 8.96 mmol) was tosylated as described for compound **57** to yield white solid which was reduced with $LiAlH_4$ in THF as described for **56** to afford compound **14** as white solid (93 %) ^{1}H NMR (500 MHz, $CDCl_3$): δ (ppm) 0.84-0.86 (overlapping d, 6H), 1.75-1.80 (m, 2H), 2.29-2.34 (dd, 1H, J = 5.3, 13.3 Hz), 2.39-2.43 (dd, 1H, J = 6.5, 13.6 Hz), 2.55-2.59 (dd, 1H, J = 7.7, 13.6 Hz), 2.75-2.78 (dd, 1H, J = 9.3, 13.3 Hz), 3.83 (s, 4H), 3.86 (s, 8H), 6.59 (s, 1H), 6.62 – 6.66 (m, 2H), 6.70-6.72 (m, 1H), 6.76-6.80 (m, 2H).

3.3.39 Synthesis of 4-(3,4-dimethoxyphenyl)butan-1-ol (66)

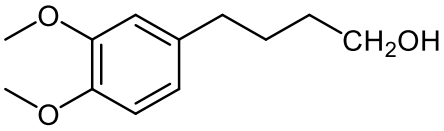

A 4-(3,4-dimethoxyphenyl)butyric acid (3.0 g, 13.4 mmol) was reduced with $LiAlH_4$ as described for compound **56** to obtain **66** (86 %). ^{1}H NMR (500 MHz, $CDCl_3$): δ (ppm) 1.26 (s, 2H), 1.60-1.65 (m, 2H), 1.66-1.72 (m, 2H,), 2.60 (t, J = 7.2 Hz, 2H), 3.68 (bs, 1H), 3.86 (s, 3H), 3.88 (s, 3H), 6.72 (d, J = 8.0, 2H), 6.79 (d, 1H, J = 7.8 Hz).

3.3.40 Synthesis of 4-(3,4-dimethoxyphenyl)butanal (67)

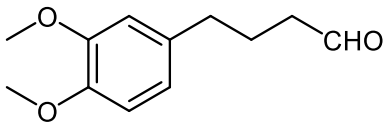

A solution of **66** (2.0 g, 9.5 mmol) in dried CH_2Cl_2 (10 ml) was treated with pyridinium chlorochromate (PCC) (4.10 g, 19.0 mmol) in dried CH_2Cl_2 (20 ml). The mixture was allowed to stir for 2.5 h and filtered through a pad of silica gel. The residue was washed thoroughly with CH_2Cl_2 and solvent removed in vacuo to afford **67** (84%). ^{1}H NMR (500 MHz, $CDCl_3$): δ (ppm) 1.94 (m, 2H), 2.46 (t, J = 7.2 Hz, 2H), 2.61 (t, J = 7.6 Hz, 2H,), 3.86 (s, 3H), 3.87 (s, 3H), 6.70 (d, J = 8.7 Hz, 2H), 6.79 (d, J = 7.8 Hz, 1H), 9.76 (s 1H).

3.3.41 Synthesis of compound 70

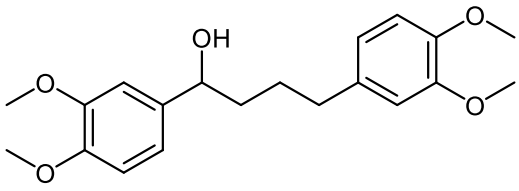

The Grignard reagent 3,4-dimethoxyphenylmagnesium bromide generated *in situ* refluxing a mixture of magnesium turning (0.46 g), 3,4-dimethoxyphenyl bromide (2.69 ml), iodine (1 crystal) in THF under N_2. The reagent was cooled to -78 ^{o}C under N_2 and treated with a solution of **67** (2.6 g, 12.5 mmol) in anhydrous THF (10 ml). The mixture was warmed to RT, and after 2 h the reaction was judged complete by TLC. Et_2O (35 ml) was added and the product mixture was washed with 20 ml NH_4Cl (5 % aq) followed by NaCl (satd aq). The crude product mixture was dried over $MgSO_4$, concentrated, and purified by flash column chromatography to afford **70** (71%). ^{1}H NMR (500 MHz, $CDCl_3$): δ (ppm) 1.52-1.60 (m, 1H), 1.68-1.75 (m, 2H), 1.80-1.86 (m, 1H)

3.57 (t, J = 7.0, 2H), 3.84 (s, 6H), 3.86 (s, 3H), 3.87 (s, 3H), 4.61 (t, J = 7.0, 1H), 6.67 (m, 2H), 6.76 (d, J = 7.8 Hz, 1H), 6.82 (m, 2H), 6.87 (s, 1H).

3.3.42 Synthesis of compund 72

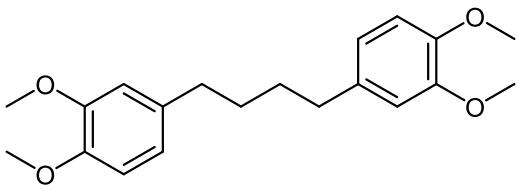

Compound **70** (2.3 g, 6.64 mmol) was treated with excess hydrogen gas as described for **28** to afford **71** in 91% yield. ^{1}H NMR (500 MHz, $CDCl_3$): δ (ppm) 1.65 (s, 4H), 2.58 (s, 4H), 3.85 (s, 12H) 6.70 (m, 4H), 6.79 (m, 2H).

3.3.43 Synthesis of 4,4'-butane-1,4-diyldibenzene-1,2-diol (A6)

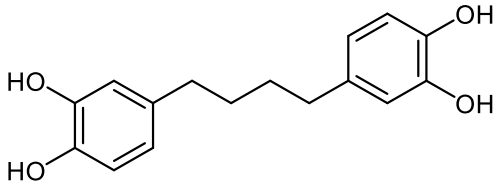

Compound **71** (0.61 g, 1.83 mmol) was demethylated with BBr_3 in DCM as described for **A1** to afford A6 as brown solid (> 99%).^{1}H NMR (500 MHz, CD_3OD): δ (ppm) 1.52 (4H, s, H8, 8'), 2.43 (4H, s, H7, 7'), 6.44 (2H, d, J = 8.0, H6, 6'), 6.56 (2H, s, H2, 2'), 6.63 (2H, d, J = 8.0, H5, 5'). ^{13}C NMR (500 MHz, CD_3OD): δ (ppm) 32.58 (C8, 8'), 36.26 (C7, 7'), 116.31 (C6, 6'), 116.64 (C5, 5'), 120.78 (C2, 2'), 135.75 (C1, 1'), 144.20 (C4, 4'), 146.13 (C3, 3').

3.4 Characterization of NDGA Analogues

3.4.1 High Performance Liquid Chromatography (HPLC) Analyses

A reverse phase, high performance liquid chromatography (RP-HPLC) method was developed to determine purity of the prepared analogues. Standard NDGA was run alongside for comparison. The RP-HPLC method employed a 150 × 2.1 mm Hypersil GOLD, ODS 3µ, microbore column at a flow rate of 200 µL/min using gradient elution. Solvent A consisted of water with 0.1% formic acid and Solvent B was acetonitrile containing 0.1% formic acid. A gradient of 90% A for 2 min, decreased to 60% A over 10 min, then 10% A over 5 min, held isocratic for 10 min, returned to 90% A in 5min and held isocratic for 2 min. All eluates were monitored by UV diode array detection.

3.4.2 Nuclear Magnetic Resonance (NMR) Spectroscopy Experiments

The prepared analogues were characterized by ^{1}H-NMR, 2-D COSY and ^{13}C-NMR experiments.

3.4.3 Mass Spectroscopy Experiments

The molecular masses of the prepared analogues were confirmed by ESI-MS analyses. The molecular ions and isotopic masses were determined by Enhanced Resolution (ER) scanning in negative ionization mode. Fragmentation patterns were studied by tandem ESI-MS/MS in negative ion mode. Tandem ESI-MS/MS data for NDGA was obtained for comparison. Instrument parameters were set as follows: Cur = 0, Temp = 200, GS1 = 14, GS2 = 40, ihe = on, IS = -4500, CAD = high, DP = 50, EP = -10, CE = -40 and CXP = -15.

3.4.4 Characterization of NDGA

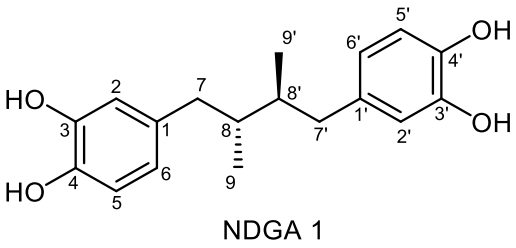

NDGA 1

Figure 2-1: Molecular structure of NDGA ($C_{18}H_{22}O_4$, 302.36 g/mol)

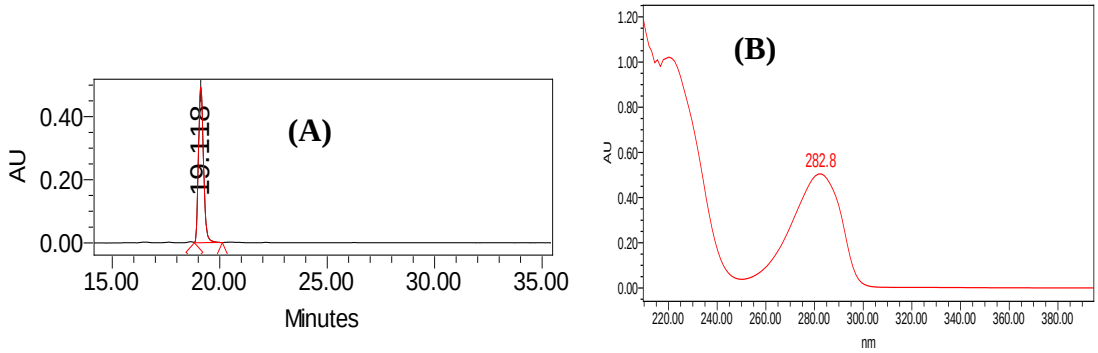

Figure 2-2: HPLC chromatogram (Panel A) and UV absorption maxima (Panel B) for NDGA.

A retention time of 19.1 min by the method described in section 3.4.1 was observed with a characteristic absorption at 282.8 nm obtained by UV-PDA detection.

Summary of NMR data for NDGA

[1H] NMR (500 MHz, DMSO-d6) δ(ppm): 0.74 (6H, d, J=6.6 Hz, H9,9'), 1.60 (2H, m, H8,8'), 2.09 (2H, dd, J=4.8, 13.3 Hz, H7α,7'α), 2.56 (2H, dd, J=9.3, 13.2 Hz, H7β,7'β), 6.38 (2H, dd, J=1.8, 7.8 Hz, H6,6'), 6.52 (2H, d, J=1.8 Hz, H2,2'), 6.61 (2H, d, J=7.8 Hz, H5,5'), 8.58b (2H, s, o,p Ar-OH), 8.65b (2H, s, o,p Ar-OH)

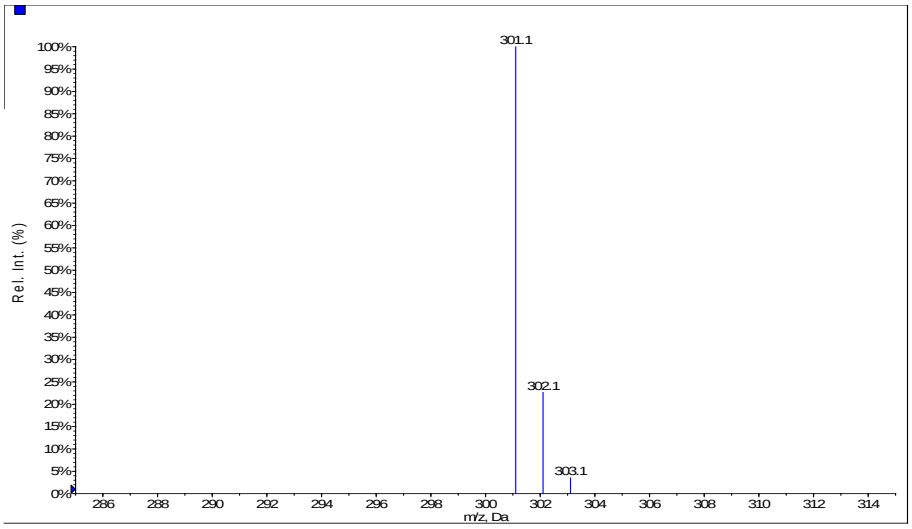

Figure 2-3: ER-ESI-MS in negative ionization mode for NDGA

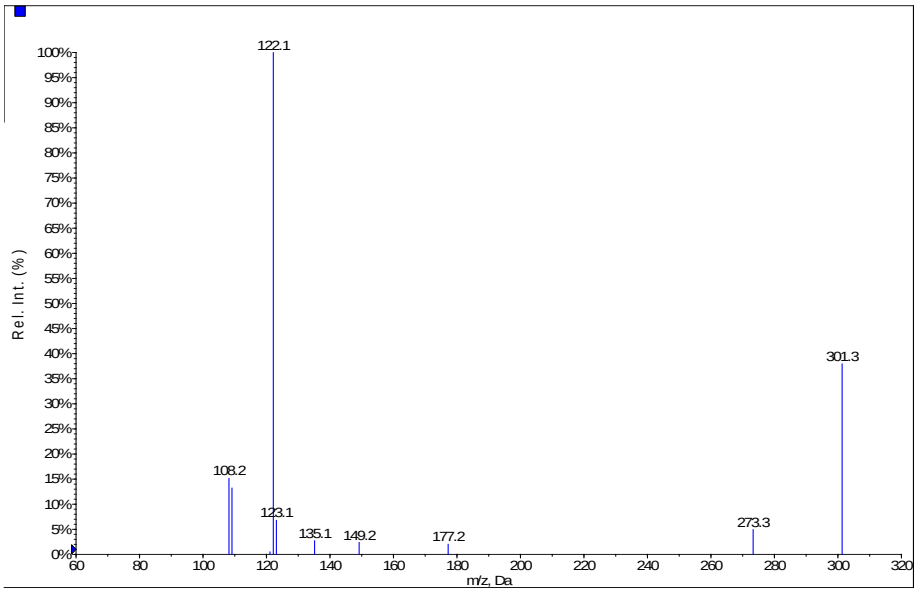

Figure 2-4: Tandem ESI-MS/MS in negative ionization mode for NDGA.

A *m/z* 301.1 was observed consistent with calculated mass of NDGA **1** (302.36 g) based on molecular formula ($C_{18}H_{22}O_4$). Product ions observed were consistent with predicted fragmentation patterns NDGA with a base peak at *m/z* 122.1 Da.

3.4.5 Characterization of A1

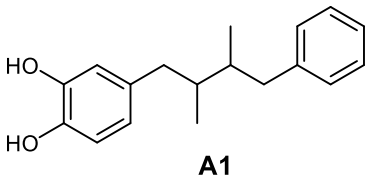

Figure 2-5: Molecular structure of **A1** ($C_{18}H_{22}O_2$, 270.36 g/mol).

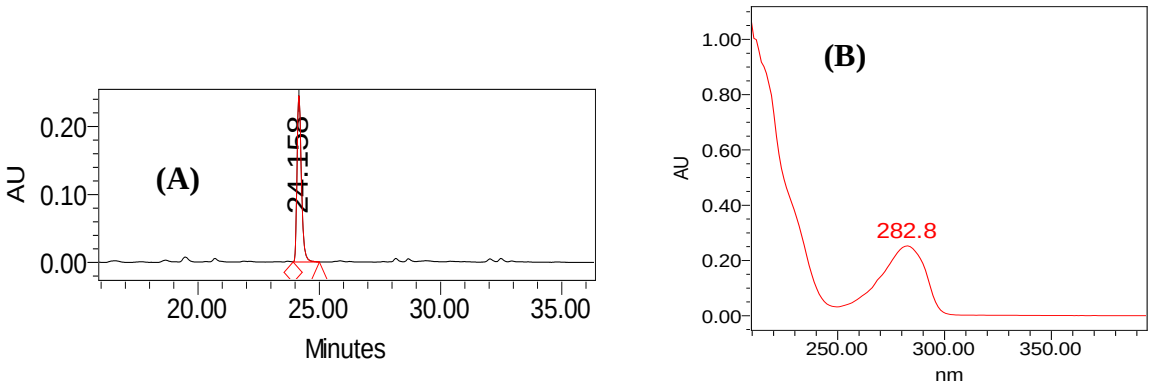

Figure 2-6: HPLC chromatogram (Panel A) and UV absorption maximum (Panel B) for **A1.**

A retention time of 24.2 min by the method described in section 3.4.1 was observed with a characteristic absorption at 282.8 nm obtained by UV-PDA detection.

Summary of NMR data for **A1**

[^{1}H] NMR (500 MHz, $CDCl_3$): δ (ppm) 0.84-0.87 (6H, 2×d, J = 4.3, H9, 9'), 1.74-1.84 (2H, m, H8, 8'), 2.32-2.36 (1H, dd, J = 8.5, 13.4, H7α), 2.43-2.48 (1H, dd, J = 8.6, 13.4, H7α'), 2.55-2.59 (1H, dd, J = 6.4, 13.6, H7β), 2.66-2.70 (1H, dd, J = 6.2, 13.6, H7β'), 5.78 (2H, bs, o, p-ArO<u>H</u>), 6.55-6.57

(1H, dd, J = 1.9, 8.1, H6), 6.64 (1H, d, J = 1.9, H2), 6.79 (1H, d, J = 7.9, H5), 7.14 (2H, d, J = 7.2, H2', 6'), 7.21 (1H, t, J = 7.4, H4'), 7.30 (2H, t, H3', 5').

[^{13}C] NMR (500 MHz, $CDCl_3$): δ (ppm) 13.97, 16.24, 38.10, 39.33, 40.67, 41.45, 115.18, 116.08, 121.55, 125.64, 128.17, 128.23, 129.13, 129.17, 134.89, 141.28, 141.78, 143.25.

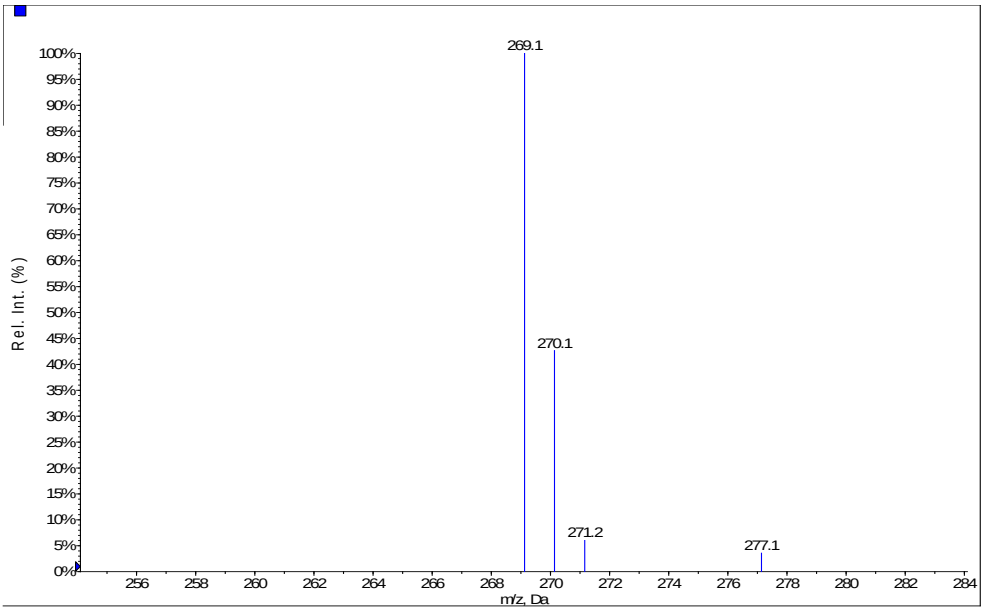

Figure 2-7: ER-ESI-MS in negative ionization mode for **A1**.

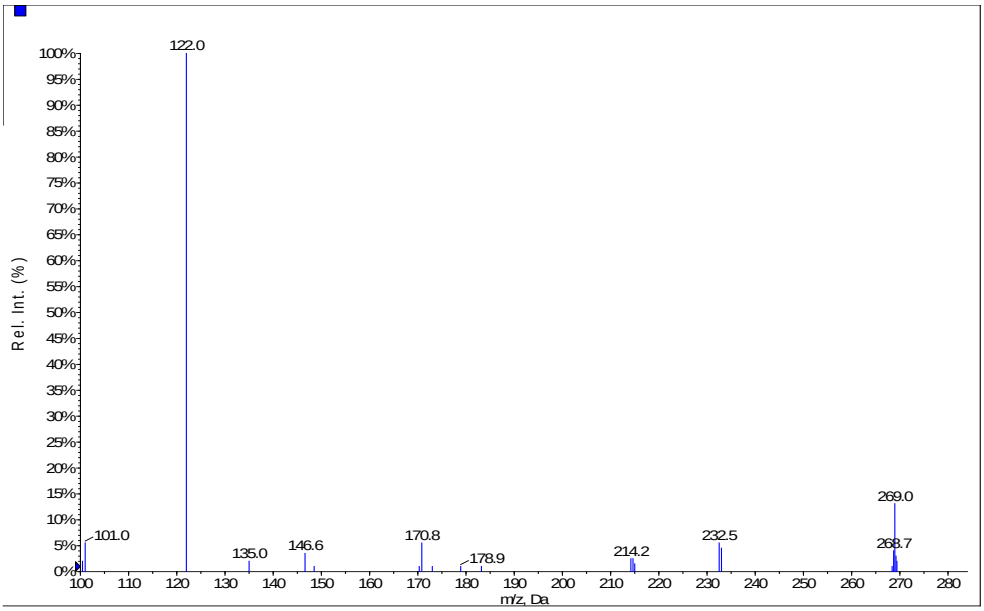

Figure 2-8: Tandem ESI-MS/MS in negative ionization mode for **A1**.

A *m/z* 269.1 was observed consistent with calculated mass of **A1** (270.36 g) based on molecular formula ($C_{18}H_{22}O_2$). Product ions observed were consistent with fragmentation patterns observed for standard NDGA with a base peak at *m/z* 122.0 Da.

3.4.6 Characterization of A2

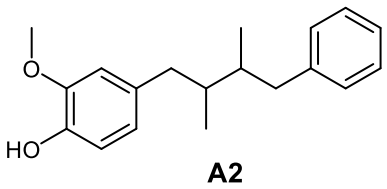

A2

Figure 2-9: Molecular structure of **A2** ($C_{19}H_{24}O_2$, 284.39 g/mol).

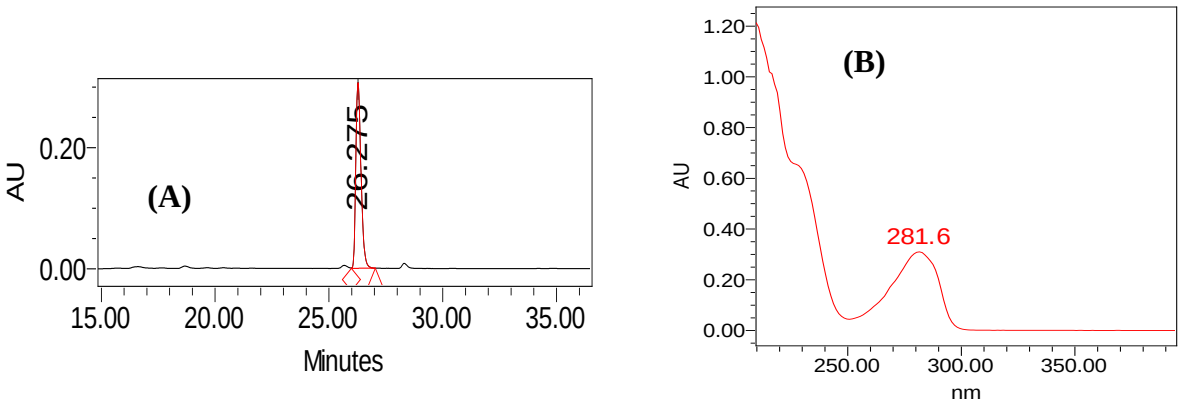

Figure 2-10: HPLC chromatogram (Panel A) and UV absorption maximum (Panel B) for **A2**.

A retention time of 26.3 min by the method described in section 3.4.1 was observed with a characteristic absorption at 281.6 nm obtained by UV-PDA detection.

Summary of NMR data for **A2**

^{1}H NMR (500 MHz, $CDCl_3$): δ (ppm) 0.86-0.88 (6H, d×2, H9, 9'), 1.77-1.85 (2H, m, H8, 8'), 2.38-2.49 (2H, m, H7α, 7α'), 2.57-2.68 (2H, m, H7β, H7β'), 3.84 (3H, s, OC$\underline{H_3}$), 5.51 (1H, bs, p-ArO$\underline{H}$), 6.58 (s, 1H), 6.62-6.65 (1H, m,), 6.84-6.88 (1H, m,), 7.13 (d, J = 7.2, 1H), 7.18-7.23 (m, 2H), 7.23-7.33 (m, 2H).

^{13}C NMR (500 MHz, $CDCl_3$): δ (ppm) 13.95, 16.11, 37.81, 38.94, 41.09, 41.45, 55.84, 111.34, 113.97, 121.67, 125.64, 128.15, 129.08, 133.57, 141.73, 143.55, 146.29.

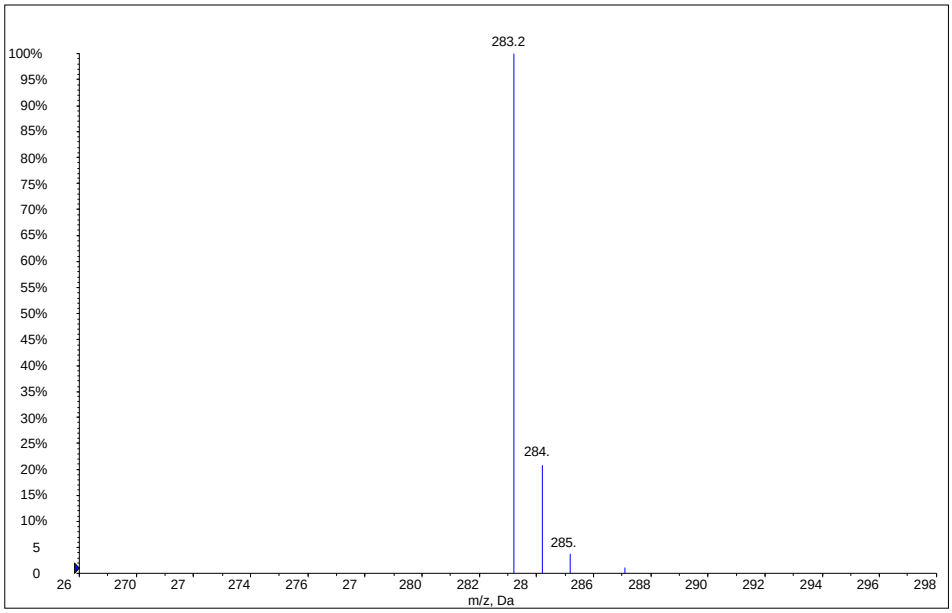

Figure 2-11: ER-ESI-MS in negative ionization mode for **A2**.

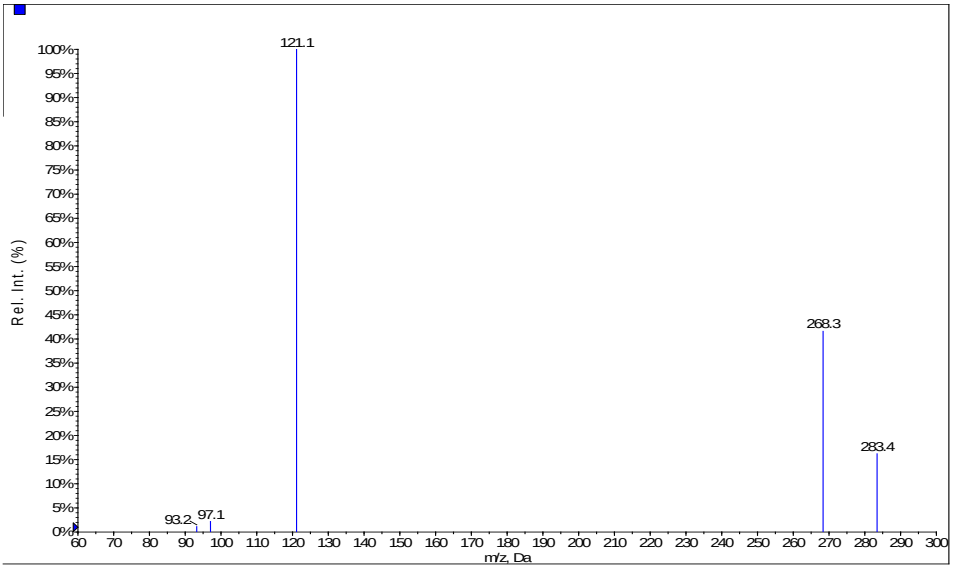

Figure 2-12: Tandem ESI-MS/MS in negative ionization mode for **A2**.

A *m/z* 283.2 was observed consistent with calculated mass of **A2** (284.39 g) based on molecular formula ($C_{19}H_{24}O_2$). Product ions observed were consistent with fragmentation patterns observed for standard NDGA with a base peak at *m/z* 121.0 Da.

3.4.7 Characterization of A3

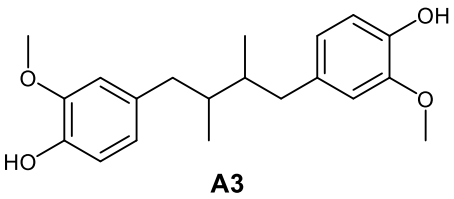

A3

Figure 2-13: Molecular structure of **A3** ($C_{20}H_{26}O_4$, 330.42 g/mol).

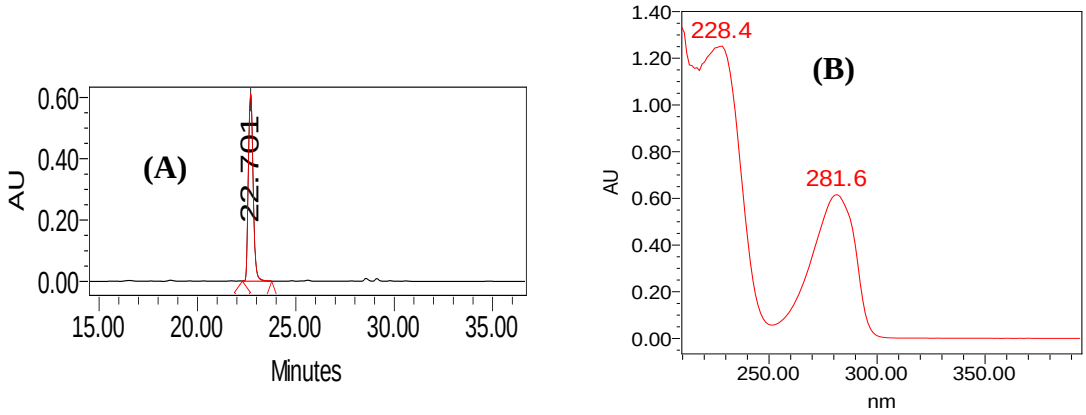

Figure 2-14: HPLC chromatogram (Panel A) and UV absorption (Panel B) for **A3**.

A retention time of 22.7 min by the method described in section 3.4.1 was observed with a characteristic absorption at 281.6 nm obtained by UV-PDA detection.

Summary of NMR data for **A3**

A3a, ^{1}H NMR (500 MHz, $CDCl_3$): δ (ppm) 0.83-0.86 (6H, 2×d, J = 6.4, H9, 9'), 1.72-1.76 (2H, m, H8, 8'), 2.26-2.32 (1H, dd, J = ,H7α), 2.37-2.41 (1H, dd, J = 7.4, 13.4, H7α'), 2.51-2.55 (1H, dd, J = 7.4, 13.7, H7β), 2.72-2.76 (1H, dd, J = 4.1, 12.9, H7β'), 3.82 (3H, s, *p*-OC<u>H</u>$_3$), 3.87 (3H, s, *o*-OC<u>H</u>$_3$), 5.58 (2H, bs, p-ArO<u>H</u>), 6.55 (1H, s, H2), 6.60 (1H d, J = 7.8, H6), 6.64 (1H, s, H2'), 6.68 (1H, d, J = 7.8, H6'), 6.83 (1H, d, J = 8.0, H5), 6.85 (1H, d, J = 8.0, H5')

^{13}C NMR (500 MHz, $CDCl_3$) δ (ppm) 14.04, 16.40, 21.25, 37.62, 39.07, 39.36, 41.26, 55.95, 56.03, 60.62, 111.46, 111.61, 114.04, 114.15, 121.81, 121.89, 133.77, 133.97, 143.67, 143.73, 146.42, 146.50.

A3b, δ (ppm) 0.83-0.86 (6H, 2×d, J = 6.8, H9, 9'), 1.72-1.76 (2H, m, H8, 8'), 2.28-2.32 (1H, dd, J = 9.3, 13.3 ,H7α), 2.37-2.42 (1H, dd, J = 7.7, 13.7, H7α'), 2.51-2.55 (1H, dd, J = 7.3, 13.7, H7β), 2.72-2.76 (1H, dd, J = 5.2, 13.7, H7β'), 3.82 (s, 3H, *p*-OC<u>H</u>$_3$), 3.87 (s, 3H, *o*-OC<u>H</u>$_3$), 5.50 (bs, 2H, p-ArO<u>H</u>), 6.53 (1H, s, H2), 6.60 (1H, d, J = 7.7, H6), 6.63 (1H, s, H2'), 6.68 (1H, d, J = 8.0, H6'), 6.81 (1H, d, J = 7.7, H5), 6.84 (1H, d, J = 7.7, H5')

^{13}C NMR (500 MHz, $CDCl_3$) δ (ppm) 13.89, 16.25, 37.45, 38.91, 39.21, 41.10, 55.79, 55.87, 111.31, 111.47, 113.89, 114.00, 121.66, 121.74, 133.62, 133.82, 143.51, 143.57, 146.27, 146.34.

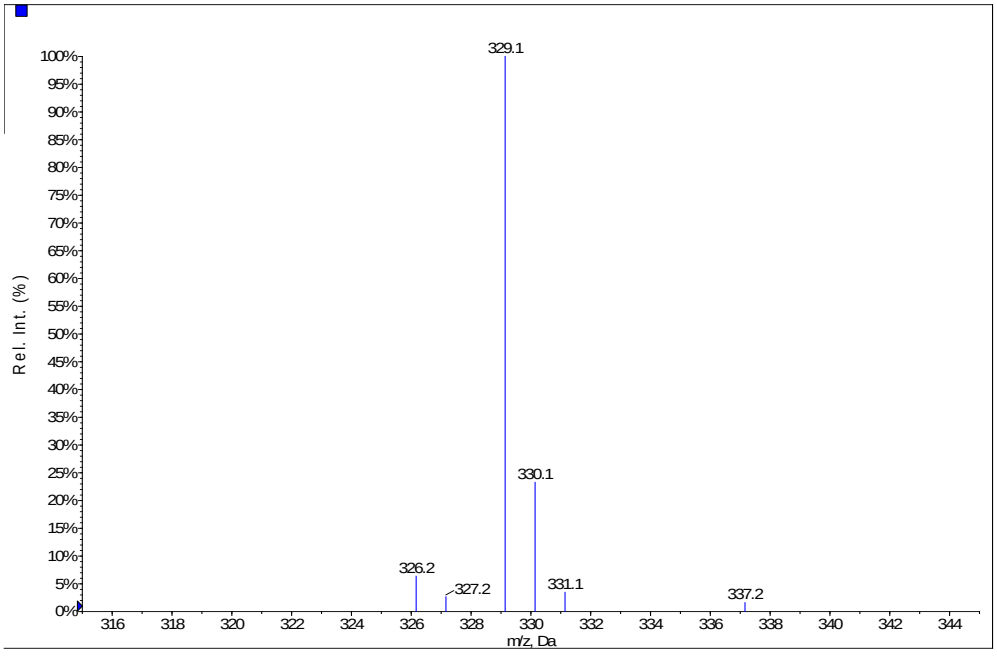

Figure 2-15: ER-ESI-MS in negative ionization mode for **A3**.

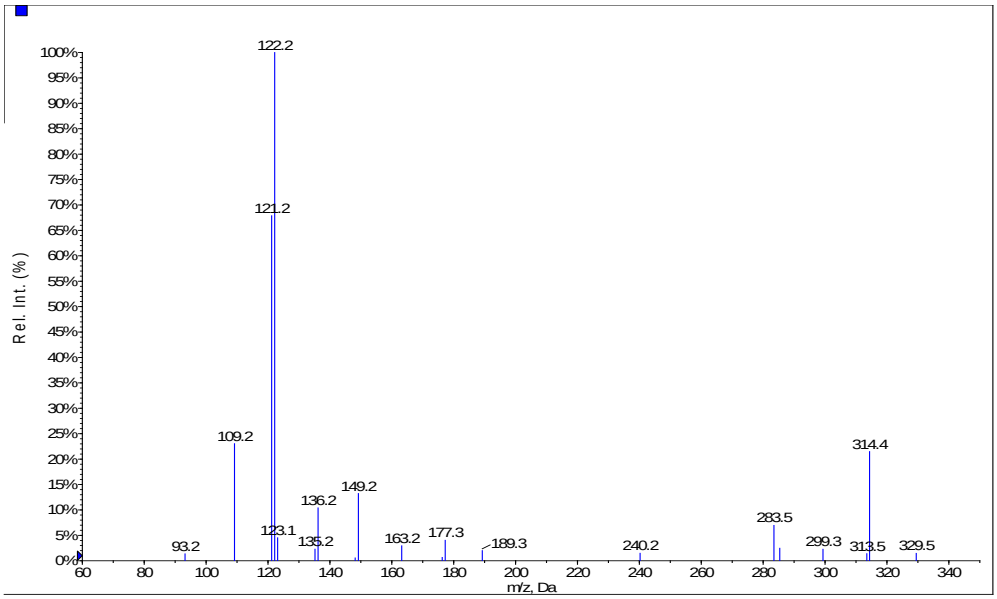

Figure 2-16: Tandem ESI-MS/MS in negative ionization mode for **A3.**

A *m/z* 329.1 was observed consistent with calculated mass of **A3** (330.42 g) based on molecular formula ($C_{20}H_{26}O_4$). Product ions observed were consistent with fragmentation patterns observed for standard NDGA with a base peak at *m/z* 122.3 Da.

3.4.8 Characterization of A4

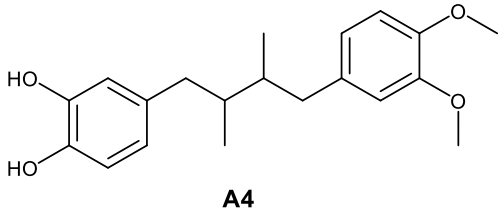

A4

Figure 2-17: Molecular structure of **A4** ($C_{20}H_{26}O_4$, 330.42 g/mol).

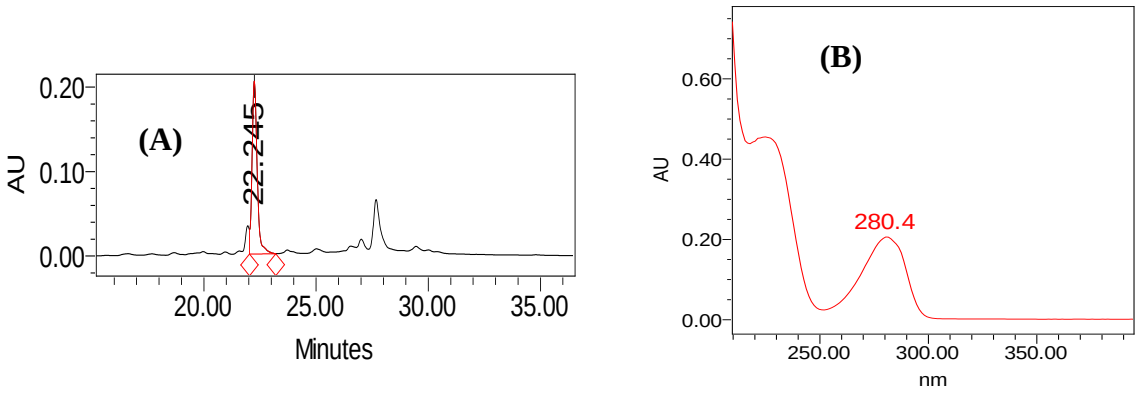

Figure 2-18: HPLC chromatogram (Panel A) and UV absorption maximum (Panel B) for **A4**.

A retention time of 22.2 min by the method described in section 3.4.1 was observed with a characteristic absorption at 280.4 nm obtained by UV-PDA detection.

Summary of NMR data for **A4**

A4a, ^{1}H NMR (500 MHz, $CDCl_3$): δ (ppm) 0.81-0.83 (6H, overlapping d, J = 4.5, H9, 9'), 1.69-1.76 (2H, m, H8, 8'), 2.31- 2.33 (2H, dd, J = 7.8, 13.4, H7α), 2.38-2.42 (1H, dd, J = 7.7, 13.4, 7α'), 2.46-2.51 (1H, dd, J = 7.0, 13.3, H7β), 2.51-2.55 (1H, dd, J = 7.3, 13.5, 7β'), 3.82 (3H, s, *p*-OC$\underline{H}_3$), 3.86 (3H, s, *o*-OC$\underline{H}_3$), 6.50 (1H, d, J = 6.2), 6.56 (1H, s), 6.58 (1H, s), 6.77-6.78 (m, 2H),

^{13}C NMR (500 MHz, MeOD): δ (ppm) 13.82, 13.89, 37.31, 37.44, 40.69, 40.98, 55.89, 55.92, 110.99, 112.28, 115.04, 115.96, 121.16, 121.49, 134.40, 134.69, 141.52, 143.29, 146.96, 148.55.

A4b, ^{1}H NMR (500 MHz, $CDCl_3$): δ (ppm) 0.81-0.85 (6H, overlapping d, J = 6.3, H9, 9'), 1.69-1.76 (2H, m, H8, 8'), 2.24-2-29 (m, 1H), 2.31-2.42 (m, 1H), 2.46-2.56 (m, 1H), 2.67-2.75 (2H, m), 3.82 (3H, s), 3.86 (3H, s), 6.55 (2H, m), 6.67 (2H, m), 6.79 (2H, m)

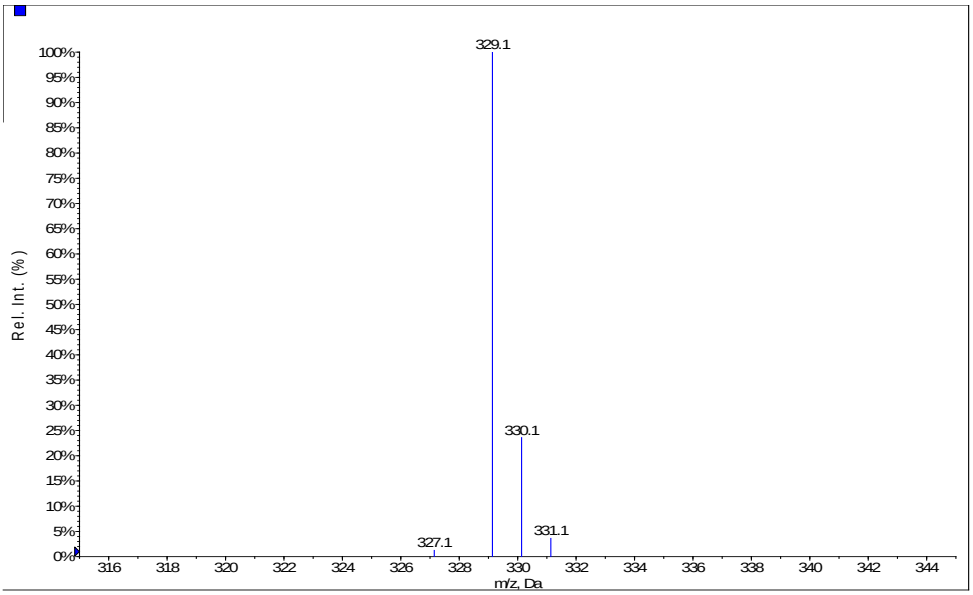

Figure 2-19: ER-ESI-MS in negative ionization mode for **A4**.

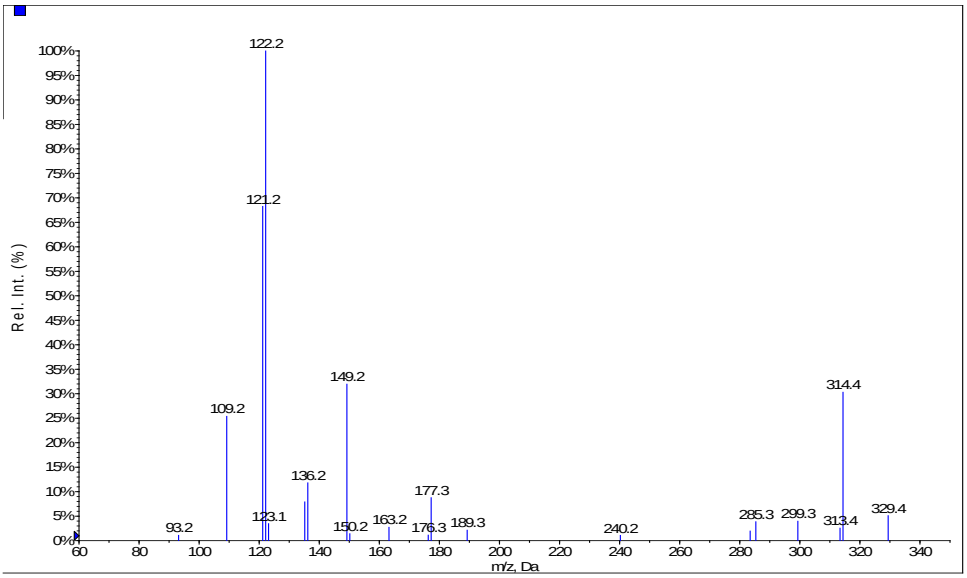

Figure 2-20: Tandem ESI-MS/MS in negative ionization mode for **A4**.

A *m/z* 329.1 was observed consistent with calculated mass of **A4** (330.42) based on molecular formula ($C_{20}H_{26}O_4$). Product ions observed were consistent with fragmentation patterns observed for standard NDGA with a base peak at *m/z* 122.2 Da

3.4.9 Characterization of A6

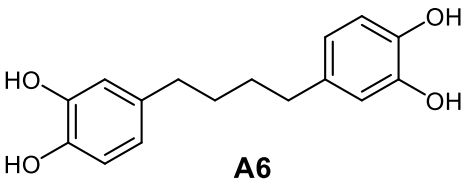

Figure 2-21: Molecular structure of **A6** ($C_{16}H_{18}O_4$, 274.31 g/mol).

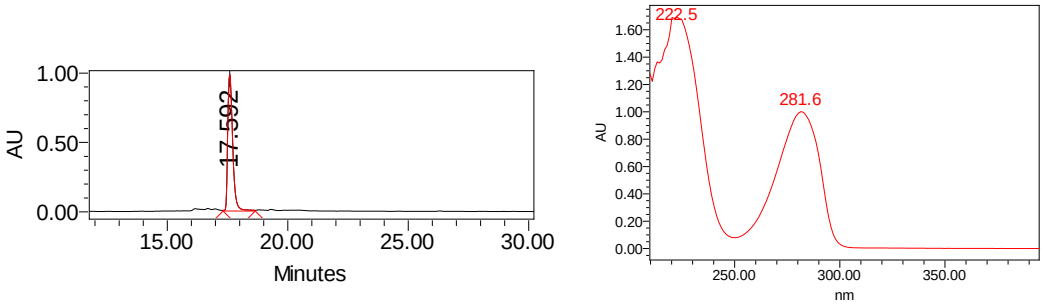

Figure 2-22: HPLC chromatogram (Panel A) and UV absorption for **A6**.

A retention time of 17.5 min by the method described in section 3.4.1 was observed with a characteristic absorption at 281.6 nm obtained by UV-PDA detection

Summary of NMR data for **A6**

^{1}H NMR (500 MHz, CD_3OD): δ (ppm) 1.52 (4H, s, H8, 8'), 2.43 (4H, s, H7, 7'), 6.44 (2H, d, J = 8.0, H6, 6'), 6.56 (2H, s, H2, 2'), 6.63 (2H, d, J = 8.0, H5, 5')

^{13}C NMR (500 MHz, CD_3OD): δ (ppm) 32.58 (C8, 8'), 36.26 (C7, 7'), 116.31 (C6, 6'), 116.64 (C5, 5'), 120.78 (C2, 2'), 135.75 (C1, 1'), 144.20 (C4, 4'), 146.13 (C3, 3')

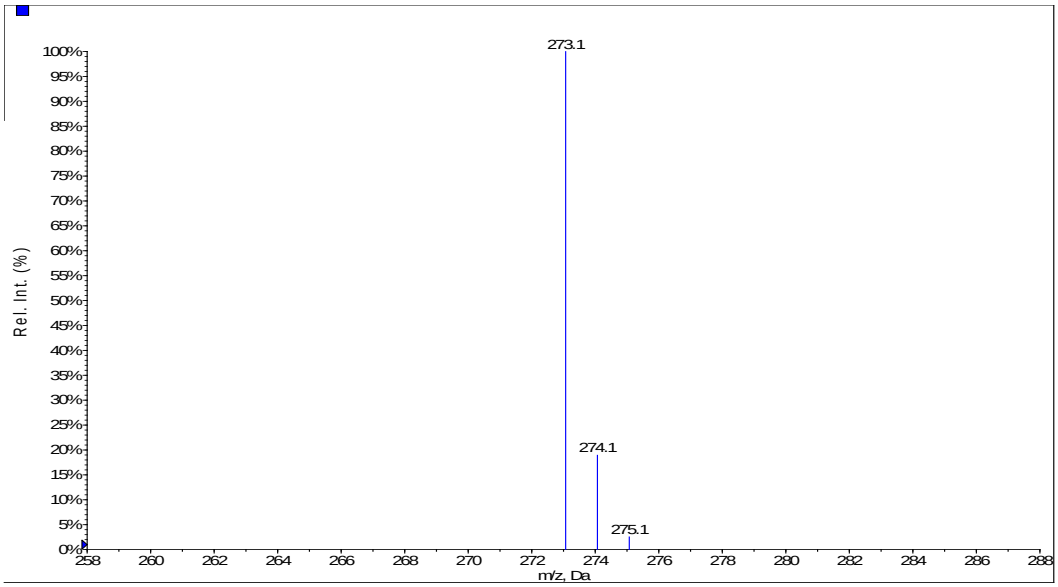

Figure 2-23: ER-ESI-MS in negative ionization mode for **A6**.

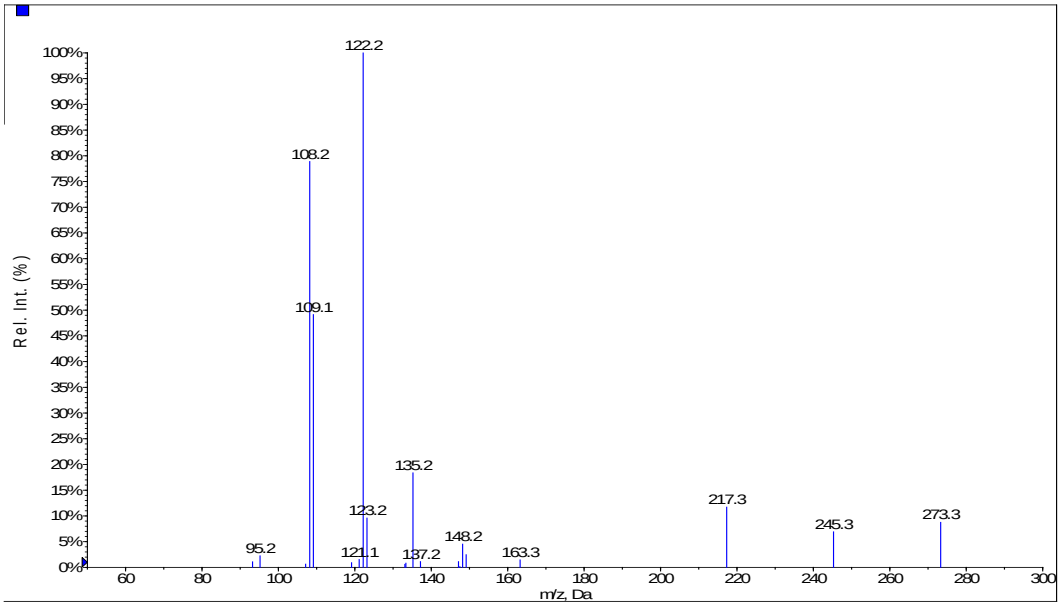

Figure 2-24: Tandem ESI-MS/MS in negative ionization mode for **A6**.

A *m/z* 273.1 was observed consistent with calculated mass of **A6** (274.31 g) based on molecular formula ($C_{16}H_{18}O_4$). Product ions observed were consistent with fragmentation patterns observed for standard NDGA with a base peak at *m/z* 122.2 Da.

3.4.10 Characterization of A7

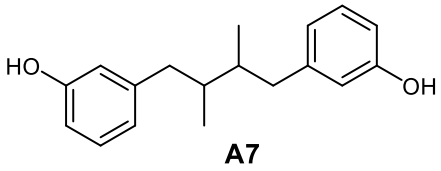

A7

Figure 2-25: Molecular structure of **A7** ($C_{18}H_{22}O_2$, 270.36 g/mol).

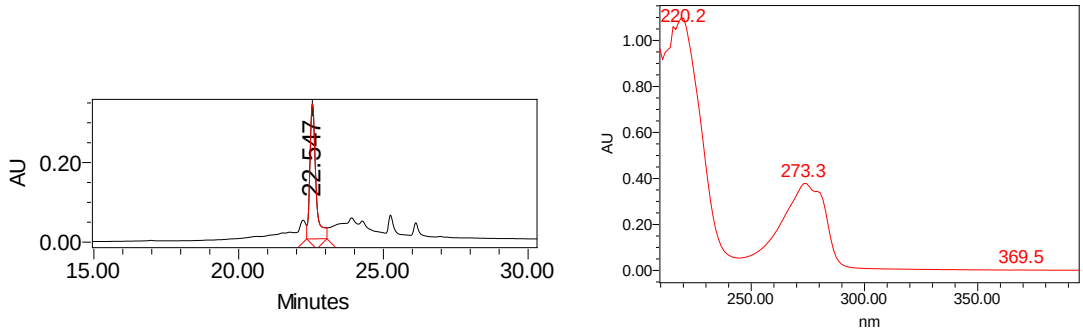

Figure 2-26: HPLC chromatogram (Panel A) and UV absorption for **A7**.

A retention time of 22.5 min by the method described in section 3.4.1 was observed with a absorption at 273.3 nm obtained by UV-PDA detection

Summary of NMR data for **A7**

^{1}H NMR (500 MHz, $CDCl_3$): δ (ppm) 0.87-0.89 (6H, 2×d, J = 6.5, H9, 9'), 1.61-1.69 (2H, m, H8, 8'), 2.32-2.36 (2H, dd, J = 8.3, 13.3, H7α, H7α'), 2.59-2.63 (2H, dd, J = 6.3, 13.4, H7β, H7β'), 5.56 (2H, bs, ArO<u>H</u>), 6.68-6.60 (2H, s), 6.70 (1H, d, J = 1.6), 6.76 (2H, d, J = 7.3), 6.83-6.86 (1H, m), 7.14-7.17 (2H, m)

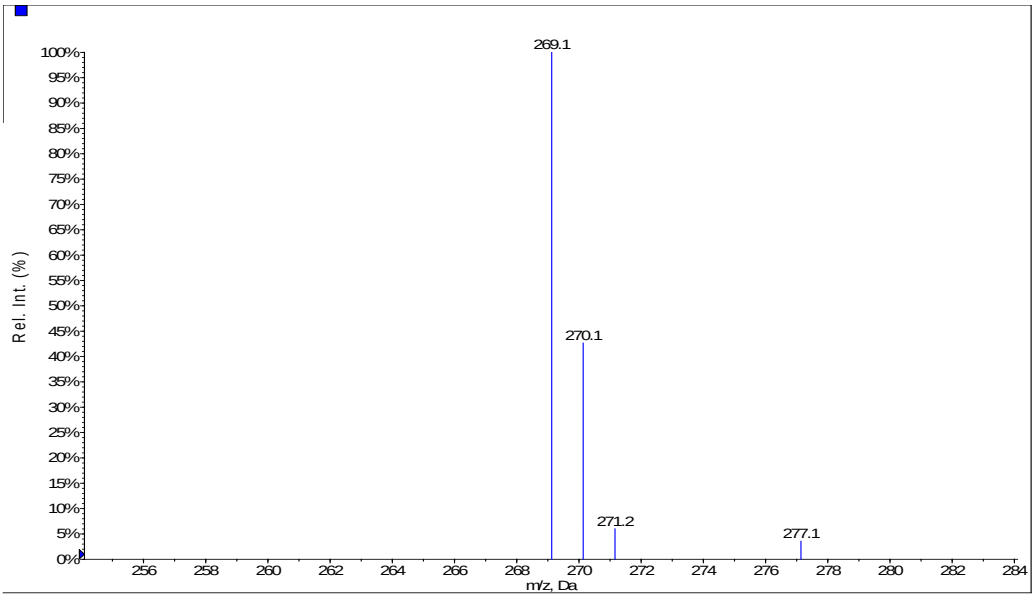

Figure 2-27: ER-ESI-MS in negative ionization mode for **A7**.

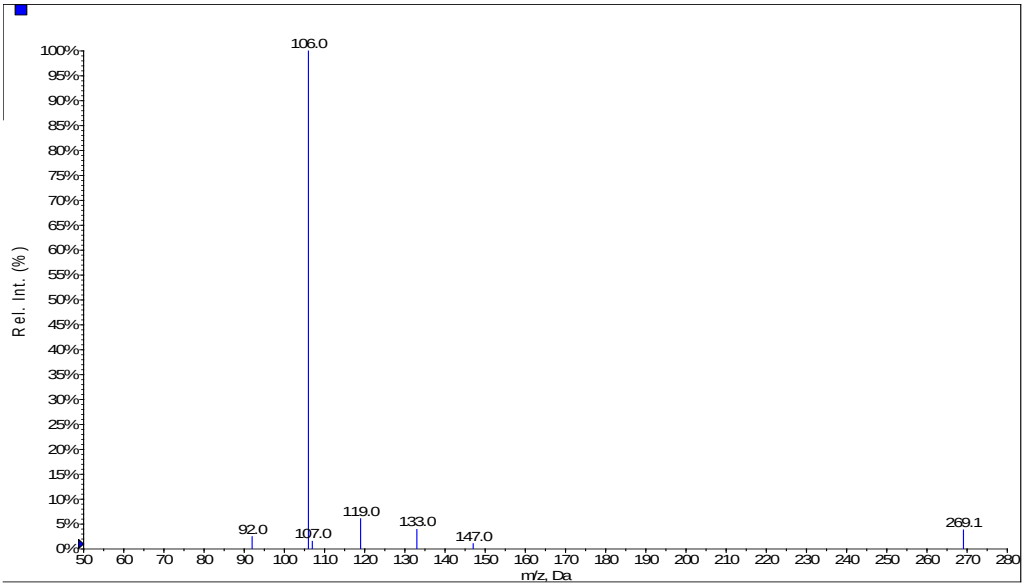

Figure 2-28: Tandem ESI-MS/MS in negative ionization mode for **A7**.

A *m/z* 269.1 was observed consistent with calculated mass of **A7** (270.36 g) based on molecular formula ($C_{18}H_{22}O_2$). Product ions observed were consistent with fragmentation patterns observed for standard NDGA with a base peak at *m/z* 106.0 Da.

3.4.11 Characterization of A8

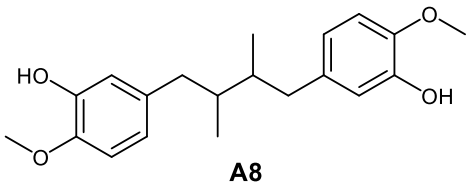

A8

Figure 2-29: Molecular structure of **A8** ($C_{20}H_{26}O_4$, 330.42 g/mol).

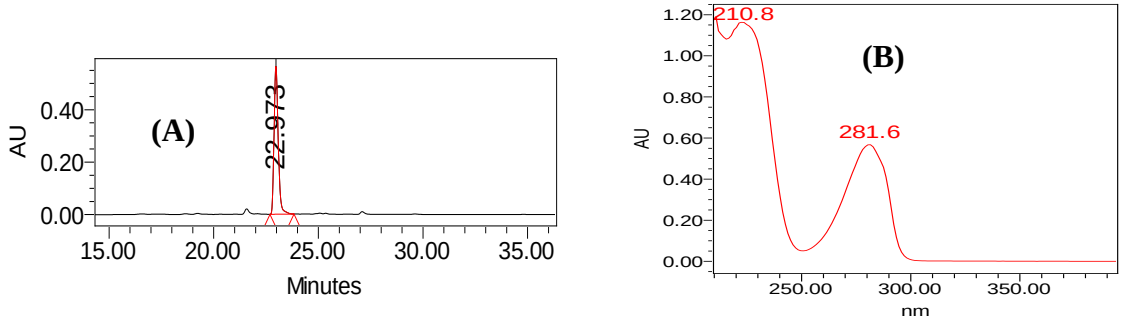

Figure 2-30: HPLC chromatogram (Panel A) and UV absorption maximum (Panel B) for **A8**.

A retention time of 22.9 min by the method described in section 3.4.1 was observed with a characteristic absorption at 281.6 nm obtained by UV-PDA detection.

Summary of NMR data for **A8**

A8a, ^{1}H NMR (500 MHz, $CDCl_3$): δ (ppm) 0.80-0.84 (6H, 2×d, J = 6.7, H9, 9'), 1.74-1.78 (2H, m, H8, 8'), 2.22-2.27 (1H, dd, J = 9.6, 13.3, H7α), 2.31-2.35 (1H, dd, J = 7.9, 12.8, H7α'), 2.54-2.58 (1H, dd, J = 5.8, 13.5, H7β), 2.70-2.74 (1H, dd, J = 4.5, 13.4, H7β'), 3.89 (6H, s, 3,3' OC<u>H</u>$_3$), 5.58 (2H, bs, ArO<u>H</u>), 6.58-6.60 (1H, dd, J = 1.6, 8.1), 6.63-6.65 (1H, dd, J = 1.6, 8.1), 6.71 (1H, d, J = 1.6), 6.75-6.79 (3H, m)

A8b, ^{1}H NMR (500 MHz, $CDCl_3$): δ (ppm) 0.81-0.84 (6H, 2×d, H9, 9'), 1.73-1.79 (2H, m, H8, 8'), 2.23-2.28 (1H, dd, J = 9.5, 13.3, H7α), 2.32-2.36 (1H, dd, J = 8.5, 13.5, H7α'), 2.55-2.59 (1H, dd, J = 5.8, 13.5, H7β), 2.71-2.74 (1H, dd, J = 4.6, 13.4, H7β'), 3.87 (6H, s, 3,3' OC<u>H</u>$_3$), 5.68 (2H, bs, ArO<u>H</u>), 6.59-6.61 (1H, dd, J = 1.7, 7.9), 6.64-6.66 (1H, dd, J = 1.7, 7.9), 6.71 (1H, d, J = 1.7), 6.75-6. 79 (3H, m)

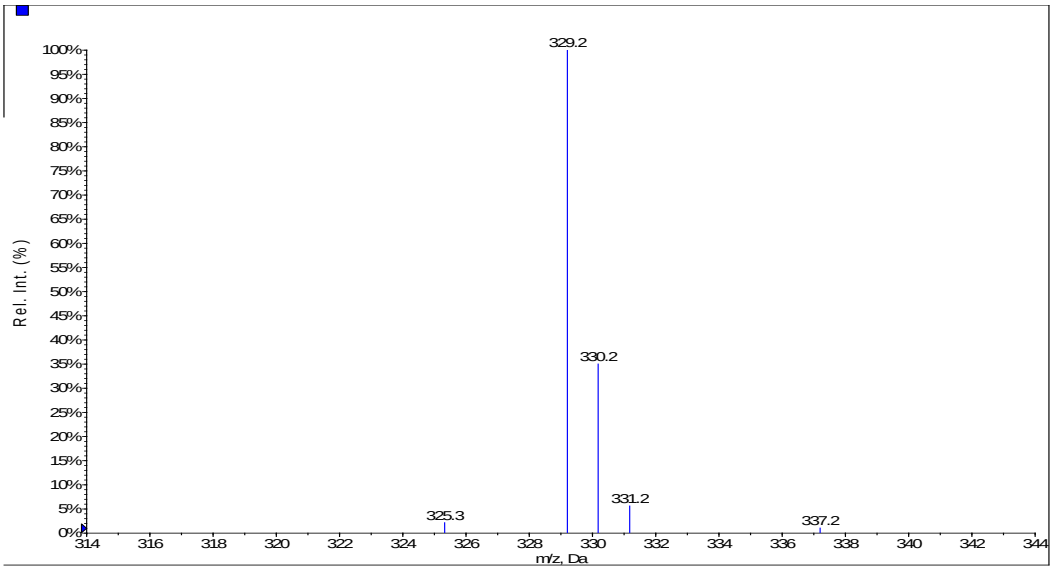

Figure 2-31: ER-ESI-MS in negative ionization mode for **A8**.

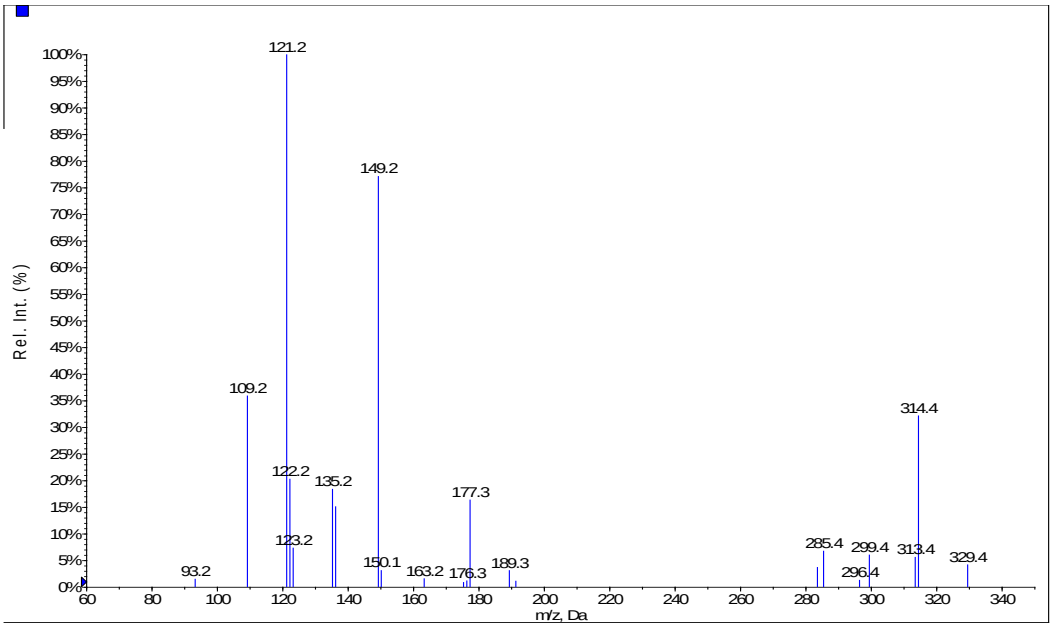

Figure 2-32: Tandem ESI-MS/MS in negative ionization mode for **A8**.

A *m/z* 329.2 was observed consistent with calculated mass of **A8** (330.42 g) based on molecular formula ($C_{20}H_{26}O_4$). Product ions observed were consistent with fragmentation patterns observed for standard NDGA with a base peak at *m/z* 121 Da.

Table 2-1: Summary of ESI-MS analyses data for NDGA and its analogues.

Compound (M)	[a][M-H]- found	[b][M-H]- calcd	[c]Product ion following CID	[a]Isotopic Peaks
NDGA (302)	301.1	301.1	177, 149, 135, **122**, 109	301.1, 302.1, 303.1
A1 (270)	269.1	269.2	149, 135, **122**, 108	269.1, 270.1, 271.1
A2 (284)	283.2	283.2	268, **121**	283.2, 284.2. 285.2
A3 (330)	329.1	329.2	314, 177, 149, 136, **122**, 109	329.1, 330.1, 331.1
A4 (330)	329.1	329.2	314, 177, 149, 136, **122**, 109	329.1, 330.1, 331.1
A6 (274)	273.1	273.1	245, 217, 149, 135, **122**, 109	273.1, 274.1, 275.1
A7 (270)	269.1	269.1	147, 133, 119, **106**	269.1, 270.1, 271.2
A8 (330)	329.1	239.2	314, 177, 149, 135, **121**, 109	329.1, 330.1, 331.1

[a]The parent ion and isotopic peaks were determined by ER scanning in negative ion mode. [b]The calculated parent ions were obtained from ACD/ChemSketch software. [c]The product ion determine by MS-MS scannind using the following instrument parameters: CUR = 10, Temp = 200ºC, GS1 = 14, GS2 = 40, ihe = on, IS = 4500, CAD = high, DP = -50, EP = -10, CE = -30 to -55, CXP = -15. The boldface type denotes base peak.

3.5 Experimental 2: Autoxidative Cyclization Potential of NDGA Analogues

3.5.1 General HPLC Method

An HPLC method was developed to monitor autoxidation and glutathione trapping experiments. The RP-HPLC method employed a 150 × 2.1 mm Hypersil GOLD, ODS 3µ, microbore column at a flow rate of 200 µL/min using gradient elution. Solvent A consisted of water with 0.1% formic acid and Solvent B was acetonitrile containing 0.1% formic acid. An initial isocratic phase of 90% A for 2 min, decreased to 60% A over 8 min, then 10% A over 12 min, held isocratic for 10 min, and finally increased to 90% A over 1 min and held isocratic at 90% A for 6 min to equilibrate the column. All eluates were monitored by UV diode array detection.

3.5.2 Autoxidative Cyclization Studies

The potential of the prepared analogues to autoxidize to their corresponding dibenzocyclooctadiene lignans was examined using a method developed by Billinsky et al.[35] Briefly, the substrate in CH_3CN (20 mM) is added to phosphate-citric acid buffer (0.5 M, pH 8.5) pre-equilibrated to 37 °C to give a final substrate concentration of 0.1 mM. The reaction mixture was stirred at the same temperature for 90 min and monitored by HPLC. The reaction was stopped by acidification to pH 1.5 with HCl. The mixture was extracted with ethyl acetate, dried over $MgSO_4$ and solvent evaporated in *vacuo.* The oxidation product was purified over a C-18 column (RedSep®Rf GOLD, Teledyne Isco) on a Tris Pump connected to UA-6 UV/Vis Detector (Teledyne Isco) separation system using 70:30 H_2O/CH_3CN (v/v) containing 0.1% formic acid. The product was analyzed by HPLC, MS and NMR techniques. Standard NDGA was used as positive control.

3.5.2.1 Chemical Stability Determination

The test compound in CH_3CN (20 mM) and internal standard (DMPA) were added to a phosphate-citric acid buffer (0.5 M, pH 7.4) pre-equilibrated to 37 °C to give final concentrations of 0.5 mM each. The mixture was incubated at 37 ºC in incubating Orbital Shaker (VWR). Aliquots were taken at various time intervals and the reactions quenched by acidification to pH 1.5 with HCl. Samples were analyzed directly by HPLC. Test analogues were verified by the elution time of standards and quantitated by their corresponding standard curves (R^2 = 0.97-1.0). All calibration curves were developed by plotting peak area ratios of substrate versus internal standard as a function of concentration

3.5.2.2 Dibenzocyclooctadiene Formation via o-Q intermediate

The experiment as described in section 3.5.2.1 was repeated in the absence and presence of GSH (added at time t = 0 h) and also with GSH added in aliquots over time. All samples were treated as in section 3.5.2.1 and analyzed by HPLC. A separate experiment was conducted without and with 20 fold excess of GSH at 37 ºC for 6 h to further investigate the involvement of o-Q intermediate in the intramolecular cyclization process.

3.5.2.3 Reaction Kinetics

The concentrations of the test analogues that remained in solution over time were used to establish the kinetics of the loss of each analogue in phosphate buffer at pH 7.4. The loss of NDGA in phosphate buffer at pH 7.4 follows apparent first-order kinetics.[33] Thus, the disappearance rate of the analogues can be described by:

$$ln\frac{C}{C_o} = -kt$$

where C_o and C are initial concentration and concentration at different time points respectively; k is the reaction rate constant and t is time. A plot of ln C against time is expected to give a straight line with intercept ln C_0 and a gradient -k for a first order degradation reaction.

3.6 Experimental 3: Reactive Metabolites Formation Potential of NDGA Analogues

3.6.1 Enzymatic Oxidation Studies

Each test compound (1 mM), glutathione (5.0 mM) and mushroom tyrosinase (47.25 units) in 500 µl $NA2HPO_4$ buffer (50 mM, pH 6.0) was vortexed for 60 min at room temperature (25 °C). The reaction was stopped by addition of perchloric acid (20 µl). After centrifugation (14,000 for 10 min), aliquots of the supernatant were analyzed directly by HPLC and further by MS. Control experiments were performed in the absence of GSH, in the absence of mushroom tyrosinase, and with the addition of GSH after the 60 min vortex. Each reaction was performed in triplicate.

3.6.1.1 Pilot Enzymatic Oxidation Study

4-Propylbenzene-1,2-diol (PC1) and 2-methoxy-4-propylphenol (PC2) were synthesized from eugenol. The PC1 and PC2 were used as mimics of the catechol analogues (**A1**, **A4** and **A6)** and phenol analogues (**A2, A3, A7 and A8)** respectively. HPLC and MS conditions for oxidative metabolism studies were validated using PC1, PC2 and standard NDGA. The compounds were oxidized as described in section 3.6.1

3.6.1.2 Mushroom Tyrosinase-catalysed Oxidation of the prepared Analogues

The analogues prepared for this study were oxidized with mushroom tyrosinase as described in section 3.6.1 and the oxidation products analyzed by HPLC and MS technique

3.6.1.3 Isomerization of o-Q to p-QM Studies

Analogues **A1** or **A4** was oxidized with mushroom tyrosinase in the presence and absence of GSH for 60 min. For the incubations containing GSH, salicylamide (internal standard) was added at 60 min and quenched with perchloric acid. For the experiments conducted in the absence of GSH, an aliquot was stirred in a phosphate buffer after 60 min incubation and sampled at various time points. To each 1 hour interval aliquot, GSH was added and treated similarly as incubations with GSH. Samples were taken for 8 hours. Samples were analysed by HPLC and LS-MS.

3.6.2 Chemical Oxidation Studies

Freshly prepared silver oxide (300 mg) was added to the test sample in dried acetonitrile (2.5 mM) pre-equibilirated to 60ºC. 1 ml aliquots were taken at 30 s or 30 min and centrifuged at 14,000 for 10 min. The resulting supernatant was added to a potassium phosphate buffer (pH 7.4) containing GSH to a final concentration ratio of 1:5 substrate-GSH. Control experiments contained no GSH and were all performed in duplicates. The samples were analyzed directly by HPLC. For MS analysis, samples were loaded on C-18 extraction cartridges (Bond Elut, Varian) and eluted with methanol.

3.6.2.1 Pilot Chemical Oxidation Studies

The two pilot compounds (PC1 and PC2) and standard NDGA were oxidized as described in section 3.6.2 to validate the oxidation, HPLC and MS method.

3.6.2.2 Silver oxide-catalysed Oxidation of prepared Analogues

The analogues prepared for this study were oxidized with Ag_2O as described in section 3.6.2 and the oxidation products analyzed by HPLC and MS techniques

3.6.3 Cytochrome P450 Oxidation Studies

Test compounds in DMSO (0.5 mM) were incubated in N**A2**HPO_4 buffer (50 mM, pH 7.4) containing GSH (5 mM), rat liver microsomes (0.5 mg/ml) and $MgCl_2$ at 37 °C for 60 min. The final reaction volume (500 µl) contained 0.5% DMSO solvent. The reaction was initiated with NADPH after 5 min pre-incubation and terminated by chilling in ice bath followed by addition of ice cold acetonitrile (200 µl). After centrifugation at 14,000 rpm for 10 min, the supernatant was analyzed by HPLC and LC-MS. Samples for LC-MS were loaded on C-18 extraction cartridges (Bond Elut, Varian) and eluted with methanol. Control experiments contained no NADPH. All experiments were run in duplicates.

4 RESULTS

4.1 Syntheses of NDGA Analogues

4.1.1 Syntheses of A1: 4-(2,3-dimethyl-4-phenylbutyl)benzene-1,2-diol

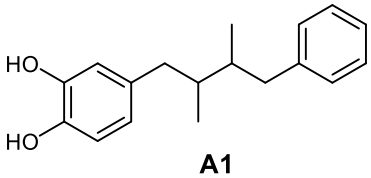

A1

Figure 4-1: Molecular structure of NDGA analogue **1** (**A1**).

The basic lignan skeleton was constructed using a Stobbe condensation followed by alkylation.[58, 102] Reaction of the aromatic aldehyde **24** with succinate ester **19** gave a trans-benzylidene succinate monoester **25** in 98% yield (Scheme 4-1). The monoester **25** was esterified to **26** using CH_3I/K_2CO_3 in DMSO in 93% yield. Alkylation with benzyl bromide and LDA in THF at -78 °C afforded the basic lignan skeleton **27** as orange oil (73%). Compound **27** was hydrolyzed to a diacid to allow resolution via quinine salts. However, this theoretically possible step proved practically challenging as the expected fractional crystallization did not occur. This separation step was not pursued further. Instead, compound **27** was hydrogenated under H_2 atmosphere using Pd-C(10%) catalyst to give **28** as yellowish oil (87%) which was reduced with $LiAlH_4$ in THF to the diol **29**, a white solid in 65% yield. Tosylation of compound **29** in pyridine gave the resulting tosylate **30** as white crystals in low yield (26%). Contrary to our expectation, this step does not seem to provide separation into two pairs of enantiomers for **A1**. The ^1H NMR and ESI-MS data of only one of the two isolated products was consistent with the expected product. A further reduction of **30** with $LiAlH_4$ in THF gave **31** as yellowish oil (82 %). Demethylation of compound **31** with

BBr_3 in DCM at -78 °C afforded the final NDGA mono-catechol **A1** as a purple oil in quantitative yield.

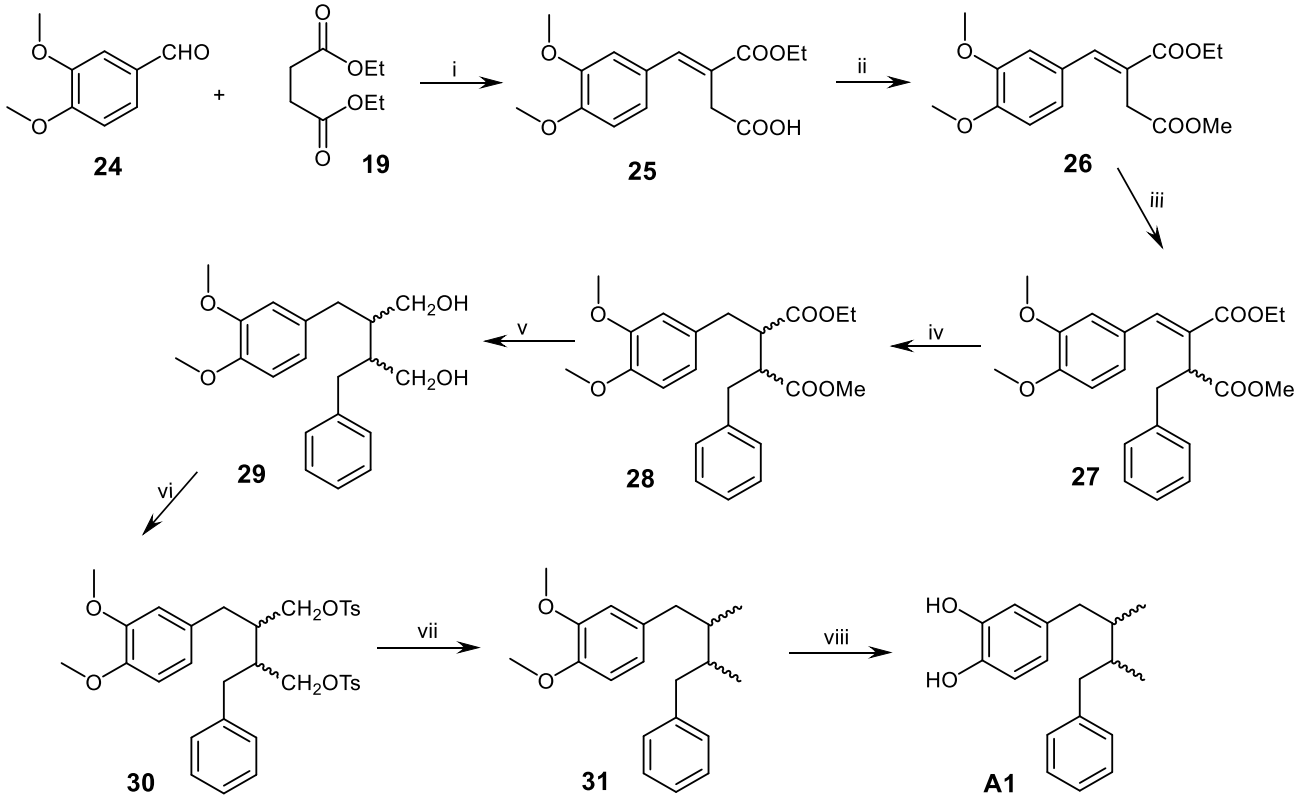

Scheme 4-1: Synthetic pathway to NDGA analogue **1** (**A1**).

Reagents and Conditions: i) EtONa/EtOH, reflux, 98%; ii) MeI, K_2CO_3/DMSO, rt, 93%; iii) BnBr, LDA/THF, -78 °C, 73%; iv) H_2, Pd-C, 88%; v) $LiAlH_4$/THF, rt, 65%; vi) TsCl, Pyridine, 0 °C 26%; vii) $LiAlH_4$/THF, rt, 82%; viii) BBr_3/DCM, -78 °C, > 99%.

4.1.2 Synthesis of A2: 4-(2,3-dimethyl-4-phenylbutyl)-2-methoxyphenol

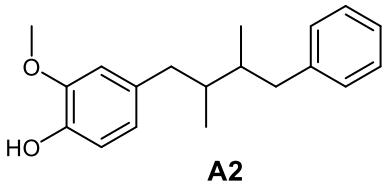

A2

Figure 4-2: Molecular Structure of NDGA analogue **2** (**A2**).

Benzylation of vanillin gave compound **32** which was treated with diethyl succinate **19** via a Stobbe condensation reaction to give the trans-benzylidene succinate monoester **33** (Scheme 4-2). After methylation, the resulting diester **34** was alkylated with BnBr/LDA in THF to give the basic lignan structure **35**. Compound **35** was hydrolyzed to diacid **36** to allow resolution of the enantiomeric pair via diastereomeric quinine salts. As observed in the case of **A1**, the desired fractional crystallization of diastereomeric quinine salts did not occur even though ESI-MS data showed successful reaction. Compound **35** was subsequently reduced with $LiAlH_4/AlCl_3$ mixture in THF to the diol **37**. Compound **35** required a more vigorous condition obtained by using $LiAlH_4$ in the presence of a Lewis acid, $AlCl_3$to undergo reduction. Reduction with $LiAlH_4$ in the absence of a Lewis acid was unsuccessful. It is noteworthy that this reduction step does not cleave the benzyl protecting group and therefore offers synthetic advantage as it shortens the synthetic steps by one. Attempts to tosylate diol **37** led to undesired lactone **38a** and **38b** possibly through tosylation of one OH group followed by elimination. When compound **37** was hydrogenated to **39**, subsequent tosylation easily gave the desired tosylate **40** in good yield (62%). This step however tosylates the de-protected aromatic OH group as well. $LiAlH_4$ reduction followed by aromatic detosylation with refluxing KOH (3%) in ethanol-water (1:1) mixture afforded **A2** as a yellow oil. Compound **A2** was

also prepared via consecutive Stobbe condensation reaction on **34** using benzylaldehyde **41** followed with methylation to give the diester **42.** Compound **42** was hydrogenated and the resulting mixture reduced with $LiAlH_4$ to give **43.** Compound **43** was treated with mesyl chloride and the resulting mesylate reduced with $LiAlH_4$ and further with refluxing KOH (3%) in ethanol-water (1:1) mixture afforded **A2** as yellow oil.

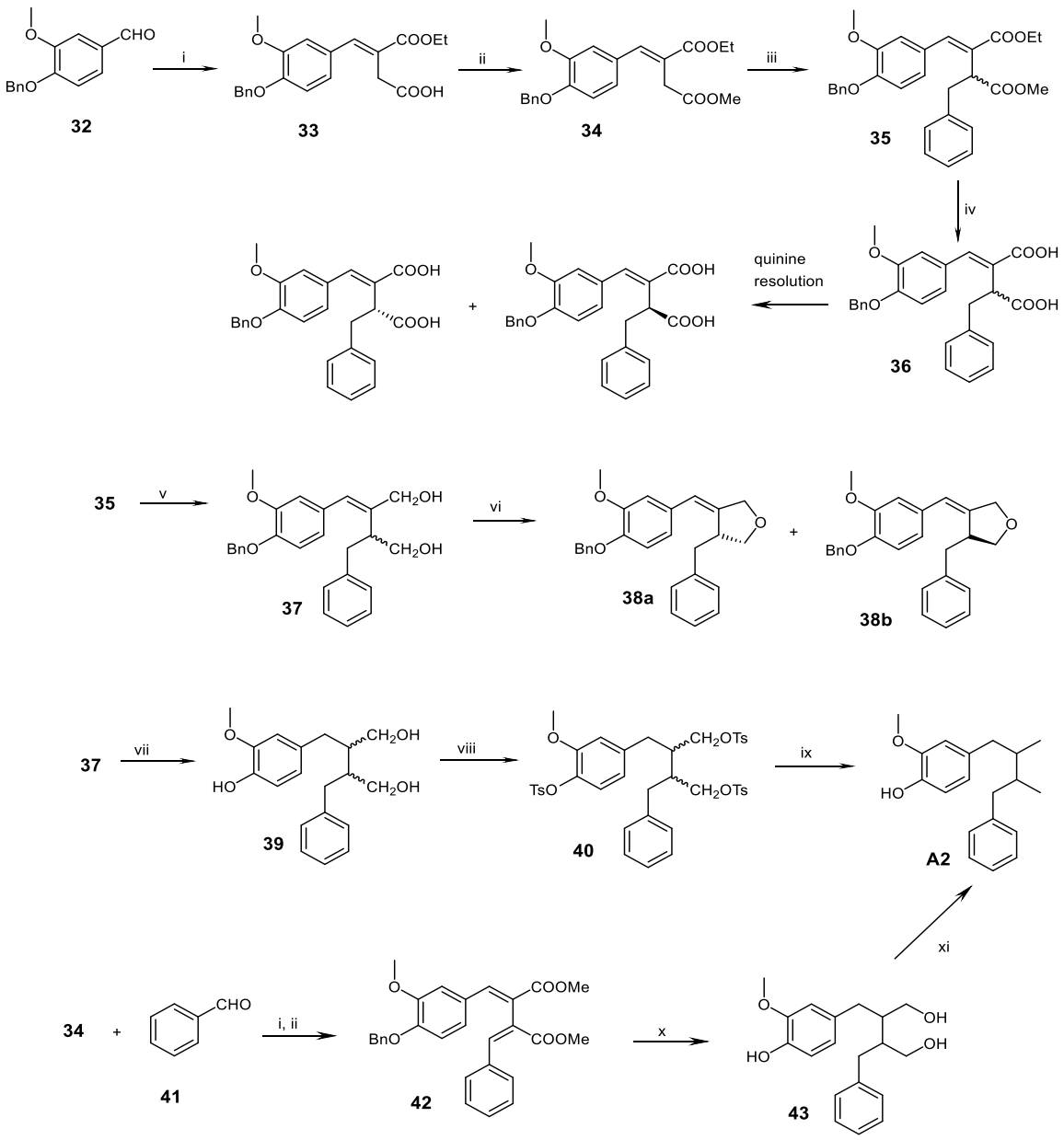

Scheme 4-2: Synthetic pathway to NDGA analogues **2** (**A2**).

Reagents and Conditions: i) EtONa/EtOH, reflux, 98%; ii) MeI, K_2CO_3/DMSO, rt, 92%; iii) BnBr, LDA/THF, -78 ºC, 92%; iv) NaOH/H_2O, reflux, H_3O^+, 57%; v) $LiAlH_4$/$AlCl_3$, THF, rt, 74%, vi) 63%; vii) H_2, Pd/C (10%), EtOH, 99% viii) TsCl, Pyridine, 0 ºC 62%; ix) (a) $LiAlH_4$, THF, rt; (b) KOH/EtOH-H_2O (1:1), reflux, 41%; x) (a) H_2, Pd/C (10%), EtOH; (b) $LiAlH_4$, THF, rt; xi (a) MsCl, Pyridine, 0 ºC; (b) $LiAlH_4$, THF, rt; (c) KOH/EtOH-H_2O (1:1), reflux.

4.1.3 Synthesis of A3: 4,4′-(2,3-dimethylbutane-1,4-diyl)bis(2-methoxyphenol)

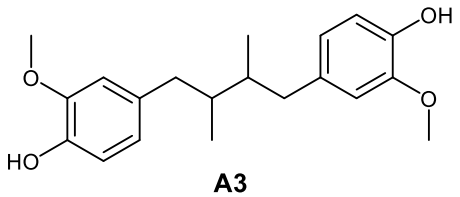

A3

Figure 4-3: Molecular Structure of NDGA analogue **3** (**A3**).

A second Stobbe condensation reaction on **34** using benzylated vanillin **32** in EtONa/EtOH gave the basic lignan skeleton **44** (Scheme 4-3). Compound **44** was esterified to **45** and reduced under similar conditions as **35** to give the diol **46**. Flash chromatography over silica on the hydrogenation product of **46** led to *meso*-secoisolariciresinol **47a** and racemic (±)-secoisolariciresinol **47b**. Treatment of **47a** or **47b** with toluenesulfonyl chloride in pyridine at 0 ºC, followed by $LiAlH_4$ reduction and refluxing the resulting crude product in KOH (3%) in ethanol-water (1:1) mixture afforded **A3** as the *meso*-compound **A3a** or *rac* (±)-compound **A3b**.

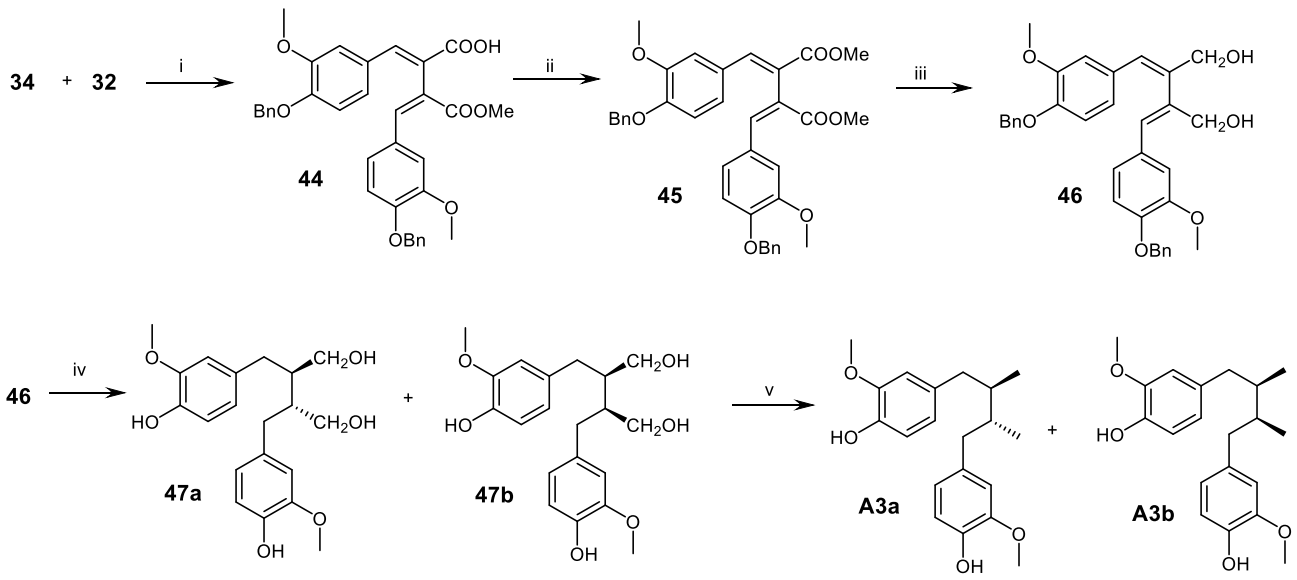

Scheme 4-3: Synthetic pathway to NDGA analogues **3** (**A3**).
Reagents and Conditions: i) EtONa/EtOH, reflux, 72%; ii) MeI, K_2CO_3/DMSO, rt, 87%; iii) $LiAlH_4/AlC_3$, THF, rt., 74%, iv) H_2, Pd-C, EtOH, 47% **23a**, 48% **23b;** v) (a) TsCl, Pyridine, 0 ºC; (b) $LiAlH_4$, THF, rt.; (c) KOH/EtOH-H_2O (1:1), reflux, 74% **24a**, 64% **24b.**

4.1.4 Synthesis of A4: 4[4-(3,4-dimethoxyphenyl)-2,3-dimethylbutyl]benzene-1,2-diol

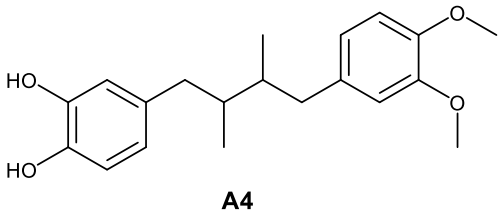

A4

Figure 4-4: Molecular Structure of NDGA analogue **4** (**A4**).

Benzylation of 3,4-dihydroxybenzyladehyde **48** gave **49** as white crystals in 84% yield (Scheme 4-4). Treatment of **49** with a succinate ester **19** via Stobbe condensation followed by esterification gave **50** and **51** respectively. A second Stobbe condensation reaction on **51** using **24** in EtONa/EtOH afforded the half-ester **52** which on esterification gave **53**, the basic lignan skeleton for **A4**. After hydrogenation of **53** under H_2 atmosphere, the de-protected OH groups of the

resulting compound **54** were protected again via benzylation to give **55**. Compound **55** was reduced with $LiAlH_4$ in THF. Treatment of the resulting diol **56** with tosyl chloride in pyridine at 0 ºC and a flash chromatography over silica gel resulted in **57a** and **57b**. Reduction of **57a** or **57b** with $LiAlH_4$ in THF gave **58a** or **58b** which were separately hydrogenated under H_2 atmosphere to afford **A4** as two enantiomeric pairs **A4a** or **A4b**.

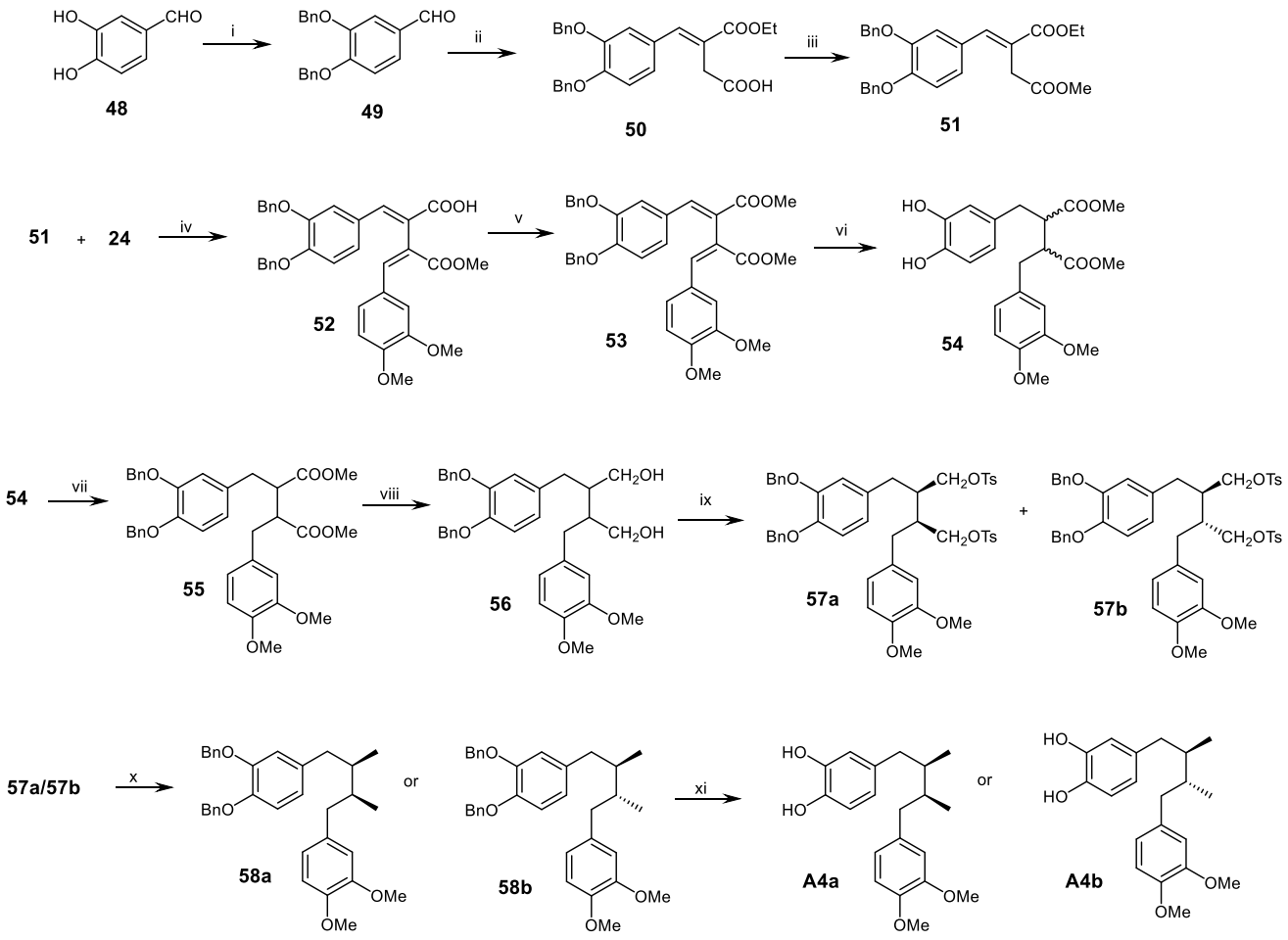

Scheme 4-4: Synthetic pathway to NDGA analogue **4** (**A4**).
Reagents and Conditions: i) BnBr, K_2CO_3/DMF, rt., 84%; ii) EtONa/EtOH, reflux; 98%, iii) MeI, K_2CO_3/DMSO, r.t., 98%; iv) EtONa/EtOH, reflux; > 90 % v) MeI, K_2CO_3/DMSO, rt., 98%; vi) H_2, Pd-C, vacuum; > 99%; vii) BnBr, K_2CO_3/DMF, rt., 63 %; viii) $LiAlH_4$/THF, rt; ix) TsCl, pyridine, 0 °C; x) $LiAlH_4$/THF, rt; 67 %; xi) H_2, Pd-C, vacuum; > 98%.

4.1.5 Attempted synthesis of A5: 4,4'-(2,2,3,3-tetramethylbutane-1,4-diyl)dibenzene-1,2-diol

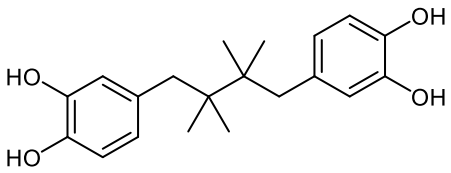

A5

Figure 4-5: Molecular structure of NDGA analogue **5** (**A5**).

Treatment of compound **26** with **24** in a refluxing EtONa/EtOH followed by esterification afforded the basic lignan structure **59** which on hydrogenation gave **60** (Scheme 4-6). We have previously observed that base-catalyzed esterification of a dicarboxylic acid **61** with iodomethane (Scheme 4-5) resulted in additional methylation at the α-position to produce **62** as the major product. Although **62** was a side-product not useful for the synthesis of the intended target compound **A2**, we thought this reaction could be exploited to make **A5**. However, treatment of **60** with powdered KOH in anhydrous DMSO in the presence of iodomethane surprisingly failed to form the expected di-methylated product **63**. After a number of unsuccessful attempts, compound **60** was reduced with $LiAlH_4$ to **64** followed by tosylation and a further reduction with $LiAlH_4$ to obtain tetra-O-methyl NDGA (M4N **14**)

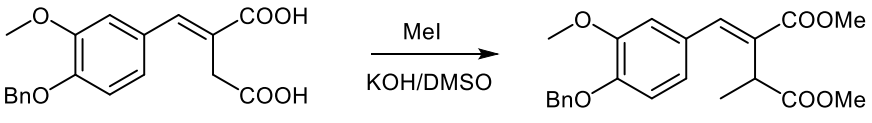

61 **62**

Scheme 4-5: Base-catalysed esterification of a di-carboxylic acid using KOH in DMSO.

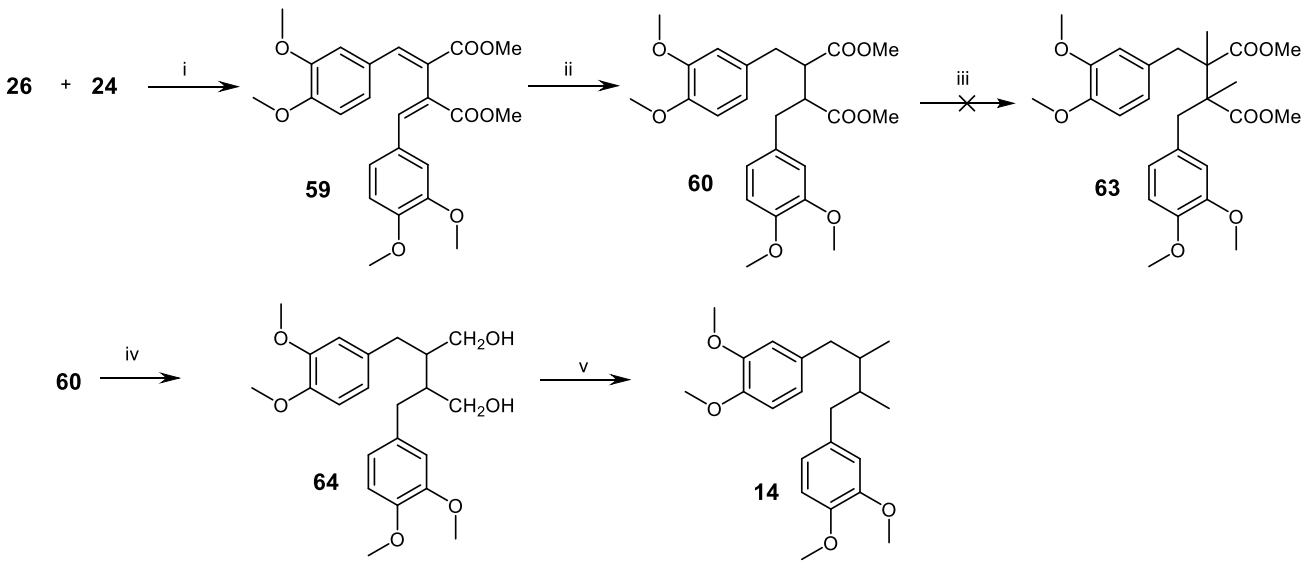

Scheme 4-6: Attempted synthesis of NDGA analogue **5** (**A5**) led to tetra-O-methyl NDGA **14**. *Reagents and Conditions:* i) (a) EtONa/EtOH, reflux, 98%; (b), MeI, K_2CO_3/DMSO, 92%; ii) H_2, Pd/C (10 %), EtOH, 99%; iii) MeI, KOH/DMSO, rt.; iv) $LiAlH_4$, THF, rt., v) (a) TsCl, Pyridine, 0 ºC; (b) $LiAlH_4$, THF, rt.

4.1.6 Synthesis of A6: 4,4'-butane-1,4-diyldibenzene-1,2-diol

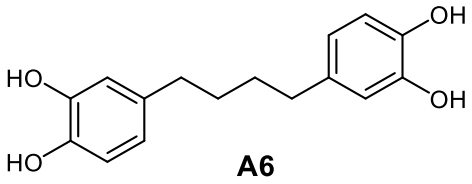

Figure 4-6: Molecular structure of NDGA analogue **6** (**A6**).

Compound **A6** was prepared according to previously reported literature method[131] with minor modification as shown in Scheme 4-7. Reduction of carboxylic acid **65** with $LiAlH_4$ gave the alcohol **66** which was oxidized with pyridinium chlorochromate (PCC) to the intermediate aldehyde **67.** Treatment of **67** with the Grignard reagent **68** which was generated in-situ gave **70** which upon hydrogenolysis resulted in compound **71**. Compound **71** was treated with BBr_3 in DCM to afford the target compound **A6.**

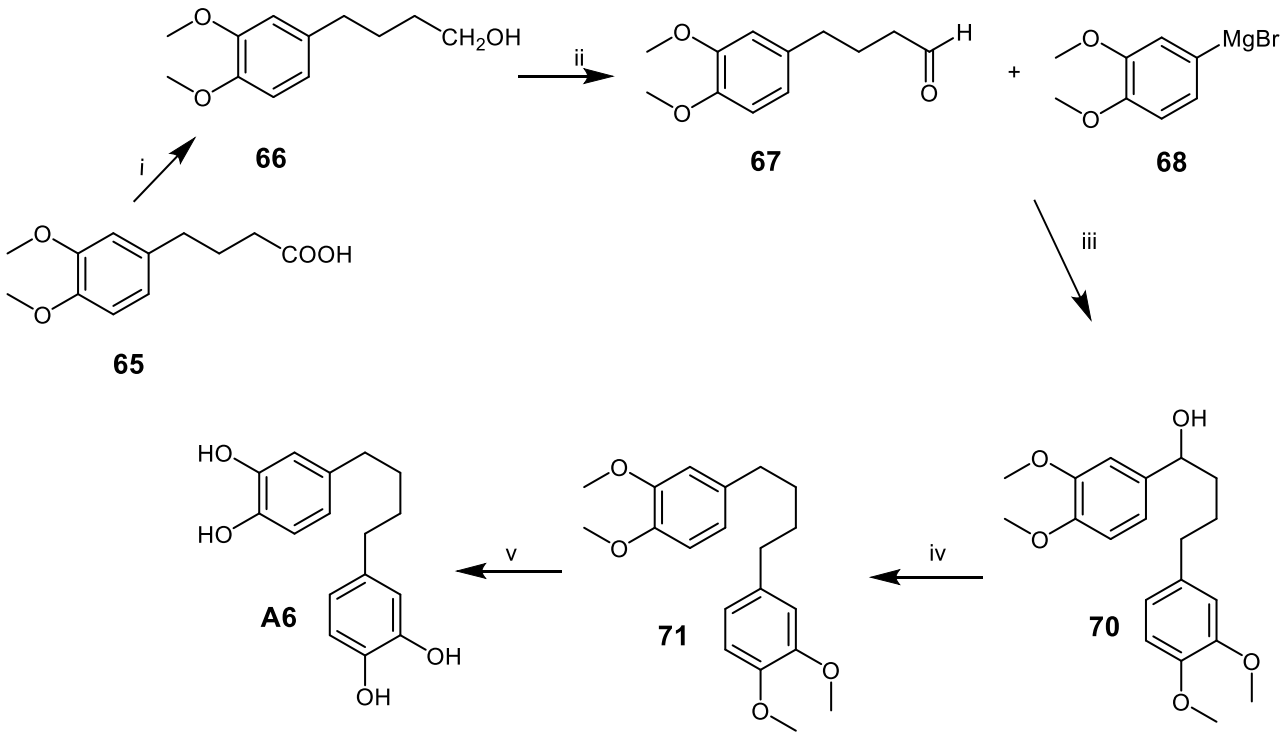

Scheme 4-7: Synthetic pathway to NDGA analogue **6** (**A6**).
Reagents and conditions: i) $LiAlH_4$, THF, rt. 86%; ii) PCC, DCM, rt 84%; iii) THF, -78 ºC, then rt 71%; iv) H_2, Pd-C, EtOH 91%; v) BBr_3, DCM, -78 ºC, then rt > 99%.

4.1.7 Synthesis of A7: 3,3'-(2,3-dimethylbutane-1,4-diyl)diphenol

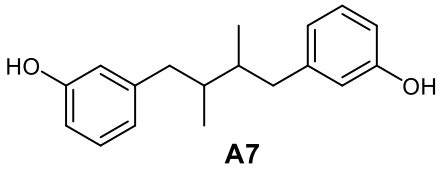

A7

Figure 4-7: Molecular structure of NDGA analogue **7** (**A7**).

Benzylation of 3-hydroxybenzyladehyde **72** followed by treatment with succinate ester **19** in refluxing EtONa/EtOH and esterification of the resulting half-ester gave **73** (Scheme 4-8). Compound **73** was subsequently treated with benzylated **72** in refluxing EtONa/EtOH and esterified to generate the basic lignan skeleton **74**. Following hydrogenation of **74** and reduction of the

resulting mixture with $LiAlH_4$, compound **75** was isolated. Tosylation of **75** with TsCl in pyridine followed by reduction with $LiAlH_4$ gave **76** which upon refluxing in KOH (3%) in ethanol-water (1:1) mixture afforded **A7** as yellowish brown oil.

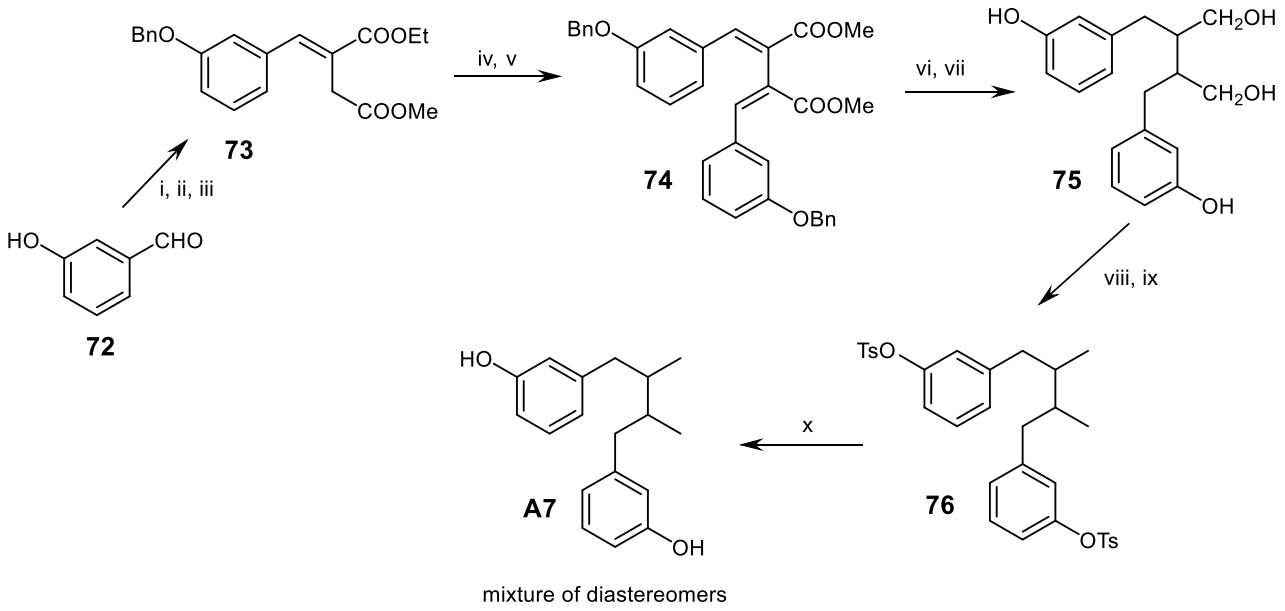

Scheme 4-8: Synthetic pathway to NDGA analogue **7** (**A7**).
Reagents and conditions: i) BnBr, K_2CO_3/DMF, rt; ii) diethyl succinate, EtONa/EtOH, reflux; iii or v) MeI, K_2CO_3/DMSO, rt; iv) 3-(benzyloxy)benzaldehyde, EtONa/EtOH, reflux; vi) H_2, Pd-C, EtOH, vii) $LiAlH_4$, THF, rt., viii) TsCl, Pyridine, 0 ºC; ix) $LiAlH_4$, THF, rt.; (x) KOH/EtOH-H_2O (1:1), reflux.

4.1.8 Synthesis of A8: 3,3'-(2,3-dimethylbutane-1,4-diyl)bis(6-methoxyphenol)

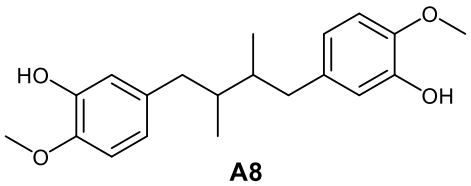

Figure 4-8: Molecular structure of NDGA analogue **8** (**A8**).

Benzylation of 4-methoxy-3-hydroxybenzaldehyde **77** followed by Stobbe condensation reaction with succinate ester **19** and esterification of the resulting half-ester gave the di-ester **78**

(Scheme 4-9). Compound **78** was treated with benzylated **77** and the resulting acid esterified to give **79**. Reduction of **79** with a mixture of $LiAlH_4$ and $AlCl_3$ in THF gave the unsaturated diol **80** which upon hydrogenation and purification via flash column chromatography resulted in easily separable **81a** and **81b.** Compound **81a** or **81b** was tosylated to **82a** or **82b** and reduced with $LiAlH_4$ to **83a** or **83b.** Refluxing of **83a** or **83b** in KOH (3%) in ethanol-water (1:1) mixture afforded the target compound as **A8a or A8b**.

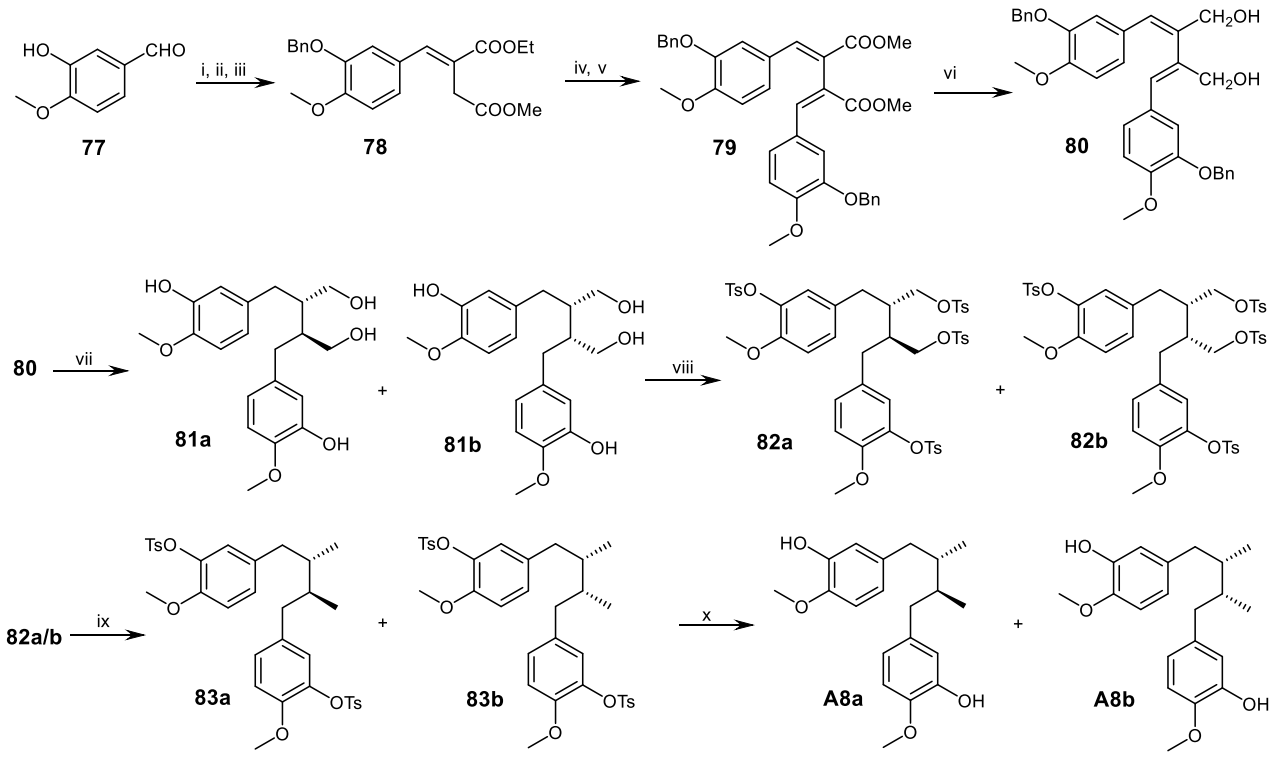

Scheme 4-9: Synthetic pathway to NDGA analogue **8** (**A8**).
Reagents and conditions: i) BnBr, K_2CO_3/DMF, rt.; ii) diethyl succinate, EtONa/EtOH, reflux; iii or v) MeI, K_2CO_3/DMSO, rt.; iv) 3-(benzyloxy)-4-methoxybenzaldehyde, EtONa/EtOH, reflux; vi) $LiAlH_4/AlCl_3$, THF, rt.; vii) H_2, Pd-C, EtOH; viii) TsCl, Pyridine, 0 ^oC; ix) $LiAlH_4$, THF, rt.; (x) KOH/EtOH-H_2O (1:1), reflux.

4.2 Autoxidation Cyclization Potential of NDGA Analogues

4.2.1 Autoxidation Studies

Two possible mechanisms were proposed (Schemes 2-1 and 2-3) for NDGA autoxidation based on literature reports.[35, 59, 66] We hypothesized that NDGA autoxidation is a radical-mediated process in which the slightly lower pKa of the meta hydroxyl group resulted in preferential oxidation and cyclization of the carbon-centered resonance form. The NDGA analogues prepared for this study were examined for their potential to undergo autoxidative cyclization under previously described conditions.[35] Compound **A6** cyclized into its corresponding dibenzocyclooctadiene derivative as shown below in Scheme 4-10.

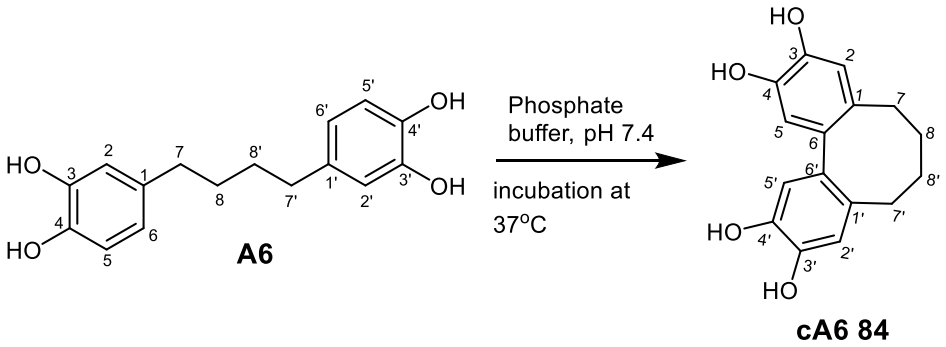

Scheme 4-10: Intramolecular cyclization of **A6** to its dibenzocyclooctadiene derivative **84**.

A decrease in retention time and the 3.5 nm shift to a higher absorbance observed by HPLC (Figure 4-9) is consistent with previous[35] and current results obtained for NDGA under the same condition. The λ_{max} for NDGA and **A6** changed from 282.8 to 286.3 and 281.6 to 285.1 respectively (Figure 4-10). ESI-MS in negative ion mode (Figure 4-11) was consistent with predicted *m/z* 299.1 and 271.1 Da for NDGA and **A6** dibenzocyclooctadiene derivatives respectively. Both were two mass units less than their respective *m/z* 301.1 and 273.2 prior to oxidative cyclization. Fragmentation patterns following collision induced dissociation (CID) in Tandem MS/MS

experiments were consistent for dibenzocyclooctadiene derivatives for NDGA and **A6** as shown in Figure 4-12.

^{1}H and ^{13}C NMR data as summarized below confirmed intramolecular cyclization of **A6** under oxidative conditions to dibenzocyclooctadiene derivative **84**. ^{1}H NMR (500 MHz, CD_3OD): δ (ppm) 1.37 (2H, m), 1.94 (2H, m), 2.00 (2H, m), 2.47 (2H, m'), 6.54 (2H, s, H2, 2'), 6.60 (2H, s, H5, 5'). ^{13}C NMR (500 MHz, CD_3OD): δ (ppm) 31.3 (C8, 8'), 33.4 (C7, 7'), 117.0 (C2, 5, 2', 5'), 133.8 (C1, 1'), 135.6 (C6, 6'), 143.9 (C4, 4'), 145.7 (C3, 3'). The loss of C6, 6' proton, coupling of C7, 7' and well as C8, 8' protons are all consistent with cyclization.

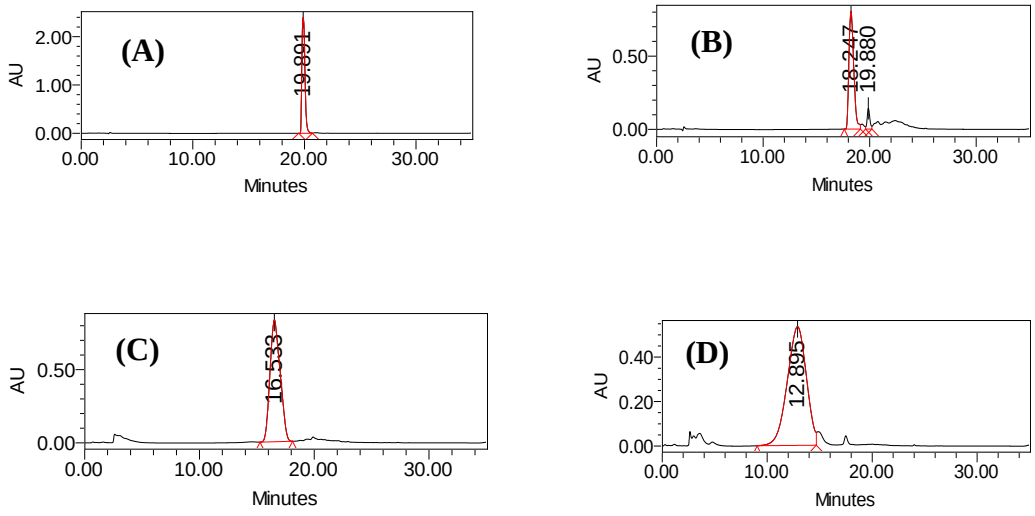

Figure 4-9: HPLC Chromatogram for incubation in phosphate-citrate buffer pH 7.4 at 37 °C for 90 min for NDGA (panel A) before and (panel B) after incubation; **A6** (panel C) before and (panel D) after incubation.

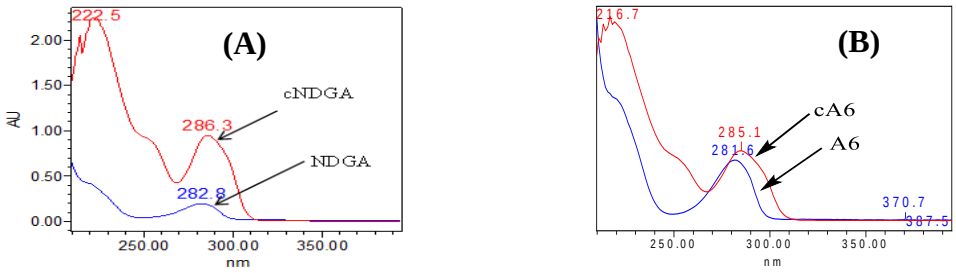

Figure 4-10: UV absorption of dibenzocyclooctadiene derivatives for NDGA (panel A) and A6 (panel B).

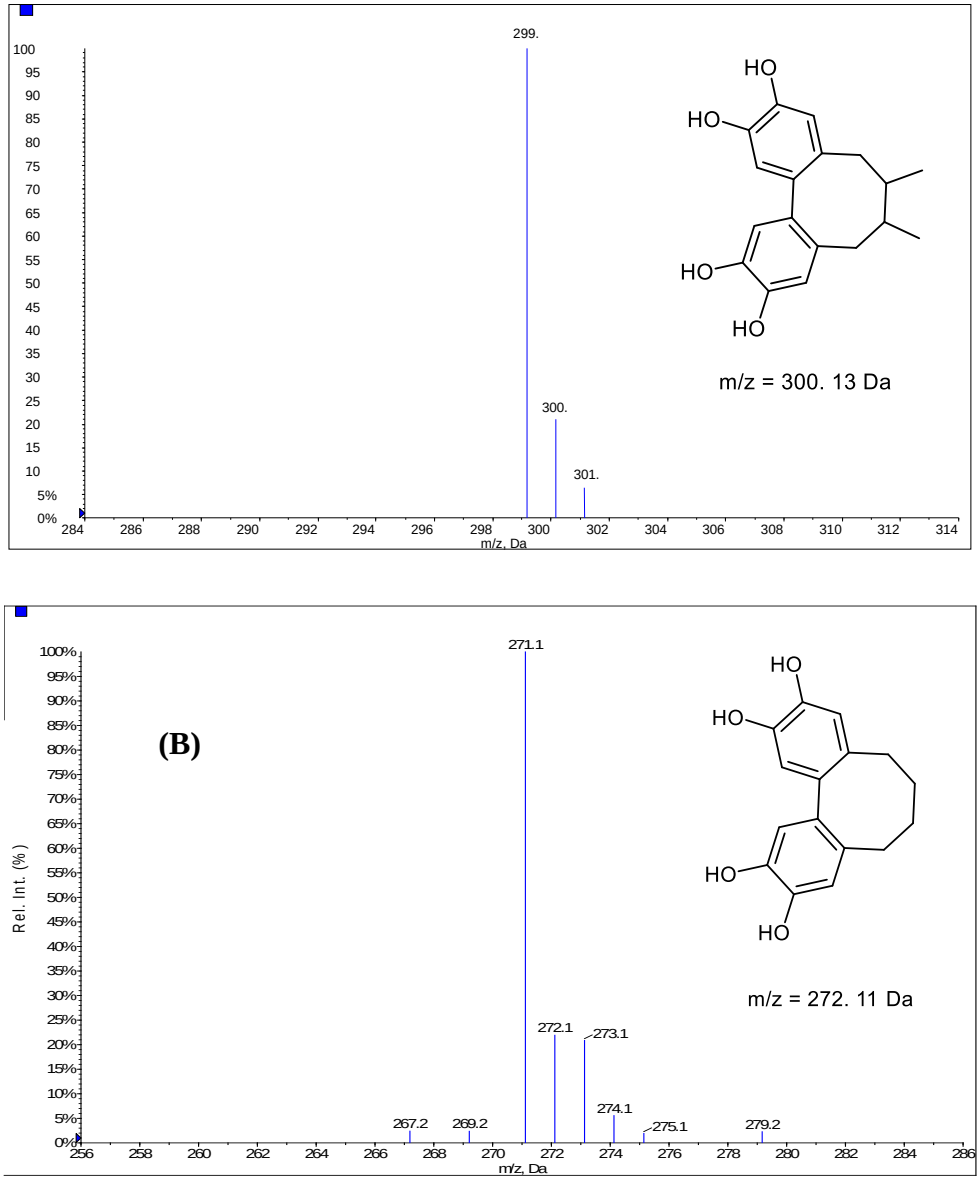

Figure 4-11: ER-ESI-MS scanning in negative ionization mode for dibenzocyclooctadiene derivative of NDGA (panel A) and **A6** (panel B).

The *m/z* 299.1 and 271.1 Da observed were consistent with calculated monoisotopic masses of dibenzocyclooctadiene derivatives for NDGA (300.13 g) and **A6** (272.10 g) respectively. The observed masses were two mass units less than their respective *m/z* 301.1 and 273.2 prior to oxidative cyclization.

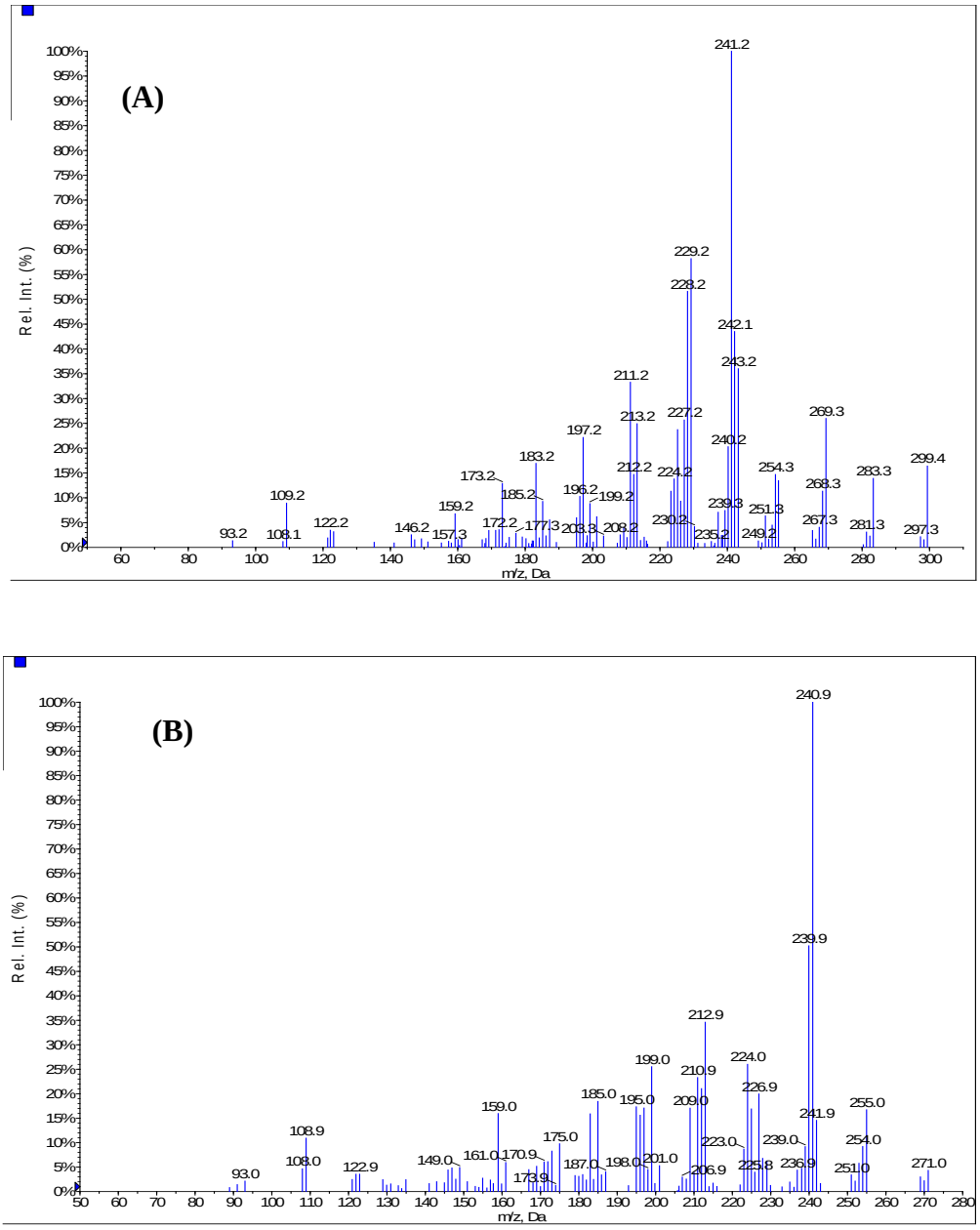

Figure 4-12: ESI-MS/MS of dibenzocyclooctadiene derivative for NDGA (panel A) and **A6** (panel B).

A consistent fragmentation pattern was observed generating product ions which were different than those observed for standard NDGA (Figure 3-4) and **A6** (Figure 3-24).

When the other catechol (**A1** or **A4**) and phenol (**A2** or **A3**) analogues were subjected to the same oxidative conditions as describe in section 3.5.2, no evidence of intramolecular cyclization was observed. Unlike NDGA or **A6**, no changes in retention time and UV absorption characteristics were seen by HPLC (Figure 4-13) although concentration of the starting materials appeared to decrease over time. This prompted us to determine the chemical stability of these compounds and also establish their rates of disappearance in the phosphate buffer (pH 7.4).

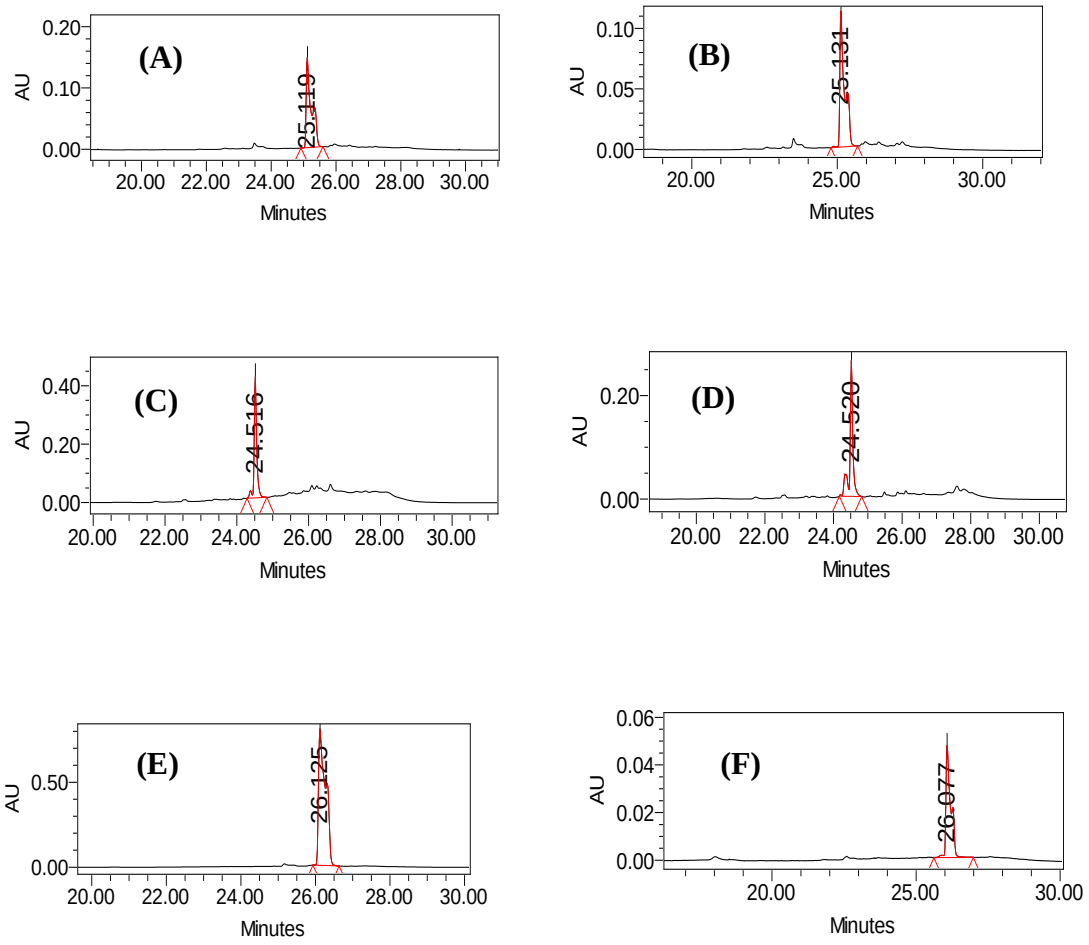

Figure 4-13: HPLC chromatograph for **A1** before (panel A) and after (panel B) reaction; **A4** before (panel C) and after (panel D) reaction; **A2** before (panel E) and after (panel F) reaction. Reactions were performed by incubating substrates in phosphate-citrate buffer (7.4) at 37ºC for 90 min.

We predicted that **A4** will cyclize at a comparable rate to NDGA if the intramolecular cyclization follows electrophilic substitution mechanism and that absence of cyclization could imply that the radical-mediated pathway more accurately describes NDGA autoxidation. Based on our observations with **A1** and **A4,** an electrophilic substitution mechanism (Scheme 2-9, pathway B) was ruled out. We synthesized and evaluated **A7** to advance more support for the radical-mediated pathway. Contrary to our expectations, **A7** did not cyclize although it meets the minimum structural requirements for di-radical ion formation.[77, 78] We thought stability of a possible radical or di-radical intermediate might be important for cyclization[60] although this does not appear to be the case. We predicted that methoxy substituents of compound **A8** should stabilize the di-radical intermediate via a positive inductive effect to allow for cyclization. Surprisingly, we found no evidence of intramolecular cyclization for **A8**. We could detect the starting material quantitatively even after 48 h incubation at 37 °C in a phosphate buffer (pH 7.4) by HPLC (Figure 4-14). A further analysis of the reaction mixture by MS techniques gave no evidence of cyclization for **A8.** The predicted mass at m/z 327.16 Da in negative ionization mode was not detected.

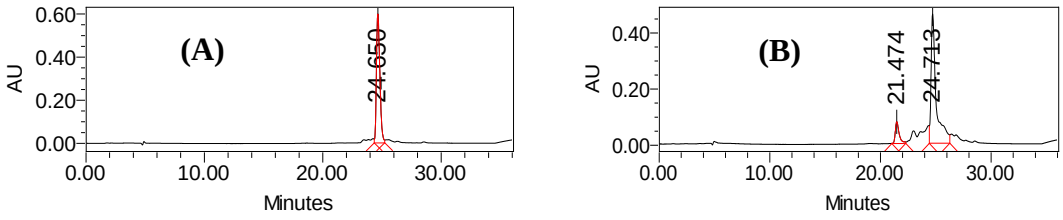

Figure 4-14: HPLC Chromatogram for **A8** incubation in phosphate-citrate buffer (pH 7.4) at 37°C for 90 min: Before (panel A) and after (panel B) incubation. The UV absorption of the 21.5 min peak was inconsistent with dibenzocyclooctadiene product.

4.2.2 Chemical Stability and Reaction Kinetics

Autoxidation experiments revealed a decrease in concentration of the analogues over time although no product peaks were seen by HPLC. This prompted us to determine the chemical stability of these compounds and also establish their rates of disappearance in the phosphate-citric acid buffer (pH 7.4) at 37ºC.

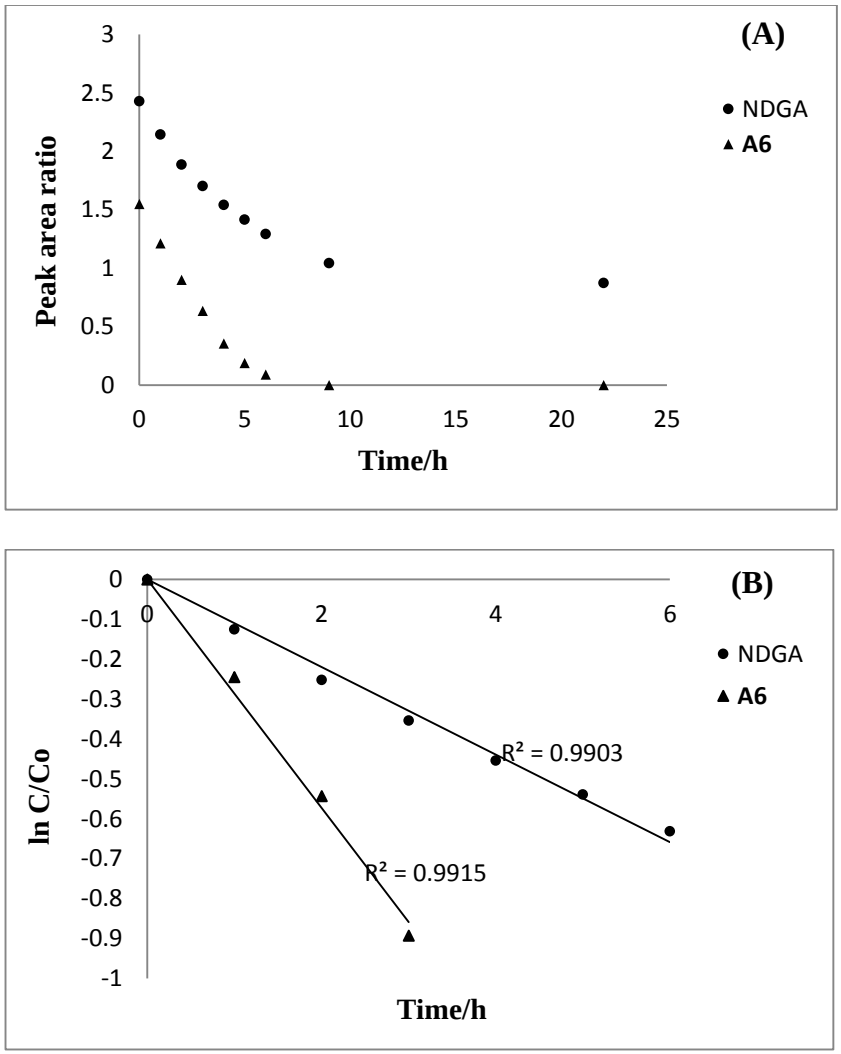

Figure 4-15 : Chemical degradation profiles (panel A) and first-order degradation regression lines (panel B) for NDGA (●) and **A6** (▲) in 0.5 M phosphate-citric acid buffer (pH 7.4) at 37ºC. Changes in concentration of substrates were determined from the peak area ratios and plotted as a function of time.

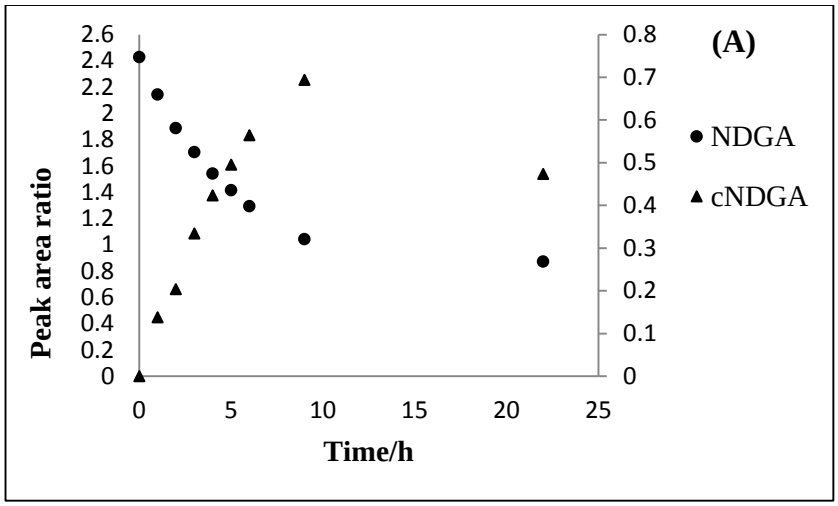

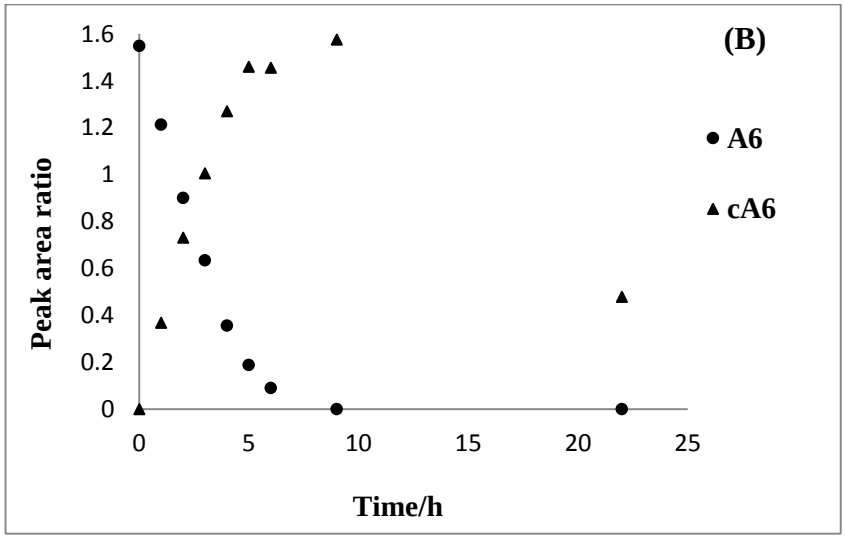

Figure 4-16: The disappearance of substrates (●) and appearance of corresponding dibenzocyclooctadiene derivatives (▲) for NDGA (panel A) and **A6** (panel B) in 0.5 M phosphate-citric acid buffer (pH 7.4) at 37ºC. The decrease and increase in concentrations of substrates and dibenzocyclooctadiene derivatives respectively were determined from the peak area ratios and plotted as a function of time.

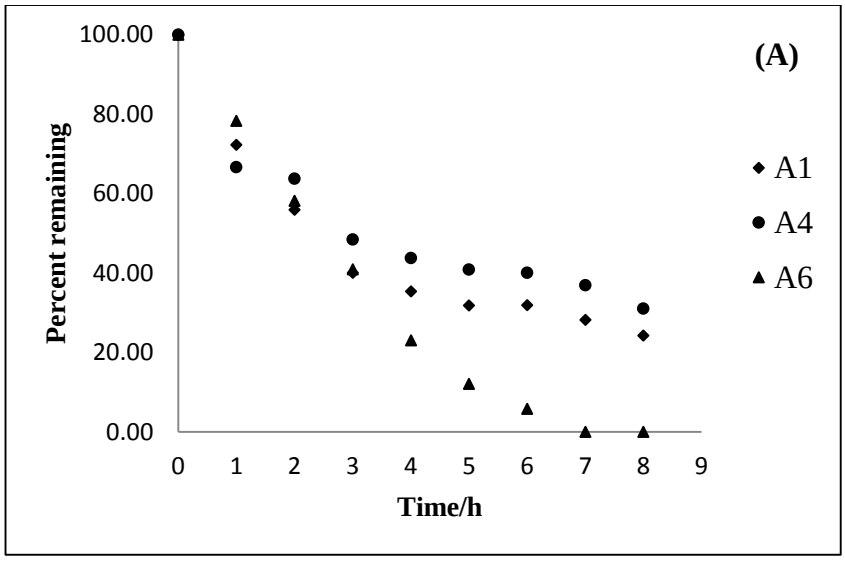

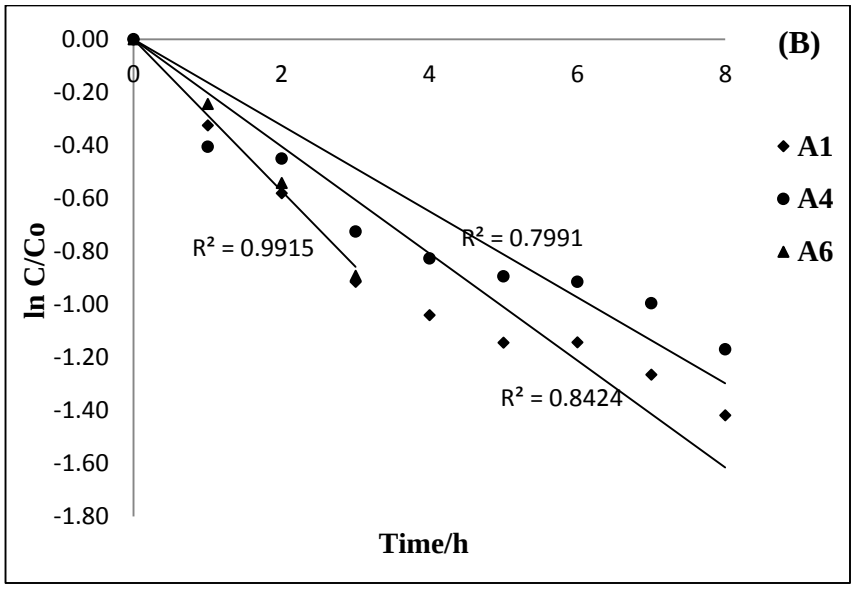

Figure 4-17: Chemical degradation profiles (panel A) and first-order regression lines (panel B) for the catechol analogues **A1** (♦), **A4** (●) and **A6** (▲) in 0.5 M phosphate-citric acid buffer (pH 7.4) at 37ºC. Changes in concentration of substrates were determined from peak area ratios and plotted as a function of time.

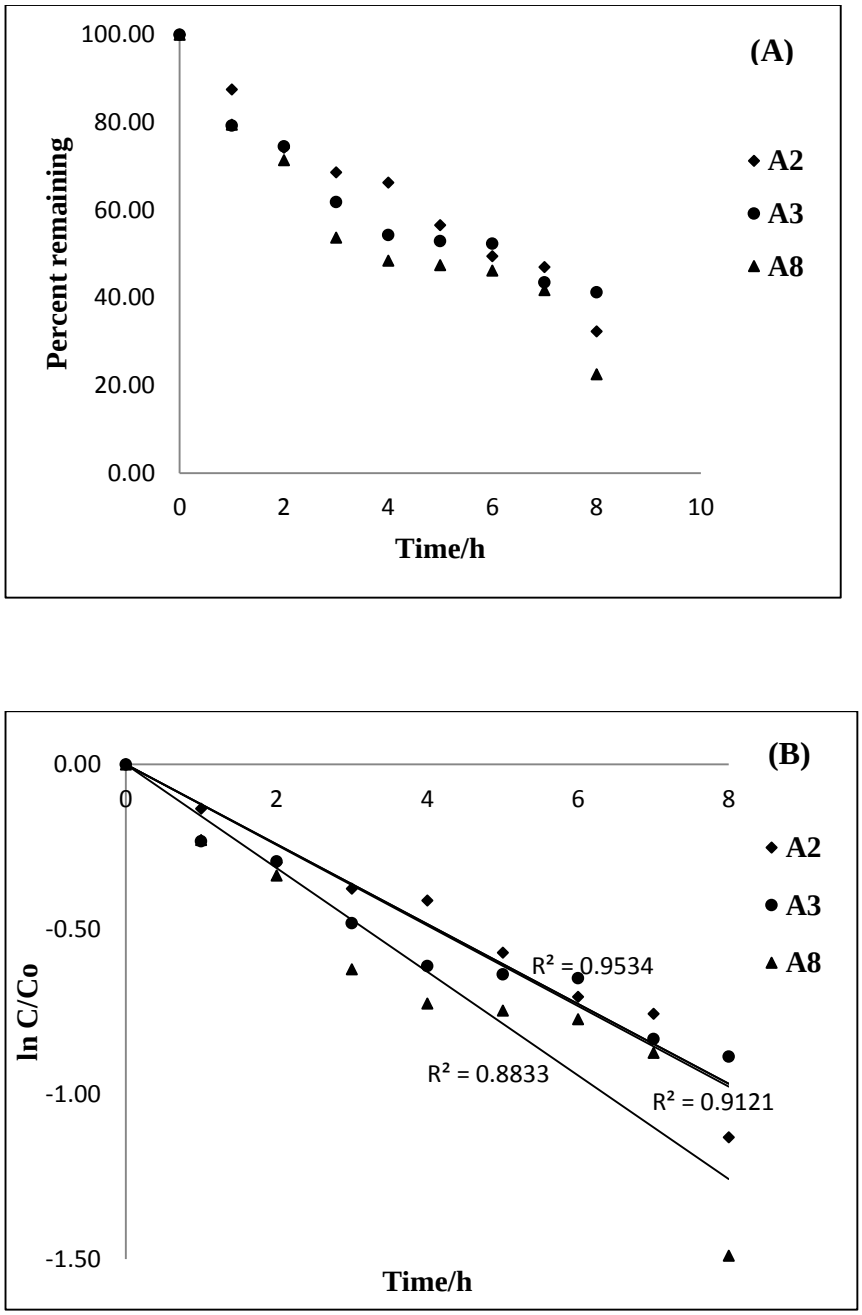

Figure 4-18: Chemical degradation profiles (panel A) and first-order regression lines (panel B) for the phenol analogues **A2** (♦), **A3** (●) and **A8** (▲) in 0.5 M phosphate-citric acid buffer (pH 7.4) at 37ºC. Changes in concentration of substrates were determined from peak area ratios and plotted as a function of time.

Table 4-1: Rate of autoxidative degradation of NDGA and its analogues in 0.5 M phosphate-citric acid buffer (pH 7.4) at 37ºC.

Compound	Rate constant k (s^{-1})	Half-life $t_{1/2}$ (h)	Coefficient of determination R^2
NDGA	4.8778×10^{-5}	3.94	0.9936
A6	13.1111×10^{-5}	1.47	0.9598
A1	4.5611×10^{-5}	4.22	0.9116
A2	3.5027×10^{-5}	5.49	0.9473
A3	2.8722×10^{-5}	6.70	0.9512
A4	4.1583×10^{-5}	4.62	0.9413
A8	4.1138×10^{-5}	4.68	0.888

A plot of lnC as a function of time t gave the rate constant k as the gradient. Half-life $t_{1/2}$ was determined from $t_{1/2}$ = 0.693/k(h).

4.2.3 Dibenzocyclooctadiene Formation via o-Q intermediate

We monitored the rate of formation of dibenzocyclooctadiene derivatives for NDGA and **A6** in the presence (i.e. added to the incubation mixture at time t = 0 min) and absence of GSH as well as addition of GSH at different time intervals. The results show a significant decrease in the formation of the dibenzocyclooctadiene derivatives for NDGA and **A6** in the presence of GSH (Figure 4-19). The detection of GSH conjugates and significant reduction in the amount of dibenzocyclooctadiene derivatives when GSH was added to the incubation mixture suggested that an o-quinone intermediate is possibly involved in the intramolecular cyclization process. It is possible that competition exists between intramolecular cyclization and an intermolecular reaction with GSH and that after 3h for NDGA or 2 h for **A6**, the intramolecular cyclization pathway is favoured leading to a rise in the amount of dibenzocyclooctadiene derivatives as observed by

HPLC. Given the apparent suppression of intramolecular cyclization in the presence of GSH, the effect of GSH on the formation of dibenzocyclooctadiene derivatives was further investigated with the aim of establishing whether the observed inhibition is concentration dependent. The substrate-GSH ratio in the incubation mixture was increased from a 1:2 ratio to a 20 fold excess of GSH (1:20). Incubations were done with and without GSH at 37ºC for 6 h and the percent compositions estimated by comparison of peak area ratios with time zero samples. The results (Figure 4-20, Table 4-2) indicate that excess GSH significantly inhibits intramolecular conversion of **A6** or NDGA to dibenzocyclooctadiene derivatives. Over 91% conversion was observed in the absence of GSH compared to barely 5% in the presence of 20 fold excess GSH for **A6**. NDGA formed no dibenzocyclooctadiene derivative in the presence of a 20 fold excess GSH compared to 33% conversion in the absence of GSH.

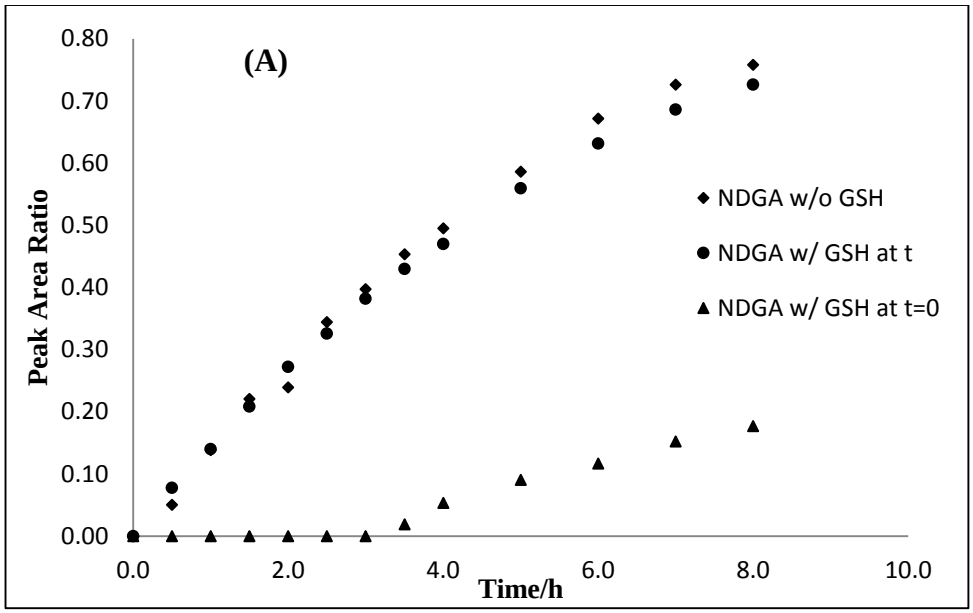

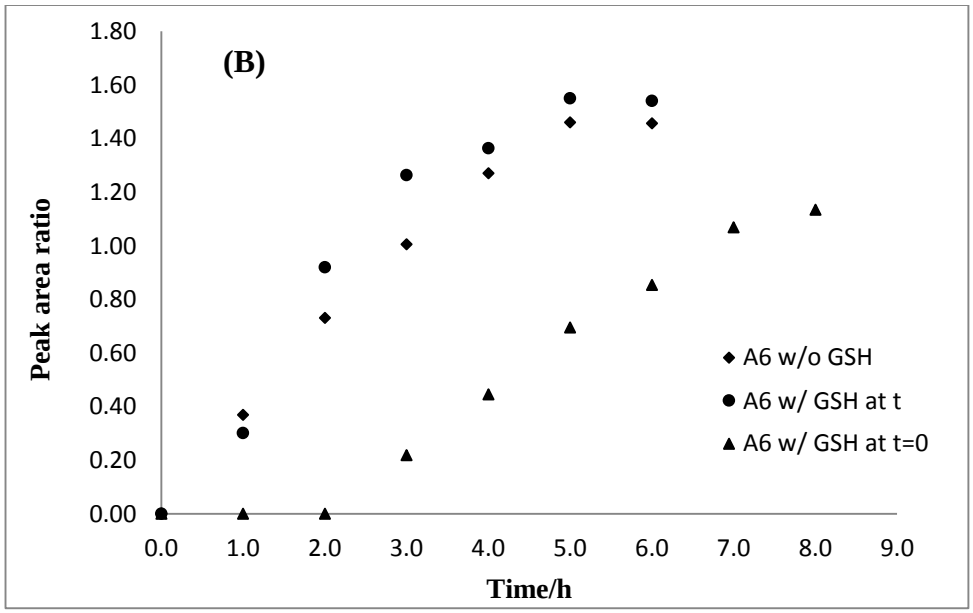

Figure 4-19: Formation of dibenzocyclooctadiene derivatives for NDGA (panel A) and **A6** (panel B) over time in the absence of GSH (♦), GSH added at time points (●) and GSH added at time t = 0 h (▲). The graphs show that the presence of GSH in the incubation mixture significantly affected the amount of dibenzocyclooctadiene formed over time.

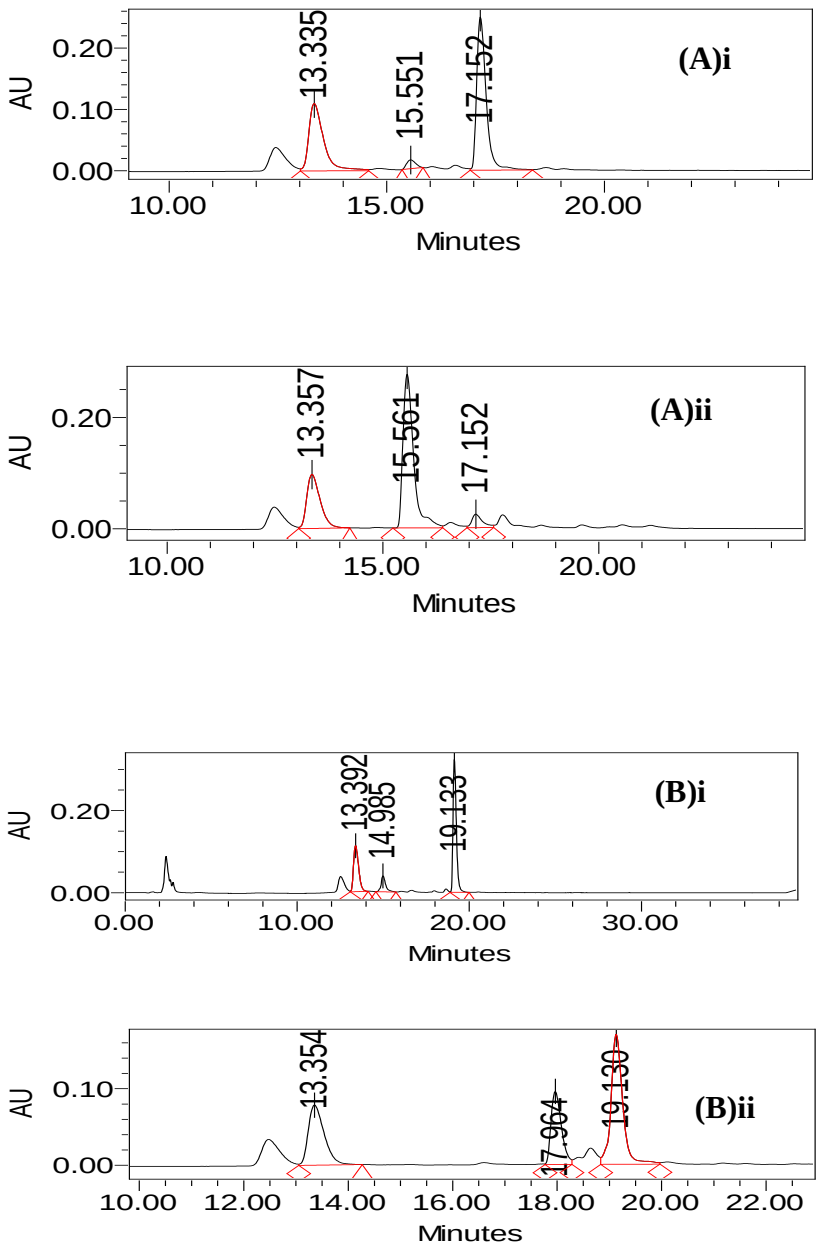

Figure 4-20: HPLC Chromatogram for **A6** (panel A) and NDGA (panel B) incubation in phosphate-citrate buffer (pH 7.4) at 37°C for 6 hr in the presence (i) and absence (ii) of glutathione. The 17.2 or 19.1 min peaks represent **A6** or NDGA while the corresponding dibenzocyclooctadienes derivatives gave 15.6 or 17.9 min peaks respectively. Peak at 13.4 min represent internal standard.

Table 4-2: Relative composition of **A6** or NDGA and their dibenzocyclooctadiene derivatives following 6 h incubation in phosphate-citrate buffer (pH 7.4) at 37°C in the absence or presence of 20 fold excess glutathione. Concentrations were calculated from peak area ratios.

Compound	Incubation for 6h at 37 °C in the presence of GSH, (%)			Incubation for 6h at 37 °C in the absence of GSH, (%)		
	SM	CycloL	Adduct	SM	CycloL	Adduct
A6	95.46	4.54	-	8.52	91.47	-
NDGA	87.08	-	12.91	66.90	33.09	-

SM = starting material; CycloL = dibenzocyclooctadiene derivative

We determined that the dibenzocyclooctadiene derivatives **2** and **84** are unstable in the phosphate buffer over time. Compound **84** degraded at a rate of 1.75×10^{-5} s^{-1} in comparison with 0.470×10^{-5} s^{-1} for compound **2.**

Table 4-3: The rate of formation[a] and degradation[b] of dibenzocyclooctadiene derivatives **2** and **84** in a phosphate buffer (pH 7.4) at 37°C.

Compound	[a]k × 10^{-5} s^{-1}	[a]Rel rate	[b]k× 10^{-5} s^{-1}	[b]Rel rate
2	2.78	1	0.47	1
84	8.70	3.1	1.75	3.7

4.3 Assessment of Reactive Metabolites Formation of NDGA analogues

4.3.1 Synthesis of Pilot Compounds PC1 and PC2

Two pilot compounds **PC1** and **PC2** were prepared from eugenol according to Scheme 4-11 below. PC1 and PC2 were used to mimic the catechol and phenol NDGA analogues respectively under oxidative conditions.

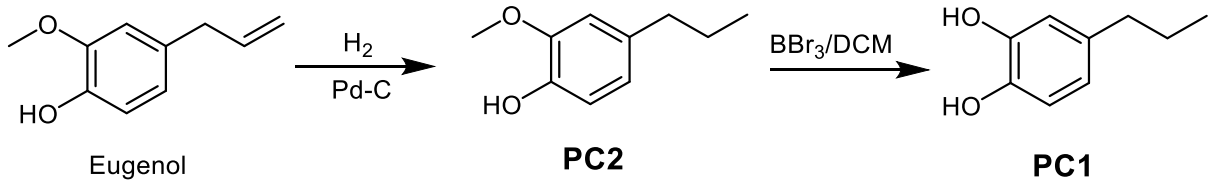

Scheme 4-11: Synthesis of pilot compounds from eugenol.

4.3.2 Enzymatic Oxidation Studies

Enzymatic oxidation experiments were performed using mushroom tyrosinase and the resulting quinoid species trapped as GSH conjugates. Tyrosinase-catalyzed oxidization of catechol is a common method for producing an o-Q moiety.[77, 78, 87] Pilot studies were done using **PC1**, **PC2** and standard NDGA. The experiments were repeated using **A1, A2, A3, A4 or A6**. All glutathione conjugates were analyzed by HPLC and further by MS techniques.

4.3.2.1 Neutral Loss (NL) ESI-MS Analysis

Glutathione conjugates were detected by NL scanning for protonated ions that fragment to give *m/z* 129 Da corresponding to the pyroglutamic acid moiety. This MS technique has been extensively utilized in the literature for detecting GSH adducts although it lacks general applicability.[116] As exemplified by **PC1**, NDGA, **A1** and **A4** in Figure 4-21, a NL 129 scanning in

positive ion mode gave the masses *m/z* 458.2, 608.3, 576.2 and 636.3 Da consistent with mono-GSH conjugates of **PC1**, NDGA, **A1** and **A4** respectively. In addition, GSH is capable of losing *m/z* 129 Da as indicated by the presence of *m/z* 308.1 Da for excess GSH.

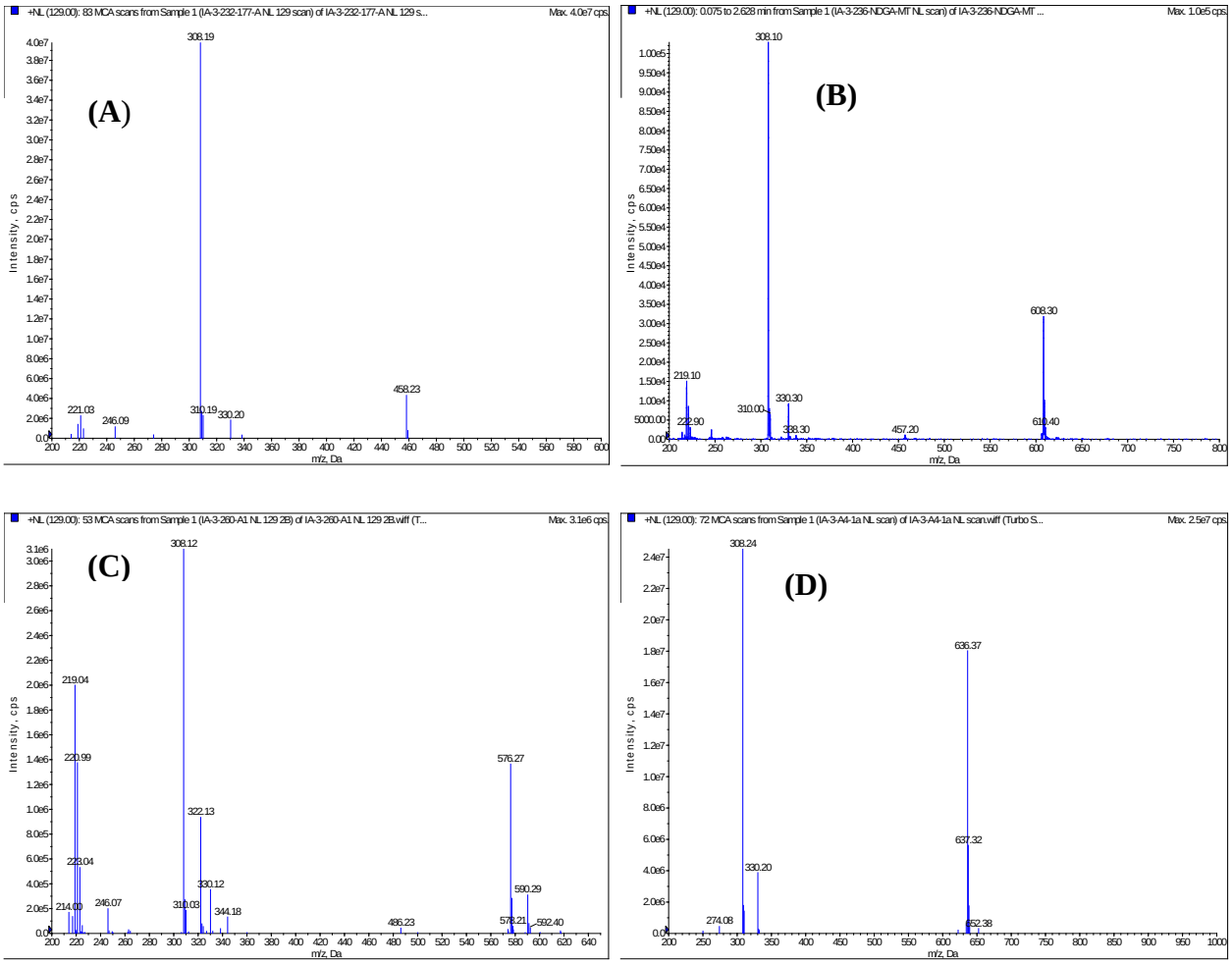

Figure 4-21: Positive ion ESI-MS in NL scan mode (129 Da) for detection of GSH conjugates for **PC1** (panel A), NDGA (panel B), **A1** (panel C) and **A4** (panel D). The masses *m/z* 458.2, 608.3, 576.2 and 636.3 Da detected by NL 129 scanning in positive ion mode are consistent with mono-GSH conjugates of PC1, NDGA, **A1** and **A4** respectively. The ion at *m/z* 308 Da is due to a NL 129 from excess GSH present in all the samples.

4.3.2.2 Enhanced Resolution ESI-MS Analysis

To further confirm the presence of GSH conjugates, parent ions (MH^+) were determined by ESI-MS in enhanced resolution (ER) positive ionization scanning mode. This gave isotopic peaks separated by one mass unit indicating singly charged adducts (Figure 4-22). Doubly charged adducts will be expected to have one-half mass unit difference between isotopic peaks. The ratio of substrate to GSH (1:5) was optimized to favour addition of one GSH molecule[33] although trace amounts of di-conjugate were observed in the case of NDGA and **A4** which is consistent with results of Billinsky et al.[33]

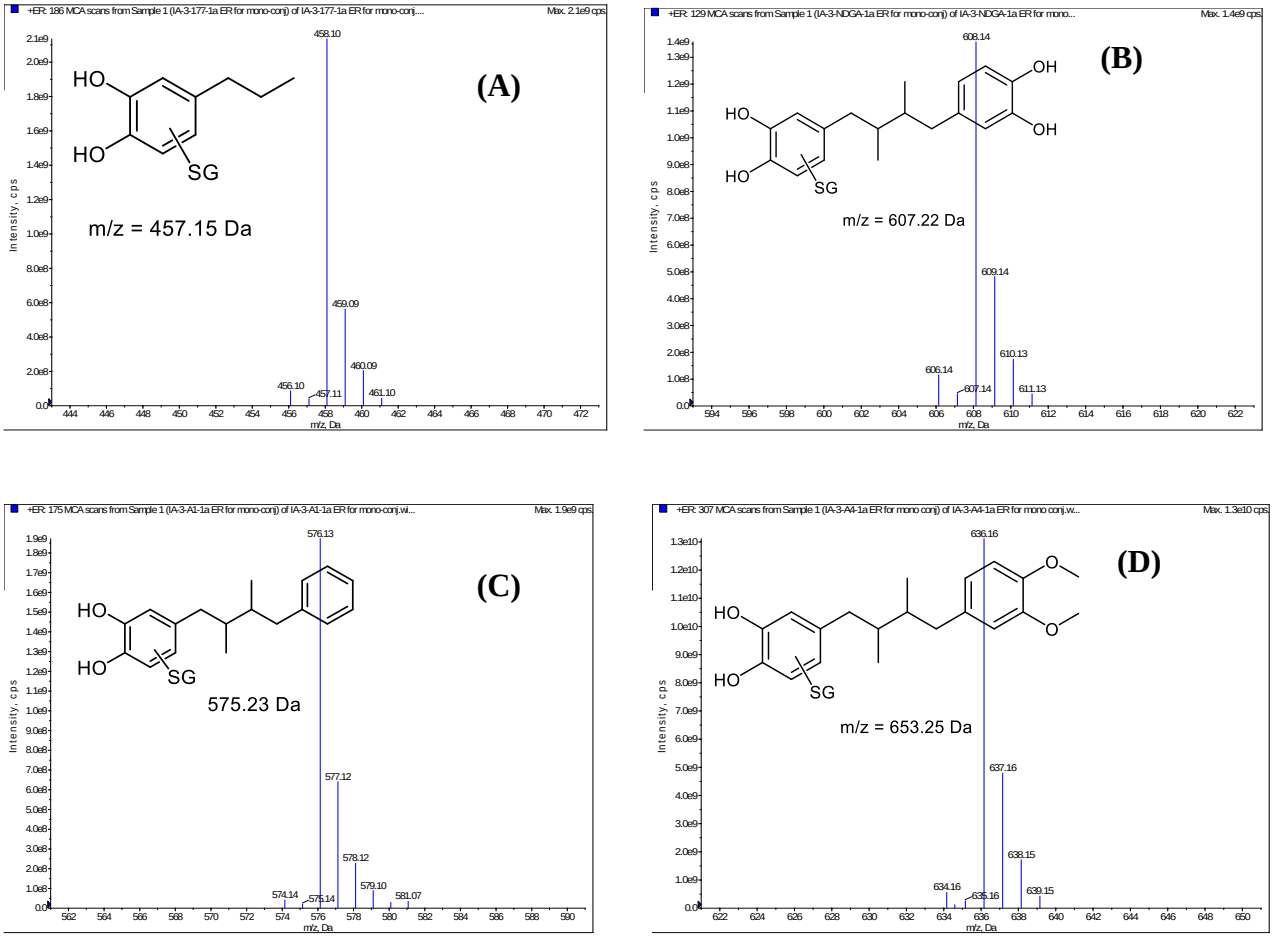

Figure 4-22: Positive ion ESI-MS in ER scan mode for detection of GSH conjugates for PC1 (panel A), NDGA (panel B), **A1** (panel C) and **A4** (panel D). The isotopic peaks obtained following ER scanning for the parent ions $[M+H^+]^+$ differed by one mass unit for all observed masses. This is

consistent with addition of one GSH molecules as di-conjugates will be expected to have one-half mass unit difference.

4.3.2.3 Tandem ESI-MS-MS Analysis

In order to obtain further information for structural elucidation, tandem ESI-MS/MS analyses were performed on all suspected GSH conjugates. This was preceded by MS/MS analysis of standard GSH. The product ions generated by MS/MS analyses (Figure 4-23, Table 4-4) were consistent with fragmentation patterns reported for glutathione adducts[116, 126, 132] and mirrored those obtained for standard GSH (Figure 4-23A). The fragmentation pathways were consistent for all GSH conjugates examined including standard NDGA-GSH conjugate (Figure 4-23B). The mass loss patterns and the resulting product ions suggest that fragmentation mainly occurred in the GSH moiety consistent with previous reports.[116, 132]

The common neutral losses of glycine (75 Da), pyroglutamic acid (129 Da) and 146 Da mass units observed for standard GSH were also seen for GSH conjugates of **PC1**, NDGA and the cateccol analogues (**A1, A4, A6**). In addition, other typical losses from the parent ion MH^+ including 232, 249 and 275 Da mass units were consistently observed for all GSH conjugates analyzed.

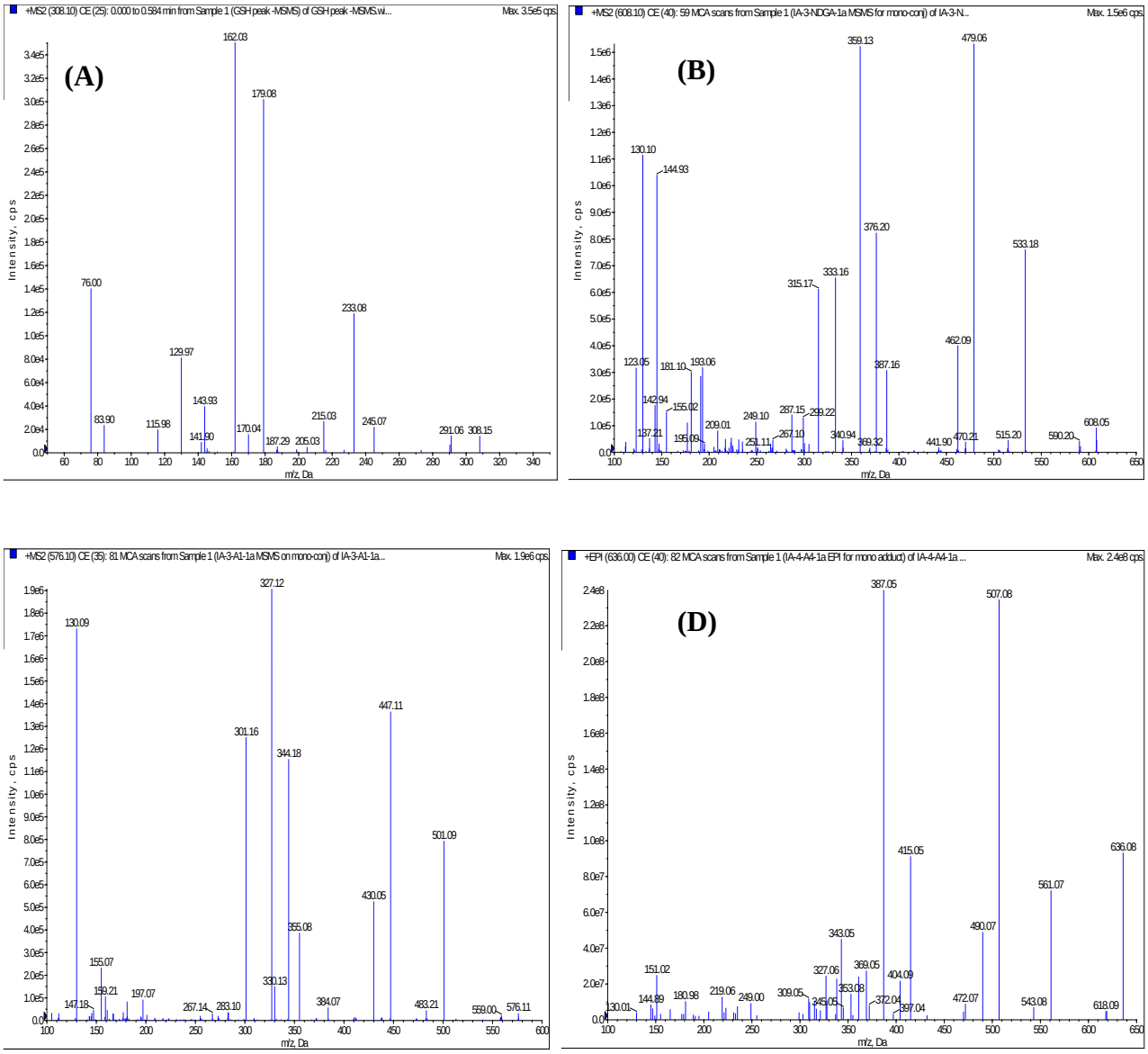

Figure 4-23: Tandem ESI-MS/MS in positive ion mode for standard GSH (Panel A); NDGA-GSH (Panel B), **A1**-GSH (Panel C) and **A4**-GSH (Panel D) conjugates.

Table 4-4: Summary of Tandem MS/MS data for GSH conjugates following mushroom tyrosinase-catalysed oxidation.

Compound (M)	MH^+ and (Major fragments) of GSH adduct[b]	Adduct composition	Isotopic peaks[c]
PC1 (152)	[a]458 (383, **329**, 312, 237, 266, 183, 130)	P + GSH – 2H	458.1, 459.1, 460.1
PC2 (166)	-	-	-
NDGA (302)	[a]608 (533, **479**, 462, 387, 376, 359, 333, 130)	P + GSH – 2H	608.1, 609.1, 610.1
A1 (270)	[a]576 (501, **447**, 430, 355, 344, 327, 301, 130)	P + GSH – 2H	576.1, 577.1, 578.1
A2 (284)	-	-	-
A3 (330)	-	-	-
A4 (330)	[a]636 (561, **507**, 490, 415, 404, 387, 361, 130)	P + GSH – 2H	636.2, 637.2, 638.2
A6 (274)	[a]580 (505, **451**, 434, 359, 348, 331, 305, 130)	P + GSH – 2H	580.1, 581.1, 582.1

[a]The GSH adducts detected were the peaks detected by NL scan for m/z 129 Da. [b]Product ions listed were greater than 5% relative intensity. The boldface type denotes the product ions from the loss of 129 Da mass units from the parent ion. [c]Isotopic peaks were obtained by ER in positive ion scanning mode.

In summary, the pilot compound **PC1** easily oxidized in the presence of mushroom tyrosine to reactive quinone. Enhanced resolution MS gave *m/z* 458.1 Da consistent with addition of one glutathione molecule to **PC1** (Table 4-4). NDGA and its catechol analogues (**A1**, **A4** and **A6)** were

similarly oxidized to their corresponding quinoid species in the presence of mushroom tyrosinase and were stably trapped as glutathione conjugates for analysis (Table 4-4). As expected, we found no evidence of GSH conjugates for **PC2** and the phenol analogues of NDGA (**A2** and **A3**) in the mushroom tyrosinase-catalyzed oxidations indicating that the phenols do not form reactive intermediates under these conditions.

4.3.3 Isomerization of NDGA *o*-Q to *p*-QM

In theory, the structure of NDGA suggests possible direct oxidation to either o-Q or p-QM (Scheme 4-12). Surprisingly, NDGA does not appear to form the p-QM[33] even though its o-Q meets the structural requirements for isomerization.[77,78] The presence of benzyl protons available for abstraction suggests that the NDGA o-Q **5b** can tautomerize to a p-QM **5c.**[79] We investigated a possible isomerization of o-Q to p-QM using **A1** and **A4**. This study was expected to provide insight into the contribution of NDGA p-QM to its toxicity. Based on our observation that **A1** and **A4** form o-Qs but do not cyclize to dibenzocyclooctadiene derivatives in aqueous phosphate buffer (pH 7.4), we selected both compounds for this study. This was based in part on the assumption that competition between isomerization and intramolecular cyclization should not occur for **A1** or **A4** as may be the case for NDGA. We therefore predicted that **A1** or **A4** will form p-QM.

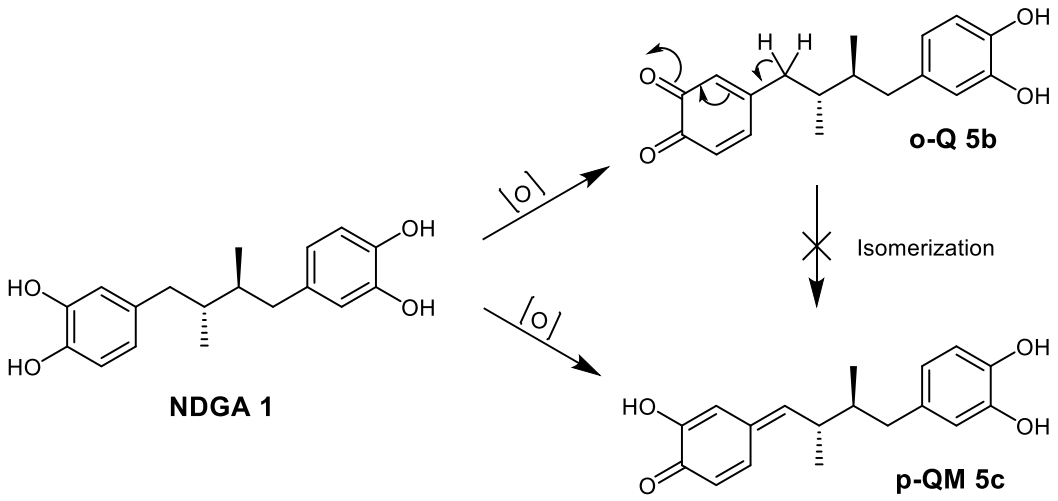

Scheme 4-12: Proposed oxidation of NDGA 1 to p-QM 5c either directly or via isomerization of its o-Q 5b.

A1 or **A4** was oxidized with mushroom tyrosinase in the presence and absence of GSH for 60 min. An aliquot from the experiment conducted in the absence of GSH was stirred in phosphate buffer after the 60 min incubation to allow for isomerization. GSH was added at different time points and samples were analyzed by HPLC and LC-MS. As shown in Figure 4-24, suspected GSH conjugate peaks were observed at 21.7 and 20.6 min respectively for **A1** and **A4** from the experiment conducted in the presence of GSH. However, HPLC analyses of time point samples obtained from 60 min incubation without GSH followed by stirring in a phosphate buffer experiment gave no evidence of conjugates formation.

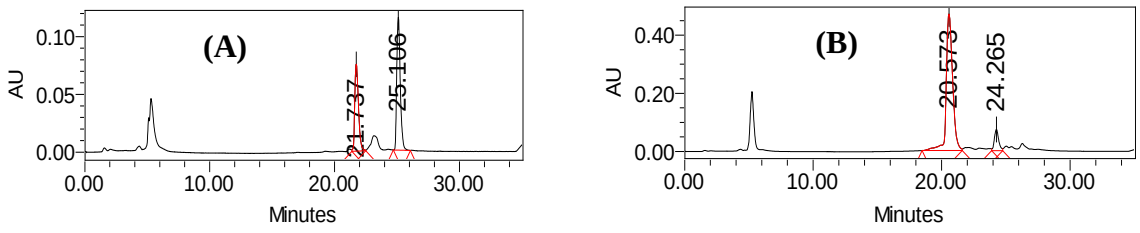

Figure 4-24: HPLC chromatograms for **A1** (panel A) and **A4** (panel B) following mushroom tyrosinase-catalyzed incubation for 60 min in the presence of GSH.

Following LC-MS analyses, the peaks observed at 21.7 and 20.6 min by HPLC from **A1** and **A4** incubations in the presence of GSH gave *m/z* 576 and 636 consistent with the $[M+H]^+$ for **A1**-GSH and **A4**-GSH conjugates respectively. Product ions generated from the extracted ion chromatogram (XIC) (Figure 4-25) were consistent with fragmentation patterns oberved for **A1** or **A4** conjugates derived from their respective o-Qs via mushroom-tyrosinase catalyzed oxidations. No GSH conjugates were detected in the time point experiments where the initial incubation was done in the absence of GSH, suggesting that quinones were not stably present after 60 min incubations. The results of this study suggest that isomerization of o-Q to p-QM did not occur for **A1** or **A4**.

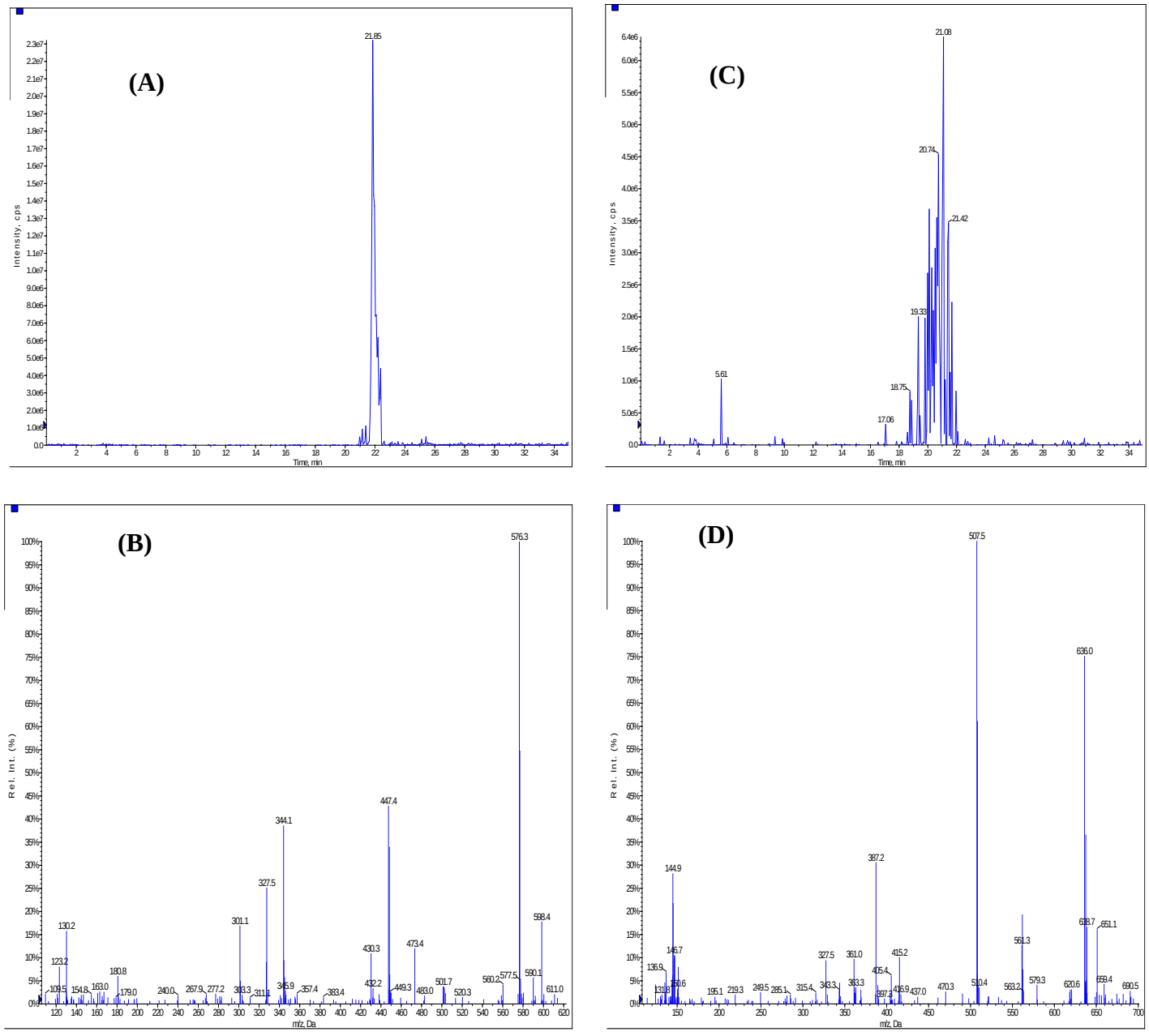

Figure 4-25: LC-MS data for **A1** and **A4** incubation for 60 min with mushroom tyrosinase in the presence of GSH: (A) XIC chromatogram and (B) product ion for **A1**-GSH conjugate; (C) XIC chromatogram and (D) product ion for **A4**-GSH conjugate.

4.4 Chemical Oxidation Studies

Chemical oxidations were performed using silver oxide and the resultant electrophilic entities were trapped as GSH adducts. This is a classical approach utilized to generate p-quinone methides from catechols and/or phenols.[78, 80] Previous attempts to oxidize NDGA directly to a p-quinone methide with silver oxide was unsuccessful but resulted in a complex mixture of products none of which was glutathione reactive.[35] The reported results were based only on HPLC-UV analysis and are possibly limited by instrument sensitivity. To further probe this observation, eugenol, **PC1** and **PC2** were used to establish and validate the chemical oxidation protocol. Eugenol and **PC2** have previously been oxidized to p-quinone methide with Ag_2O.[78, 133] The experiments were repeated with NDGA and its prepared analogues. The conditions used for HPLC and MS analysis were the same as those used for enzyme oxidation studies. However, additional MS experiments using PI scan for *m/z* 272 Da in the negative ESI mode and NL scan for *m/z* 307 Da in positive ion mode were done. Table 4-5 shows the sensitivities of various MS scan modes used in detecting GSH adducts following Ag_2O oxidation experiment

4.4.1 Precursor Ion (PI) ESI-MS Analysis

Following the non-detection of GSH conjugates for eugenol, **PC2** and the phenol NDGA analogues by NL 129 Da scanning experiment even though eugenol and **PC2** are known to oxidize to p-QM in the presence of Ag_2O,[78, 133] the potential of PI 272 Da scanning in negative ionization mode as an alternative detection method was explored. The PI scan for 272 Da appears to be more sensitive and has broader applicability in detecting GSH conjugates of different classes for compounds.[116] The results of this study revealed that, PI 272 Da scan was successful in detecting GSH adducts of **PC1**, **A1** and NDGA at *m/z* 456.2, 574.1 and 606.3 Da respectively (Table 4-5). In

addition, the observed *m/z* 306.1 Da was consistent with excess GSH. Surprisingly, we saw no evidence of GSH conjugates for eugenol, **PC2**, **A2** and **A3** by PI 272 Da scanning in negative ion mode.

4.4.2 Neutral Loss (NL) ESI-MS Analysis

In addition to NL 129 Da scanning in positive ionization mode, NL 307 Da corresponding to a loss of GSH moiety has been employed in detection of GSH conjugates, albeit to a lower extent.[116] To determine the potential utility of NL 307 Da for detecting GSH conjugates, the Ag_2O-catalysed oxidation samples were analyzed. Interestingly, adducts generated from **PC1**, NDGA and its catechol analogues could not be detected by NL 307 scanning in positive ion mode. However, GSH adducts of eugenol, **PC2** and **A2** could easily be detected by NL 307 Da scan (Table 4-5). A *m/z* 470.2, 472.2 and 590.3 Da detected by NL 307 Da is consistent with GSH adducts of eugenol, PC2 and **A2** respectively.

Table 4-5: Detection of GSH adducts using different ESI-MS scanning techniques.

Compound-GSH conjugate (M, Da)	MS Detection Technique		
	ESI-MS (+) NL 129	ESI-MS (+) NL 307	ESI-MS (-) PI 272
Eugenol-GSH (469)	ND	470.1	ND
PC1-GSH (457)	458.1	ND	456.2
PC2-GSH (471)	ND	472.2	ND
NDGA-GSH (607)	608.3	ND	606.3
A1-GSH (575)	576.1	ND	574.2
A2-GSH (598)	ND	590.2	ND
A3-GSH (635)	ND	ND	ND
A4-GSH (635)	636.2	ND	634.2

ND = not detected

4.4.3 Tandem ESI-MS-MS Analysis

Tandem MS/MS experiments were performed on all suspected GSH conjugates to obtain further information for structure elucidation. Examples of MS/MS spectral data and summary of product ions following Ag_2O catalyzed oxidation in the presence of GSH are shown in Figure 4-26 and Table 4-6 respectively.

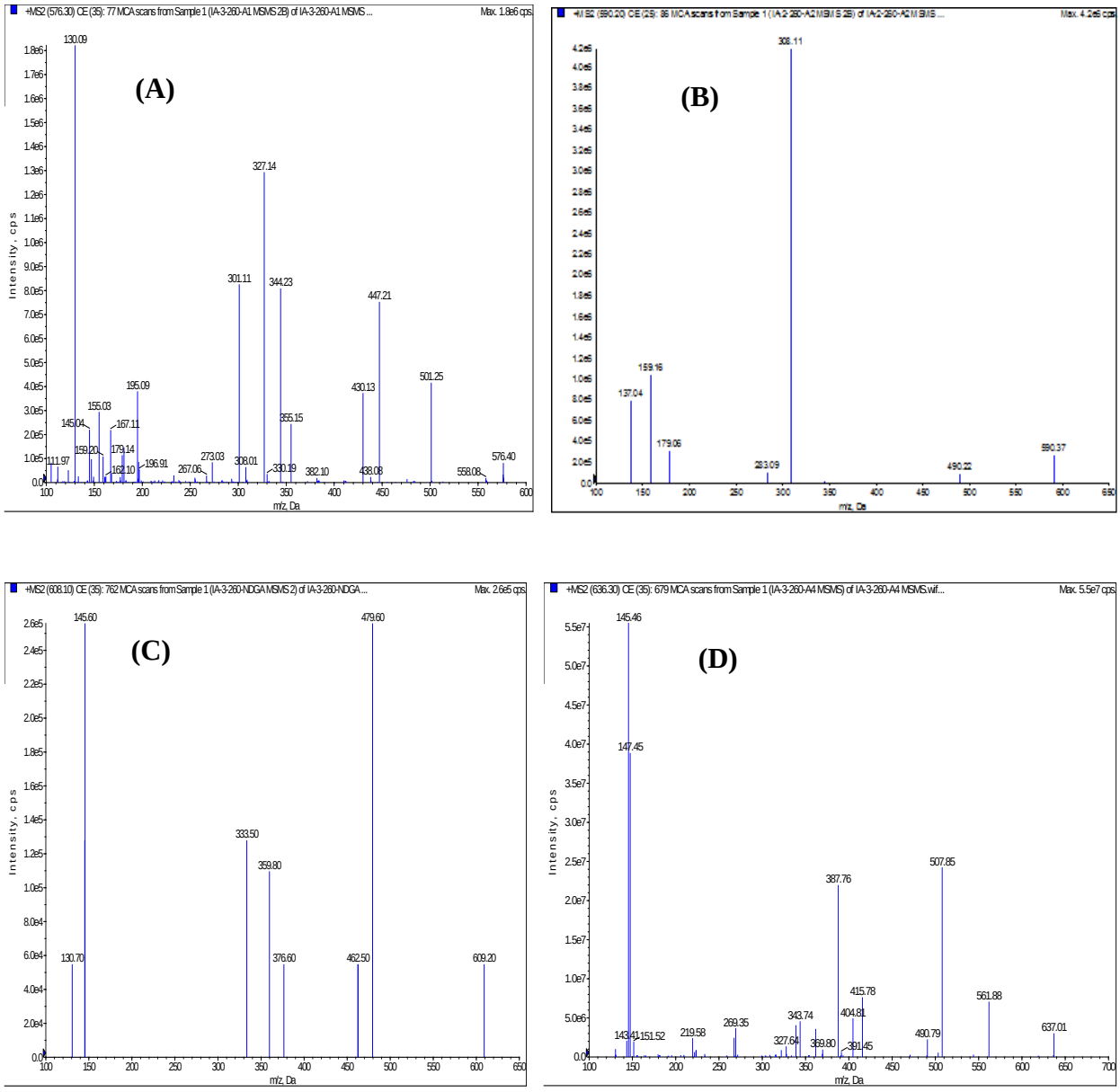

Figure 4-26: Tandem ESI-MS/MS in positive ion mode for GSH conjugates of **A1** (Panel A), **A2** (Panel B), NDGA (Panel C) and **A4** (Panel D) following silver oxide oxidation.

Table 4-6: Summary of Tandem MS/MS data for GSH conjugates following Silver oxide oxidation experiment.

Compound (M)	MH^+ and (Major fragments) of GSH adduct[c]	Adduct composition	Isotopic peaks[f]
Eugenol (164)	[a]470 (308, 233, 179, 163[d])	P + GSH – 2H	470.1, 471.1, 472.1
PC1 (152)	[b]458 (329[e], 312, 226, 209, 183, 145, 130)	P + GSH – 2H	458.1, 459.1, 460.1
PC2 (166)	[a]472 (308, 233, 179, 165[d])	-	472.2, 473.2, 474.2
NDGA (302)	[b]608 (479[e], 462, 376, 359, 333, 145, 130)	P + GSH – 2H	608.1, 609.1, 610.1
A1 (270)	[b]576 (501, 447[e], 430, 355, 344, 327, 301, 130)	P + GSH – 2H	576.1, 577.1, 578.1
A2 (284)	[a]590 (308, 283[d], 159, 179, 137)	-	-
A3 (330)	-	-	-
A4 (330)	[b]636 (561, 507[e], 490, 415, 404, 387, 343, 327, 145)	P + GSH – 2H	636.2, 637.2, 638.2

[a]The GSH adducts were detected by NL scan for m/z 307 Da in positive ion mode only. [b]The GSH adducts were detected by either NL scan for m/z 129 Da in positive ion mode or PI scan for m/z 272 Da in negative ion mode. [c]The product ions were obtained in positive ion mode and the major ions listed were greater than 5% relative intensity. [d]The product ions from the loss of 307 mass unit from the parent ions. [e]The product ions from the loss of 129 Da mass unit from the parent ion. [f]Isotopic peaks were obtained by ER in positive ion scanning mode.

4.5 Cytochrome P450 Oxidation Studies

In order to assess the relevance of the observed reactive metabolites in biological systems, *in-vitro* microsomal incubations using rat liver microsomes were performed. The results were compared with those obtained from chemical or enzyme-catalyzed oxidation studies. HPLC analyses showed significant loss of substrates although product peaks were barely seen. The samples were further analyzed by LC-ESI-MS using NL 129 or 307 Da scan in positive ion mode or PI 272 in negative ion mode as detection techniques. Suspected GSH adducts were subjected to tandem MS/MS analysis to obtain further information for structure elucidation in a second LC-ESI-MS run.

Glutathione conjugates of NDGA and its catechol analogues were detected by NL 129 Da scan in the LC-ESI-MS experiments. GSH-trapped conjugates of NDGA, **A1**, **A4** and **A6** gave parent ions (MH^+) at *m/z* 608.1, 576.1, 636.2 and 580.1 respectively. Tandem MS/MS analyses gave product ions (Table 4-7) generated from common neutral losses of glycine (75 Da) and pyroglutamic acid (129 Da) in addition to other typical losses including 146, 232, 249 and 275 Da mass units from the parent ion (MH^+) for all GSH-trapped conjugates. Also, cytochrome P450 mediated oxidation of NDGA-derived dibenzocyclooctadiene lignan **2** gave a parent ion MH^+ at 606.2 Da and product ions consistent with GSH conjugates. Like the parent ion, observed product ions (Table 4-7) were two mass units lower than their corresponding product ions obtained for NDGA. An example of an ion chromatogram from the LC-ESI-MS analysis is shown in Figure 4-27 for RLM incubation of **A1** in the presence of GSH. Incubations performed in the absence of NADPH gave the same results for NDGA and its catechol analogues suggesting that oxidation was independent of NADPH and possibly results from autoxidation. There was no evidence of P450 enzyme mediated oxidation to reactive quinones for the phenolic analogues **A2**, **A3** and **A8** by NL

129 Da or 307 scanning in positive ion mode. The results were no different when the samples were re-analyses using PI 272 Da scan in negative ion mode as detection method.

Table 4-7: Summary of Tandem MS/MS data for GSH conjugates following RLM incubation experiments.

Compound (M)	MH^+ and (Major fragments) of GSH adduct[b]	Adduct composition	Isotopic peaks[f]
NDGA (302)	[a]608 (533, **479**, 462, 444, 376, 359, 341, 333, 315, 191, 130)	P + GSH – 2H	608.1, 609.1, 610.1
A1 (270)	[a]576 (501, **447**, 430, 355, 344, 327, 301, 130)	P + GSH – 2H	576.1, 577.1, 578.1
A4 (330)	[a]636 (561, **507**, 415, 404, 387, 361, 343, 327, 315, 233, 219)	P + GSH – 2H	636.1. 637.1, 638.1
A6 (274)	[a]580 (505, **451**, 442, 331, 305, 287, 199, 163, 147, 130)	P + GSH – 2H	580.1, 581.1, 582.1
cNDGA **2** (300)	[a]606 (531, **477**, 460, 374, 357, 331, 313, 298, 261, 130)	P + GSH – 2H	636.2, 637.2, 638.2

[a]The GSH adducts were detected by NL scan for m/z 129 Da in positive ion mode. [b]The product ions were obtained in positive ion mode and the major ions listed were greater than 5% relative intensity. The boldface type denotes product ions from the loss of 129 Da mass units from the parent ion. [f]Isotopic peaks were obtained by ER in positive ion scanning mode.

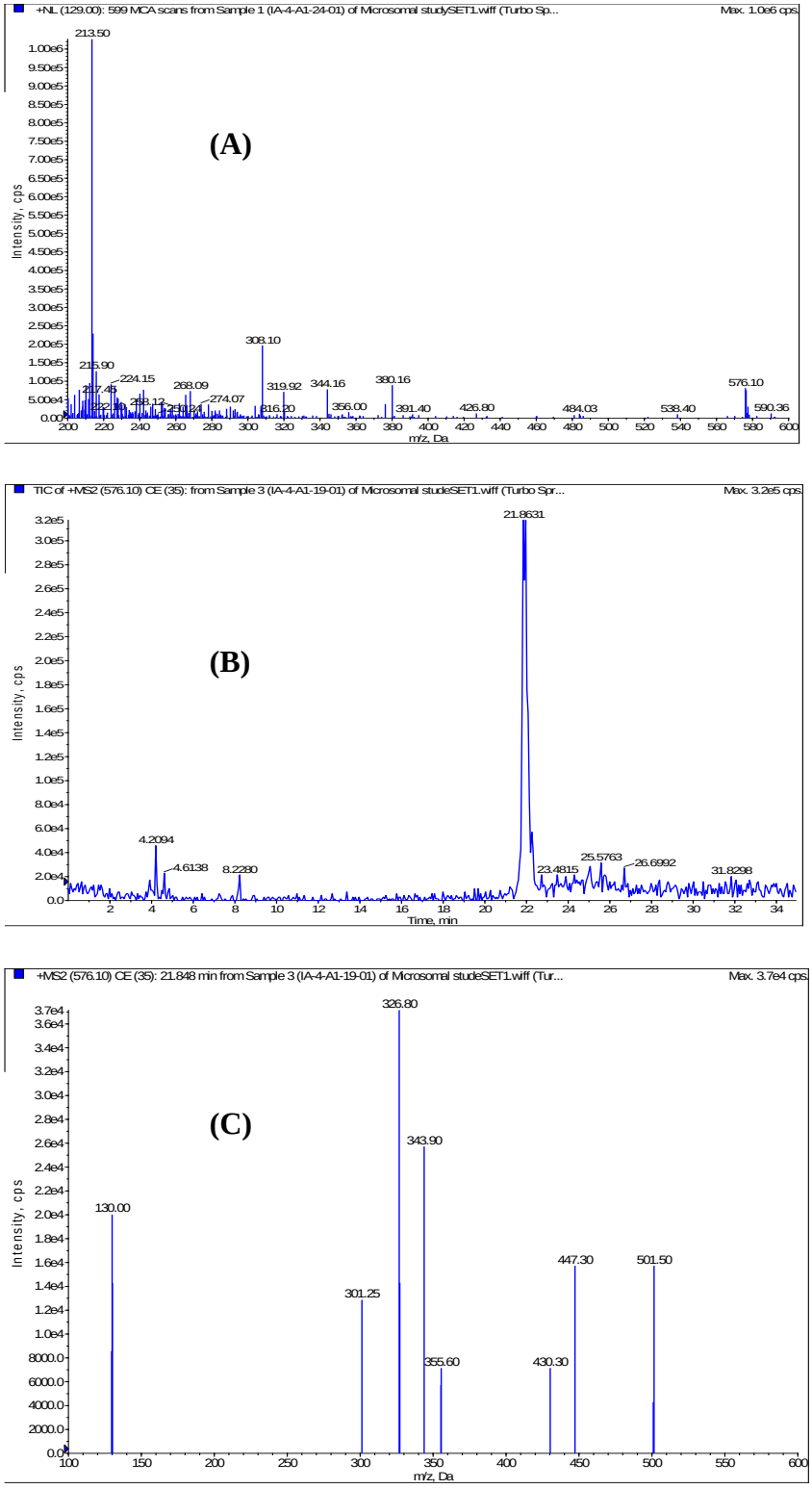

Figure 4-27: NL and LC/MS/MS analysis of NDGA analogue **A1**-GSH conjugate formed in the RLM incubation. (A) NL scanning of 129 Da; (B) TIC of MSMS for 576.1 Da; (C) Product ion spectrum of MH^+ (576.1) for **A1**-GSH conjugate.

4.5.1 MRM-EPI MS Analysis of Microsomal Incubations

Rat liver microsomal incubations were analyzed further using the quadrupole-linear ion trap mass spectrometry (Q-trap) which combines MS/MS scan functions of both the triple quadrupole and the ion trap.[128] Multiple reactions monitoring (MRM) was used as a survey scan to trigger acquisition of enhance product ion (EPI) data. As exemplified by **A1** (Figure 4-28) and **A4 (**Figure 4-29**)**, the results of this study was consistent with data obtained by using the NL 129 Da detection method. Again, no evidence of reactive metabolites formation was seen for the phenol analogues of NDGA by the MRM-EPI technique.

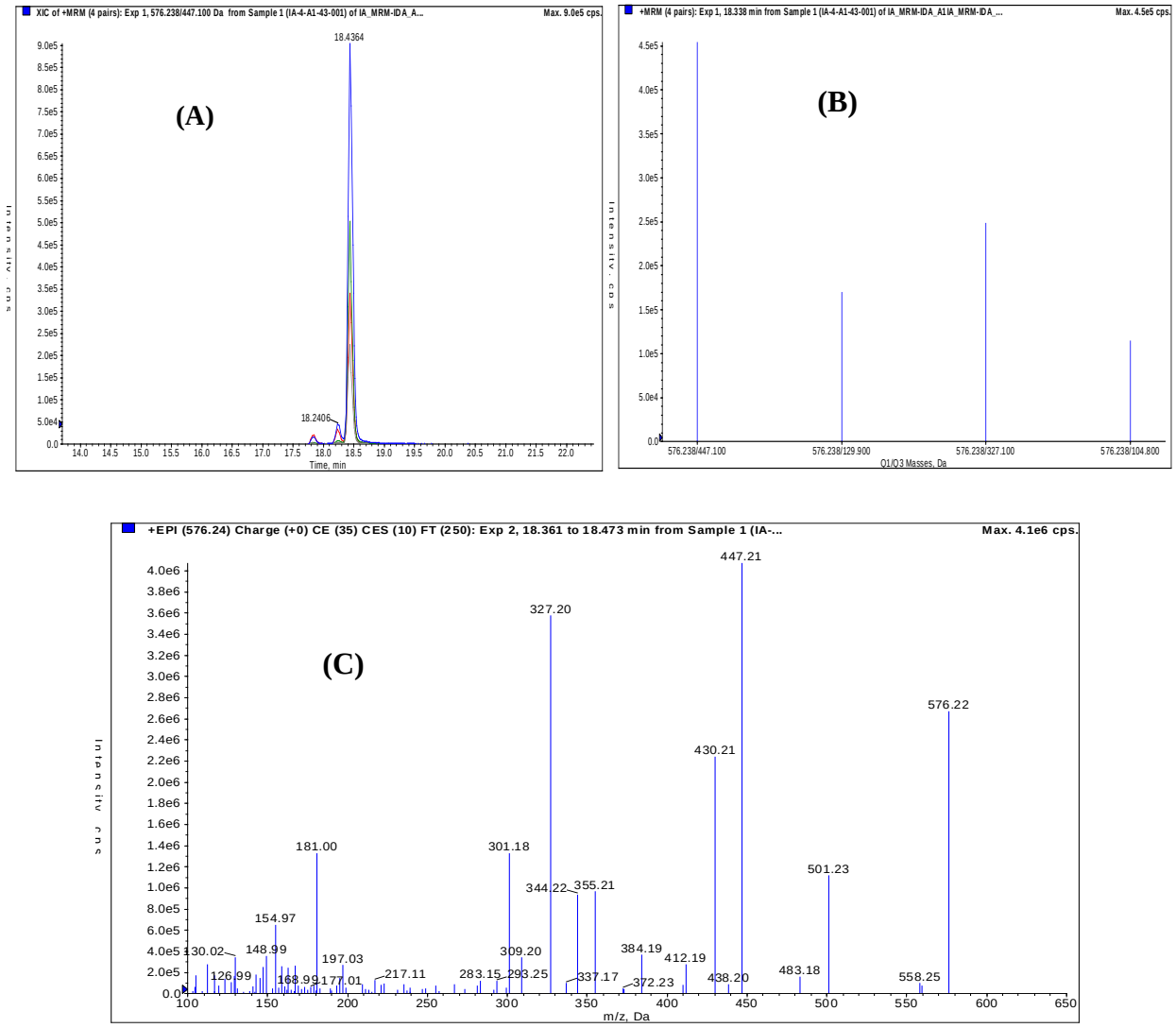

Figure 4-28: MRM-EPI analysis of GSH conjugate formed in the RLM incubation for **A1**-GSH conjugate: XIC (panel A); MRM (panel B) and EPI (panel C).

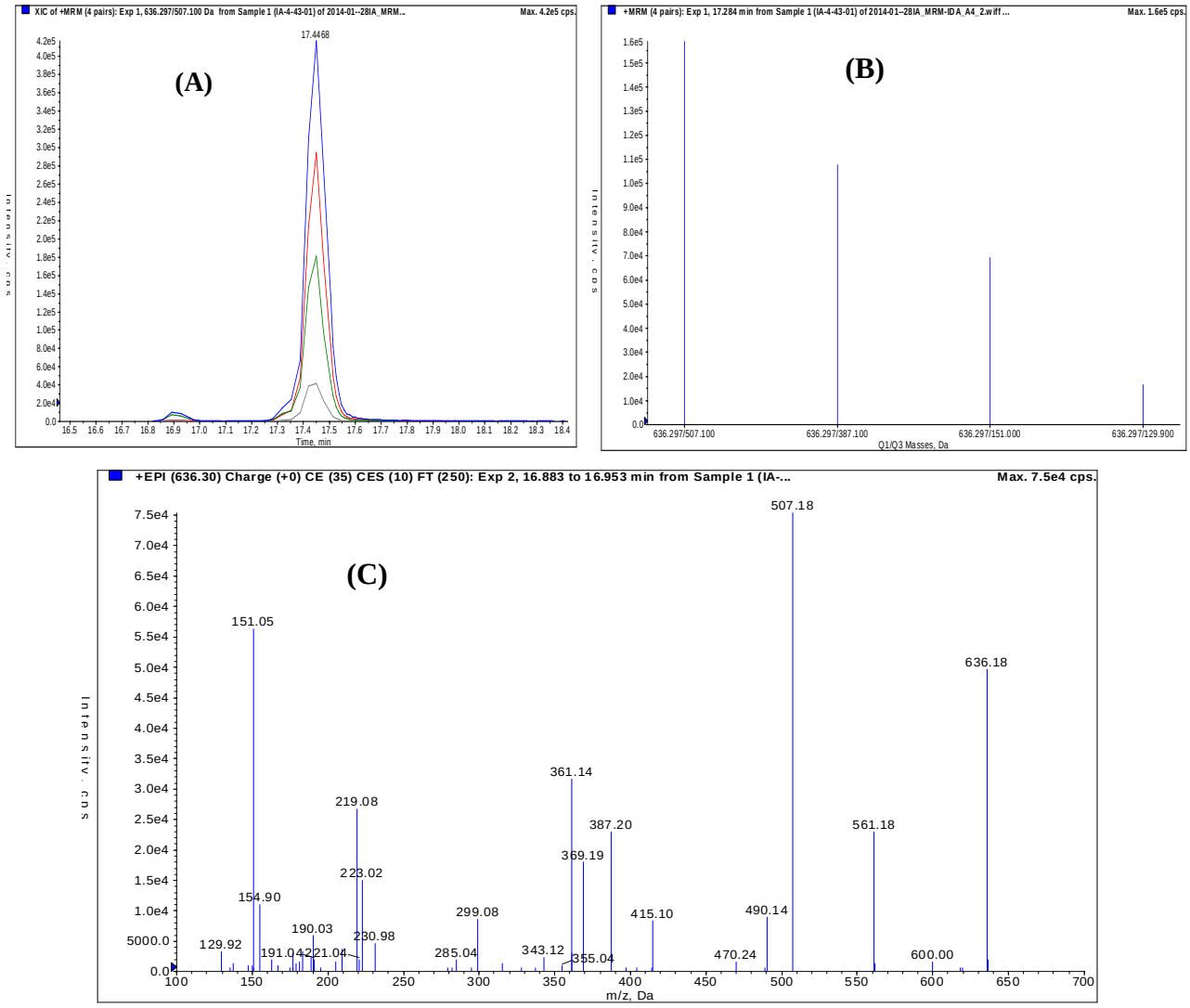

Figure 4-29: MRM-EPI analysis of GSH conjugate formed in the RLM incubation for **A4**-GSH conjugate: XIC (panel A); MRM (panel B) and EPI (panel C).

4.6 Preliminary Cytotoxicity Evaluation

NDGA **1**, cNDGA **2** and analogues synthesized for this study were evaluated for cytotoxicity against four human breast cancer cell lines T47D, MDA-MB-231 (M231), MDA-MB-468 (M468), MCF7, and a lung cancer cell line A549 by our collaborator (J. Tuszynski) at the Cross Cancer Institute (Edmonton, AB). The cell lines were selected based on availability and

establilshed cell lines used in the Tuszynski. The MTS tetrazolium dye assay[40] was used to measure changes in metabolism based on which the cytotoxicity of treatments were inferred (Table 4-8). Thiocolchicine and linoleic acid were used as positive and negative controls respectively. NDGA, the parent compound was tested for comparison.

Table 4-8: Cytotoxicity of NDGA and its prepared analogues in the human lung cancer cell line A549 and four different human breast cancer cell lines.

Compound	Cell lines, IC_{50} (μM)				
	A549	MCF7	MDA-MB-231	MDA-MB-468	T47D
Thiocolchicine	0.035	0.078	0.002	0.021	0.004
Linoleic acid	229.08	371.53	870.96	199.53	239.88
NDGA **1**	676.08	190.54	-	-	-
A1	125.48	199.53	-	?	-
A2	257.04	281.84	218.78	?	190.55
A3b	295.12	190.55	95.45	83.18	75.86
A6	891.25	1288.25	-	-	-
cNDGA **2**	1258.92	-	-	-	-
c**A6 84**	724.43	2041.74	-	-	-
M4N **14**	234.42	100.00	389.05	758.58	588.84

Note: dash (-) indicates no growth inhibition effect, and "?" indicates results discarded due to problems with the plate

As shown in Table 4-8, NDGA and its analogues had no significant growth inhibition effect against all the cell lines tested in comparison with the positive control thiocolchicine although the

phenol analogues **A3b** and **A2** were generally better than the parent compound NDGA against the cell line used. Given that the phenol analogues are oxidatively more stable than the catechol analogues and NDGA, further biological assays in appropriate cell lines where NDGA shows cytotoxic effects are required for better comparison. Contrary to our expectation, cNDGA had no inhibitory activity or was less active in comparison to NDGA at inhibiting the growth the cancer cell lines tested

5 DISCUSSION

5.1 Synthesis and Characterization of NGDA Analogues

A number of approaches have been reported in the literature for synthesis of dibenzylbutane type lignans.[48, 97, 100, 100-102, 102, 106, 107] Two of these approaches were exploited for constructing the basic lignan skeleton in this project. We were initially interested in preparing analogues with defined relative and absolute configuration. An approach utilizing Stobbe condensation-alkylation and resolution of intermediate (±)-diacid via diastereomeric quinine salts is reported to yield enantiomerically enriched lignans.[102] However, we could not successfully resolve our intermediate (±)-diacids as the expected fractional crystallization of the diastereomeric quinine salts did not occur. Whether this resulted from the different substituents on the aromatic rings was not investigated. The second approach involved consecutive Stobbe condensation reactions as an alternative pathway to the basic 18-carbon lignan skeleton. Although relative configuration about the two stereogenic centers could not be controlled, the double Stobbe condensation pathway was versatile in providing access to all the desired compounds for this study. In addition, we could obtain separation into two pairs of enantiomers or a meso-compound and racemic product following flash chromatography of intermediate diols for **A3** and **A8**. In the case of **A3**, the NMR of separated intermediate diols was compared with that of SECO **9** to obtain some information about which fraction is the meso-compound. We have also seen similar separation following a flash column on intermediate tosylates of **A3** and **A8**. Thus, the target analogues were successfully synthesized in yields ranging from 8-45% by literature methods with modifications where appropriate. The prepared analogues were characterized by HPLC-UV-PDA, ESI-MS and NMR methods as reported in Chapter 3. The UV absorptions were consistent with that observed for NDGA.

Molecular mass of each of the prepared analogues was confirmed by ER-ESI-MS analysis. The parent ions $[M-H]^-$ and isotopic masses observed by ER-ESI-MS in negative ionization mode were in agreement with calculated masses. The fragmentation patterns observed by tandem MS/MS analysis were consistent with those obtained for NDGA with a base peak at *m/z* 122 Da as illustrated in Scheme 5-1 for NDGA. The product ions obtained for each analogue are tabulated in Table 3-1 and were in agreement with those obtained for standard NDGA.

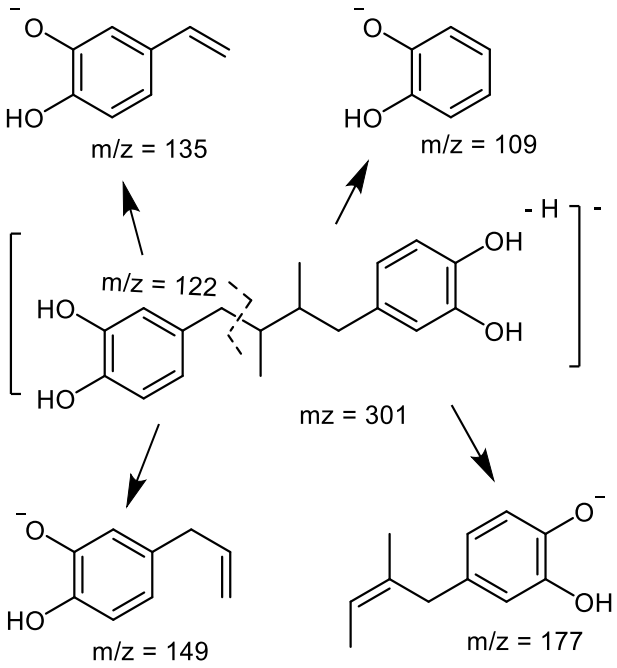

Scheme 5-1: Proposed Fragmentation of the $[M-H]^-$ ion of NDGA (*m/z* 301) following CID.

5.2 Autoxidation of NDGA

The objective of this phase of the study was to investigate the mechanisms of intramolecular cyclization of NDGA and its analogues in phosphate buffer (pH 7.4) at 37ºC to dibenzocyclooctadiene lignans. The dibenzocyclooctadiene family of lignans exhibits numerous pharmacological activities[38, 39, 55] including antiviral,[40-42] anticancer,[41] anti-inflammatory[42] and hepatoprotective effects.[43] Billinsky et al.,[35] reported a unique schisandrin-like dibenzocyclooctadiene lignan derived from NDGA via autoxidation under physiologically relevant conditions. Given the important biological activities of dibenzocyclooctadiene lignans,[38, 49] and the fact that conditions of biological evaluations involving NDGA[5, 36] as well as methods of Chaparral tea preparation[24, 35] favour autoxidation, we speculated that the intramolecular cyclization product probably contributes to the broad spectrum of beneficial properties reported for NDGA. Wagner et al., suggested that any biological action by NDGA treatment could result from either NDGA itself or its oxidation products[37] since many antimicrobial and antineoplastic agents are known to function by interacting with DNA and subsequently affecting nucleic acid metabolism.[53, 54] The authors[37] report that NDGA converts to "activated" NDGA in the presence of molecular oxygen which formed a stable complex with duplex DNA although the structure of the oxidation product was not elucidated. This "activated" NDGA was later confirmed as the dibenzocyclooctadiene derivative.[35]

There is growing evidence in the literature that chemical modification of NDGA reduces toxicity, combined with enhanced therapeutic effects, indicating that derivatives of NDGA may become important drugs in the future.[6] Therefore, investigating the mechanism of autoxidation to dibenzocyclooctadiene derivatives of NDGA and its analogues will aid in understanding the structural features which influence the previously reported intramolecular cyclization process. We

hypothesized that intramolecular cyclization of NDGA to the dibenzocyclooctadiene lignan follows a radical-mediated pathway rather than an electrophilic substitution mechanism. A radical-mediated mechanism has been proposed by Galano et al.,[22] using a combination of theoretical and electrochemical techniques. In these studies, we designed and synthesized a series of NDGA analogues and evaluated their autoxidative potential in a phosphate buffer under aerobic condition at physiological pH and 37 ºC[35] in our effort to unravel the exact mechanism of NDGA cyclization.

Like NDGA, compound **A6** underwent autoxidation to the corresponding dibenzocyclooctadiene lignan, although at a faster rate than NDGA. The rate enhancement seems to correlate with conformational flexibility as the absence of substitution on the butane bridge in the case of **A6** could be expected to confer a less restrictive intramolecular interaction between the two aromatic rings allowing for a faster cyclization than NDGA. Although a Thorpe-Ingold effect is typically experienced by geminal substituents,[134] the vicinal methyl groups attached to the butane-bridge of NDGA likely generate CH_3-CH_3 as well as CH_3-CH_2-Ar steric interactions as shown in Figure 5-1. It is unlikely that the most stable conformations I and IV for NDGA and **A6** respectively favour cyclization and that the required conformations for cyclization are II or III and V or VI. The presence of additional CH_3-CH_3 and CH_3-CH_2-Ar steric interactions suggests conformations II or III are more difficult to attain in comparison with V or VI. This conformational flexibility probably explain the faster rate of cyclization observed for **A6**.

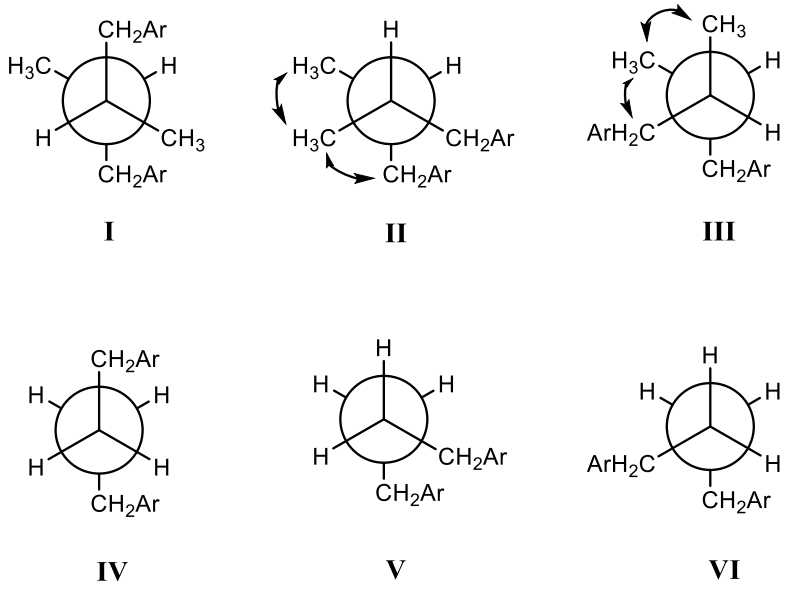

Figure 5-1: Conformational representations for NDGA (I, II, III) and **A6** (IV, V, VI). I and IV represent the most stable conformations for NDGA and **A6** respectively; II or III and V or VI conformers are the required formations for cyclization.

Compounds **A1** and **A4** oxidized to yield o-Q although subsequent nucleophilic attack by the unoxidized ring did not occur. Given that intramolecular reactions are generally kinetically favoured over intermolecular reactions and that the dimethoxy substituted ring of **A4** is comparable to the unoxidized ring of NDGA in nucleophilicity, **A4** was expected to form a dibenzocyclooctadiene derivative if the mechanism involves electrophilic substitution. Compound **A1** was also expected to autoxidize although we predicted it to occur at a slower rate than NDGA. Oxidation of polyphenols by molecular oxygen have resulted in intermolecular reaction products[66, 67] and oxidation of polyphenols present in tea have resulted in dimers and other oligomers via intermolecular nucleophilic attack of an unoxidized ring on an o-Q.[66, 67] The absence of intramolecular cyclization in **A1** or **A4** could imply that a radical-mediated process more accurately describes NDGA oxidative cyclization. This is supported by the biosynthesis of dibenzocyclooctadiene series of lignans in plants, which is known to involve enzymatic

intramolecular oxidative coupling of phenolic precursors via a radical cation intermediate.[60] The biosynthetic approach has been exploited in many synthetic strategies to construct the biaryl linkage of the dibenzocyclooctadiene lignan core structure.[38, 59, 60] In this vein, lignans belonging to the dibenzylbutane class have served as precursors to dibenzocyclooctadiene derivatives via intramolecular coupling reactions using coupling reagents such as ruthenium dioxide (RuO_2) for phenols[60] or 2,3-dichloro-5,6-dicyano-1,4-benzoquinone (DDQ) for non-phenols.[38] No such similar report exists in the literature involving a catechol-containing substrate such as NDGA. The role of conformational rigidity in preventing intramolecular cyclization has not been clarified. However, this hypothesis may not explain the situation for **A1** or **A4** given that both compounds are conformationally equivalent to NDGA.

Attempts to confirm a radical-mediated pathway for cyclization using compound **A7** was unsuccessful, although our observation was similar to a result reported by Robin et al., using RuO_2 for cyclization of an *ortho*-phenol substituted lignan.[60] Robin found however that additional methoxy substituents on the aromatic ring facilitated cyclization, suggesting that the electron-donating methoxy substituents may be critical to cyclization, possibly due to enhanced stability of a radical intermediate. We investigated this hypothesis with compound **A8** where the methoxy substituents were expected to stabilize the intermediate radical to allow for cyclization. In spite of the presence of methoxy groups on both aromatic rings, incubation of **A8** at pH 7.4 gave no intramolecular cyclization product. The intermediate radical of **A8** may be too stable to react or the intramolecular cyclization mechanism is not a simple di-radical coupling as proposed by us[35] and Galano et al.[22] An intriguing possibility, outlined in Scheme 5-2, involves attack of an *ortho*-quinone by an ionized ring. A sequential 2 proton 2 electron loss is expected to yield **5a** or **5b** with

a deprotonation step expected to be pH dependent. This hypothesis would require an analogue consisting of one catechol substituted ring and one 3-hydroxy-4-methoxy substituted ring.

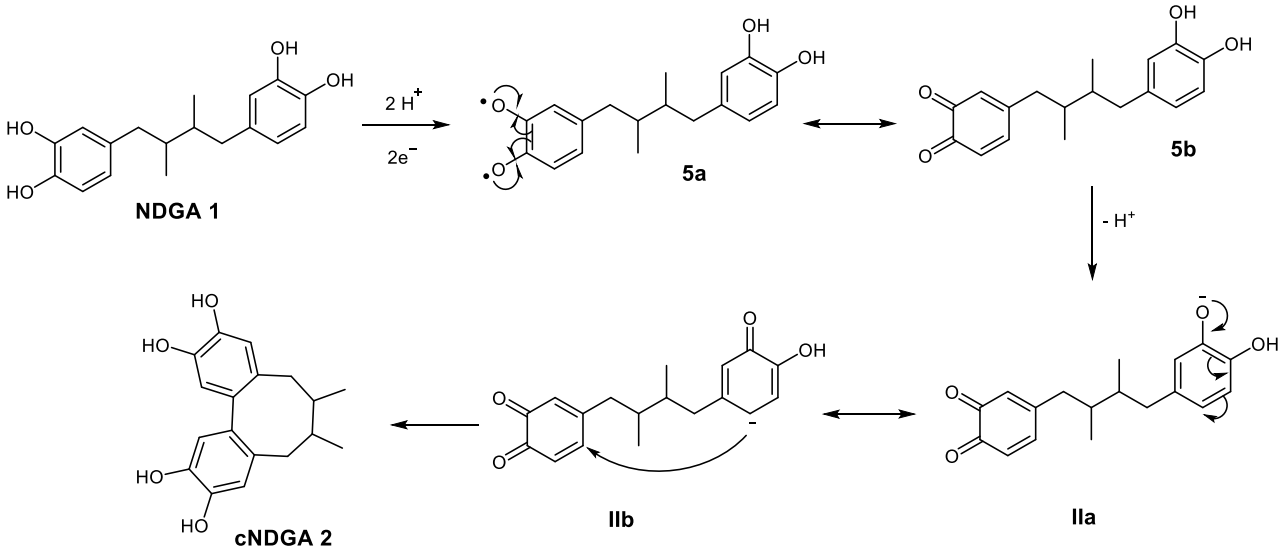

Scheme 5-2: Modification to the proposed mechanism of intramolecular cyclization of dibenzylbutane lignans to dibenzocyclooctadiene derivatives.

Another interesting finding of this study is the inhibition of autoxidation by glutathione, a nucleophilic trapping agent used in this study. As shown in Figure 4-19 and Table 4-2, the rate of intramolecular cyclization and the amount of dibenzocyclooctadiene derivative produced decreased significantly in the presence of GSH. An o-Q will be expected to decrease the concentration of NDGA or **A6** as a result of irreversible conversion to GSH conjugates whilst a semiquinone radical or a di-radical intermediate could regenerate the starting material in the presence of GSH via one electron reduction[135, 136] as shown in Scheme 5-3. In addition, thiol compounds can regenerate the catechol moiety *in situ* during the oxidation reaction of polyphenols and are reported to exhibit potent synergistic effects on the antioxidant activity of polyphenols.[137] Superoxide dismutase (SOD) suppresses oxidation of polyphenols by purging the system of superoxide ions.[67] GSH is

also known to react with superoxide ion to generate oxidized GSH (GSSG)[135] which will be expected to decrease the rate of superoxide-dependent chain oxidation. The proposed radical-mediated or electrophilic substitution mechanisms can both generate superoxide ions, suggesting that incubation in the presence of SOD might not clarify the intramolecular oxidation process. The inhibition of intramolecular cyclization suggests that GSH acts as radical scavenger as illustrated in Scheme 5.3 and that the dibenzocyclooctadiene product only formed atfter GSH was depleted. This supports the involvement of free radicals as opposed to o-Q in the intramolecular cyclization process.

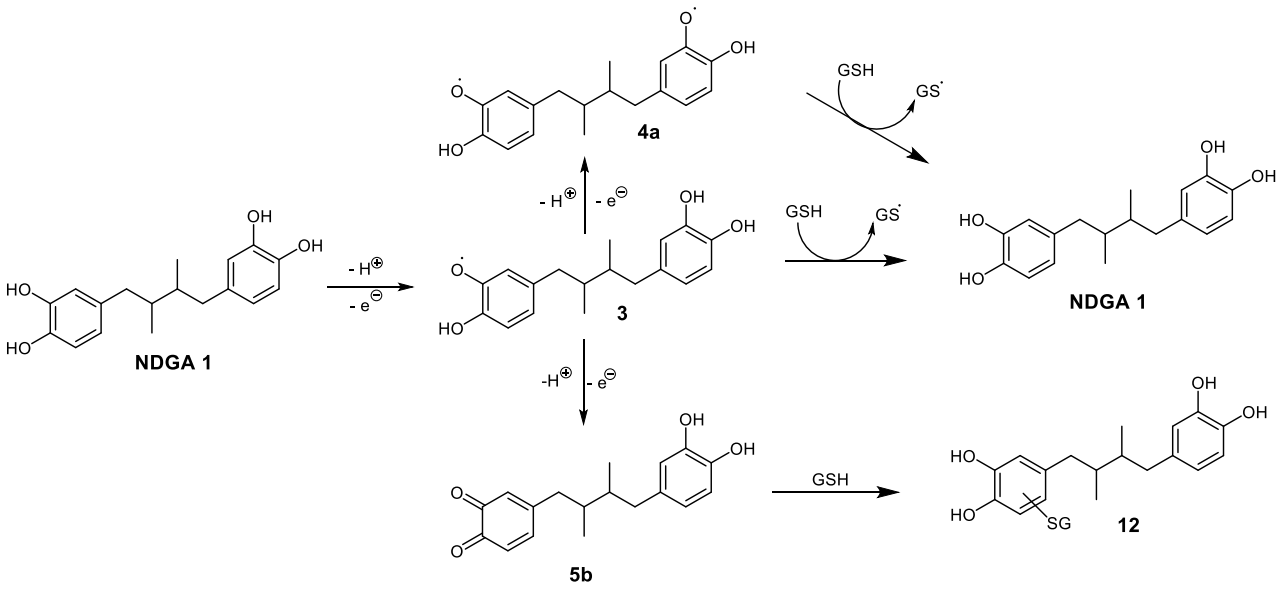

Scheme 5-3: Proposed mechanism of regeneration of NDGA following incubation with excess GSH.

Another important factor in polyphenol oxidation is the catalytic effect of transition metals. Chelating agents such as EDTA and Desferal have been employed to suppress or eliminate this catalytic effect.[67] We did not determine whether any metals were present in our incubation system as our intent was to examine the analogues in our previously established conditions where NDGA

was observed to form a dibenzocyclooctadiene lignan. It is possible that the use of metal-ions-free buffer will inhibit or slow down the intramolecular oxidation reactions and also improve the stability of the NDGA and its analogues although this seems impractical for the purpose of biological evaluation studies. Also, the instability of NDGA in the extraction process is well known and likely oxidizes during traditional preparation of creosote bush. Our results suggest that electrophilic substitution makes no contribution to the intramolecular cyclization process and that NDGA autoxidative cyclization is a radical mediated process. This notwithstanding the inability of compound **A8** to undergo intramolecular cyclization is intriguing and raises the question of whether a radical-mediated mechanism as a standalone is sufficient to explicitly describe autoxidation of dibenzylbutane lignans to dibenzocyclooctadiene derivatives especially for the non-dicatechol lignans.

5.3 Assessment of Reactive Metabolites Formation of NDGA Analogues

In order to minimize bioactivation of new chemotypes during the drug discovery process, a variety of experimental approaches have been developed and incorporated into early optimization of lead compounds including routine in vitro evaluation for reactive metabolite (RM) formation.[129, 138] RMs have been implicated in many drug-induced toxicities including hepatotoxicity.[139] Despite the numerous known pharmacological properties of NDGA, its use is also associated with toxic outcomes including hepatic injury possibly mediated by RMs.[32] Therefore, this phase of the project evaluated the metabolic activation potential of NDGA and its analogues with the overall goal of eliminating RMs liability through rational structural modification. This study was also expected to provide better appreciation of the nature of RMs such as why NDGA does not appear to form p-QM and how ring substitutions affect RMs formation. The potential of the dibenzocyclooctadiene

lignan **2** derived from NDGA under physiological conditions to contribute to its toxicological properties via reactive metabolite formation was also evaluated. This compound has been postulated to contribute to pharmacological properties attributed to NDGA and therefore assessment of its potential reactive metabolite liability is critical to its safety profile. We incubated NDGA and its analogues in rat liver microsomes (RLM) in the presence of glutathione as a nucleophilic trapping agent. Standards for comparison were generated by performing glutathione trapping experiments with chemical and enzyme oxidation systems.

The results of this study demonstrate that NDGA and its catechol-type analogues were oxidized to their corresponding quinoid reactive intermediates by cytochrome P450s. We saw no evidence of RMs when the phenol-type analogues were incubated with microsomes. GSH conjugates were detected by ESI-MS scanning for neutral loss NL 129 Da or 307 Da in positive ionization mode or PI 272 Da scanning in negative ionization mode. These methods have been described in the literature for detecting different classes of GSH adducts[116, 127] although none of them has general applicability. To obtain further information for structure determination, GSH conjugates were subjected to tandem MS/MS analysis or MRM-EPI analysis. Product ions obtained from these studies were consistent with previous reports.[116, 127] As reported in Chapter 4, common neutral losses of glycine (75 Da) and pyroglutamic acid (129 Da) as well as other typical losses from the parent ion MH^+ of GSH conjugates including 146, 232, 249 and 275 Da mass units were observed indicating that NDGA, **A1**, **A4**, **A6**, and cNDGA **2** were oxidized by P450 enzymes to their respective reactive metabolites. The typical fragmentation patterns observed for the GSH conjugates of NDGA and its analogues are summarized in Figure 5-2. The product ions are indicated by *a*- to *k*- in accordance with the literature[117, 132, 140]

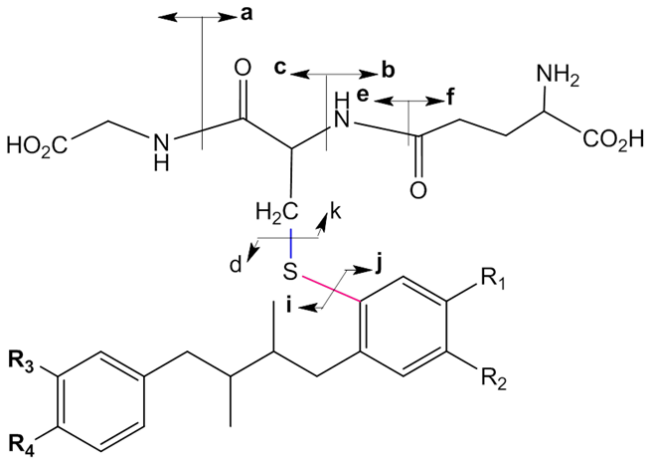

Fragment type	Positive m/z
a	P-75
b	145
c	P-146
d	P-275
e	P-129
f	130
g	P-232
h	P-249
i	308
j	P-307
k	274

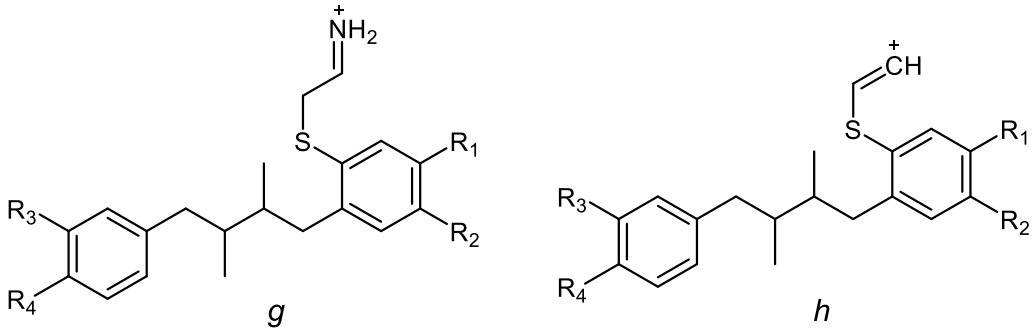

Figure 5-2: Typical fragmentation pathways for GSH conjugates following CID for dibenzylbutane type lignans. P represents the parent ion (MH^+).

Fragmentation-based methods have been used to differentiate glutathione conjugates belonging to different structural classes.[132] In particular, the cleavage of the cysteinyl C-S bond leading to formation of *d/k*-type ions is diagnostic for aromatic conjugates whereas benzylic conjugates primarily yield *i/j*-type ions upon cleavage of the C-S bond between the drug molecule and GSH.[132] As speculated by the authors, the strong π–backbonding interaction between the lone-pair electron of the glutathionyl sulfur atom and the aromatic ring may increase the resistance of the C-S bond between the drug and GSH to CID. The product ions obtained for NDGA and its catechol-type analogues following P450-mediated bioactivation are consistent with aromatic

conjugates indicating that the conjugates were derived from o-Qs. The product ions (Table 4-7) were mainly derived from cleavage of bonds within the glutathionyl moiety as observed in the enzyme oxidation system (Table 4-4) and included the *a*-, *b*-, *c*-, *d*-, *e*-, *f*-, *g*- and *h*-type ions for NDGA and its catechol-type analogues except **A6** where *b*-, *c*- and *g*-type ions were not detected in the P450 oxidation system. It is worth noting that the *d*-type ion formed by the cleavage of the cysteinyl C-S bond and characteristic of ring adducts[132] was observed for NDGA and all its catechol-type analogues. The only evidence of benzylic conjugates which primarily yield i/j-type ions upon cleavage of the C-S bond between the drug molecule and GSH[132] was seen for the phenolic analogue **A2** following Ag_2O catalyzed oxidation. A similar observation was made for the phenolic compounds eugenol and **PC2** (Table 4-6).

Another noteworthy observation from this study is the potential diagnostic utility of the MS detection methods NL 129 and NL 307 in distinguishing aromatic and benzylic conjugates respectively. GSH conjugates of NDGA and its catechol analogues were consistently detected by NL 129 but not NL 307 scanning in positive ionization mode whilst conjugates of the phenol analogue **A2**, eugenol and **PC2** formed in Ag_2O catalyzed oxidation system were only detectable by NL 307 Da scanning. This is in agreement with the findings of Xie et al.,[132] who reported that cleavage of the C-S bond between the test compound and GSH is a less favourable pathway when addition occurs on the ring than when is exocyclic. Tandem MS/MS analysis provided further support for this potential utility when GSH conjugates of NDGA and its catechol analogues all gave a product ion at *m/z* 130 Da consistent with the loss of pyroglutamic acid whilst conjugates of **A2**, eugenol and **PC1** gave *m/z* 308 Da resulting from the loss of glutathione moiety (Tables 4-4, 4-6 and 4-7).

Although the method of scanning for NL 129 Da is a widely used approach for detecting GSH adducts, especially when protonated molecules of GSH conjugates cannot be predicted, it suffers low LC/MS sensitivity and limited selectivity resulting from the interference of endogenous compounds and background noise.[127] Also, neutral loss fragmentation patterns are compound-dependent making the effectiveness of NL experiments vary among different classes of GSH adducts. To improve the selectivity of NL scanning for GSH adducts, the following MS techniques have been explored in the literature: (a) methods using a mixture of GSH and stable-isotope labelled GSH (1:1 ratio) as trapping agent;[124, 141] (b) high-resolution LC/MS;[118] (c) multiple reaction monitoring (MRM) method to monitor typical transitions of protonated (MH^+) potential reactive metabolite trapped as GSH adduct;[142] and (d) precursor ion (PI) scanning in negative electrospray ionization mode.[116] Although an MRM-based approach seems to provide superior sensitivity and selectivity for GSH adducts, especially where isotope labelled GSH is not available, it only detects the GSH adducts pre-set on an MRM transition protocol.[127] Therefore the MRM approach has been used in conjunction with PI or NL when comprehensive analysis of predicted and unpredicted GSH conjugates is desired.[127] In order to further confirm the RMs formed in P450s mediated oxidation system, MRM was used as a survey scan to trigger acquisition of EPI. As shown in Figures 4-28 and 4-29, the results of this study were consistent with those of NL 129 scanning and tandem MS/MS studies. The P450-mediated bioactivation study also revealed that the NDGA-derived dibenzocyclooctadiene lignan **2** potentially makes contribution to NDGA toxicity via oxidation to reactive quinones. Results of ESI-MS/MS experiments (Table 4-7) clearly demonstrate evidence of P450-mediated oxidation to a reactive quinone. Notably, the 2 mass unit difference between NDGA (302 Da) and the cNDGA (300 Da) was maintained in the corresponding MH^+ for GSH monoconjugates at *m/z* 608 and 606 Da respectively. Additionally,

major product ions obtained for NDGA-GSH and cNDGA-GSH conjugates differed by 2 mass units. This observation is in agreement with findings by Galano et al.[22] who recently reported that NDGA forms a cyclic compound which can be further oxidized, although at a higher potential than NDGA.

5.3.1 Isomerization of NDGA *o*-Q to *p*-QM

The results of this study revealed that isomerization of NDGA o-Q **5b** to p-QM **5c** does not occur for either **A1** or **A4**, suggesting that NDGA o-Q is the major toxicophore and likely responsible for RMs-mediated toxicities. Steric hindrance at the benzyl carbon has been previously invoked to explain why NDGA does not form a p-QM. Compound **A2** has the same steric bulk at the benzyl carbon and yet formed a GSH conjugate derived from p-QM in the chemical oxidation system. Also conversion of SECO to lariciresinol has been proposed to occur via p-QM intermediate, although the benzyl carbon has the same chemical environment. It is likely that p-QM formation from the dibenzylbutane-type lignans is a direct oxidation process and that isomerization contributes negligibly to its formation, as may be the case for NDGA. Like **A2** and SECO, compound **A3** lacks the potential to form an o-Q and was expected to oxidize directly to a p-QM. Surprisingly, **A3** did not form a GSH reactive product in the P450 oxidation system nor in the Ag_2O catalyzed oxidation system. No direct evidence of RMs formation has been reported for the standard compounds meso-dihydroguaiaretic acid (DGA) as well as SECO in the literature.

Taken together, the results demonstrate that RMs formation is dependent on substituents and/or substitution pattern on the two aromatic rings of NDGA. It was observed that P450-mediated oxidation of the dibenzylbutane family of lignans do not form p-QM and that the o-Q is the major reactive toxicophore which likely leads to some of the toxic effects associated with NDGA use. It is

concluded that structural modification efforts should focus on phenol-type analogues to potentially enhance safety profile of NDGA. Notably, phenols such as **A3** and **A8** require further investigation as these phenols demonstrated improved stability at pH 7.4 and *meta*-OH substituted lignans, such as enterolactone, display pharmacological activity.[69, 143]

5.4 Preliminary Cytotoxicity Evaluation

NDGA derived-dibenzocyclooctadiene lignan (cNDGA **2**) was evaluated for the first time for biological activity. We have speculated based on the conditions of its formation and the known pharmacological properties of the dibenzocyclooctadiene family of lignans that cNDGA possibly makes contribution to biological activities reported for NDGA. Thus, NDGA, cNDGA and the analogues synthesized for this project were evaluated for cytotoxicity against four human breast cancer cell lines T47D, MDA-MB-231 (M231), MDA-MB-468 (M468), MCF7, and a lung cancer cell line A549 by our collaborator (J. Tuszynski) at the Cross Cancer Institute (Edmonton, AB). As shown in Table 4-8, NDGA and its analogues had no significant growth inhibition effect against all the cell line tested in comparison with the positive control thiocolchicine although the phenol analogues **A3b** and **A2** were generally better than the parent compound NDGA against the cell line used. Given that the phenol analogues are oxidatively more stable than the catechol analogues and NDGA, further biological assays in appropriate cell lines where NDGA shows cytotoxic effects are required for better comparison.

6 SUMMARY AND CONCLUSIONS

In summary, a series of NDGA analogues were designed, synthesized and characterized for the purpose of investigating the structural features that influence pharmacological and toxicological properties of NDGA. The potentials of the prepared analogues to undergo intramolecular cyclization under our previously established physiologically relevant conditions[35] where NDGA was observed to form a dibenzocyclooctadiene lignan were evaluated. This study was intended to help explain the mechanisms of NDGA intramolecular cyclization to a dibenzocyclooctadiene derivative and provide information about structural features that influence pharmacological properties of NDGA. The results demonstrate that electrophilic substitution makes no contribution to the intramolecular cyclization process and that NDGA autoxidative intramolecular cyclization is a radical-mediated process. NDGA and **A6** (both containing a di-catechol) autoxidized to their corresponding dibenzocyclooctadiene derivatives **2** and **84** respectively which were fully characterized by MS and NMR techniques. However, the mono-catechol analogues **A1** and **A4** underwent oxidation to o-Q but no evidence of cyclization was found implying that electrophilic substitution cannot account for NDGA cyclization. Attempts to confirm the radical-mediated pathway with **A7** were unsuccessful although our observation was similar to a result reported by Robin et al., using RuO_2 for cyclization of an *ortho*-phenol substituted lignan.[60] The pronounced suppression of cyclization for NDGA and **A6** observed in the presence of 20 fold excess GSH supports the involvement of free radicals as opposed to o-Q in the intramolecular cyclization process. We also evaluated the stability of the analogues under the conditions used for this study. It was observed that stability of the analogues is dependent on the degree of substitution of the aromatic rings. At pH 7.4, the catechol-type analogues were generally less stable in comparison to

the phenol-type analogues. Compound **A6** which lacks substitution on the butane-bridge degraded faster than NDGA possibly as a result of its conformational flexibility.

Oxidative metabolism and bioactivation studies on NDGA and its analogues revealed that reactive metabolites formation is dependent on substitution and/or substitution pattern of the aromatic rings. Cytochrome P450-mediated oxidation of NDGA and its catechol-type analogues yielded electrophilic intermediates which reacted with GSH. LC-ESI-MS analysis in positive ionization mode gave parent ions at *m/z* 608, 576, 636 and 580 Da, consistent with addition of GSH to NDGA, **A1**, **A4** and **A6** respectively. A further tandem MS/MS studies gave products ions consistent with typical fragmentation patterns reported for GSH conjugates.[116, 127, 129] The fragmentation patterns were used to identify the GSH conjugates as ring adducts derived from o-Q[132] although the position of attachment on the aromatic ring could not be determined. We also found that NL 129 or 307 scanning in positive ionization mode has potential diagnostic utility in distinguishing between aromatic and benzylic GSH conjugates. GSH conjugates of NDGA and its catechol-type analogues were consistently detected by NL 129 but not NL 307 scanning whilst conjugates of the phenol analogue **A2**, eugenol and **PC2** formed in a Ag_2O catalyzed oxidation system were only detectable by NL 307 Da scanning. This is in agreement with the findings of Xie et al.[132] We found no evidence of p-QM formation either directly or via isomerization of o-Q intermediates suggesting that o-Q is the major reactive toxicophore responsible for reactive metabolite generated toxicities associated with NDGA use. In addition, we demonstrated that the NDGA-derived dibenzycyclooctadiene lignan (cNDGA **2**) undergoes P450-mediated oxidation to a reactive metabolite which might contribute to the toxicological properties of NDGA. There was no evidence of P450-mediated oxidation to reactive metabolites for the phenol-type NDGA analogues. It is concluded that structural modification efforts should focus on phenol-type analogues.

Cytotoxicity of the NDGA analogues and the possible involvement of cNDGA in pharmacological properties attributed to NDGA were examined against human breast cancer cell lines T47D, MDA-MB-231 (M231), MDA-MB-468 (M468), MCF7, and a lung cancer cell line A549. This preliminary study gave growth inhibition (GI_{50}) at micro molar concentration levels or showed no growth inhibitory effect. The results indicate that the analogues are several folds less potent in comparison to a known cytotoxic compound thiocolchicine against the cell lines used. The cNDGA showed no growth inhibition against human breast cancer cells and about two fold less potent than NDGA against the lung cancer cell line A549.

7 FUTURE RESEARCH

On the basis of the findings made in these studies, the following are intended to direct future efforts at advancing this research project.

Given the interesting observation that absence of substituents on the butane-bridge of the two aromatic rings enhances intramolecular cyclization to dibenzocyclooctadiene derivatives, a successful synthesis of **A5** and evaluation of its autoxidation potential under similar conditions used for NDGA and **A6** will provide further information about structural features which influence the oxidative cyclization rate. From our observation with **A6**, compound **A5** will be expected to cyclize at a reduced rate in comparison to NDGA. The synthetic challenge that remained was introduction of the additional methyl substituents at positions C2 and C3 of the butane-bridge. One potential approach to forming the required basic lignan skeleton is shown in Scheme 7-1. Step 1 of this scheme involves esterification of 2,3-dimethylsuccinic acid. The use of MeI in DMSO/K_2CO_3 gave access to esters in good yield in this project and may be applicable. It is anticipated that the basic lignan skeleton may be obtainable via alkylation although step 2 is yet unstudied. Following a successful LDA alkylation, a couple of reductive steps and demethylation using BBr_3 as reported in this project should allow access to compound **A5.**

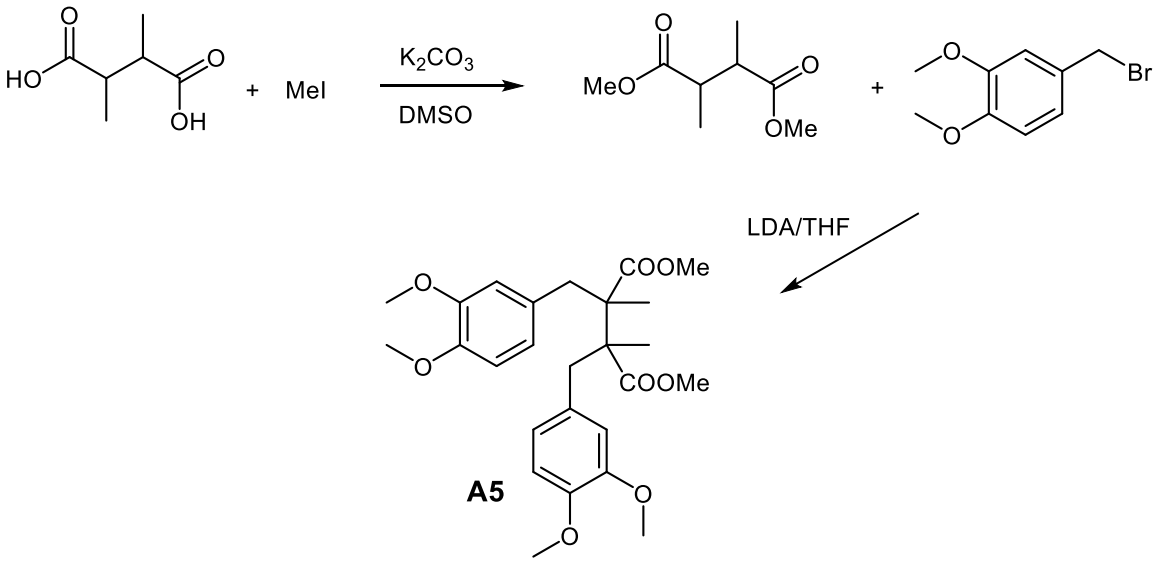

Scheme 7-1: Potential synthetic approach to basic lignan skeleton for compound **A5**.

Also, the inability of compound **A8** to undergo intramolecular cyclization raises the question of whether radical-mediated mechanism as a standalone is sufficient to explicitly describe autoxidation of dibenzylbutane lignans to dibenzocyclooctadiene derivatives especially for non-dicatechol lignans. Access to NDGA analogues shown in Figure 7-1 will be useful in verifying an intriguing possibility outlined in Scheme 5-2 of this project. This modified mechanism involves attack of an *ortho*-quinone by an ionized ring suggesting that compound 7-1 but not 7-2 should cyclize. The proposed compounds are obtainable by consecutive Stobbe condensation approach used in this project.

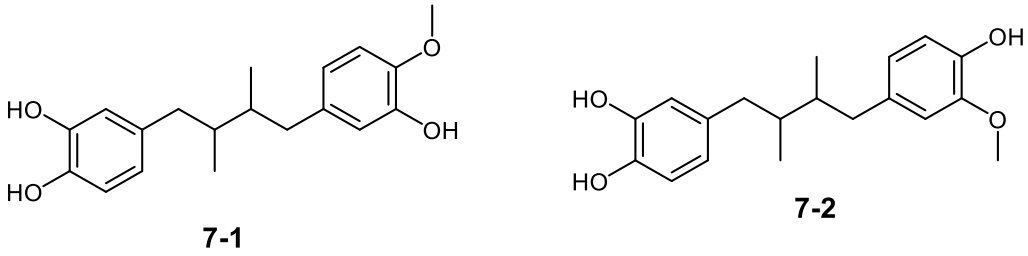

Figure 7-1: Proposed compounds for verifying the modified mechanism of intramolecular cyclization of NDGA.

Another potential direction for this research is isolation of the GSH conjugates formed via P450 mediated oxidations of **A1**, **A4**, and **A6** for NMR studies. The conjugates were identified as ring adducts derived from o-Qs by MS.[132] However, NMR studies will be useful to define the position at which the GSH binds to these analogues and provide further support for the nature of the electrophilic entities. Following successful NMR determination of positions of GSH attachment, the pure isolates could be used in MS studies for validation of the diagnostic utility of NL 129 and NL 307 scanning modes for aromatic and benzylic adducts respectively. This will be extremely useful in the early drug discovery and optimization process for providing insight into the nature of reactive metabolites in real-time without the need for reference standards or the tedious and time-consuming isolations for nuclear magnetic resonance (NMR) identification.

Analogues of NDGA have been assessed for their growth inhibitory activity against human breast cancer, human colon cancer and human melanoma cell lines. The lignans had IC50 values of 5–60 μM.[5] M4N **14** inhibits the growth of a number of tumor cell lines in vitro and also the growth of both murine and human melanomas and human colon cancer in vivo without apparent hepatic and renal toxicity.[92] Given that our preliminary cytotoxicity evaluation results varied widely from previous reports, it is recommended that biological activity screening of the analogues prepared for this project be repeated. Anti-viral activity has also been reported for NDGA and its derivatives.[21] It may be interesting to evaluate the analogues prepared for this project in a similar model. M4N **14**, which is being developed as an anticancer and antiviral drug, was also synthesized in addition to the analogues studied in this project. This presents a great opportunity to compare the biological activities of the analogues with two standards, NDGA and M4N to establish whether the findings support the idea that the "free" phenolic hydroxyl groups facilitate intolerable in vivo toxicity.

8 REFERENCES

1. Lambert, J. D.; Dorr, R. T.; Timmermann, B. N. Nordihydroguaiaretic Acid: A review of its numerous and varied biological activities. *Pharm. Biol.* **2004**, *42*, 149-158.

2. Arteaga, S.; Andrade-Cetto, A.; Cardenas, R. Larrea tridentata (Creosote bush), an abundant plant of Mexican and US-American deserts and its metabolite nordihydroguaiaretic acid. *J. Ethnopharmacol.* **2005**, *98*, 231-239.

3. Tyler, V. E. *The honest herbal, a sensible guide to the use of herbs and related remedies;* Pharmaceutical Products Press: New York, 1994; , pp 375 pp.

4. Lambert, J. D.; Zhao, D.; Meyers, R. O.; Kuester, R. K.; Timmermann, B. N.; Dorr, R. T. Nordihydroguaiaretic acid: hepatotoxicity and detoxification in the mouse. *Toxicon* **2002**, *40*, 1701-1708.

5. Lambert, J. D.; Sang, S.; Dougherty, A.; Caldwell, C. G.; Meyers, R. O.; Dorr, R. T.; Timmermann, B. N. Cytotoxic lignans from Larrea tridentata. *Phytochemistry* **2005**, *66*, 811-815.

6. Lu, J. M.; Nurko, J.; Weakley, S. M.; Jiang, J.; Kougias, P.; Lin, P. H.; Yao, Q.; Chen, C. Molecular mechanisms and clinical applications of nordihydroguaiaretic acid (NDGA) and its derivatives: an update. *Med. Sci. Monit.* **2010**, *16*, RA93-100.

7. Kumar, S.; Wedgwood, S.; Black, S. M. Nordihydroguaiaretic acid increases endothelial nitric oxide synthase expression via the transcription factor AP-1. *DNA Cell Biol.* **2007**, *26*, 853-862.

8. Ramasamy, S.; Drummond, G. R.; Ahn, J.; Storek, M.; Pohl, J.; Parthasarathy, S.; Harrison, D. G. Modulation of expression of endothelial nitric oxide synthase by nordihydroguaiaretic acid, a phenolic antioxidant in cultured endothelial cells. *Mol. Pharmacol.* **1999**, *56*, 116-123.

9. Aktan, S.; Aykut, C.; Yegen, B. C.; Okar, I.; Ozkutlu, U.; Ercan, S. The effect of nordihydroguaiaretic acid on leukotriene C4 and prostaglandin E2 production following different reperfusion periods in rat brain after forebrain ischemia correlated with morphological changes. *Prostaglandins Leukot. Essent. Fatty Acids* **1993**, *49*, 633-641.

10. Goodman, Y.; Steiner, M. R.; Steiner, S. M.; Mattson, M. P. Nordihydroguaiaretic acid protects hippocampal neurons against amyloid beta-peptide toxicity, and attenuates free radical and calcium accumulation. *Brain Res.* **1994**, *654*, 171-176.

11. Guzman-Beltran, S.; Pedraza-Chaverri, J.; Gonzalez-Reyes, S.; Hernandez-Sanchez, F.; Juarez-Figueroa, U. E.; Gonzalez, Y.; Bobadilla, K.; Torres, M. Nordihydroguaiaretic acid attenuates the oxidative stress-induced decrease of CD33 expression in human monocytes. *Oxid. Med. Cell Longev.* **2013**, *2013*, 375893.

12. Rothman, S. M.; Yamada, K. A.; Lancaster, N. Nordihydroguaiaretic acid attenuates NMDA neurotoxicity--action beyond the receptor. *Neuropharmacology* **1993**, *32*, 1279-1288.

13. Shishido, Y.; Furushiro, M.; Hashimoto, S.; Yokokura, T. Effect of nordihydroguaiaretic acid on behavioral impairment and neuronal cell death after forebrain ischemia. *Pharmacol. Biochem. Behav.* **2001**, *69*, 469-474.

14. Ansar, S.; Iqbal, M.; Athar, M. Nordihydroguairetic acid is a potent inhibitor of ferric-nitrilotriacetate-mediated hepatic and renal toxicity, and renal tumour promotion, in mice. *Carcinogenesis* **1999**, *20*, 599-606.

15. Hofmanova, J.; Soucek, K.; Pachernik, J.; Kovarikova, M.; Hoferova, Z.; Minksova, K.; Netikova, J.; Kozubik, A. Lipoxygenase inhibitors induce arrest of tumor cells in S-phase of the cell cycle. *Neoplasma* **2002**, *49*, 362-367.

16. Huang, J. K.; Chen, W. C.; Huang, C. J.; Hsu, S. S.; Chen, J. S.; Cheng, H. H.; Chang, H. T.; Jiann, B. P.; Jan, C. R. Nordihydroguaiaretic acid-induced C**A2**+ handling and cytotoxicity in human prostate cancer cells. *Life Sci.* **2004**, *75*, 2341-2351.

17. Moody, T. W.; Leyton, J.; Martinez, A.; Hong, S.; Malkinson, A.; Mulshine, J. L. Lipoxygenase inhibitors prevent lung carcinogenesis and inhibit non-small cell lung cancer growth. *Exp. Lung Res.* **1998**, *24*, 617-628.

18. Rowe, D. L.; Ozbay, T.; Bender, L. M.; Nahta, R. Nordihydroguaiaretic acid, a cytotoxic insulin-like growth factor-I receptor/HER2 inhibitor in trastuzumab-resistant breast cancer. *Mol. Cancer. Ther.* **2008**, *7*, 1900-1908.

19. Soriano, A. F.; Helfrich, B.; Chan, D. C.; Heasley, L. E.; Bunn, P. A.,Jr; Chou, T. C. Synergistic effects of new chemopreventive agents and conventional cytotoxic agents against human lung cancer cell lines. *Cancer Res.* **1999**, *59*, 6178-6184.

20. Seufferlein, T.; Seckl, M. J.; Schwarz, E.; Beil, M.; v Wichert, G.; Baust, H.; Luhrs, H.; Schmid, R. M.; Adler, G. Mechanisms of nordihydroguaiaretic acid-induced growth inhibition and apoptosis in human cancer cells. *Br. J. Cancer* **2002**, *86*, 1188-1196.

21. Craigo, J.; Callahan, M.; Huang, R. C.; DeLucia, A. L. Inhibition of human papillomavirus type 16 gene expression by nordihydroguaiaretic acid plant lignan derivatives. *Antiviral Res.* **2000**, *47*, 19-28.

22. Galano, A.; Macias-Ruvalcaba, N. A.; Medina Campos, O. N.; Pedraza-Chaverri, J. Mechanism of the OH radical scavenging activity of nordihydroguaiaretic acid: a combined theoretical and experimental study. *J Phys Chem B* **2010**, *114*, 6625-6635.

23. Floriano-Sanchez, E.; Villanueva, C.; Medina-Campos, O. N.; Rocha, D.; Sanchez-Gonzalez, D. J.; Cardenas-Rodriguez, N.; Pedraza-Chaverri, J. Nordihydroguaiaretic acid is a potent in vitro scavenger of peroxynitrite, singlet oxygen, hydroxyl radical, superoxide anion and hypochlorous acid and prevents in vivo ozone-induced tyrosine nitration in lungs. *Free Radic. Res.* **2006**, *40*, 523-533.

24. Sheikh, N. M.; Philen, R. M.; Love, L. A. Chaparral-associated hepatotoxicity. *Arch. Intern. Med.* **1997**, *157*, 913-919.

25. Bhattacherjee, P.; Boughton-Smith, N. K.; Follenfant, R. L.; Garland, L. G.; Higgs, G. A.; Hodson, H. F.; Islip, P. J.; Jackson, W. P.; Moncada, S.; Payne, A. N. The effects of a novel series of selective inhibitors of arachidonate 5-lipoxygenase on anaphylactic and inflammatory responses. *Ann. N. Y. Acad. Sci.* **1988**, *524*, 307-320.

26. Salari, H.; Braquet, P.; Borgeat, P. Comparative effects of indomethacin, acetylenic acids, 15-HETE, nordihydroguaiaretic acid and BW755C on the metabolism of arachidonic acid in human leukocytes and platelets. *Prostaglandins Leukot. Med.* **1984**, *13*, 53-60.

27. Batchelor, W. B.; Heathcote, J.; Wanless, I. R. Chaparral-induced hepatic injury. *Am. J. Gastroenterol.* **1995**, *90*, 831-833.

28. Gordon, D. W.; Rosenthal, G.; Hart, J.; Sirota, R.; Baker, A. L. Chaparral ingestion. The broadening spectrum of liver injury caused by herbal medications. *JAMA* **1995**, *273*, 489-490.

29. Stickel, F.; Egerer, G.; Seitz, H. K. Hepatotoxicity of botanicals. *Public Health Nutr.* **2000**, *3*, 113-124.

30. Smith, A. Y.; Fau, F. R.; Gardner, K. D. J.; Fau-Davis, C. J. J.; Davis, C. J. Cystic renal cell carcinoma and acquired renal cystic disease associated with consumption of chaparral tea: a case report. *The Journal of urology JID - 0376374* **1212**, .

31. Goodman, T.; Grice, H. C.; Becking, G. C.; Salem, F. A. A cystic nephropathy induced by nordihydroguaiaretic acid in the rat. Light and electron microscopic investigations. *Lab. Invest.* **1970**, *23*, 93-107.

32. Grice, H. C.; Becking, G.; Goodman, T. Toxic properties of nordihydroguaiaretic acid. *Food Cosmet. Toxicol.* **1968**, *6*, 155-161.

33. Billinsky, J. L.; Marcoux, M. R.; Krol, E. S. Oxidation of the lignan nordihydroguaiaretic acid. *Chem. Res. Toxicol.* **2007**, *20*, 1352-1358.

34. Cavalieri, E. L.; Li, K.; Balu, N.; Saeed, M.; Devanesan, P.; Higginbotham, S.; Zhao, J.; Gross, M. L.; Rogan, E. G. Catechol ortho-quinones : the electrophilic compounds that form depurinating DNA adducts and could initiate cancer and other diseases. *Carcinogenesis* **2002**, *23*, 1071-1077.

35. Billinsky, J. L.; Krol, E. S. Nordihydroguaiaretic acid autoxidation produces a schisandrin-like dibenzocyclooctadiene lignan. *J. Nat. Prod.* **2008**, *71*, 1612-1615.

36. McDonald, R. W.; Bunjobpon, W.; Liu, T.; Fessler, S.; Pardo, O. E.; Freer, I. K.; Glaser, M.; Seckl, M. J.; Robins, D. J. Synthesis and anticancer activity of nordihydroguaiaretic acid (NDGA) and analogues. *Anticancer Drug Des.* **2001**, *16*, 261-270.

37. Wagner, P.; Lewis, R. A. Interaction between activated nordihydroguaiaretic acid and deoxyribonucleic acid. *Biochem. Pharmacol.* **1980**, *29*, 3299-3306.

38. Chang, J.; Reiner, J.; Xie, J. Progress on the chemistry of dibenzocyclooctadiene lignans. *Chem. Rev.* **2005**, *105*, 4581-4609.

39. Charlton, J. L. Antiviral activity of lignans. *J. Nat. Prod.* **1998**, *61*, 1447-1451.

40. Lee, K. H. Current developments in the discovery and design of new drug candidates from plant natural product leads. *J. Nat. Prod.* **2004**, *67*, 273-283.

41. Kuo, Y.; Huang, H.; Kuo, L. Y.; Chen, C. Novel C19 Homolignans, Taiwanschirin A, B, and Cytotoxic Taiwanschirin C, and a New C18 Lignan, Schizanrin A, from Schizandra arisanensis. *J. Org. Chem.* **1999**, *64*, 7023-7027.

42. Wang, J. P.; Raung, S. L.; Hsu, M. F.; Chen, C. C. Inhibition by gomisin C (a lignan from Schizandra chinensis) of the respiratory burst of rat neutrophils. *Br. J. Pharmacol.* **1994**, *113,* 945-953.

43. Ko, K. M.; Ip, S. P.; Poon, M. K.; Wu, S. S.; Che, C. T.; Ng, K. H.; Kong, Y. C. Effect of a lignan-enriched fructus schisandrae extract on hepatic glutathione status in rats: protection against carbon tetrachloride toxicity. *Planta Med.* **1995**, *61,* 134-137.

44. Niemeyer, H. B.; Honig, D. M.; Kulling, S. E.; Metzler, M. Studies on the metabolism of the plant lignans secoisolariciresinol and matairesinol. *J. Agric. Food Chem.* **2003**, *51,* 6317-6325.

45. Smolewski, P. Terameprocol, a novel site-specific transcription inhibitor with anticancer activity. *IDrugs* **2008**, *11,* 204-214.

46. Romanczyk, L. J.; Sharma, P. K.; Gou, D.; Gou, Y. US Patent US20100048920 **A1**, 2010.

47. Moss, G. P. Nomenclature of Lignans and Neolignans (IUPAC Recommendations 2000). *Pure and Applied Chemistry* **2000**, *72,* 1493-1523.

48. Chen, Q. Nordihydroguaiaretic acid analogues: their chemical synthesis and biological activities. *Curr. Top. Med Chem* **2009**, *9,* 1636-1659.

49. Ward, R. S. Lignans, neolignans, and related compounds. *Nat. Prod. Rep.* **1995**, *12,* 183-205.

50. Ayres, D. C.; Loike, J. D. Chemical, Biological and Clinical Properties. In Cambridge University Press, Cambridge: 1990; .

51. Hosseinian, F. S.; Muir, A. D.; Westcott, N. D.; Krol, E. S. AAPH-mediated antioxidant reactions of secoisolariciresinol and SDG. *Org. Biomol. Chem* **2007**, *5,* 644-654.

52. Chipault, J. R. *Autoxidation and Antioxidants;* Interscience Publisher: New York, 1962; , pp 396.

53. Cozzarelli, N. R. In *In Annual Reviews in Biochemistry;* Annual Reviews, Inc: Palo Alto, CA, 1977; pp 641.

54. Wells, R. D.; Larson, J. E. Studies on the binding of actinomycin D to DNA and DNA model polymers. *J. Mol. Biol.* **1970**, *49,* 319-342.

55. Choi, Y. W.; Takamatsu, S.; Khan, S. I.; Srinivas, P. V.; Ferreira, D.; Zhao, J.; Khan, I. A. Schisandrene, a dibenzocyclooctadiene lignan from Schisandra chinensis: structure-antioxidant activity relationships of dibenzocyclooctadiene lignans. *J. Nat. Prod.* **2006**, *69,* 356-359.

56. Fujihashi, T.; Hara, H.; Sakata, T.; Mori, K.; Higuchi, H.; Tanaka, A.; Kaji, H.; Kaji, A. *Antimicrob. Agents Chemother.* **1995**, *39,* .

57. Chen, D.; Zhang, S.; Xie, L.; Xie, J.; Chen, K.; Kashiwada, Y.; Zhou, B.; Wang, P.; Cosentino, L. M.; Lee, K. Anti-aids agents—XXVI. Structure-activity correlations of Gomisin-G-related anti-HIV lignans from Kadsura interior and of related synthetic analogues. *Bioorg. Med. Chem.* **1997**, *5,* 1715-1723.

58. Xia, Y.; Bi, W.; Zhang, Y. Synthesis of dibebzylbutanediol lignans and their Anti-HIV, Anti-HSV, Anti-tumor Activities. *J. Chil. Chem. Soc.* **2009**, *54,* 428-431.

59. Coleman, R. S.; Gurrala, S. R.; Mitra, S.; Raao, A. Asymmetric total synthesis of dibenzocyclooctadiene lignan natural products. *J. Org. Chem.* **2005**, *70*, 8932-8941.

60. Robin, J. P.; Landais, Y. Ruthenium(IV) dioxide in fluoro acid medium. An efficient biaryl phenol coupling process, exemplified with a biomimetic access to the skeleton of steganacin from presteganes. *J. Org. Chem.* **1988**, *53*, 224-226.

61. Kupchan, S. M.; Leip, A. J.; Kameswaran, V.; Bryan, R. F. Novel nonphenol oxidative coupling. *J. Am. Chem. Soc.* **1973**, *95*, 6861-6863.

62. Taylor, E. C.; Andrade, J. G.; Rall, G. J. H.; Mackillop, A. Thallium in organic synthesis. 59. Alkaloid synthesis via intramolecular nonphenolic oxidative coupling. Preparation of (.+-.)-ocoteine, (.+-.)-acetoxyocoxylonine, (.+-.)-3-methoxy-n-acetylnornantenine, (.+-.)-neolitsine, (.+-.)-kreysigine, (.+-.)-O-methylkreysigine, and (.+-.)-multifloramine . *J. Am. Chem. Soc.* **1980**, *102*, 6513.

63. Pelter, A.; Ward, R. S.; Abd-El-Ghani, A. Preparation of dibenzocyclooctadiene lignans and spirodienones by hypervalent iodine oxidation of phenolic dibenzylbutyrolactones. *J. Chem. Soc. , Perkin Trans. 1* **1992**, 2249-2251.

64. Xie, L.; Chen, L. H.; Xie, J. X. *Chin. J. Org. Chem* **1991**, *11*, 371.

65. Chattopadhyay, S. K.; Rao, K. V. Chemistry of saururus cernuus IV: cyclooctadiene systems derived from austrobailignan-5. *Tetrahedron* **1987**, *43*, 669-678.

66. Krafczyk, N.; Heinrich, T.; Porzel, A.; Glomb, M. A. Oxidation of the dihydrochalcone aspalathin leads to dimerization. *J. Agric. Food Chem.* **2009**, *57*, 6838-6843.

67. Roginsky, V.; Alegria, A. E. Oxidation of tea extracts and tea catechins by molecular oxygen. *J. Agric. Food Chem.* **2005**, *53*, 4529-4535.

68. Spanos, G. A.; Wrolstad, R. E. Phenolics of apple, pear, and white grapes juices and their changes with processing and storage: a review. *J. Agric. Food Chem.* **1992**, *40*, 1478-1487.

69. Adolphe, J. L.; Whiting, S. J.; Juurlink, B. H.; Thorpe, L. U.; Alcorn, J. Health effects with consumption of the flax lignan secoisolariciresinol diglucoside. *Br. J. Nutr.* **2010**, *103*, 929-938.

70. Bolton, J. L.; Trush, M. A.; Penning, T. M.; Dryhurst, G.; Monks, T. J. Role of quinones in toxicology. *Chem. Res. Toxicol.* **2000**, *13*, 135-160.

71. O'Brien, P. J. Molecular mechanisms of quinone cytotoxicity. *Chem. Biol. Interact.* **1991**, *80*, 1-41.

72. Wahllander, A.; Soboll, S.; Sies, H.; Linke, I.; Muller, M. Hepatic mitochondrial and cytosolic glutathione content and the subcellular distribution of GSH-S-transferases. *FEBS Lett.* **1979**, *97*, 138-140.

73. Kaplowitz, N. The importance and regulation of hepatic glutathione. *Yale J Biol Med.* **1981**, *54*, 497-502.

74. Schweigert, N.; Zehnder, A. J.; Eggen, R. I. Chemical properties of catechols and their molecular modes of toxic action in cells, from microorganisms to mammals. *Environ. Microbiol.* **2001**, *3*, 81-91.

75. Halliwell, B.; Gutteridge, J. M. C. *Free Radicals in Biology and Medicine;* Oxford University Press Inc: New York, 1999; Vol. 3rd.

76. Jordan, R. T.; Allen, L. M. Patent WO8801509, 1988.

77. Bolton, J. L.; Acay, N. M.; Vukomanovic, V. Evidence that 4-allyl-o-quinones spontaneously rearrange to their more electrophilic quinone methides: potential bioactivation mechanism for the hepatocarcinogen safrole. *Chem. Res. Toxicol.* **1994**, *7,* 443-450.

78. Iverson, S. L.; Hu, L. Q.; Vukomanovic, V.; Bolton, J. L. The influence of the p-alkyl substituent on the isomerization of o-quinones to p-quinone methides: potential bioactivation mechanism for catechols. *Chem. Res. Toxicol.* **1995**, *8,* 537-544.

79. Thompson, D. C.; Thompson, J. A.; Sugumaran, M.; Moldeus, P. Biological and toxicological consequences of quinone methide formation. *Chem. Biol. Interact.* **1993**, *86,* 129-162.

80. Bolton, J. L.; Wu, H. M.; Hu, L. Q. Mechanism of isomerization of 4-propyl-o-quinone to its tautomeric p-quinone methide. *Chem. Res. Toxicol.* **1996**, *9,* 109-113.

81. Naish-Byfield, S.; O'Reilly, P. A. Oxidation of monohydric phenol substrates by tyrosinase: An oximetric study. *Biochem. J.* **1992**, *288,* 63-67.

82. Sayre, L. M.; Nadkarni, D. V. Direct conversion of phenols to o-quinones by copper (I) dioxygen: Questions regarding the monophenolase activity of tyrosinase mimics. *J. Am. Chem. Soc.* **1994**, *116*, 3157-3158.

83. Thompson, D. C.; Teodosiu, D.; Egestad, B.; Mickos, H.; Moldeus, P. Formation of glutathione conjugates during oxidation of eugenol by microsomal fractions of rat liver and lung. *Biochem. Pharmacol.* **1990**, *39*, 1587-1595.

84. Tajima, K.; Yamamoto, K.; Mizutani, T. Biotransformation of butylated hydroxytoluene (BHT) to BHT-quinone methide in rats. *Chem. Pharm. Bull.* **1981**, *29*, 3738-3741.

85. Thompson, D. C.; Trush, M. A. Enhancement of peroxidase-mediated oxidation of butylated hydroxytoluene to a quinone methide by phenolic amd amine compounds. *Chem. Biol. Interact.* **1989**, *72*, 157-173.

86. Thompson, D. C.; Teodosiu, D.; Norbeck, K.; Svensson, B.; Moldeus, P. Metabolic activation of eugenol by myeloperoxidase and polymorphnuclear leucocytes. *Chem. Res. Toxicol.* **1989**, *2*, 186-192.

87. Krol, E. S.; Bolton, J. L. Oxidation of 4-alkylphenols and catechols by tyrosinase: ortho-substituents alter the mechanism of quinoid formation. *Chem. Biol. Interact.* **1997**, *104*, 11-27.

88. Powis, G. Metabolism and reactions of quinoid anticancer agents. *Pharmacol. Ther.* **1987**, *35*, 57-162.

89. Huang, R. C.; Li, Y.; Giza, P. E.; Gnabre, J. N.; Abd-Elazem, I. S.; King, K. Y.; Hwu, J. R. Novel antiviral agent tetraglycylated nordihydroguaiaretic acid hydrochloride as a host-dependent viral inhibitor. *Antiviral Res.* **2003**, *58*, 57-64.

90. Hwu, J. R.; Tseng, W. N.; Gnabre, J.; Giza, P.; Huang, R. C. Antiviral activities of methylated nordihydroguaiaretic acids. 1. Synthesis, structure identification, and inhibition of tat-regulated HIV transactivation. *J. Med. Chem.* **1998**, *41*, 2994-3000.

91. Chen, Q.; Heller, J. D.; Lopez, R. A.; Morris, A. J. US Patent 2031/0053378 **A1**, 2013.

92. Lambert, J. D.; Meyers, R. O.; Timmermann, B. N.; Dorr, R. T. tetra-O-Methylnordihydroguaiaretic acid inhibits melanoma in vivo. *Cancer Lett.* **2001**, *171*, 47-56.

93. Kemal, C.; Louis-Flamberg, P.; Krupinski-Olsen, R.; Shorter, A. L. Reductive inactivation of soybean lipoxygenase 1 by catechols: a possible mechanism for regulation of lipoxygenase activity. *Biochemistry* **1987**, *26*, 7064-7072.

94. Whitman, S.; Gezginci, M.; Timmermann, B. N.; Holman, T. R. Structure-activity relationship studies of nordihydroguaiaretic acid inhibitors toward soybean, 12-human, and 15-human lipoxygenase. *J. Med. Chem.* **2002**, *45*, 2659-2661.

95. Hansch, C.; Leo, A. *Substituent constants for correlation analysis in chemistry and biology;* Wiley-Interscience: 1979.; .

96. Eklund, P. C.; Långvik, O. K.; Wärnå, J. P.; Salmi, T. O.; Willför, S. M.; Sjöholm, R. E. Chemical studies on antioxidant mechanisms and free radical scavenging properties of lignans. *Org. Biomol. Chem.* **2005**, *3*, 3336-3347.

97. Johnson, W. S.; McCloskey, A. L.; Dunnigan, D. A. The Mechanism of the Stobbe Condensation. *J. Am. Chem. Soc.* **1950**, *72*, 514-517.

98. Anjaneyulu, A. S. R.; Raghu, P.; Ramakrishna Rao, K. V.; Sastry, C. V. M.; Umasundari, P.; Satyanarayana, P. In *In On The Stereoselectivity of Stobbe Condensation with Ortho Substituted Aromatic Aldehydes: (E, Z) Configuration of Monobenzylidenesuccinates and Dibenzylidenesuccinic Anhydrides;* 1984; Vol. 53, pp 239-243.

99. Mizufune,H, Nakamura,M,Mitsudera,H, Process research on arylnaphthalene lignan aza-analogues: a new palladium-catalyzed benzannulation of alpha, beta-bisbenzylidenesuccinic acid derivatives. *Tetrahedron* **2006**, *62,* 8539-8549.

100. Xia, Y. M.; Cao, X. P.; Peng, K.; Ren, X. F.; Pan, X. F. An efficient synthetic methood of nordihydroguaiaretic acid (NDGA). *Chinese Chem. Lett* **2003**, *14,* 359-360.

101. Wang, Q.; Yang, Y.; Li, Y.; Yu, W.; Hou, Z. J. An efficient method for the synthesis of lignans. *Tetrahedron* **2006**, *62,* 6107-6112.

102. Xia, Y.; Zhang, Y.; Wang, W.; Ding, Y.; He, R. Synthesis and bioactivity of erythro-nordihydroguairetic acid, threo-(-)-saururenin and their analogues. *J.Serb.Chem.Soc* **2010**, *75,* 1325-1335.

103. Dahl, R.; Landais, Y.; Lebrun, A.; Lanain,V,Robin,J.-P. Ruthenium dioxide in fluoro acid medium V. Application to the non phenolic oxidative coupling of diarylbutanes. Comformational studies of cis and trans deoxyschizandrins. *Tetrahedron* **1994**, *50,* 1153-1164.

104. Lieberman, S. V.; Mueller, G. P.; Stiller, E. T. A synthesis of nordihydroguaiaretic acid. *J. Am. Chem. Soc.* **1947**, *69*, 1540.

105. Hearon, W. M.; MacGregor, W. S. The natuarally occuring lignans. *Chem. Rev.* **1995**, *55*, 957.

106. Son, J.; Lee, S. H.; Nagarapu, L.; Jahng, Y. A simple synthesis of Nordihydroguaiaretic Acid and its analogues. *Bull. Korean Chem. Soc* **2005**, *26,* 1117-1120.

107. Gezginci, M. H.; Timmermann, B. N. A short synthetic route to nordihydroguaiaretic acid (NDGA) and its stereoisomer using Ti-induced carbonyl-coupling reaction. *Tetrahedron Lett.* **2001**, *42,* 6083-6085.

108. Richards, I. C. Titanium(IV) Chloride-Zinc. In John Wiley: London, 2001; .

109. Takei, Y.; Mori, K.; Matsui, M. Synthesis of dl-matairesinol dimethyl ether, dehydrodimethyl conidentrin and dehydrodimethyl retrodendrin from ferulic acid. *Agric. Biol. Chem.* **1973**, *37,* 637-641.

110. Zhu, F.; Li, W.; Wang, Q.; Hou, Z. Regioselective Oxidative Coupling Approach to the Synthesis of (ñ)-Matairesinol and (ñ)-Secoisolariciresinol. *Synlett* **2006**, *11,* 1780-1782.

111. Sarkanen, K. V.; Wallis, A. F. A. Oxidative dimerizations of (E)- and (Z)-isoeugenol (2-methoxy-4-pro-penylphenol) and (E)- and (Z)-2,6-dimethoxy-4-propenylphenol. *J. Chem. Soc. Perkins Trans.* **1973**, *1,* 1869-1878.

112. Li, A. P. Overview: Evaluation of metabolism-based drug toxicity in drug development. *Chem. Biol. Interact.* **2009**, *179,* 1-3.

113. Ma, S.; Zhu, M. Recent advances in applications of liquid chromatography-tandem mass spectrometry to the analysis of reactive drug metabolites. *Chem. Biol. Interact.* **2009**, *179,* 25-37.

114. Friedlander, T. W.; Weinberg, V. K.; Huang, Y.; Mi, J. T.; Formaker, C. G.; Small, E. J.; Harzstark, A. L.; Lin, A. M.; Fong, L.; Ryan, C. J. A phase II study of insulin-like growth factor receptor inhibition with nordihydroguaiaretic acid in men with non-metastatic hormone-sensitive prostate cancer. *Oncol. Rep.* **2012**, *27*, 3-9.

115. Haley, S. L.; Lamb, J. G.; Franklin, M. R.; Constance, J. E.; Dearing, M. D. "Pharm-ecology" of diet shifting: biotransformation of plant secondary compounds in creosote (Larrea tridentata) by a woodrat herbivore, Neotoma lepida. *Physiol. Biochem. Zool.* **2008**, *81*, 584-593.

116. Dieckhaus, C. M.; Fernandez-Metzler, C. L.; King, R.; Krolikowski, P. H.; Baillie, T. A. Negative ion tandem mass spectrometry for the detection of glutathione conjugates. *Chem. Res. Toxicol.* **2005**, *18*, 630-638.

117. Baillie, T. A.; Pearson, P. G.; Rashed, M. S.; Howald, W. N. The use of mass spectrometry in the study of chemically-reactive drug metabolises. Application of MS/MS and LC/MS to the analysis of glutathione- and related S-linked conjugates of N-methylformamide. *J. Pharm. Biomed. Anal.* **1989**, *7*, 1351-1360.

118. Castro-Perez, J.; Plumb, R.; Liang, L.; Yang, E. A high-throughput liquid chromatography/tandem mass spectrometry method for screening glutathione conjugates using exact mass neutral loss acquisition. *Rapid Commun. Mass Spectrom.* **2005**, *19*, 798-804.

119. Hopfgartner, G.; Husser, C.; Zell, M. Rapid screening and characterization of drug metabolites using a new quadrupole-linear ion trap mass spectrometer. *J. Mass Spectrom.* **2003**, *38*, 138-150.

120. Zhang, K. E.; Naue, J. A.; Arison, B.; Vyas, K. P. Microsomal metabolism of the 5-lipoxygenase inhibitor L-739,010: evidence for furan bioactivation. *Chem. Res. Toxicol.* **1996**, *9*, 547-554.

121. Xu, S.; Zhu, B.; Teffera, Y.; Pan, D. E.; Caldwell, C. G.; Doss, G.; Stearns, R. A.; Evans, D. C.; Beconi, M. G. Metabolic activation of fluoropyrrolidine dipeptidyl peptidase-IV inhibitors by rat liver microsomes. *Drug Metab. Dispos.* **2005**, *33*, 121-130.

122. Meneses-Lorente, G.; Sakatis, M. Z.; Schulz-Utermoehl, T.; De Nardi, C.; Watt, A. P. A quantitative high-throughput trapping assay as a measurement of potential for bioactivation. *Anal. Biochem.* **2006**, *351*, 266-272.

123. Argoti, D.; Liang, L.; Conteh, A.; Chen, L.; Bershas, D.; Yu, C. P.; Vouros, P.; Yang, E. Cyanide trapping of iminium ion reactive intermediates followed by detection and structure identification using liquid chromatography-tandem mass spectrometry (LC-MS/MS). *Chem. Res. Toxicol.* **2005**, *18*, 1537-1544.

124. Yan, Z.; Maher, N.; Torres, R.; Caldwell, G. W.; Huebert, N. Rapid detection and characterization of minor reactive metabolites using stable-isotope trapping in combination with tandem mass spectrometry. *Rapid Commun. Mass Spectrom.* **2005**, *19*, 3322-3330.

125. Mitchell, M. D.; Elrick, M. M.; Walgren, J. L.; Mueller, R. A.; Morris, D. L.; Thompson, D. C. Peptide-based in vitro assay for the detection of reactive metabolites. *Chem. Res. Toxicol.* **2008**, *21*, 859-868.

126. Chen, W. G.; Zhang, C.; Avery, M. J.; Fouda, H. G. In *In Biological Reactive Intermediates;* Dansette, P. M., Delaforge, R. S. M., Gibson, G. G., Greim, H., Jallow, D. J., Monks, T. J. and Sipes, I. G., Eds.; Kluwer Academic/Plenum Publishers: NY, 2001; Vol. I, pp 521-524.

127. Zheng, J.; Ma, L.; Xin, B.; Olah, T.; Humphreys, W. G.; Zhu, M. Screening and identification of GSH-trapped reactive metabolites using hybrid triple quadruple linear ion trap mass spectrometry. *Chem. Res. Toxicol.* **2007**, *20,* 757-766.

128. Hopfgartner, G.; Varesio, E.; Tschappat, V.; Grivet, C.; Bourgogne, E.; Leuthold, L. A. Triple quadrupole linear ion trap mass spectrometer for the analysis of small molecules and macromolecules. *J. Mass Spectrom.* **2004**, *39,* 845-855.

129. Zhu, M.; Wen, B. Applications of Quadrupole-Linear Ion Trap Mass Spectrometry to the Analysis of Reactive Metabolites in Drug Discovery and Development. In *Advances in Molecular Toxicology;* Elsevier B.V.: United Kingdom, 2009; Vol. 3, pp 59-98.

130. Yu, L.; Liu, H.; Li, W.; Zhang, F.; Luckie, C.; van Breemen, R. B.; Thatcher, G. R.; Bolton, J. L. Oxidation of raloxifene to quinoids: potential toxic pathways via a diquinone methide and o-quinones. *Chem. Res. Toxicol.* **2004**, *17,* 879-888.

131. Blecha, J. E.; Anderson, M. O.; Chow, J. M.; Guevarra, C. C.; Pender, C.; Penaranda, C.; Zavodovskaya, M.; Youngren, J. F.; Berkman, C. E. Inhibition of IGF-1R and lipoxygenase by nordihydroguaiaretic acid (NDGA) analogs. *Bioorg. Med. Chem. Lett.* **2007**, *17,* 4026-4029.

132. Xie, C.; Zhong, D.; Chen, X. A fragmentation-based method for the differentiation of glutathione conjugates by high-resolution mass spectrometry with electrospray ionization. *Anal. Chim. Acta* **2013**, *788*, 89-98.

133. Wang, X.; Thomas, B.; Sachdeva, R.; Arterburn, L.; Frye, L.; Hatcher, P. G.; Cornwell, D. G.; Ma, J. Mechanism of arylating quinone toxicity involving Michael adduct formation and induction of endoplasmic reticulum stress. *Proc. Natl. Acad. Sci. U. S. A.* **2006**, *103*, 3604-3609.

134. Jung, M. E.; Piizzi, G. Gem-Disubstituent Effect: Theoretical Basis and Synthetic Applications. *Chem. Rev.* **2005**, *105*, 1735-1766.

135. Winterbourn, C. C.; Metodiewa, D. The reaction of superoxide with reduced glutathione. *Arch. Biochem. Biophys.* **1994**, *314*, 284-290.

136. Masuda, T.; Yamada, K.; Akiyama, J.; Someya, T.; Odaka, Y.; Takeda, Y.; Tori, M.; Nakashima, K.; Maekawa, T.; Sone, Y. Antioxidation mechanism studies of caffeic acid: identification of antioxidation products of methyl caffeate from lipid oxidation. *J. Agric. Food Chem.* **2008**, *56*, 5947-5952.

137. Fujimoto, A.; Inai, M.; Masuda, T. Chemical evidence for the synergistic effect of a cysteinyl thiol on the antioxidant activity of caffeic and dihydrocaffeic esters. *Food Chem.* **2013**, *138*, 1483-1492.

138. Evans, D. C.; Watt, A. P.; Nicoll-Griffith, D. A.; Baillie, T. A. Drug-protein adducts: an industry perspective on minimizing the potential for drug bioactivation in drug discovery and development. *Chem. Res. Toxicol.* **2004**, *17*, 3-16.

139. Walgren, J. L.; Mitchell, M. D.; Thompson, D. C. Role of Metabolism in Drug-Induced Idiosyncratic Hepatotoxicity. *Crit. Rev. Toxicol.* **2005**, *35*, 325-361.

140. Haroldsen, P. E.; Reilly, M. H.; Hughes, H.; Gaskell, S. J.; Porter, C. J. Characterization of glutathione conjugates by fast atom bombardment/tandem mass spectrometry. *Biomed. Environ. Mass Spectrom.* **1988**, *15*, 615-621.

141. Yan, Z.; Caldwell, G. W. Stable-isotope trapping and high-throughput screenings of reactive metabolites using the isotope MS signature. *Anal. Chem.* **2004**, *76*, 6835-6847.

142. Soglia, J. R.; Harriman, S. P.; Zhao, S.; Barberia, J.; Cole, M. J.; Boyd, J. G.; Contillo, L. G. The development of a higher throughput reactive intermediate screening assay incorporating micro-bore liquid chromatography-micro-electrospray ionization-tandem mass spectrometry and glutathione ethyl ester as an in vitro conjugating agent. *J. Pharm. Biomed. Anal.* **2004**, *36*, 105-116.

143. Kitts, D. D.; Yuan, Y. V.; Wijewickreme, A. N.; Thompson, L. U. Antioxidant activity of the flaxseed lignan secoisolariciresinol diglycoside and its mammalian lignan metabolites enterodiol and enterolactone. *Mol. Cell. Biochem.* **1999**, *202*, 91-100.

144. Wu, Q.; Liu, H.; Liu, H.; Chen, X.; Wang, H.; Zhang, Q.; Li, Y. Practical and Efficient Acylation and Tosylation of Sterically Hindered Alcohols Catalyzed with 1-Methylimidazole. *Chem. Res. Chin. Univ.* **2010**, *26*, 55-59.